DIRECT UV RESONANCE RAMAN MONITORING OF PROTEIN FOLDING REACTION COORDINATE: α-HELIX MELTING AND FORMATION REVISITED

by

Aleksandr V. Mikhonin

B.S., Moscow Institute of Physics and technology, 1995

M.S., Moscow Institute of Physics and technology, 1997

Submitted to the Graduate Faculty of

Arts and Sciences in partial fulfillment

of the requirements for the degree of

Doctor of Philosophy

University of Pittsburgh

2006

UNIVERSITY OF PITTSBURGH

FACULTY OF ARTS AND SCIENCES

This dissertation was presented

by

Aleksandr V. Mikhonin

It was defended on

November 22, 2006

and approved by

David Waldeck, Professor, Department of Chemistry

Christian Schafmeister, Professor, Department of Chemistry

Ivet Bahar, Professor, Department of Computational Biology

Dissertation Advisor: Sanford A. Asher, Professor, Department of Chemistry

Advisor: Prof. Sanford A. Asher

DIRECT UV RESONANCE RAMAN MONITORING OF PROTEIN FOLDING REACTION COORDINATE: α-HELIX MELTING AND FORMATION REVISITED

Aleksandr V. Mikhonin, PhD

University of Pittsburgh, 2006

Abstract. Spectroscopic investigations of protein folding mechanism(s) require the elucidation of the relationship between spectral features and the protein folding reaction coordinate(s). This thesis describes the development and demonstrates the applications of a novel UV resonance Raman (UVRR) spectroscopic methodology, which quantitatively correlates the UVRR amide III_3 ($AmIII_3$) frequency of a peptide bond to its Ψ Ramachandran angle (which is arguably the most important folding reaction coordinate). This information, then, allows us, for the first time, to obtain Ψ angular population distributions of peptide bonds in peptides and proteins from their UVRR $AmIII_3$ band profiles, as well as the Gibbs free energy landscapes along the Ψ Ramachandran angle folding coordinate. Application of this methodology allows us to quantitatively characterize the ensembles of folded and unfolded states in peptides and proteins. We show that the unfolded state ensembles show no evidence of completely disordered "random coil" conformation, and are usually dominated by PPII-like conformations. In addition, we for the first time experimentally detected the extended 2.5_1-helix conformation in poly-L-lysine and poly-L-glutamic acid, which is stabilized by electrostatic repulsion between side-chain charges. Most importantly, we resolved and quantitatively characterized the 3_{10}-helix and π-bulge contributions within the "α-helix melting" of ala-rich peptides. We for the first time obtained their individual experimental melting curves, estimated their Zimm and Bragg parameters, and estimated their individual kinetic (un)folding rates. These results challenge the classical view of protein folding and provide an important quantitative basis for future studies.

TABLE OF CONTENTS

LIST OF TABLES

LIST OF FIGURES

ACKOWLEDGEMENTS

Work described in this thesis would not be possible without contributions of many different people listed below, whome I would like to greatfully acknowledge.

I would like to thank Dr. Sanford Asher for intellectual supervising of this work; for creating an encouraging environment and for letting me be a part of the outstanding research group, where the scientific accomplishments are basically limited only by the abilities.

I would like to acknowledge Dr. Waldeck, Dr. Schafmeister and Dr. Bahar for careful reading of this manuscript.

I am very grateful to Anton Karnoup, Mark Sparrow, Dr. Igor Lednev and Dr. Mary Boyden, who taught me at the early beginning of my carreer as a graduate student how to use the state-of-the-art laboratory equipment. They also helped me to better understand the basic concepts of both protein folding and Raman spectrosocopy. I also would like to thank Anton Karnoup for verifying the AdP-peptide sequence for us using MALDI-MS analysis.

I would like to thank Dr. Nataliya Myshakina for performing theoretical calculations, which helped to understand a significant fraction of the experimental results, and allowed to make make much more valuable conclusions.

I would like to acknowledge Sergei Bykov, Dr. Anatoli Ianoul, Konstantin Pimenov and Zeeshan Ahmed for measuring some of the experimental data, which is included in this thesis. I am especially thankful to Sergei Bykov for measuring UV resonance Raman spectra of peptide crystals. These measurements allowed us to obtain the homogenious linewidth of of single peptide bond conformations, and were crucially needed for further developments of the data deconvolution methodology.

I am also thankful for help and financial support of Dr. John Jackovitz while my travel to PittCon Conferences. This opened me new opportunities, which otherwise would not be possible.

I would like to also acknowledge all the above people as well as Dr. Jon Scaffidi, Bhavya Sharma, Lu Ma, Dr. Marta Kamenjicki-Maurer, Dr. Chad Reese, Dr. Vladimir Alexeev, Benjamin Kabagambe, Dr. Adrien Murza and all the other Asher's group members for helpful discussions and friendly environment.

I would like to also acknowledge NIH Grants GM8RO1EB002053021 and GM30741 for financial support.

Finally, I am very grateful to my wife Irina for her patience, support, understanding and encouragement. I sincerely appreciate her contribution, which is extremely valuable.

1.0 CHAPTER 1. INTRODUCTION

1.1 PROTEIN FOLDING

Protein folding is one of the major problems in modern biochemistry. This problem refers to the questions of how a protein adopts a unique biologically active conformation under specific conditions, and how this information is encoded in protein primary sequences.[1-3] A vast theoretical and experimental literature exists on peptide and protein folding and unfolding.[1-97] A number of mechanisms have been proposed.[8-11,16-18,36,45-48,51,54,58-61,64,69,74,75,94-97] However, only limited progress is made in *de novo* design of proteins;[98-103] because still little insight exists on how the primary sequences dictate the protein folding mechanism. In general case, it is still impossible to predict the protein 3D-structure from primary structure unless these sequences have been previously observed in a protein with known structure. Thus, the arguably most important problem in enzymology is to translate the primary sequence into the encoded protein folding mechanism(s), and to use this information to predict the ultimate native structure from the primary sequence information. Solving this problem will directly lead to a number of practical applications in biochemistry, biotechnology and medicine.

For example, the recent completion of the human genome project elucidated the primary sequence of all human proteins. Thus, solving protein folding problem will also reveal the mechanisms of many diseases of humans. Specifically, mutations in the secondary structure of proteins lead to diseases such as Huntington's, Parkinson's, cystic fibrosis, as well as Alzheimer's and prion diseases.[104-109] In addition, solving the protein folding problem will open new opportunities in drug design and drug delivery.[110]

1.1.1 Levels of Protein Structural Organization

Proteins are biological macromolecules consisting of one or more polypeptide chains. Monomer units in a polypeptide chain are called amino acid residues. The amino acid residues in polypeptide chains are linked together by covalent bonds. There are 20 naturally occurred amino-acids, which serve as building blocks for all proteins found in live organisms. The covalent structure of proteins is determined by the structure of each amino acid, and by the order of these amino acids in the polypeptide chain.[3]

Protein structure is very complex. The number of all possible conformations of a polypeptide chain is too large to be sampled exhaustively. For the sake of simplicity, four levels of structural organization of proteins are usually considered: so called primary, secondary, tertiary, and quaternary structures (IUPAC-IUB, 1970).

The term ***primary structure*** means the chemical structure of the polypeptide chain(s) in a given protein - i.e., the number and sequence of amino acid residues linked together by peptide bonds.

The term ***secondary structure*** means the local spatial arrangement of main-chain atoms of a polypeptide chain segment. The spatial arrangements of side-chain atoms as well as the relationship of the polypeptide chain segment with other segments is not included in this level. The ***tertiary structure*** of a protein molecule, or of a subunit of a protein molecule, takes into account the spatial organization of all its atoms. However, the relationship of the protein molecule (or the subunit) to neighboring molecules or subunits is disregarded at this level.

Finally, the term ***quaternary structure*** of a protein molecule means the arrangement of its subunits (for example, folded domains) in space as well as the intersubunit contacts and interactions. The internal geometry of subunits is disregarded at this level. The subunits in a quaternary structure must be in noncovalent association. For example, haemoglobin contains four polypeptide chains ($alpha_2b_2$) held together noncovalently in a specific conformation as required for its function.

1.1.2 Definition of Native and Denatured States of Proteins.

The term “native state” or “folded state” usually denotes the biologically active state of a protein. Generally, native states are assumed to exist as either a single well defined conformation or a restricted subset of similar conformations, which occur at the minimum (or minima) of its conformational energy landscape at biological conditions, at which the environment favors folding.[3,9,13,15,18,45,46,51,58,61,92,96] It is believed that the biological properties of a protein are determined by the specific main chain and side chain topologies of its unique native conformation.

Term “denatured state” or “unfolded state” usually denotes any conformational state of a protein, which is different from the compact native state. Denatured states of proteins are much less defined[58,111-115] than native state(s), since, at least in principle, there exists a huge number of all possible protein chain conformations, which are different from that of native state(s).

Usually, the transition from the native state to the denaterd state is called “unfolding” or “denaturation” (Fig. 1). In contrast, the transition from the unfolded (denatured state) to the native state is denoted as “folding” (Fig. 1). However, these definitions should be used with care, because there is an evidence, that the unfolded states of proteins may also have biological functions.[116,117]

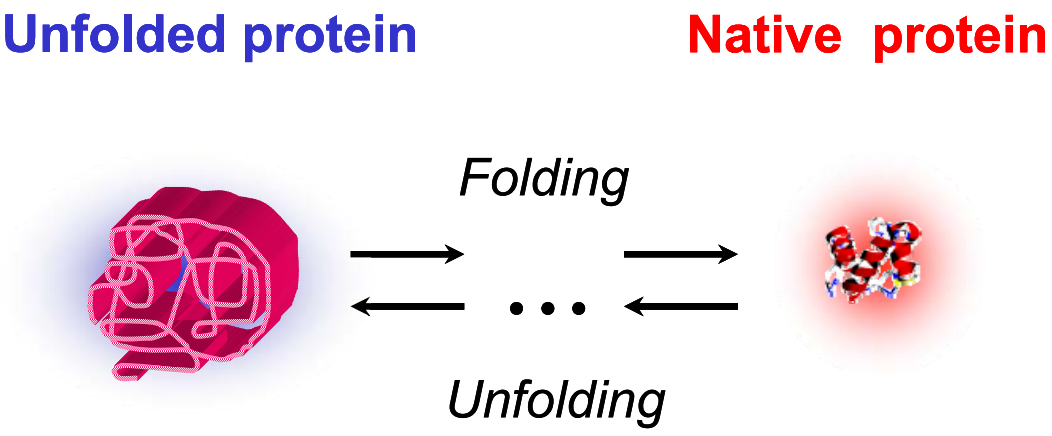

Figure 1. Schematic Diagram of folding and unfolding of a protein.

It should be also noted that the unfolded proteins, until recently, were assumed to exist in a completely disordered “random coil” conformation.[118-123] However, this view has been challenged by Tiffany and Krimm[124,125] as well as by Dukor and Keiderling,[126] who suggested

that the unfolded conformations of peptides and proteins exhibit a local order, which often can be explained in terms of polyproline II (PPII) conformation. There is an accumulating number of recent studies, which also suggest that the unfolded states of proteins,[127-131] long and medium peptides[132-137] and even short peptides[129,138-141] contain a significant fraction of PPII conformation. In Chapters 2 and 6 of this thesis we discuss this issue in more detail.

1.1.3 Elucidation of Protein Folding Reaction Coordinate(s).

Any attempt to understand protein folding mechanism(s) requires the elucidation of the important protein folding reaction coordinate(s). Then, monitoring of the chosen reaction coordinate(s) should provide the understanding of the relationships between the different levels of protein structure organization (see sub-Section 1.1.1 above), and ultimately allow the prediction of the complex 3D-structure of proteins from their primary sequences.

First arguably most important step in understanding the protein folding mechanism is to reveal the relationship between proteins primary sequences and their secondary structure compositions, since protein folding reaction unavoidably involves secondary structure changes. Thus, both the characterization of the most common protein secondary structure motifs as well as the elucidation of secondary structure protein folding reaction coordinates, are crucially needed.

The secondary structure of a polypeptide/protein backbone can be characterized by three dihedral angles: Φ, Ψ and ω (Fig. 2).[1,2] Φ angle is defined as an angle of rotation around N-C_α bond (Φ=0° if C_α-C is trans to N-H); Ψ angle is defined as an angle of rotation around C_α-C bond (Ψ=0° if C_α-N is trans to C=O); ω angle is defined as an angle of rotation around C-N bond (ω=0° if C_α-C is cis to N-C_α).

It should be noted that there is a strong preference of a peptide bond to be trans,[142-145] so the ω angle is almost always ~180°. In actual structures, this angle can vary only up to 10°-15°. Thus, the peptide bonds can often be considered as a rigid plates, which rotate about Φ and Ψ angles (Fig. 2).[1,2]

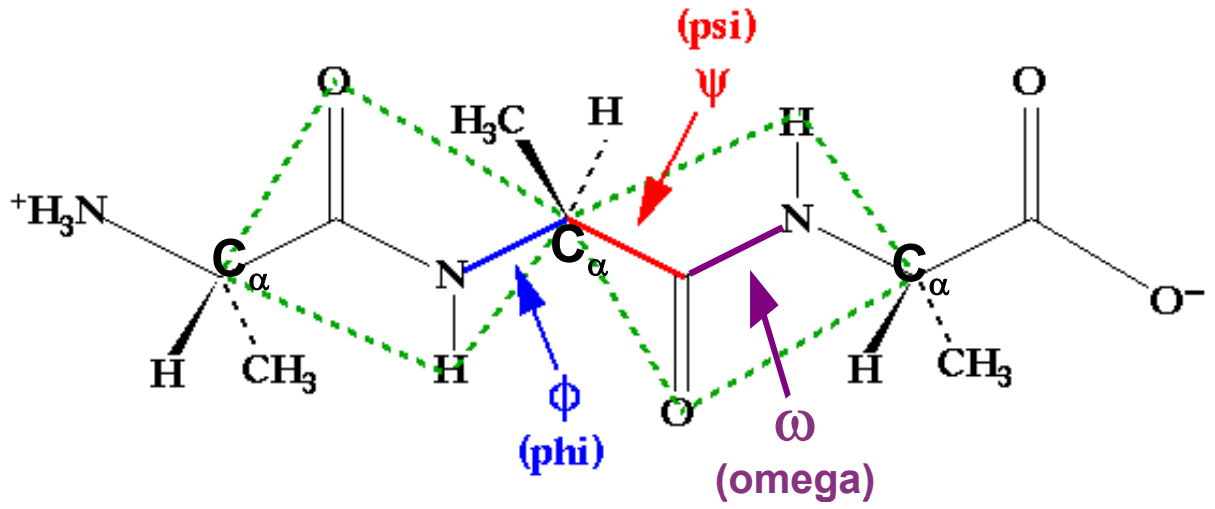

Figure 2. Φ, Ψ and ω angle definitions in alanine tripeptide. Note that ω angle is essentially constant (~180°) for most abundant secondary structures. Thus, the peptide bonds on either side of the central alpha carbon can be treated as rigid plates, which rotate about, Φ and Ψ.[1,2] Obtained from: http://www.cgl.ucsf.edu/home/glasfeld/ tutorial/AAA/AAA.html

Summarizing, almost all secondary structure changes in peptides/proteins can be characterized by the changes in Φ and Ψ angles. Thus, these two angles are the main protein folding reaction coordinates. In the Chapter 5 of this thesis, we show, that Ψ angle changes dominate the overall (Ψ,Φ) secondary structure changes. **Thus, Ψ angle is arguably the most important protein (un)folding reaction coordinate.**

1.1.4 Ramachandran Plot.

An enormous number of all possible conformations of a polypeptide chain can be significantly reduced, if one takes into account the steric constraints. These constraints were first described by Ramachandran and coworkers.[142] The original Ramachandran plot for ala, which shows the sterically allowed Φ and Ψ angles is shown in Fig. 3.

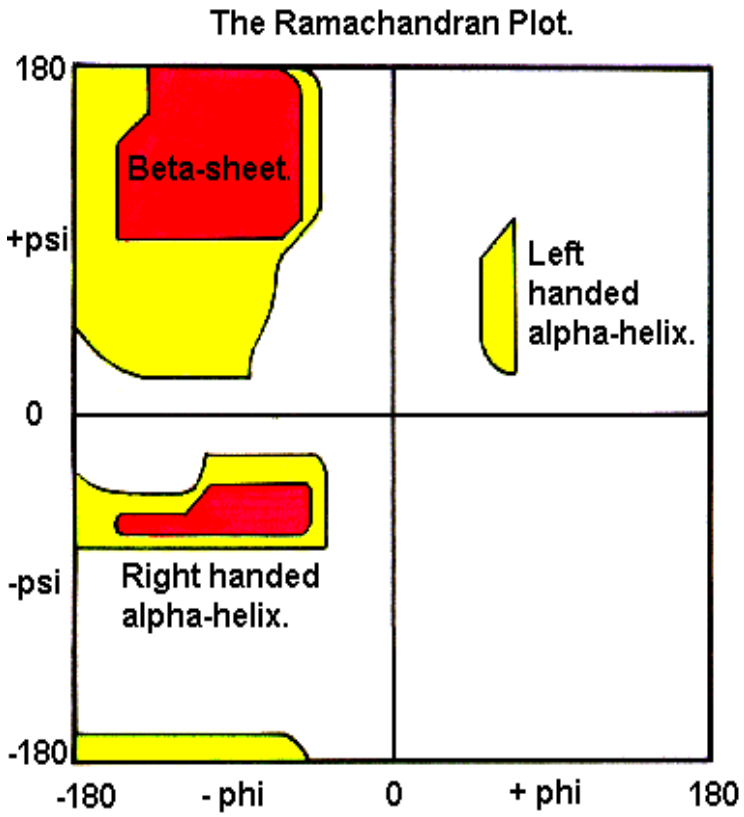

Figure 3. The original Ramachandran plot for alanine.[142] Yellow and red regions show the allowed Ψ and Φ Ramachandran angles. Obtained from: http://www.cryst.bbk.ac.uk/PPS95/course/3_geometry/rama.html.

The original Ramachandran plot for alanine (Fig. 3) have broken an important new ground in understanding of protein folding mechanism(s). However, side chains which differ from that of alanine, may result in different steric constraints for a protein backbone (Fig. 4).

Recently, number of groups[146-148] have updated the Ramachandran plot. Specifically, using protein x-ray structure data banks, they obtained the Ramachandran plots for most of individual amino acid residues; the combined Ramachandran plots for non-Gly residues, for non-Gly and non-Pro residues; as well as the combined Ramachandran plot for all residues (Fig. 4).

Ramachandran plots for most of individual amino acid residues, except for Gly and Pro, are similar to that for Ala (Fig. 4). Gly is unique because its smallest side chain significantly increases the allowed range of Φ angles. In contrast, the existence of the bond from the side chain to the imino nitrogen significantly reduces the allowed range of Φ angles for Pro (Fig. 4).

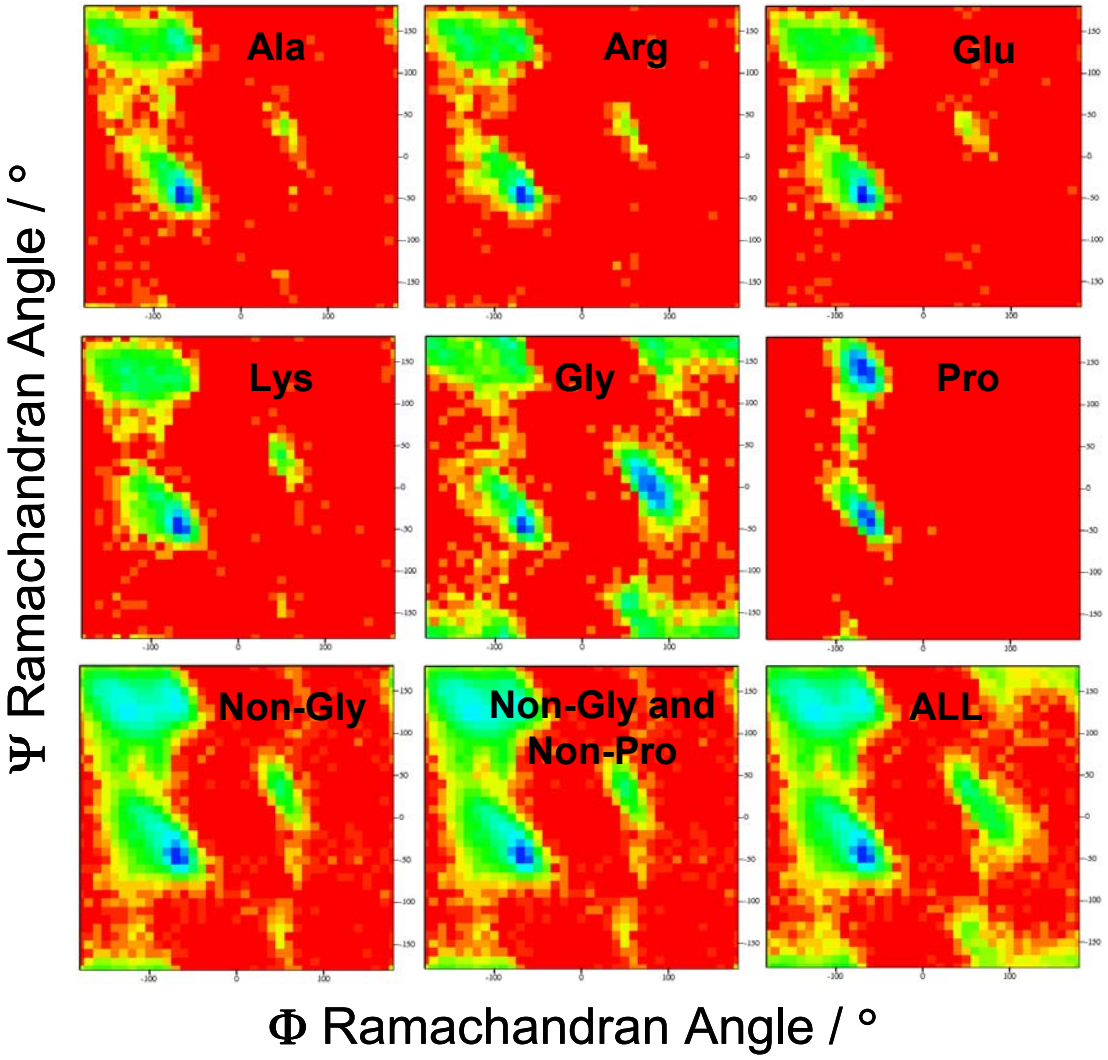

Figure 4. Recent Ramachandran plots for individual amino acid residues (such as Ala, Arg, Glu, Lys, Gly and Pro), as well as that for non-Gly residues, non-Gly and non-Pro residues and all amino acid residues.[146] All these Ramachandran plots were obtained from: http://alpha2.bmc.uu.se/gerard/rama/ramarev.html.

The general conclusion, which can be made from the Ramachandran plots shown in Fig. 4, is that typically much larger range of Ψ angles is allowed compared to that of Φ (except for Gly). It also can be seen that α-helix melting is likely to also involve the much greater change in Ψ angle compared to that of Φ. In the Chapter 5 of the thesis we provide a method, which can be used to qualitatively monitor Ψ Ramachandran angles using UV Resonance Raman (UVRR) spectroscopy. We believe that this quantitative methodology makes the UVRR spectroscopy competitive to the ^{13}C NMR analysis.

1.1.5 Common Secondary Structure Motifs in Proteins

The most abundant types of protein secondary structures are α-helix and β-sheet (Appendix A, Fig. 84). Until recently, various turns are thought to be the third most frequent types of protein secondary structure (Chapter 5, Fig. 56). However, the polyproline II helix (PPII) was also recently found to be common in proteins[127-131] and peptides[129,132-141] (Chapter 5, Fig. 55). There are also a number of less abundant protein secondary structures such as 3_{10}- and π-helices (Chapter 5, Fig. 55). In addition, polypeptides with charged side chains may create unusual secondary structure motifs, such as for example 2.5_1-helix[135] (Chapter 5, Fig. 55). Ψ and Φ Ramachandran angles for the secondary structure motifs, mentioned throughout this thesis are summarized in Tables 1 and 2.

Table 1. Ψ and Φ Ramachandran angles for common protein and peptide secondary structure motifs.

Secondary Structure	Φ Ramachandran angle	Ψ Ramachandran angle
α-helix	–57°	–47°
Anti-parallel β-sheet	–139°	135°
Parallel β-sheet	–119°	113°
PPII helix	–75°	145°
2.5_1-helix	–130°	170°
3_{10}-helix	–60°	–26°
π-helix	–57°	–70°
γ-turn	70°	–60°
Inverse γ-turn	–70°	60°

Table 2. Ψ and Φ Ramachandran angles for i+1 and i+2 residues in various β-turns.

β-turn	Φ (i+1)	Ψ (i+1)	Φ (i+2)	Ψ (i+2)
Type I	–60°	–30°	–90°	0°
Type I'	60°	30°	90°	0°
Type II	–60°	120°	80°	0°
Type II'	60°	–120°	–80°	0°
Type III	–60°	–30°	–60°	–30°
Type III'	60°	30°	60°	30°
Type V	–80°	80°	80°	–80°
Type V'	80°	–80°	–80°	80°
Type VIII	–60°	–30°	–120°	120°

The α-, 3_{10}-, π-helices as well as β-sheets are mainly stabilized by peptide bond-to-peptide bond hydrogen bonding (PB-PB HB).[1,2] Most of the turn motifs are also stabilized mainly by PB-PB HB. Primary sequence may also favor a specific turn formation, since some amino acids, for example Gly and Pro, have a strong preference to occur only at a certain position in the specific turn(s). In contrast, PPII conformation is mainly stabilized by peptide bond-water (PB-water) interactions.[149-153] Alternatively, Hinderaker and Raines[154] proposed that the PPII stabilization is substantially aided by electronic effects such as hyperconjugation. The unusual secondary structure motifs, which occur in polypeptides with relatively long and ionized side chains (such as 2.5_1-helix conformation in poly-L-lysine and poly-L-glutamic acid), are stabilized by the electrostatic repulsion between the side chain charges.[135]

1.1.6 Classical View of α-Helix Melting and Formation

The α-helix is far the most abundant secondary structure motif in native proteins. Specifically, the analysis of modern protein databases indicates that ~32-38% of all amino-acid residues in globular proteins occur in α-helical conformation.[1,155] Thus, the understanding of of α-helix melting (formation) mechanism(s) is a key task in the peptide and protein conformational dynamics, because this is the most common process in peptide and protein conformational search between folded and unfolded structures.

The α-helix melting process has been extensively studied for over 50 years. The classical view, which describes α-helix melting, was proposed by Zimm and Bragg[118], Lifson and Roig[119] and Polland and Sheraga[122,123]. This theory envisiones the α-helix melting as a transition between an ordered α-helix structure and a disordered random coil structure with uncorrelated, but allowed Ψ and Φ Ramachandran angles. Such a melting involves the breakage of intra-α-helical hydrogen bonds.

This theory, which appears to adequately describe the thermodynamics of α-helix↔random coil transition in most of cases (however, see Section 1.3. below), is based on the following assumptions. It is assumed that each peptide bond unit exists either in **"helix"(h)** or **"coil" (c)** state. Residue is considered α-helical (in "h" state) if all its dihedral angles correspond to α-helix. If one or more of the unit dihedral angles are different from those of the α-helix then this resudue is considered to be in a coil state. It is also assumed that free energy of successive sequences of h's and c's are independent, that is free energy of a sequence depends only on its length and does not depend on its position in the chain or on the parameters (length etc.) of the neighboring sequences. In addition, it is also assumed that there exist two types of helical residues: involved in hydrogen bonding, and not involved in hydrogen bonding.

Under the above assumptions, it is possible to assign the statistical weights for each conformational state of a peptide bond unit (Table 3). This procedure is described in detail in the Polland and Sheraga's book.[122] Briefly, the statistical weights of coil residue, helix residue participating in hydrogen bonding, and helix residue not participating in hydrogen bonding residue are **u**, **w**, and **v**. The assignments of statistical weights are based on the following physical picture: the stability of α-helix depends mainly on the formation of hydrogen bonds,

therefore **$w \sim \exp(-E_{HB}/RT)$**; while the main contribution to free energy of random coil is the entropy of internal rotations (conformational entropy), so **$u \sim \exp(S/R) = \Omega$**, where **Ω** is the average number of isoenergetic positions of internal rotations per residue. When ratio **w/u=s** is greater, less than, or equal to unity, than α-helix conformation is, respectively, favored, unfavored, and equal probability with respect to coil. The **s** parameter, thus, is directly related to the α-helix annealing and is also known as a propagation parameter.

In addition, this classical theory proposes that there exist a nucleation free energy barrier for the formation of first α-helical turn. This barrier is associated with an entropic cost due to compulsory restriction of four consecutive peptide bonds at α-helical Ψ and Φ angles prior to enthalpic compensation by the intra-α-helix hydrogen bonds. This barrier is reflected in this theory by small nucleation parameter, **$\sigma=(v/u)^2$** (see Table 3). It is estimated by Zimm and Bragg[118] that **σ** is equal or less than $\sim 10^{-2}$. This estimate is consistent with later experimental studies of α-helix melting,[156-162] which usually report the σ-values of $\sim 10^{-3} - 10^{-4}$. However, we suggest in Chapter 8 of this thesis (see also ref[163]), that the actual pure α-helix melting nucleation parameter in a 21-residue ala-rich peptide, AP is much less ($\leq \sim 10^{-5}$); i.e. that the pure α-helix melting shows much higher cooperativity than it is typically assumed. The origin of this inconsistency is the inability of earlier researches to resolve the 3_{10}-helix and π-bulge contributions to so-called "α-helix" melting, which resulted in less cooperative net melting curve than that for pure α-helix melting.[163]

Using the Table 3 assignments for statistical weights, it is possible to calculate the partition function for any system of interest in terms of three parameters: **σ** (nucleation parameter)**, s** (propagation parameter) and **N** (peptide chain length). To reduce the number of possible states while performing the summation, Poland and Sheraga[122] proposed three models applicable for different chain lengths (see below). Their proposition is based on the following arguments. On the one hand, if an α-helical segment exists in a polypeptide chain; then it tends to elongate to maximize the negative free energy per peptide bond in the α-helical segment. On the other hand, the α-helical segment tends to shorten to maximize the configurational entropy for the rest of the chain. This competition between the free energy benefit per residue and the configurational entropy of the peptide molecule largely determines the physics of α-helix melting, dictating different scenaria, which primarily depend on the chain length.

Table 3. Classical Notations for Statistical Weights of Individual Peptide Bond Units in a Peptide Chain.[122]

State	Statistical Weight	
	Lifson and Roig Notation	Zimm and Bragg Notation
Coil	u	1=u/u
Helix involved in Hydrogen Bonding	w	s=w/u
Helix not involved in Hydrogen Bonding	v	$\sigma^{1/2}$=v/u

Finally, Polland and Sheraga[122] concluded, that for very short chains the α-helix melting is likely to follow so-called "all-or-none" scenario (Fig. 5A and sub-Section 1.2.1), because the shorter the chain the less combinatorial entropy is potentially available. In case of somewhat longer chains, only one α-helical sequence of any size is likely to show up in such a chain (Fig. 5B and sub-Section 1.2.2). In contrast, a number of α-helical segments of moderate lengths are likely to occur in long chains. We do not describe the latter scenario in detail, because it is not applicable to the experimental data reported in this thesis.

1.1.6.1 "All-Or-None" Model.

The simplest "all-or-none" (AON) model assumes that a polypeptide chain can exist only in two conformations: either all peptide bond units occur in α-helical state; or all peptide bond units occur in coil state (Fig. 5A). In this case, the AON partition function, $\mathbf{Z_{AON}(N)}$, and AON fraction of hydrogen bonds, $\mathbf{\Theta_{AON}(N)}$, can be simply found as[122]:

$$\mathbf{Z_{AON}(N) = v^2 w^{N-2} + u^N = u^N \cdot [\sigma \cdot s^{N-2} + 1]} \qquad \mathbf{(1A)}$$

$$\mathbf{\Theta_{AON}(N) = [1/(N-2)] \cdot \partial \ln Z_{AON}(N)/\partial \ln s = v^2 w^{N-2}/(v^2 w^{N-2} + u^N) = \sigma \cdot s^{N-2}/(\sigma \cdot s^{N-2} + 1)} \qquad \mathbf{(1B)}$$

Fig. 6 below, which compares the α-helix melting curves obtained using AON and Zipper models with the equal propagation and nucleation parameters, agrees well with a proposition of Sheraga and Polland that AON model is applicable only for very short chains.

Specifically, if we set the enthalpy of hydrogen bonding and entropy to −1.1 kcal/mol·peptide bond (kcal/mol·PB), and 2.8 cal/mol·K·PB, respectively (similar values are typically reported for α-helix-forming peptides[152-158]); then only for very short chains of N<~10 there would be a good agreement between AON and more realistic Zipper models (see text below for detail).

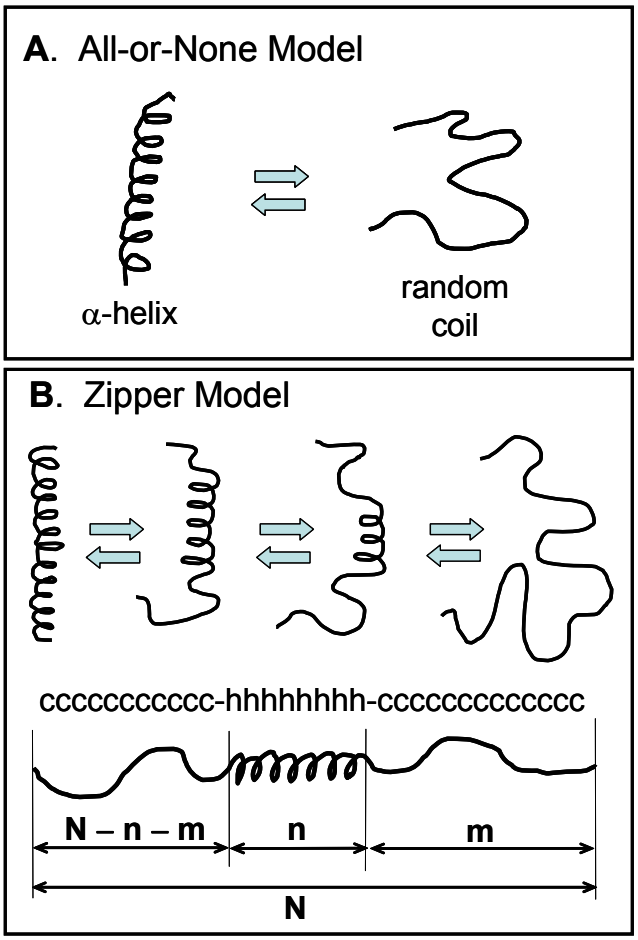

Figure 5. Typical models, which serve as a basis for classical description of α-helix melting in very short and/or moderately short α-helix-forming peptides[122]: **A**. All-or-none model; **B**. Zipper model.

1.1.6.2 Zipper Model

To study α-helix↔random coil transition in case of moderately long peptide chains (~10 < N < ~40), one should use more realistic zipper model (Fig. 5B).[122] This model generally assumes that only one α-helical segment of any length **n** may occur in the polypeptide chain of length **N**. In addition, this model proposes that the unwinding of α-helical peptide bonds during melting starts

from the ends of the α-helical segments and then propagates toward the middle. This proposition is supported by the argument that it is necessary to break *two* intra-α-helical hydrogen bonds to enable the "uncorrelated" rotation of a peptide bond located at the middle of an α-helical segment around its Ψ and Φ Ramachadran angles; whereas it is necessary to break only *one* hydrogen bond to enable the rotation of a peptide bond at the end of the α-helical segment to enable such a rotation. In this case, fraction of hydrogen bonds Θ_Z, parametrized in terms of nucleation parameter (σ), propagation parameter (s) and chain length (N), is given by[122]:

$$\Theta(N) = \frac{1}{N-2} \cdot \frac{\partial \ln Z(N)}{\partial \ln s} = \frac{\frac{\sigma \cdot s}{(s-1)^3} \cdot \{(N-2) \cdot s^N - N \cdot s^{N-1} + N \cdot s - (N-2)\}}{(N-2) \cdot [1 + \frac{\sigma \cdot s}{(s-1)^2} \cdot \{s^{N-1} - (N-1)s + (N-2)\}]} \quad \textbf{(2)}$$

Fig. 6 below, which compares the α-helix melting curves obtained using AON and Zipper models with the equal propagation and nucleation parameters, shows that for very short chains (N ≤ ~10) AON and Zipper model melting curves are very similar to each other. In contrast, AON and Zipper model melting curves differ more and more different as the chain length increases. Thus, for very short chains, one can use simple AON model (Eq. 1B) to accurately describe α-helix melting, whereas it is necessary to use more complicated Zipper model for longer chains.

The Eqs. 1B and 2 above can be used to fit the experimentally obtained helical melting curves (see Chapter 8), so the nucleation and propagation parameters can be found using the least-square criteria.

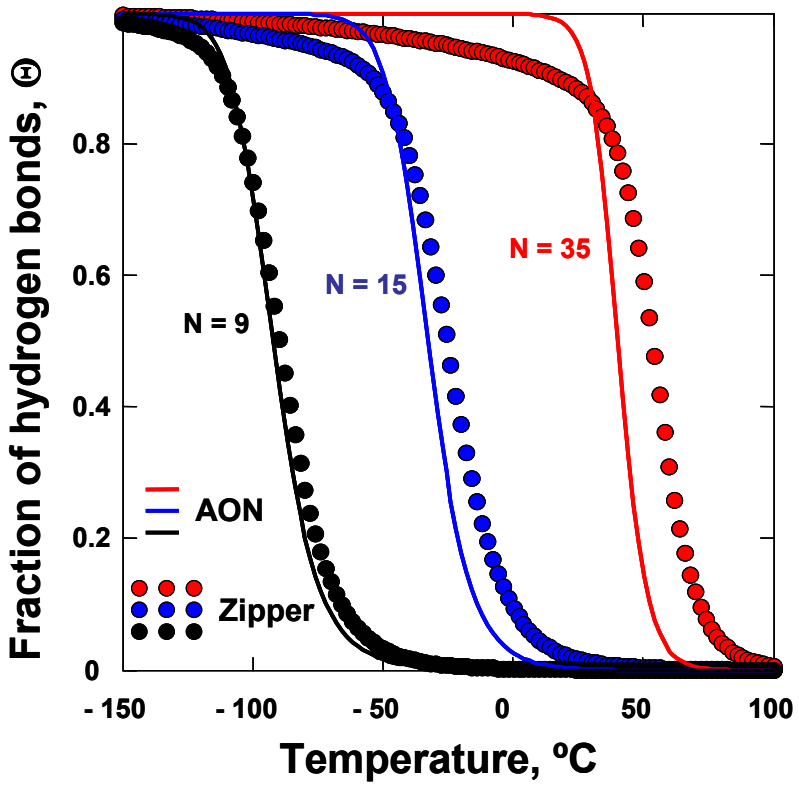

Figure 6. Comparison between the α-helix melting curves for different peptide chain lengths, N, obtained using the "All-Or-None" (AON, Eq. 1B) and Zipper (Eq. 2) models: N=9, N=15, and N=35. Nucleation parameter, enthalpy of intra-α-helical hydrogen bonding and conformational entropy are set to 10^{-5}, –1.1kcal/mol·PB, and 2.8 cal/mol·K·PB, respectively.

1.1.6.3 Physical Meaning of Propagation and Nucleation Parameters

The physical meaning of the propagation parameter $s=\exp(-E_{HB}/RT)/\exp(\Delta S/R)$ can be illustrated by Figs. 7A and 7B. For example, if we set the nucleation parameter (σ) and conformational entropy (ΔS) to 10^{-5} and 2.8 cal/mol·K·PB, respectively, then the increase in negative value hydrogen bonding enthalpy (E_{HB}) would increase the value of propagation parameter and expectedly result in stabilization of α-helix conformation. In this case, the melting temperature (T_m) of the transition shifts to higher temperatures (Fig. 7A).

In contrast, the increase of conformational entropy ΔS (at fixed $\sigma=10^{-5}$ and $E_{HB}=-1.1$ kcal/mol·PB), decreases the propagation parameter and destabilizes the α-helix conformation. In the latter case, T_m shifts to lower temperatures (Fig. 7B).

It should be also noted that the changes in the enthalpy of hydrogen bonding and/or the moderate changes in conformational entropy does not change the cooperativity of the transition, since steepness of the melting curves remains essentially the same (Figs. 7A and 7B).

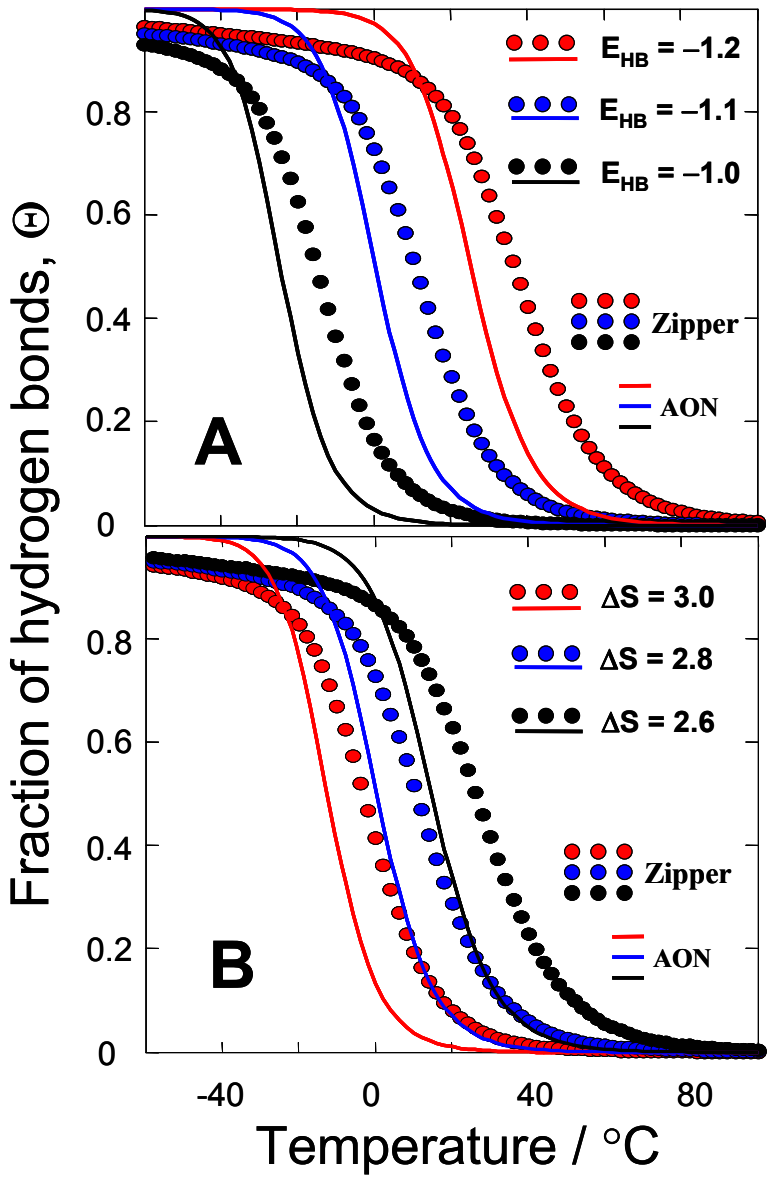

Figure 7. Zipper and AON α-helix melting curves, generated for a 21-residue peptide at fixed $\sigma=10^{-5}$, by varying either the enthalpy of hydrogen bonding (E_{HB}) or configurational entropy (ΔS): A) ΔS is fixed to 2.8 cal/mol·K·PB, whereas the E_{HB} varies from −1.2 to −1.0 kcal/mol·PB; B) E_{HB} is fixed to −1.1 kcal/mol·PB, whereas ΔS varies from 2.6 to 3.0 cal/mol·K·PB. It can be concluded that the propagation parameter, $s=\exp(-E_{HB}/RT)/\exp(\Delta S/R)$, is directly related to the α-helix stability (see text for detail).

Physical meaning of nucleation parameter, σ, can be understood from Fig. 8. Specifically, we generated three AON and three Zipper α-helix melting curves at σ-values of 10^{-3}, 10^{-5} and 10^{-7}. Simultaneously, we kept both E_{HB}=–1.1 kcal/mol·PB and ΔS=2.8 cal/mol·K·PB fixed. It is clear from Fig. 8 that σ is a measure of cooperativity of α-helix↔random coil transition, since the change in σ results in change of the melting curve steepness.

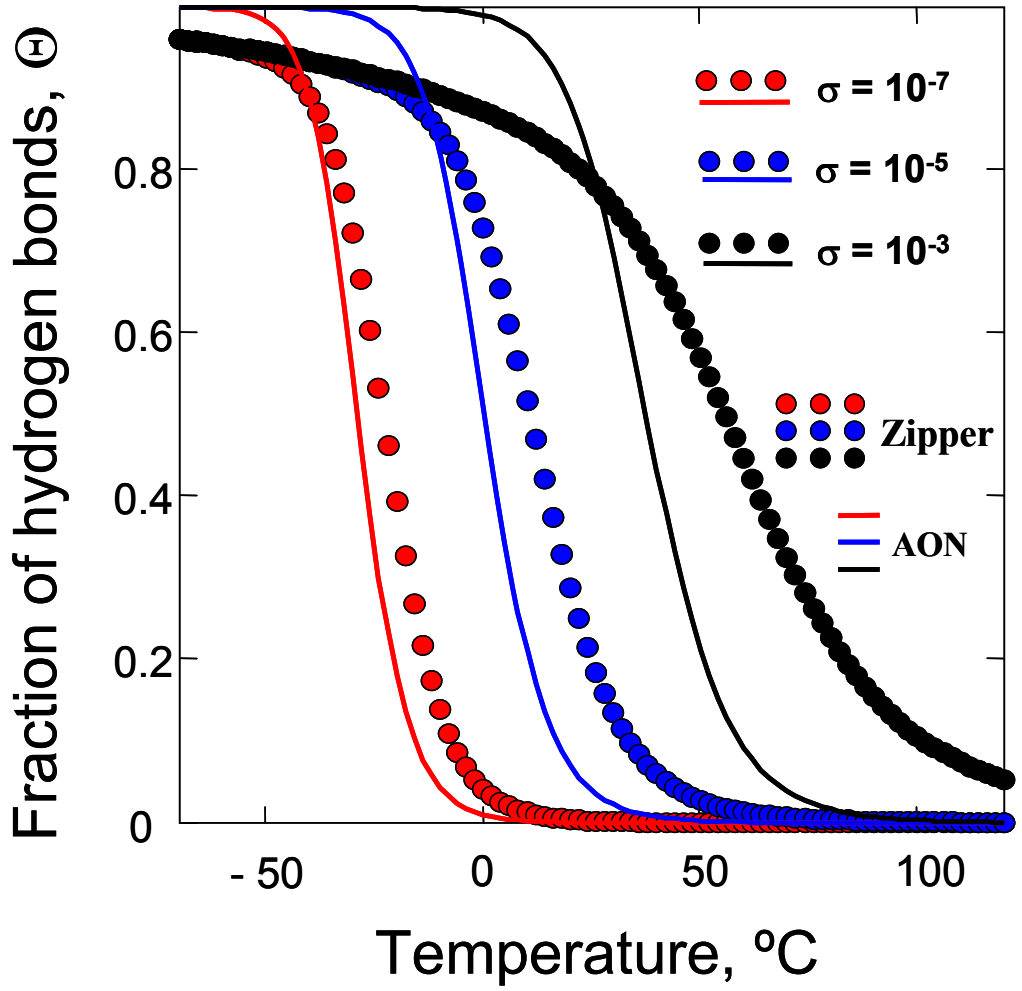

Figure 8. Zipper and AON α-helix melting curves generated for a 21-residue peptide at different nucleation parameters, σ, of 10^{-3}, 10^{-5} and 10^{-7}. Both the enthalpy of hydrogen bonding (E_{HB}) and entropy (ΔS) kept fixed at –1.1 kcal/mol·PB and 2.8 cal/mol·K·PB, respectively. It can be concluded that nucleation parameter, σ, is a measure of the cooperativity of the α-helix↔random coil transition (related to steepness of the melting curve).

1.1.7 Classical View of α-Helix Melting and Formation Must Be Revisited

The classical theories of α-helix melting (described above) have long and distinguished histories. They provided the basis for numerous recent experimental[38,55,156-158,164-203] and theoretical[9,40,77,81,137,159,204-266] works, which study the α-helix↔random coil transition in short α-helix-forming peptides. However, there is an accumulating number of recent evidences that this classical view must be carefully revisited and updated.

First challenge comes from the recent observations that simple α-helix-forming peptides often melt to a PPII conformation.[127,134,137,152,267-270] In fact, there is no evidence in favor of melting to, or even the existence of random coil peptides in solution. Even single ala peptide bonds in aqueous solutions, which are intrinsically expected to be disordered, were recently reported to show PPII-like spectra.[138] Thus, the fact that α-helix melting (formation) is rather a transition between two ordered conformations than that between ordered and completely disordered ones, must be incorporated into the new α-helix melting theories.

In addition, there exist steric restrictions, which prevent direct simple connection between the α-helical and PPII/β-strand segments in a peptide chain.[77] Thus, α-helix melting (formation) must involve at least one additional interfacial conformational state. Various turn conformations are the likely candidates for such an interfacial state, because their Ψ and Φ Ramachandran angles belong to the region of Ramachandran plot allowed for this interfacial state.

Further, it was also proposed that the additional intermediate states (presumably β-turns and 3_{10}-helices), which are involved in α-helix melting/formation, facilitate the α-helix nucleation process.[271-273] Thus, classical α-helix melting theories may have overestimated the entropic cost associated with nucleation of a first helical turn. Further, the physical meaning of classical nucleation parameter, σ, becomes no longer straightforward.

Finally, there is also evidence that the α-helical ensembles of short α-helix forming peptides rich in alanine, in fact, are not homogenious and contain the contributions not only from pure α-helices, but also from 3_{10}-helices[163,206,222,224,240,273-285] and π-bulges/helices[163,207,251,281,286-288] (see also Chapters 8 and 9). These π-bulge and 3_{10}-helical conformations show a decreased melting temperatures (T_m) compared to that of pure α-helix,[163] which results from their less

optimized intra-peptide hydrogen bonding compared to that of perfect α-helix. Whereas, the low temperature stability of these more solvent exposed π-bulges[289] and 3_{10}-helices (type III turns[272]) derives from the increase in the peptide bond-water hydrogen bonding strengths as the temperature decreases.[134,135,164,290]

Taking into account these complications, it is somewhat surprising that the existing basic theories often adequately predict the α-helix melting behavior. In most cases, the melting relaxation kinetics appears to be single-exponential within the experimental error.[156,157,164,165,169,171-174,176,181] However, there are also clear departures from simple classical theories reported by Werner et al.[169], Huang et al.[187] and Ramajo et al.[180] time-resolved IR isotopically labeled (C=O) spectroscopic studies, which observe the position-dependence of α-helix melting rates in ~20-residue long ala-rich α-helical peptides. In addition, Huang et al.[187-189], Wang et al.[190] and Bredenbeck et al.[177] found the evidence for non-exponential relaxation kinetics in their ala-rich peptides. Some of recently proposed theoretical models[9,188,291] may help to rationalize the complicated kinetic behavior of α-helix melting in proteins and peptides. However, more experimental data is needed to test the validity of these theories.

In Chapters 8 and 9 of this thesis, we also observe the unusual non-classical α-helix melting behaviors of two 21-residue mainly alanine peptides, AP and AdP, which cannot be understood from classical α-helix melting models. We succesfully explain this behavior in terms of different relative contributions of pure α-helix, π-bulge and 3_{10}-helix conformations melting into the so-called "net α-helix" melting. Our novel mathematical model succesfully explains not only the Chapter 8 and 9 results, but also the anti-Arrhenius AP kinetics of Lednev et al.[164] as well as the non-exponential kinetic behaviors of similar peptides reported earlier by Huang et al.[189] and Bredenbeck et al.[177]

1.1.8 Experimental Methods for Studying Protein Folding

1.1.8.1 Methods to Study Protein Structure (Structural Probes)

Scientists use many experimental techniques to elucidate the protein structure (Fig. 9). A brief description of the most important ones is given below.

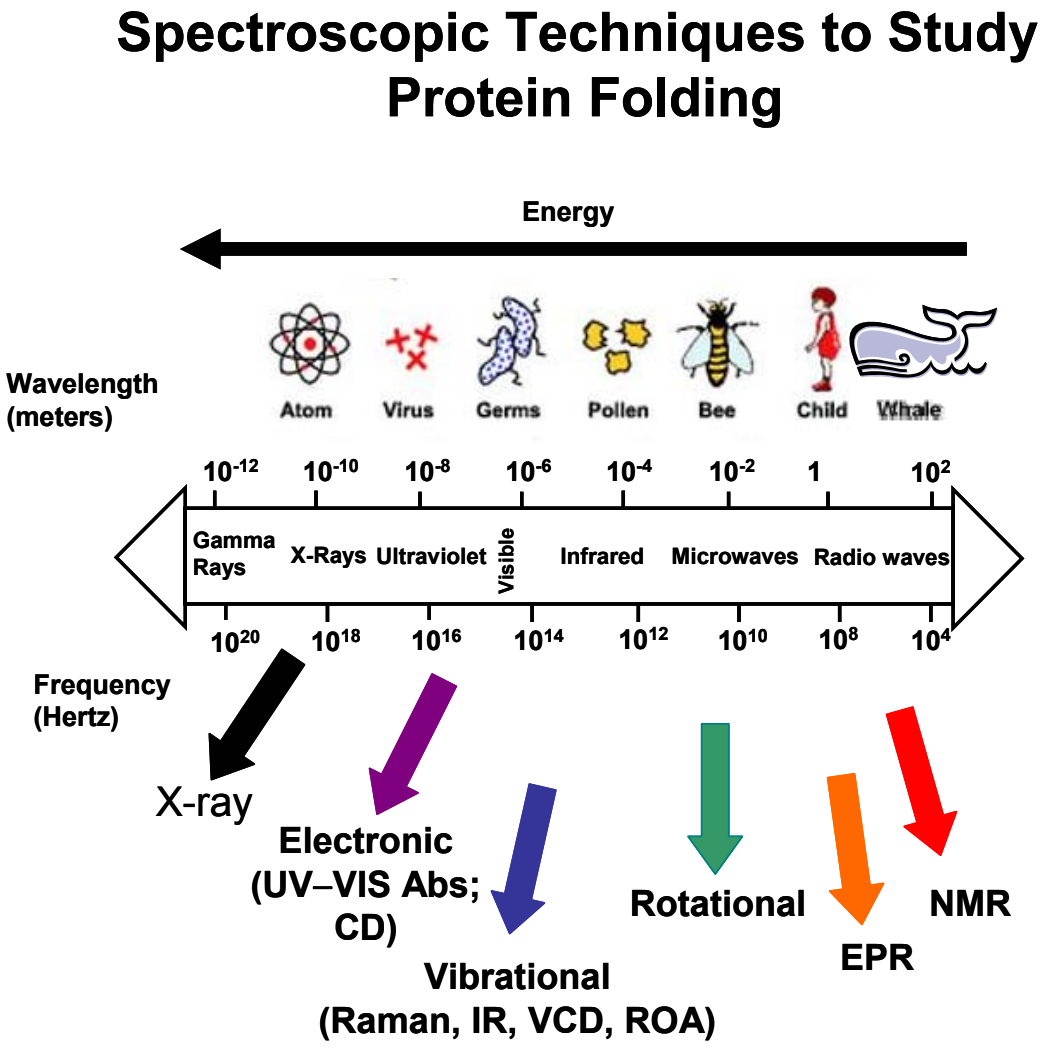

Figure 9. Spectroscopic techniques to study protein folding. Adapted from: http://scholar.hw.ac.uk/site/chemistry /topic3.asp.

X-ray. X-ray diffraction is a gold standard for the solid state studies.[292-295] In the most favorable cases (for small peptides, for example), x-ray structures can provide the equilibrium

bond distances up to 0.1 Å resolution. However, for large proteins, x-ray structures show ~Å resolution.

NM*R*. NMR (and especially 2D-NMR) techniques[296-305] are certainly a gold standard for protein solution studies at high concentrations if any dynamical processes of interest are not much faster than miliseconds. 2D-NMR, in favorable cases, can provide higher resolution than x-ray.

SAXS. Small-angle X-ray scattering (SAXS) using synchrotron source can be combined with a stopped- or continuous-flow device to directly monitor the overall size and shape of proteins during folding.[306-308] These difficult experiments, which typically consume large quantities of protein, can allow one to explore folding events in the time window from ~1 ms to a few seconds with time resolution of ~100 μs.

In contrast to NMR and X-ray techniques, optical spectroscopic methods monitors the light absorption, emission, or scattering, and allow the studies of proteins at low concentration as well as fast dynamic processes down to femtoseconds. These techniques include the ultraviolet (UV), visible (VIS) and infrared (IR) absorption; circular dichroism (CD); vibrational circular dichroism (VCD); fluorescence; visible and near-infrared Raman scattering (normal Raman); Raman optical activity (ROA), and UV resonance Raman (UVRR) scattering techniques. The brief description of some of these techniques is given below.

Absorption. Absorption techniques are usually used for submillisecond fast protein folding studies. Signals from either amide chromophore in IR,[169,309-311] or from some prosthetic groups in VIS regions[312-314] can be measured. IR absorption measurements directly probe the polypeptide backbone secondary structure, however, only the amide I region is readily available for quantitative studies in D_2O due to severe overlap of this band with the HOH bending band of water.[315]

Circular dichroism (CD). Far-UV CD spectra probe the secondary structure of the polypeptide backbone, since the $n \rightarrow \pi^*$, $\pi \rightarrow \pi^*$ electronic transitions of the amide group contribute to CD signal at 180-250 nm. Far-UV CD is widely used to quantitatively analyze protein secondary structure.[316-319] Near-UV CD can describe some tertiary structure changes during protein folding.[87,320,321] The signal in this region (260-290 nm) originates from the aromatic amino-acid side chains. Generally, standard CD spectropolarimeters allow to work in

millisecond timescales. Although, fancy laser-based nanosecond and even picosecond time-resolved CD techniques were also reported.[322,323]

Fluorescence. Fluorescence can be used to probe global kinetics of folding, solvent exposure of aromatic chromophores, motional anisotropy and the formation of specific tertiary contacts.[324-328] Intrinsic fluorescence of proteins without prosthetic groups derives from the aromatic residues, mainly tryptophan (Trp). Trp fluorescence can be excited with ~290 nm radiation; the emission maximum shifts from ~350 to ~330 nm upon burial of the Trp within a protein's hydrophobic core. Quenchers such as acrylamide can be used to probe solvent accessibility in fast-folding experiments. Although the fluorescence spectrum lifetime and quantum yield do not simply report on protein structure, fluorescence measurements can provide useful complementary information on formation of protein tertiary contacts during the folding.

UV Resonance Raman spectroscopy. UV Resonance Raman (UVRR) spectroscopy with ~200 nm excitation has been shown to be a powerful tool in protein conformational studies, since the frequencies and intensities of amide vibrations (Am I, II, III) as well as of the C_α-H bending vibration are critically depend on protein secondary structure.[135,164,329-337] It also can be used to monitor changes in local environment of prosthetic groups and aromatic amino-acid residues.[338-340] Quantitative methods for the analysis of a protein/peptide conformation by this technique has been recently developed.[164,332,336,337] Further, recent advances in UVRR spectroscopy allow to directly monitor the Ψ Ramachandran angle[134,135,163,341] (which is one of the most important protein folding reaction coordinates) as well as to obtain the information on protein energy landscape features.[135,163] (For more detail see Section 1.2. below).

1.1.8.2 Typical Methods to Initiate (Un)Folding Reaction during the Kinetic Studies.

To study protein (un)folding it is often necessary to carry out a relaxation experiment. First, it is needed to initiate the (un)folding reaction. It could be done, for example, by a fast change in the protein environment such as pH, temperature, solvent composition, etc. After that, the protein starts its relaxation towards a new thermodynamic equilibrium, and it is necessary to monitor in time the conformational changes, which occur in studied protein, using spectroscopic "structural probe" techniques. If relaxation leads the sample to the formation of higher content of its folded conformation, then we deal with refolding kinetic experiment. If the opposite is true, then we deal with the unfolding kinetic experiment.

Typical methods to initiate (un)folding reactions are:

Fast mixing techniques, such as **stopped-flow**, **continuous-flow** and **quenched-flow** techniques. These methods allow us to change rapidly the pH, denaturant concentration, temperature, etc. by a rapid mixing of two solutions. The time resolution of stopped flow mixers is typically a few milliseconds.[342,343] As for continuous-flow method, it has better submillisecond resolution time range.[344] However, the disadvantage of the latter method is that it requires relatively large volumes of the sample.

Pressure jump technique. Pressure is also one of the thermodynamic parameters which could shift a conformational equilibrium in the system. Time ranges between tens of microseconds to tens of seconds are available in this method.[345]

Temperature jump (T-jump) technique. Protein native conformations are often stable over only limited range of temperatures. Unfolding of proteins, in favorable cases, can be observed at both high and low temperatures. Thus, the temperature jump technique (T-jump) is very attractive for protein folding studies.[156,164,169,310,311,346,347] Especially, it is attractive for refolding studies of cold denaturing samples, because it is possible to reach the final native-like conditions in the absence of any denaturant. By resistive heating methods it is possible to obtain microsecond resolution times. As for recently developed laser T-jump methods they are able to easily access time-range from nanosecond to seconds.

Photochemical triggering and electron injection techniques. These techniques induce the folding process photochemically.[348-350] They can be applied to proteins with heme or other prosthetic/binding groups. Either ligand unbinding or electron transfer to/from a prosthetic group in response to a laser pulse is monitored and related to protein folding events in nanosecond-to-millisecond time range.

1.2 UV RESONANCE RAMAN (UVRR) SPECTROSCOPY

In this subsection, we explain the basic principles of UVRR spectroscopy and briefly describe the UVRR instrumentation. We also show the examples of typical UVRR spectra of proteins at different exciation wavelengths with brief explanations. In addition, we briefly describe normal mode compositions and conformational sensitivity of ~200 nm excitation UVRR bands of a polypeptide backbone, which is necessary to understand work described in this thesis. Finally, we summarize those features of UVRR spectroscopy, which make this technique especially attractive for protein folding studies.

1.2.1 Background

Raman spectroscopy is a very important method for investigation of vibrational and rotational dynamics of molecules. It is based on inelastic scattering of light from molecules, when the scattered light has different frequencies relative to incident light. Raman frequency shifts corresponds to the difference between vibrational and/or rotational energy levels of molecules. This effect was first observed by Raman in 1928 in liquids,[351-353] and by Landsberg and Mandelstam in crystals.[354,355] Raman effect can be partially understood from the classical point of view.[356] However, the quantum mechanical approach provides a more complete and accurate picture.[357-360]

Since Raman scattering discovery, many applications of this effect for studying structure and molecular interactions has been developed. Raman spectroscopy gives a lot of complementary information in addition to conventional IR spectroscopy, since very often vibrational bands, which are active in Raman spectra, are not active in IR. This comes from different selection rules: a change in dipole moment is needed for a mode to be IR active, while the change in polarizability is required for the mode to be Raman active. For example, the vibrational bands corresponding to totally symmetric vibrations of non-polar molecules are not

active in IR, because there is no change in total dipole moment. However, since there is a change in polarizability, these bands appear in Raman spectra.

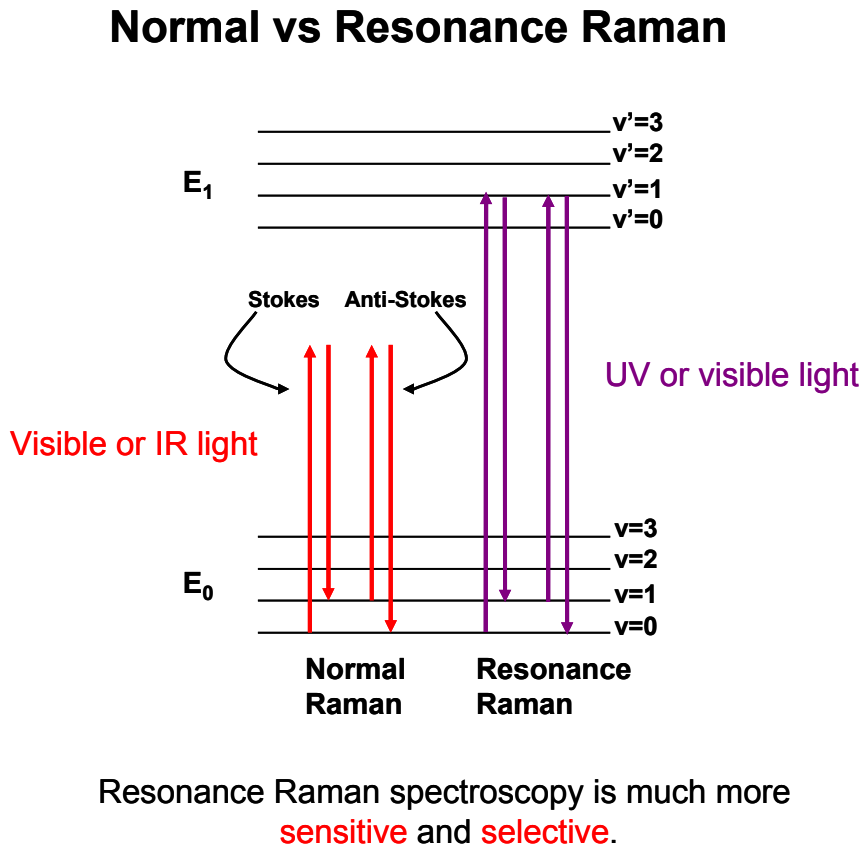

Figure 10. Schematic diagram for "Normal" and "Resonance" Raman scattering

1.2.2 Resonance Raman Can Selectively Monitor the Vibrations of Chosen Chromophore Group(s)

If Raman scattering is stimulated by light with a frequency which is far enough from any absorption band of the molecule (Fig. 10), then all electrons could be considered as equally perturbed by the external electric field. In this case Raman intensity of each species will contribute to Raman spectrum in proportion to their concentration. In contrast, if Raman excitation is within an absorption band (Fig. 10), then all the electrons involved in this electronic transition will start to oscillate with their natural frequencies, causing much larger (up to ~6 orders of magnitude) Raman intensity. Therefore, resonance Raman spectroscopy is highly

selective, and provides a very attractive opportunity to probe different chromophores in the molecule by changing the excitation wavelength.

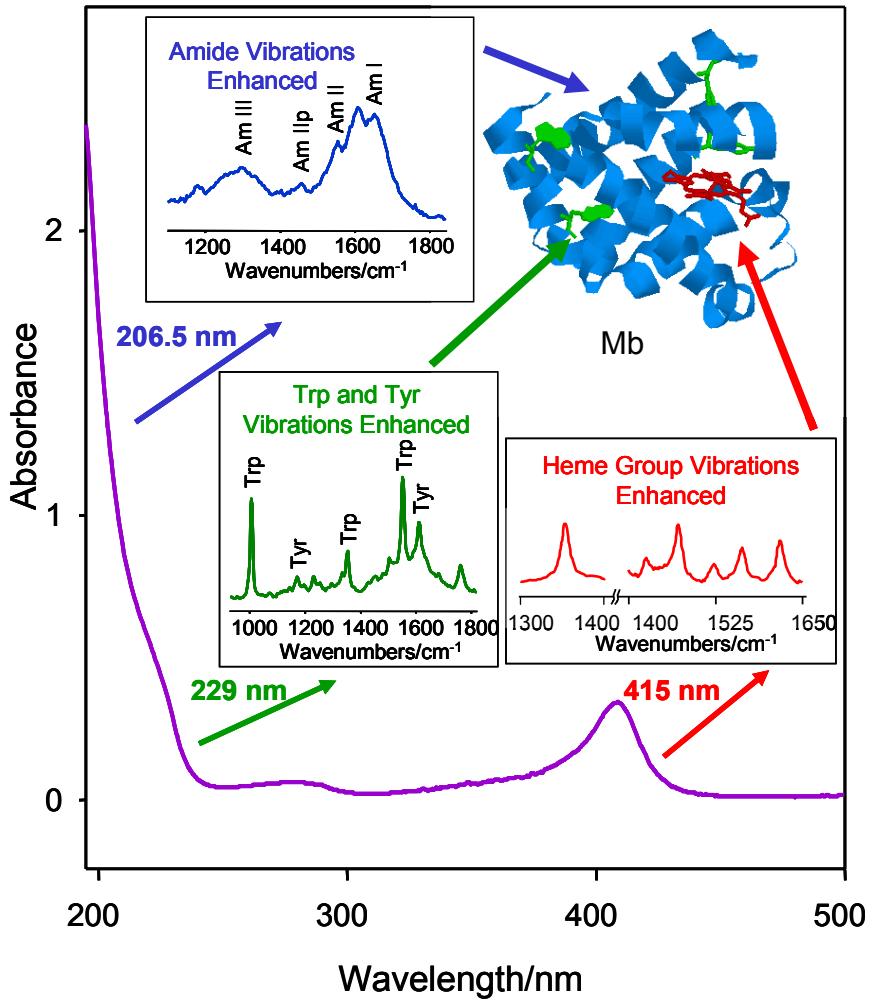

Figure 11. Absorption and resonance Raman spectra of myoglobin (Mb). Resonance excitation allows to selectively enhance the vibrations of different chromophore groups. This figure is adapted from Boyden[361].

For example, one can selectively enhance the amide bond vibrations of a protein by choosing the ~200 nm resonance excitation[361] (Fig. 11). In contrast, ~230 nm resonance excitation enhances the vibrations of aromatic amino acid side chains in the protein and allows the selective monitoring of the aromatic amino acid environment (Fig. 11). If a protein contains the heme-group, ~415 nm excitation would allow to selectively study the heme-group vibrations (Fig. 11). This selectivity dramatically simplifies the spectral analysis compared to normal

Raman, since there is no interference from the vibrational bands, which are not resonantly enhanced.

1.2.3 Normal Mode Composition of ~200 nm Excitation UVRR Amide Bands

It was mentioned above (Fig. 11), that the ~200 nm resonance excitation within the $\pi \rightarrow \pi^*$ transition[336,362-364] of a peptide bond selectively enhances the vibrations of a polypeptide backbone. Typical ~200 nm excitation UVRR spectra of a 21-residue alanine-rich peptide, AP at different temperatures are shown in Fig. 12B. The AP UVRR spectrum exhibits the Amide I band (involves mainly C=O stretch (C=O s), Fig. 12A) which typically shows up between 1620–1670 cm^{-1} depending on a peptide/protein secondary structure conformation, hydrogen bonding pattern and degree of coupling between different peptide bonds; the Amide II band at 1540–1560 cm^{-1} (mainly out-of-phase combination of CN stretch (CN s) and NH bending (NH b), Fig. 12A) and the C_α-H bending band(s) (with maybe a contribution from the CH_3-umbrella mode[156,365], Fig. 12A) at 1360–1400 cm^{-1}. The C_α-H b bands are resonancely enhanced only in PPII-like and β-strand-like conformations and do not show up in the α-helix conformation.[164,290,330,335]

Our recent study of the Amide III region UVRR bands has demonstrated the complex origin of these bands.[290] The normal mode composition of the most intense Amide III_3 band (Fig. 12A) is very close to that of "classical" Amide III band. Specifically, the Amide III_3 band mainly involves CN s and NH b vibrations coupled to C-C_α s and C_α-H b motions.[330] In contrast, the normal mode compositions of the Amide III_2 and Amide III_1 vibrations are significantly different from that of the "classical" Amide III band. Specifically, the Amide III_2 band mainly involves C_α-C s, N-C s, with possibly a small amount of C-N s and N-H b.[290] The Amide III_1 band derives from a vibration mainly involving C_α-C s and N-C s with possibly a small amount of C-N s.[290]

1.2.4 Conformational Sensitivity of UVRR Amide Bands

Fig. 12B shows the temperature dependent UVRR spectra of 21-residue mainly alanine peptide, AP, which contain three arginines for solubility. This peptide is ≥55% α-helical at 0 °C,[156,164]

whereas it is essentially in a pure PPII conformation at +65 °C.[134] It is obvious from Fig. 12B that the UVRR Amide III_3 and C_α-H bands (highlighted in yellow, Fig. 12B) are the most sensitive to secondary structure changes.

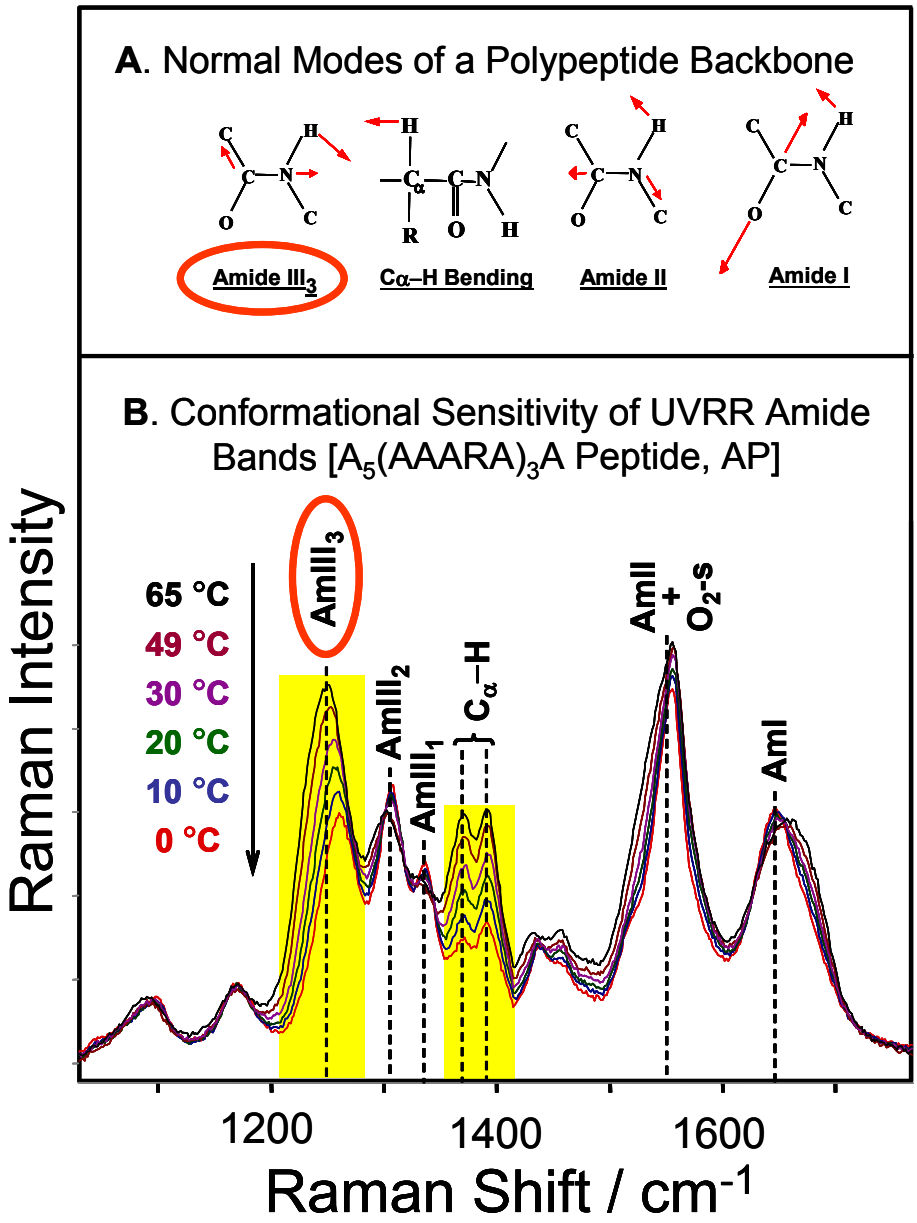

Figure 12. **A.** Assignment of ~200 nm excitation UVR amide bands, and their normal mode composition. **B**. 204 nm UVRR spectra of 21-residue mainly ala peptide, AP, at different temperatures. Note, that the $AmIII_3$ and Cα-H bands (highlighted in yellow) are the most sensitive to secondary structure changes.

The intensity of the C_α-H band(s) is directly proportional to the relative fraction of non-α-helical conformations, making these band an extremely sensitive non-α-helical

marker.[164,290,330,335] However, the frequencies of these bands are insensitive to the peptide secondary structure composition (Fig. 12B).

In contrast, both the intensity and frequency of the Amide III_3 band are highly sensitive to conformation (Fig. 12B). It was already mentioned that the Amide III_3 vibration mainly involves CN s and NH b vibrations coupled to C-C_α s and C_α-H b motions. The degree of such a coupling is sensitive to Ψ and Φ Ramachandran angles of a peptide bond, resulting in the outstanding conformational sensitivity of the Amide III_3 band frequency[290,330,341] (Fig. 12B). As we show in detail in Chapter 5, the Ψ angular dependence dominates the overall (Ψ,Φ)-dependence, so the frequency of this band sinusoidally depends on a peptide bond Ψ Ramachandran angle, allowing to directly estimate the Ψ angle (which is the most important protein folding coordinate) from the UVRR experiment.

1.2.5 Methods for Quantitative Protein and/or Peptide Secnondary Structure Determination using UVRR Spectroscopy

UVRR amide bands allow the quantitative determination of a protein/peptide secondary structure.[163,164,332,336,337] One approach to such a determination was described in detail by Chi et al.[332] Specifically, a set of UVRR basis spectra for pure secondary structures (Fig. 13) can be used to find the linear combination, which best describes the experimental spectrum of a particular protein.

Similar approach was used by Lednev et al.,[164] for 21-residue mainly alanine peptide, AP. However, the Lednev et al.'s method was improved by also taking into account the monotonic temperature dependence of pure PPII spectra. (Note, that these PPII spectra[134] were originally[164] incorrectly called "random coil"). This monotonic temperature dependence of PPII amide band frequencies, intensities and bandwidths derives from weakening of the peptide bond-water hydrogen bond strength as the temperature increases.[134,135,164,290]

Further improved method was recently proposed by Shashilov et al.[337] Specifically, these authors applied latent variable analysis of UVRR spectra to quantitatively characterize the first stages of amyloid fibril formation in lysozyme.

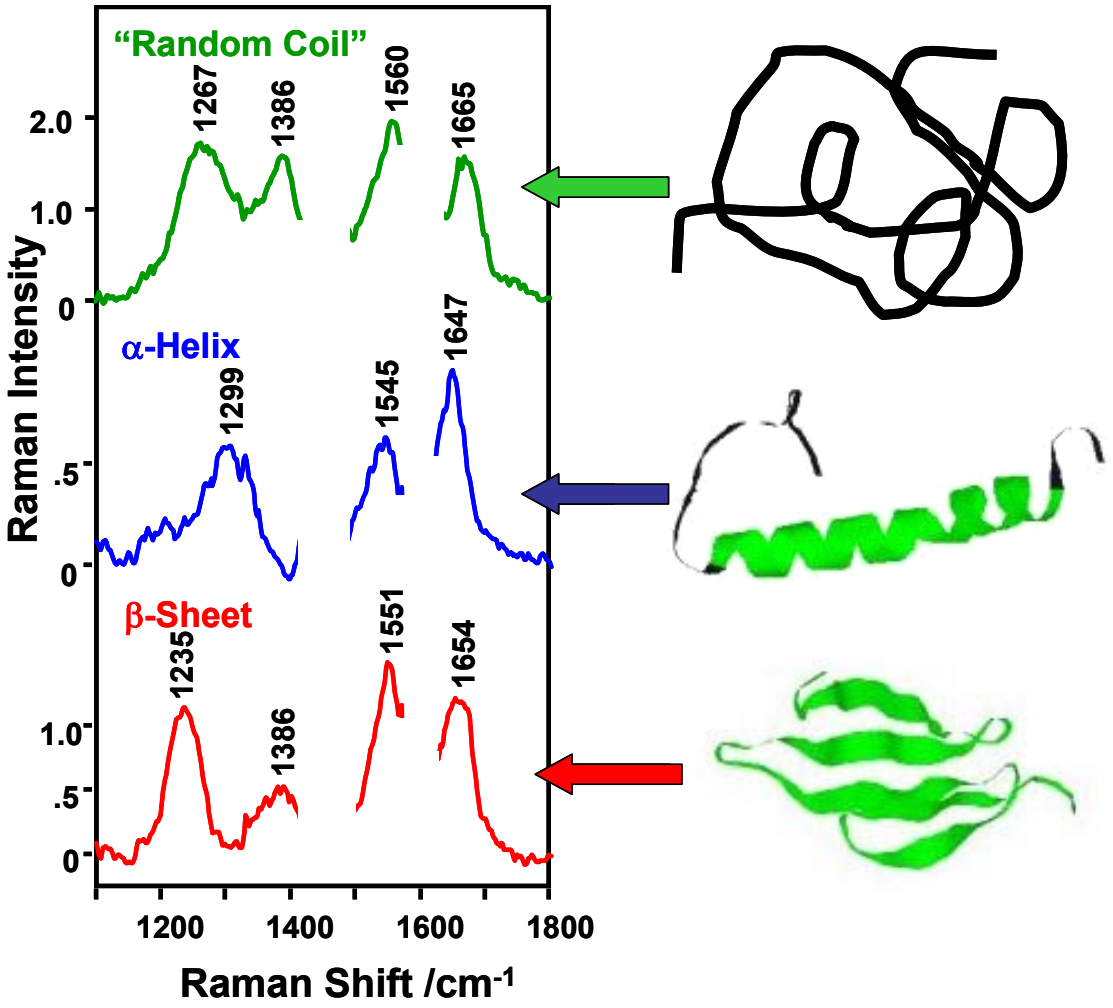

Figure 13. UVRR spectra fo pure protein secondary structures taken from Chi et al.[329]

Finally, protein and peptide secondary structure composition can be obtained from the UVRR-determined Ψ angle population distributions of peptide bonds (see Chapters 6 and 8). This novel approach is extremely powerful, because it directly monitors the folding reaction coordinate. This methodology is able to distinguish not only between major peptide and protein secondary structures, but also between similar secondary structure motifs with very similar Ramachandran angles. For example, we for the first time detected the extended 2.5_1-helix conformation in unfolded poly-L-lysine and poly-L-glutamic acid.[135] In addition, we for the first time resolved the individual contributions of pure α-helices, π-bulges and 3_{10}-helices melting to the net "α-helix-like" melting in 21-residue mainly ala peptide[163] and obtained their individual melting curves, which allows us to estimate their Zimm and Bragg parameters (see Chapter 8).

1.2.6 Summary of UVRR Spectroscopy Attractive Features

UVRR spectroscopy has many additional attractive features for protein conformational studies, compared to that of the other spectroscopic methods. For example, NMR spectroscopy, which is definitely a gold standard for conformational studies of peptides and proteins in aqueous solutions, requires relatively high sample concentrations of at least ~50-100 mg/ml.[296-305] In contrast, UVRR spectroscopy is able to measure both high and low concentrations of proteins even down to 0.15 mg/ml.[290] In addition, NMR spectroscopy is not readily available to study protein dynamics, if processes of interest are faster than microseconds. In contrast, various laser spectroscopic techniques, including the UVRR spectroscopy, allow the dynamic characterization of proteins and peptides from as slow as minutes to as fast as femtoseconds.

Circular dichroism (CD) spectroscopy, in spite of its convenience and commercial availability, allows only rough estimation of protein and peptide secondary structure composition. For example, CD is unable to detect short α-helixes.[366-368] In contrast, UVRR spectroscopy is able to detect both long and short α-helices and, thus, provides more accurate quantitative results.[366]

Typical VIS and NIR (normal) Raman spectra of peptides and proteins are very complex and not easily available for quantitative analysis.[369-371] This complexity comes from the number of severely overlapping bands, which originate from many similar covalent bonds located at both the amide backbone and different side chains. In contrast, the ability of UVRR spectroscopy to selectively monitor the vibrations of a chosen chromophore group(s) (such as, for example, amide or aromatic side chain chromophores, Fig. 11), dramatically simplifies spectral analysis, allowing the concentration only on vibrations of particular interest.

It is also known that the quantitative structural characterization of peptides and proteins using IR spectroscopic techniques are mainly limited to that in heavy water (D_2O). This is because the HOH bending band of natural abundance water severely overlaps with the most intense IR Amide I band.[315] In contrast, UVRR spectra show no significant interference from neither water nor D_2O.[156,164] Moreover, at peptide and protein concentrations of ≥ ~ 5 mg/ml, water and D_2O spectral contributions are essentially suppressed.[156,164]

In addition, there is an evidence of strong coupling, which exists between different peptide bonds in the Amide I region of the IR spectra.[372-374] Thus, the IR Amide I band

frequencies and intensities cannot be linearly related to a peptide or protein secondary structure composition. In contrast, Amide III and C_α-H (and maybe also Amide II) band regions of ~200 nm excitation UVRR spectra show essentially no coupling between different peptide bonds.[375,376] Thus, the UVRR bands (except for the Amide I band) can be considered as being independently contributed by the individual peptide bonds. This "linearity" also dramatically simplifies the use UVRR spectroscopy for peptide and protein structural studies.

One more attractive feature of UVRR, normal Raman and ROA spectroscopies is that these techniques are based on detection of ***scattered*** photons, and does not require transmission of light through samples prior to detection. This makes UVRR and normal Raman techniques applicable for studying turbid and even not transparent samples. In case of protein and peptide conformational studies, this property of UVRR spectroscopy allows to monitor, for example, the amyloid fibril formation.[331,377,378]

Finally, the recent advances in UVRR spectroscopy make this technique especially attractive for protein folding studies. Specifically, UVRR spectroscopy allows the direct monitor of peptide bond Ψ Ramachandran angle,[134,135,163,341] which is the most important folding reaction coordinate (see above). In addition, UVRR spectroscopy can be used to estimate the energy landscape features along the Ψ angle folding reaction coordinate,[135,163] providing a crucially needed quantitative basis for testing of numerous theoretical studies.

1.2.7 UV Resonance Raman Instrumentation

The UVRR T-jump apparatus used for this thesis studies is shown in the Fig. 12. It was described in detail elsewhere.[164,379] However, a brief description is given below.

The third harmonics of a Coherent Infinity Nd:YAG laser operating at 90-100 Hz with a 3 nsec pulse width was Raman shifted by five anti-Stokes harmonics in 40 psi hydrogen gas to 204 nm to excite the amide band UVRR spectra. The Raman scattered light was collected at an angle close to backscattering and was dispersed with a partially subtractive double monochromator. The Raman scattered light was detected by using a Princeton Instruments Spec-10:400B CCD camera purchased from Roper Scientific. The spectral accumulation times were ~5 min with a spectral resolution of ~10 cm^{-1}.

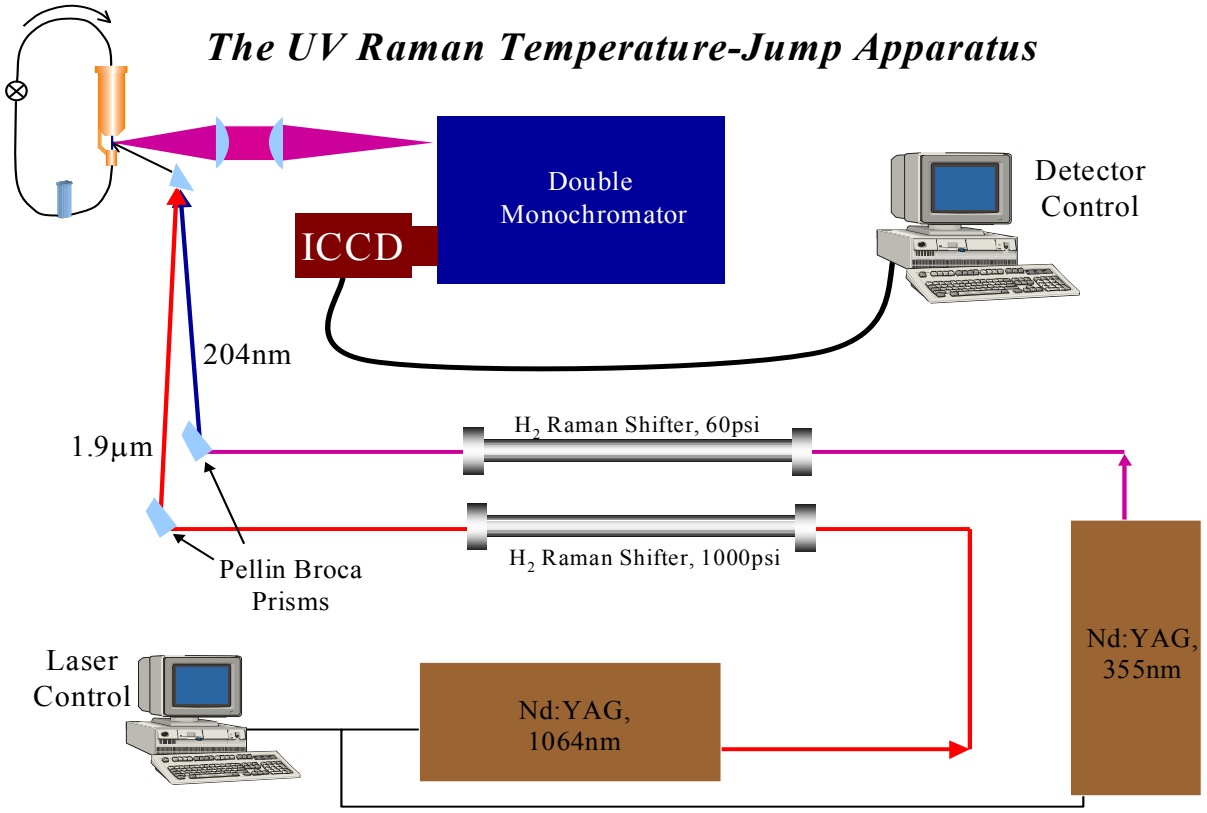

Figure 14. Schematic diagram of UVRR T-jump setup.

To initiate relaxation kinetics using the T-jump technique, we Raman-shifted the 1.06-μm Nd YAG fundamental to 1.9 μm (1st H_2 Stokes shift) by using a 1-m Raman shifter (Light Age Inc.; 1000 psi H_2) to obtain 1.5 mJ pulse energies at our 90 Hz repetition rate. This 1.9 μm excitation is absorbed by a water combination band and the energy is thermalized within picoseconds by vibrational relaxation. To accurately estimate the value of T-jump, we used the O-H stretch band(s) of water at ~3300 cm^{-1}, whose bandshape and frequency are very sensitive to temperature, using the methodology described in detail by Lednev et al.[164]

1.3 OVERVIEW OF THESIS WORK

This thesis details the most recent developments in UVRR spectroscopy, which make this technique especially attractive for protein fodling studies. Most importantly, this work establishes the relationship between UVRR spectroscopic features (such as $AmIII_3$ band profile) and a protein folding reaction coordinate (such as Ψ Ramachandran angle), allowing the direct experimental quantitative monitoring of protein and peptide (un)folding. Application of the described methodology immediately results in muber of important quantitative results, which broke an important new ground in the field of protein folding and should serve as a benchmark for future studies. Specifically:

Chapter 2 discusses a new paradigm for protein folding that finds that the unfolded states of proteins and peptides, rather than being completely disordered, exhibit local order, which often can be described as a polyproline II (PPII) conformation. In particular, we show that the 21-residue mainly alanine peptide, AP, melts from an α-helical to a PPII conformation. We also show that two central peptide bonds of penta-alanine exist essentially in a PPII conformation, as well as that a significant fraction of acid denatured apo-myoglobin peptide bonds also occur in a PPII-like conformation(s). In contrast, we find that the non-α-helical and non-β-sheet segments in a small library of folded proteins exhibit little evidence of PPII conformation. This is expected, since native-like packing in these proteins creates specific steric constrains, which are absent in acid denatured apo-myoglobin. In addition, the Chapter 2 describes our original semi-empirical relationship between the Ψ Ramachandran angle and $AmIII_3$ frequency in water solutions (which we further refine and generalize in Chapter 5). Further, Chapter 2 describes our preliminary method to obtain the Ψ angular distributions from the $AmIII_3$ band profile.

In Chapter 3, we investigated in detail the normal mode composition of α-helical and PPII UVRR amide bands, concentrating on the amide III region bands. We utilized isotopic substitutions, conformational sensitivity of the amide bands as well as their temperature dependence. Our assignments of these bands in some cases agree, but in other cases challenge previous assignments by Lee and Krimm,[365] Overman and Thomas,[380] and Diem et al.[381]

In Chapter 4, we examine the degree of vibrational coupling, which occurs between the adjacent peptide bonds. We find that negligible coupling occurs for the amide III and II' bands of both α-helical and PPII conformations as well as for the amide I, I' and II bands of PPII conformations. This dramatically simplifies the use of these vibrational bands in UVR studies of peptides and proteins. In contrast, the amide I and I' bands of the α-helical conformation show evidence for vibrational coupling. Thus, care is necessary in utilizing the amide I and I' bands of α-helical peptides and proteins, since these bands are most likely perturbed by coupling, so their parameters are not directly related to a peptide/protein secondary structure composition.

In Chapter 5, we further refine and generalize the semi-empirical relationship between the $AmIII_3$ frequency and Ψ Ramachandran angle, taking into account the hydrogen bonding. This consideration dramatically improves our ability to experimentally monitor the Ψ angle, which we believe is the most important protein folding reaction coordinate.

In Chapter 6, we apply the methods developed in Chapters 2 and 5 to obtain the Ψ angular distributions for individual poly-L-lysine (PLL) and poly-L-glutamic acid (PGA) in their unfolded states, as well as that for anti-parallel β-sheet conformation of the PLL-PGA stoichiometric mixture. This leaded us to an experimental discovery of a novel 2.5_1-helix conformation in individual PLL and PGA, which is stabilized mainly by the electrostatic repulsion between the side chain charges. In addition, applying simple Boltzmann argument, we developed a method to obtain the energy landscape features of these polypeptides from their Ψ angular population distribution.

In Chapters 7, we investigate the mechanism of of α-helix↔PPII transition in an isotopically edited analog of AP, AdP, using steady-state UVRR spectroscopy. The AdP exterior peptide bonds were perdeuterated, leaving the interior peptide bonds hydrogenated to allow separate monitoring of equilibrium melting of the middle versus the end peptide bonds. This equilibrium data demonstrates that the central peptide bonds of AdP have higher α-helix melting temperature, T_m (~32 °C) than that of exterior peptide bonds (~5 °C). We use this result in Chapter 9 to understand the AdP kinetic results.

In Chapter 8, we quantitatively characterize the mechanism of of α-helix↔PPII transition in AP, applying the methodology described in Chapters 2 and 5. Specifically, we montitored the AP equilibrium Ψ Ramachandran angular population distributions at different temperatures. The

results are striking. We resolved the contributions of pure α-helix, π-bulge and 3_{10}-helix melting to what was previously thought to be the homogenious α-helix melting. We for the first time obtained the individual melting curves for these "α-helix-like" conformations and estimated their Zimm and Bragg parameters. Strikingly, pure α-helix melting is much more cooperative and occurs at higher temperature, than it was originally reported for similar peptides. We also directly observe population of turn/β-strand conformers at higher temperatures prior to melting to a mainly PPII conformation. This novel quantitative experimental characterization of intermediates in peptide and protein (un)folding pathway will serve as the benchmark for the numerous previously untested theoretical studies of protein folding.

In Chapter 9, we kinetically investigate the mechanism of α-helix↔PPII transition in an isotopically edited analog of AP, AdP. The isotopic labeling allowed us to separately monitor the T-jump induced secondary structure relaxation of middle versus end peptide bonds. Our data indicates that the end and the middle of the peptide show significantly different and non-classical relaxation behaviors. Specifically, for a T-jump from 5 to 30 °C, the end peptide bonds show about 2-fold faster relaxation time (97±15 ns) than that of the middle (189±31 ns). In contrast, for the T-jump from 20 to 40 °C, the end peptide bonds surprisingly show a ~2-fold slower relaxation time (131±46 ns) than that of the middle peptide bonds (56±6 ns). We developed a quantitative kinetic model, which successfully explain this unusual behavior in terms of different relative contributions of different "α-helix-like" conformations, such as pure α-helices (which melt slower), and 3_{10}-helices and π-helices/bulges (which melt faster) to the melting kinetics. This methodology allowed us, for the first time, to experimentally estimate the characteristic (un)folding times for all the "α-helix-like" conformations. Strikingly, we find that the perfect α-helix (un)folding rate constants are in μsec time range at room temperature, which are ~5-10 fold slower than typically reported for similar peptides. In contrast, pure 3_{10}-helices and π-helices/bulges show ~12-fold faster (un)folding rate constants than those of pure α-helices. We also, for the first time, quantitatively estimated the spatially resolved individual relative contributions of the pure α-helix, 3_{10}-helix and π-helix/bulge melting to the overall AdP melting kinetics as well as that for AdP end and center peptide bonds melting. Strikingly, we find the evidence that the AdP N-terminus has higher pure α-helix propensity than those of the AdP center and C-terminus. These results are the first experimental ones to quantitatively show that

the folding mechanism of end residues of ala-rich peptides significantly differs from that of middle residues in terms of different relative contributions of different "α-helix-like" species to the melting kinetics.

It should be emphasized that most of novel quantitative results, reported in this thesis, seriously challenge classical theories of α-helix melting, which envision such a melting as a transition between ordered α-helix and completely disordered "random coil" conformations. First, we see no evidence for "true random coil" conformations in protein and peptide unfolded state ensembles. Rather, unfolded states of peptides and proteins exhibit a significant amount of extended polyproline II-like structures (Chapters 2 and 5). In addition, we also show that low temperature "α-helix-like" ensembles of relatively simple α-helical peptide, AP, are not homogenious and contain the additional contributions from π-bulges and 3_{10}-helices (Chapter 8). Further, we developed a quantitative kinetic model (Chapter 9), which includes the melting of all these α-helix-like conformations. This model successfully explains complicated non-classical α-helix melting kinetic behavior recently observed for short alanine-rich peptides. Specifically, Chapter 9 kinetic model accounts for the apparent anti-Arrhenius behavior of AP folding rate constant observed by Lednev et al.[164] In addition, this model also explains the complicated nonexponential kinetic behavior of ala-rich peptides reported recently by Huang et al.[189] and Bredenbeck et al.[177]

Summarizing, we developed a powerful analytical tool to, for the first time, directly monitor a major secondary structure reaction coordinate in peptides and proteins using vibrational spectroscopy. We demonstrate power of this novel methodology to quantitatively study conformational transitions in peptide and proteins. Our results not only challenge classical view of peptide and protein folding but also provide an important quantitative basis for future theoretical and experimental works in this field.

1.4 REFERENCES

(1) Creighton, T. E. *Protein Structure, Second Edition,* **1997**.

(2) Branden, C.; Tooze, J. *Introduction to Protein Structure,* **1992**.

(3) Anfinsen, C. B. *Science* **1973**, *181*, 223-230.

(4) Nemethy, G.; Scheraga, H. A. *Q. Rev. Biophys.* **1977**, *10*, 239-352.

(5) Baldwin, R. L. *Science* **2002**, *295*, 1657-1658.

(6) Baldwin, R. L.; Rose, G. D. *Trends Biochem. Sci.* **1999**, *24*, 26-33.

(7) Kim, P. S.; Baldwin, R. L. *Annu. Rev. Biochem.* **1990**, *59*, 631-660.

(8) Dill, K. A.; Chan, H. S. *Nat. Struct. Biol.* **1997**, *4*, 10-19.

(9) Chan, H. S.; Dill, K. A. *Proteins* **1998**, *30*, 2-33.

(10) Erman, B.; Dill, K. *J. Chem. Phys.* **2000**, *112*, 1050-1056.

(11) Ozkan, S. B.; Dill, K. A.; Bahar, I. *Protein Sci.* **2002**, *11*, 1958-1970.

(12) Ozkan, S. B.; Bahar, I.; Dill, K. A. *Nat. Struct. Biol.* **2001**, *8*, 765-769.

(13) Dill, K. A. *Biochemistry* **1990**, *29*, 7133-7155.

(14) Wolynes, P. G.; Onuchic, J. N.; Thirumalai, D. *Science* **1995**, *267*, 1619-1620.

(15) Hardin, C.; Eastwood, M. P.; Prentiss, M.; Luthey-Schulten, Z.; Wolynes, P. G. *J. Comp. Chem.* **2002**, *23*, 138-146.

(16) Onuchic, J. N.; Wolynes, P. G. *Curr. Opin. Struct. Biol.* **2004**, *14*, 70-75.

(17) Onuchic, J. N.; Nymeyer, H.; Garcia, A. E.; Chahine, J.; Socci, N. D. *Adv. Prot. Chem.* **2000**, *53*, 87-152.

(18) Socci, N. D.; Onucic, J. N.; Wolynes, P. G. *Proteins* **1998**, *32*, 136-158.

(19) Woody, R. W. *Methods Enzymol.* **2004**, *380*, 242-285.

(20) Nymeyer, H.; Gnanakaran, S.; Garcia, A. E. *Methods Enzymol.* **2004**, *383*, 119-149.

(21) Brooks, C. L., III; Onuchic, J. N.; Wales, D. J. *Science* **2001**, *293*, 612-613.

(22) Feig, M.; Brooks, C. L. *Curr. Opin. Struct. Biol.* **2004**, *14*, 217-224.

(23) Brooks, C. L., III; Gruebele, M.; Onuchic, J. N.; Wolynes, P. G. *Proc. Natl. Acad. Sci. U.S.A.* **1998**, *95*, 11037-11038.

(24) Bilsel, O.; Matthews, R. *Adv. Prot. Chem.* **2000**, *53*, 153-207.

(25) Dinner, A. R.; Sali, A.; Smith, L. J.; Dobson, C. M.; Karplus, M. *Trends Biochem. Sci.* **2000**, *25*, 331-339.

(26) Dinner, A. R.; Abkevich, V.; Shakhnovich, E.; Karplus, M. *Proteins* **1999**, *35*, 34-40.

(27) Lazaridis, T.; Karplus, M. *Science* **1997**, *278*, 1928-1931.

(28) Karplus, M.; Weaver, D. L. *Nature* **1976**, *260*, 404-406.

(29) Shortle, D.; Wang, Y.; Gillespie, J. R.; Wrabl, J. O. *Protein Sci.* **1996**, *5*, 991-1000.

(30) Shortle, D. *Nat. Struct. Biol.* **1999**, *6*, 203-205.

(31) Ptitsyn, O. B. *Adv. Prot. Chem.* **1995**, *47*, 83-229.

(32) Ptitsyn, O. B.; Finkelstein, A. V.; Dobson, C. M. *Mol. Biol.* **1999**, *33*, 893-896.

(33) Balbach, J.; Forge, V.; Lau, W. S.; van Nuland, N. A. J.; Brew, K.; Dobson, C. M. *Science* **1996**, *274*, 1161-1163.

(34) Dobson, C. M. *Nature* **2003**, *426*, 884-890.

(35) Clarke, J.; Itzhaki, L. S.; Fersht, A. R. *Trends Biochem. Sci.* **1997**, *22*, 284-287.

(36) Wright, C. F.; Lindorff-Larsen, K.; Randles, L. G.; Clarke, J. *Nat. Struct. Biol.* **2003**, *10*, 658-662.

(37) Ballew, R. M.; Sabelko, J.; Gruebele, M. *Nat. Struct. Biol.* **1996**, *3*, 923-926.

(38) Gruebele, M. *Annu. Rev. Phys. Chem.* **1999**, *50*, 485-516.

(39) Gruebele, M. *Curr. Opin. Struct. Biol.* **2002**, *12*, 161-168.

(40) Yang, W. Y.; Gruebele, M. *Nature* **2003**, *423*, 193-197.

(41) Snow, C. D.; Sorin, E. J.; Rhee, Y. M.; Pande, V. S. *Annu. Rev. Biophys. Biomol. Struct.* **2005**, *34*, 43-69.

(42) Snow, C. D.; Nguyen, H.; Pande, V. S.; Gruebele, M. *Nature* **2002**, *420*, 102-106.

(43) Skolnick, J. *Proc. Natl. Acad. Sci. U.S.A.* **2005**, *102*, 2265-2266.

(44) Skolnick, J.; Kolinski, A. *Science* **1990**, *250*, 1121-1125.

(45) Pokarowski, P.; Kolinski, A.; Skolnick, J. *Biophys. J.* **2003**, *84*, 1518-1526.

(46) Mirny, L.; Shakhnovich, E. *Annu. Rev. Biophys. Biomol. Struct.* **2001**, *30*, 361-396.

(47) Sali, A.; Shakhnovich, E.; Karplus, M. *Nature* **1994**, *369*, 248-251.

(48) Shakhnovich, E.; Abkevich, V.; Ptitsyn, O. *Nature* **1996**, *379*, 96-98.

(49) Lindberg, M. O.; Haglund, E.; Hubner, I. A.; Shakhnovich, E. I.; Oliveberg, M. *Proc. Natl. Acad. Sci. U.S.A.* **2006**, *103*, 4083-4088.

(50) Dokholyan, N. V. *Curr. Opin. Struct. Biol.* **2006**, *16*, 79-85.

(51) Myers, J. K.; Oas, T. G. *Annu. Rev. Biochem.* **2002**, *71*, 783-815.

(52) Lipman, E. A.; Schuler, B.; Bakajin, O.; Eaton, W. A. *Science* **2003**, *301*, 1233-1235.

(53) Schuler, B.; Lipman, E. A.; Eaton, W. A. *Nature* **2002**, *419*, 743-747.

(54) Eaton, W. A.; Munoz, V.; Hagen, S. J.; Jas, G. S.; Lapidus, L. J.; Henry, E. R.; Hofrichter, J. *Annu. Rev. Biophys. Biomol. Struct.* **2000**, *29*, 327-359.

(55) Kubelka, J.; Hofrichter, J.; Eaton, W. A. *Curr. Opin. Struc. Biol.* **2004**, *14*, 76-88.

(56) Garcia-Mira, M. M.; Sadqi, M.; Fischer, N.; Sanchez-Ruiz, J. M.; Munoz, V. *Science* **2002**, *298*, 2191-2195.

(57) Munoz, V.; Blanco, F. J.; Serrano, L. *Nat. Struct. Biol.* **1995**, *2*, 380-385.

(58) Mayor, U.; Guydosh, N. R.; Johnson, C. M.; Grossmann, J. G.; Sato, S.; Jas, G. S.; Freund, S. M. V.; Alonso, D. O. V.; Daggett, V.; Fersht, A. R. *Nature* **2003**, *421*, 863-867.

(59) Daggett, V.; Fersht, A. *Nat. Rev. Mol. Cell Biol.* **2003**, *4*, 497-502.

(60) Gianni, S.; Guydosh, N. R.; Khan, F.; Caldas, T. D.; Mayor, U.; White, G. W. N.; DeMarco, M. L.; Daggett, V.; Fersht, A. R. *Proc. Natl. Acad. Sci. U.S.A.* **2003**, *100*, 13286-13291.

(61) Englander, S. W. *Annu. Rev. Biophys. Biomol. Struct.* **2000**, *29*, 213-238, 213 Plates.

(62) Bai, Y.; Sosnick, T. R.; Mayne, L.; Englander, S. W. *Science* **1995**, *269*, 192-197.

(63) Sosnick, T. R.; Mayne, L.; Hiller, R.; Englander, S. W. *Nat. Struct. Biol.* **1994**, *1*, 149-156.

(64) Jacob, J.; Krantz, B.; Dothager, R. S.; Thiyagarajan, P.; Sosnick, T. R. *J. Mol. Biol.* **2004**, *338*, 369-382.

(65) Kallenbach, N. R.; Nelson, J. W. *Mol. Struct. Energ.* **1988**, *10*, 139-168.

(66) Kallenbach, N. R. *Nat. Struct. Biol.* **1995**, *2*, 813-816.

(67) Kallenbach, N. R.; Bell, A. J., Jr.; Spek, E. J. *Amide Linkage* **2000**, 599-625.

(68) Gilmanshin, R.; Williams, S.; Callender, R. H.; Woodruff, W. H.; Dyer, R. B. *Proc. Natl. Acad. Sci. U.S.A.* **1997**, *94*, 3709-3713.

(69) Leeson, D. T.; Gai, F.; Rodriguez, H. M.; Gregoret, L. M.; Dyer, R. B. *Proc. Natl. Acad. Sci. U.S.A.* **2000**, *97*, 2527-2532.

(70) Vu, D. M.; Peterson, E. S.; Dyer, R. B. *J. Am. Chem. Soc.* **2004**, *126*, 6546-6547.

(71) Pande, V. S.; Baker, I.; Chapman, J.; Elmer, S. P.; Khaliq, S.; Larson, S. M.; Rhee, Y. M.; Shirts, M. R.; Snow, C. D.; Sorin, E. J.; Zagrovic, B. *Biopolymers* **2003**, *68*, 91-109.

(72) Schaetzle, M.; Kiefhaber, T. *J. Mol. Biol.* **2006**, *357*, 655-664.

(73) Shea, J.-E.; Friedel, M. R.; Baumketner, A. *Rev. Comp. Chem.* **2006**, *22*, 169-228.

(74) Friedel, M.; Baumketner, A.; Shea, J.-E. *Proc. Natl. Acad. Sci. U.S.A.* **2006**, *103*, 8396-8401.

(75) Zhou, R.; Huang, X.; Margulis, C. J.; Berne, B. J. *Science* **2004**, *305*, 1605-1609.

(76) Pappu, R. V.; Srinivasan, R.; Rose, G. D. *Proc. Natl. Acad. Sci. U.S.A.* **2000**, *97*, 12565-12570.

(77) Fitzkee, N. C.; Rose, G. D. *Prot. Sci.* **2004**, *13*, 633-639.

(78) Rose, G. D. *Nat. Struct. Biol.* **1997**, *4*, 512-514.

(79) Rose, G. D.; Creamer, T. P. *Proteins* **1994**, *19*, 1-3.

(80) Creamer, T. P. *Methods Mol. Biol.* **2001**, *168*, 117-132.

(81) Kim, J. G.; Fukunishi, Y.; Nakamura, H. *Chem. Phys. Lett.* **2004**, *392*, 34-39.

(82) Duan, Y.; Kollman, P. A. *Science* **1998**, *282*, 740-744.

(83) Caflisch, A. *Curr. Opin. Struct. Biol.* **2006**, *16*, 71-78.

(84) Cavalli, A.; Haberthuer, U.; Paci, E.; Caflisch, A. *Protein Sci.* **2003**, *12*, 1801-1803.

(85) Caflisch, A.; Paci, E. *Protein Folding Handbook* **2005**, *2*, 1143-1169.

(86) Xu, Q.; Keiderling, T. A. *Biochemistry* **2005**, *44*, 7976-7987.

(87) Stelea, S. D.; Pancoska, P.; Benight, A. S.; Keiderling, T. A. *Protein Sci.* **2001**, *10*, 970-978.

(88) Keiderling, T. A. Circular Dichroism (2nd Edition) **2000**, 621-666.

(89) Miller, E. J.; Fischer, K. F.; Marqusee, S. *Proc. Natl. Acad. Sci. U.S.A.* **2002**, *99*, 10359-10363.

(90) Cecconi, C.; Shank, E. A.; Bustamante, C.; Marqusee, S. *Science* **2005**, *309*, 2057-2060.

(91) De Los Rios, M. A.; Muralidhara, B. K.; Wildes, D.; Sosnick, T. R.; Marqusee, S.; Wittung-Stafshede, P.; Plaxco, K. W.; Ruczinski, I. *Protein Sci.* **2006**, *15*, 553-563.

(92) Jewett, A. I.; Pande, V. S.; Plaxco, K. W. *J. Mol. Biol.* **2003**, *326*, 247-253.

(93) Thompson, J. B.; Hansma Helen, G.; Hansma Paul, K.; Plaxco Kevin, W. *J. Mol. Biol.* **2002**, *322*, 645-652.

(94) Plaxco, K. W.; Millett, I. S.; Segel, D. J.; Doniach, S.; Baker, D. *Nat. Struct. Biol.* **1999**, *6*, 554-556.

(95) Baker, D. *Nature* **2000**, *405*, 39-42.

(96) Alm, E.; Baker, D. *Proc. Natl. Acad. Sci. U.S.A.* **1999**, *96*, 11305-11310.

(97) Best, R. B.; Hummer, G. *Phys. Rev. Lett.* **2006**, *96*, 228104/228101-228104/228104.

(98) Floudas, C. A.; Fung, H. K.; McAllister, S. R.; Moennigmann, M.; Rajgaria, R. *Chem. Eng. Sci.* **2005**, *61*, 966-988.

(99) Sterner, R.; Schmid, F. X. *Science* **2004**, *304*, 1916-1917.

(100) Kaplan, J.; DeGrado, W. F. *Proc. Natl. Acad. Sci. U.S.A.* **2004**, *101*, 11566-11570.

(101) Schafmeister, C. E.; Stroud, R. M. *Curr. Opin. Biotech.* **1998**, *9*, 350-353.

(102) Dahiyat, B. I.; Mayo, S. L. *Science* **1997**, *278*, 82-87.

(103) Whitley, P.; Nilsson, I.; von Heijne, G. *Nat. Struct. Biol.* **1994**, *1*, 858-862.

(104) Bucciantini, M.; Giannoni, E.; Chiti, F.; Baroni, F.; Formigli, L.; Zurdo, J.; Taddei, N.; Ramponi, G.; Dobson, C. M.; Stefani, M. *Nature* **2002**, *416*, 507-511.

(105) Dobson, C. M. *Trends Biochem. Sci.* **1999**, *24*, 329-332.

(106) Ellis, R. J.; Pinheiro, T. J. T. *Nature* **2002**, *416*, 483-484.

(107) Selkoe, D. J. *Nat. Cell Biol.* **2004**, *6*, 1054-1061.

(108) Hetz, C.; Soto, C. *Cell. Mol. Life Sci.* **2003**, *60*, 133-143.

(109) Hardy, J. A.; Higgins, G. A. *Science* **1992**, *256*, 184-185.

(110) Glabe, C. G. *Trends Biochem. Sci.* **2004**, *29*, 542-547.

(111) Shortle, D. *Curr. Opin. Struc. Biol.* **1993**, *3*, 66-74.

(112) Shortle, D. R. *Curr. Opin. Struc. Biol.* **1996**, *6*, 24-30.

(113) Van Gunsteren, W. F.; Burgi, R.; Peter, C.; Daura, X. *Angew. Chem. Int. Edit.* **2001**, *40*, 352-355.

(114) Daura, X.; Glattli, A.; Gee, P.; Peter, C.; Van Gunsteren, W. F. *Adv. Prot. Chem.* **2002**, *62*, 341-360, 343 plates.

(115) Fiebig, K. M.; Schwalbe, H.; Buck, M.; Smith, L. J.; Dobson, C. M. *J. Phys. Chem.* **1996**, *100*, 2661-2666.

(116) Gast, K.; Damaschun, H.; Eckert, K.; Schulze-Forster, K.; Maurer, H. R.; Mueller-Frohne, M.; Zirwer, D.; Czarnecki, J.; Damaschun, G. *Biochemistry* **1995**, *34*, 13211-13218.

(117) Penkett, C. J.; Redfield, C.; Jones, J. A.; Dodd, I.; Hubbard, J.; Smith, R. A.; Smith, L. J.; Dobson, C. M. *Biochemistry* **1998**, *37*, 17054-17067.

(118) Zimm, B. H.; Bragg, J. K. *J. Chem. Phys.* **1959**, *31*, 526-535.

(119) Lifson, S.; Roig, A. *J. Chem. Phys.* **1961**, *34*, 1963-1974.

(120) Brant, D. A.; Flory, P. J. *J. Am. Chem. Soc.* **1965**, *87*, 2791-2800.

(121) Flory, P. J. *Statistical Mechanics of Chain Molecules,* **1969**.

(122) Poland, D.; Scheraga, H. A. *Theory of Helix-Coil Transitions in Biopolymers; Statistical Mechanical Theory of Order-Disorder Transitions in Biological Macromolecules*; Academic Press, New York and London, **1970**.

(123) Poland, D.; Scheraga, H. A. *J. Chem. Phys.* **1966**, *45*, 2071-2090.

(124) Tiffany, M. L.; Krimm, S. *Biopolymers* **1969**, *8*, 347-359.

(125) Tiffany, M. L.; Krimm, S. *Biopolymers* **1968**, *6*, 1379-1382.

(126) Dukor, R. K.; Keiderling, T. A. *Biopolymers* **1991**, *31*, 1747-1761.

(127) Adzhubei, A. A.; Sternberg, M. J. E. *J. Mol. Biol.* **1993**, *229*, 472-493.

(128) Syme, C. D.; Blanch, E. W.; Holt, C.; Jakes, R.; Goedert, M.; Hecht, L.; Barron, L. D. *Eur. J. Biochem.* **2002**, *269*, 148-156.

(129) Whittington, S. J.; Chellgren, B. W.; Hermann, V. M.; Creamer, T. P. *Biochemistry* **2005**, *44*, 6269-6275.

(130) Shi, Z.; Woody, R. W.; Kallenbach, N. R. *Adv. Prot. Chem.* **2002**, *62*, 163-240.

(131) Stapley, B. J.; Creamer, T. P. *Protein Sci.* **1999**, *8*, 587-595.

(132) Shi, Z.; Olson, C. A.; Rose, G. D.; Baldwin, R. L.; Kallenbach, N. R. *Proc. Natl. Acad. Sci. U.S.A.* **2002**, *99*, 9190-9195.

(133) McColl, I. H.; Blanch, E. W.; Hecht, L.; Kallenbach, N. R.; Barron, L. D. *J. Am. Chem. Soc.* **2004**, *126*, 5076-5077.

(134) Asher, S. A.; Mikhonin, A. V.; Bykov, S. B. *J. Am. Chem. Soc.* **2004**, *126*, 8433-8440.

(135) Mikhonin, A. V.; Myshakina, N. S.; Bykov, S. V.; Asher, S. A. *J. Am. Chem. Soc.* **2005**, *127*, 7712-7720.

(136) Rucker, A. L.; Creamer, T. P. *Protein Sci.* **2002**, *11*, 980-985.

(137) Garcia, A. E. *Polymer* **2004**, *45*, 669-676.

(138) Gokce, I.; Woody, R. W.; Anderluh, G.; Lakey, J. H. *J. Am. Chem. Soc.* **2005**, *127*, 9700-9701.

(139) Woutersen, S.; Hamm, P. *J. Phys. Chem. B* **2000**, *104*, 11316-11320.

(140) Eker, F.; Cao, X.; Nafie, L.; Schweitzer-Stenner, R. *J. Am. Chem. Soc.* **2002**, *124*, 14330-14341.

(141) Kim, Y. S.; Wang, J.; Hochstrasser, R. M. *J. Phys. Chem. B* **2005**, *109*, 7511-7521.

(142) Ramachandran, G. N.; Sasisekharan, V. *Adv. Prot. Chem.* **1968**, *23*, 283-438.

(143) Stewart, D. E.; Sarkar, A.; Wampler, J. E. *J. Mol. Biol.* **1990**, *214*, 253-260.

(144) Weiss, M. S.; Jabs, A.; Hilgenfeld, R. *Nat. Struct. Biol.* **1998**, *5*, 676.

(145) Jabs, A.; Weiss, M. S.; Hilgenfeld, R. *J. Mol. Biol.* **1999**, *286*, 291-304.

(146) Kleywegt, G. J.; Jones, T. A. *Structure* **1996**, *4*, 1395-1400.

(147) Lovell, S. C.; Davis, I. W.; Arendall, W. B., III; de Bakker, P. I. W.; Word, J. M.; Prisant, M. G.; Richardson, J. S.; Richardson, D. C. *Proteins* **2003**, *50*, 437-450.

(148) Ho, B. K.; Thomas, A.; Brasseur, R. *Protein Sci.* **2003**, *12*, 2508-2522.

(149) Bochicchio, B.; Tamburro, A. M. *Chirality* **2002**, *14*, 782-792.

(150) Woody, R. W. *Adv. Biophys. Chem.* **1992**, *2*, 37-79.

(151) Fleming, P. J.; Fitzkee, N. C.; Mezei, M.; Srinivasan, R.; Rose, G. D. *Protein Sci.* **2005**, *14*, 111-118.

(152) Mezei, M.; Fleming, P. J.; Srinivasan, R.; Rose, G. D. *Proteins* **2004**, 55, 502-507.

(153) Eisenhaber, F.; Adzhubei, A. A.; Eisenmenger, F.; Esipova, N. G. *Biofizika* **1992**, *37*, 62-67.

(154) Hinderaker, M. P.; Raines, R. T. *Protein Sci.* **2003**, *12*, 1188-1194.

(155) Kabsch, W.; Sander, C. *Biopolymers* **1983**, *22*, 2577-2637.

(156) Lednev, I. K.; Karnoup, A. S.; Sparrow, M. C.; Asher, S. A. *J. Am. Chem. Soc.* **2001**, *123*, 2388-2392.

(157) Thompson, P. A.; Eaton, W. A.; Hofrichter, J. *Biochemistry* **1997**, *36*, 9200-9210.

(158) Scholtz, J. M.; Marqusee, S.; Baldwin, R. L.; York, E. J.; Stewart, J. M.; Santoro, M.; Bolen, D. W. *Proc. Natl. Acad. Sci. U.S.A.* **1991**, *88*, 2854-2858.

(159) Scholtz, J. M.; Qian, H.; York, E. J.; Stewart, J. M.; Baldwin, R. L. *Biopolymers* **1991**, *31*, 1463-1470.

(160) Gruenewald, B.; Nicola, C. U.; Lustig, A.; Schwarz, G.; Klump, H. *Biophys. Chem.* **1979**, *9*, 137-147.

(161) Ptitsyn, O. B. *Pure Appl. Chem.* **1972**, 31, 227-244.

(162) Ptitsyn, O. B.; Skvortsov, A. M. *Biofizika* **1965**, *10*, 909-917.

(163) Mikhonin, A. V.; Asher, S. A. *J. Am. Chem. Soc.* **2006**, In Press.

(164) Lednev, I. K.; Karnoup, A. S.; Sparrow, M. C.; Asher, S. A. *J. Am. Chem. Soc.* **1999**, *121*, 8074-8086.

(165) Lednev, I. K.; Karnoup, A. S.; Sparrow, M. C.; Asher, S. A. *J. Am. Chem. Soc.* **1999**, *121*, 4076-4077.

(166) Ianoul, A.; Mikhonin, A.; Lednev, I. K.; Asher, S. A. *J. Phys. Chem. A* **2002**, *106*, 3621-3624.

(167) Lockhart, D. J.; Kim, P. S. *Science* **1992**, *257*, 947-951.

(168) Lockhart, D. J.; Kim, P. S. *Science* **1993**, *260*, 198-202.

(169) Werner, J. H.; Dyer, R. B.; Fesinmeyer, R. M.; Andersen, N. H. *J. Phys. Chem. B* **2002**, *106*, 487-494.

(170) Fesinmeyer, R. M.; Peterson, E. S.; Dyer, R. B.; Andersen, N. H. *Protein Sci.* **2005**, *14*, 2324-2332.

(171) Williams, S.; Causgrove, T. P.; Gilmanshin, R.; Fang, K. S.; Callender, R. H.; Woodruff, W. H.; Dyer, R. B. *Biochemistry* **1996**, *35*, 691-697.

(172) Dyer, R. B.; Gai, F.; Woodruff, W. H.; Gilmanshin, R.; Callender, R. H. *Acc. Chem. Res.* **1998**, *31*, 709-716.

(173) Callender, R.; Dyer, R. B.; Gilmanshin, R.; Woodruff, W. H. *Annu. Rev. Phys. Chem.* **1998**, *49*, 173-202.

(174) Thompson, P. A.; Munoz, V.; Jas, G. S.; Henry, E. R.; Eaton, W. A.; Hofrichter, J. *J. Phys. Chem. B* **2000**, *104*, 378-389.

(175) Lapidus, L. J.; Eaton, W. A.; Hofrichter, J. *Proc. Natl. Acad. Sci. U.S.A.* **2000**, *97*, 7220-7225.

(176) Lapidus, L. J.; Eaton, W. A.; Hofrichter, J. *J. Mol. Biol.* **2002**, *319*, 19-25.

(177) Bredenbeck, J.; Helbing, J.; Kumita, J. R.; Woolley, G. A.; Hamm, P. *Proc. Natl. Acad. Sci. U.S.A.* **2005**, *102*, 2379-2384.

(178) Decatur, S. M.; Antonic, J. *J. Am. Chem. Soc.* **1999**, *121*, 11914-11915.

(179) Decatur, S. M. *Biopolymers* **2000**, *54*, 180-185.

(180) Ramajo, A. P.; Petty, S. A.; Starzyk, A.; Decatur, S. M.; Volk, M. *J. Am. Chem. Soc.* **2005**, *127*, 13784-13785.

(181) Pozo Ramajo, A.; Petty, S. A.; Volk, M. *Chem. Phys.* **2006**, *323*, 11-20.

(182) Gooding, E. A.; Ramajo, A. P.; Wang, J.; Palmer, C.; Fouts, E.; Volk, M. *Chem. Commun.* **2005**, 5985-5987.

(183) Silva, R. A.; Kubelka, J.; Bour, P.; Decatur, S. M.; Keiderling, T. A. *Proc. Natl. Acad. Sci. U.S.A.* **2000**, *97*, 8318-8323.

(184) Yoder, G.; Pancoska, P.; Keiderling, T. A. *Biochemistry* **1997**, *36*, 15123-15133.

(185) Keiderling, T. A.; Silva, R. A.; Yoder, G.; Dukor, R. K. *Bioorgan. Med. Chem.* **1999**, *7*, 133-141.

(186) Decatur, S. M. *Accounts Chem. Res.* **2006**, 39, 169-175.

(187) Huang, C.-Y.; Getahun, Z.; Wang, T.; DeGrado, W. F.; Gai, F. *J. Am. Chem. Soc.* **2001**, *123*, 12111-12112.

(188) Huang, C.-Y.; Getahun, Z.; Zhu, Y.; Klemke, J. W.; DeGrado, W. F.; Gai, F. *Proc. Natl. Acad. Sci. U.S.A.* **2002**, *99*, 2788-2793.

(189) Huang, C.-Y.; Klemke, J. W.; Getahun, Z.; DeGrado, W. F.; Gai, F. *J. Am. Chem. Soc.* **2001**, *123*, 9235-9238.

(190) Wang, T.; Zhu, Y.; Getahun, Z.; Du, D.; Huang, C.-Y.; DeGrado, W. F.; Gai, F. *J. Phys. Chem. B* **2004**, *108*, 15301-15310.

(191) Wang, T.; Du, D.; Gai, F. *Chem. Phys. Lett.* **2003**, *370*, 842-848.

(192) Marqusee, S.; Baldwin, R. L. *Proc. Natl. Acad. Sci. U.S.A.* **1987**, *84*, 8898-8902.

(193) Marqusee, S.; Robbins, V. H.; Baldwin, R. L. *Proc. Natl. Acad. Sci. U.S.A.* **1989**, *86*, 5286-5290.

(194) Padmanabhan, S.; Marqusee, S.; Ridgeway, T.; Laue, T. M.; Baldwin, R. L. *Nature* **1990**, *344*, 268-270.

(195) Rohl, C. A.; Baldwin, R. L. *Biochemistry* **1994**, *33*, 7760-7767.

(196) Venyaminov, S. Y.; Hedstrom, J. F.; Prendergast, F. G. *Proteins* **2001**, *45*, 81-89.

(197) Cochran, D. A. E.; Doig, A. J. *Protein Sci.* **2001**, *10*, 1305-1311.

(198) Cochran, D. A. E.; Penel, S.; Doig, A. J. *Protein Sci.* **2001**, *10*, 463-470.

(199) Miller, J. S.; Kennedy, R. J.; Kemp, D. S. *Biochemistry* **2001**, *40*, 305-309.

(200) Goch, G.; Maciejczyk, M.; Oleszczuk, M.; Stachowiak, D.; Malicka, J.; Bierzynski, A. *Biochemistry* **2003**, *42*, 6840-6847.

(201) Gans, P. J.; Lyu, P. C.; Manning, M. C.; Woody, R. W.; Kallenbach, N. R. *Biopolymers* **1991**, *31*, 1605-1614.

(202) Kallenbach, N. R.; Lyu, P.; Zhou, H. *Circular Dichroism and the Conformational Analysis of Biomolecules* **1996**, 201-259.

(203) Spek, E. J.; Olson, C. A.; Shi, Z.; Kallenbach, N. R. *J. Am. Chem. Soc.* **1999**, *121*, 5571-5572.

(204) Doruker, P.; Bahar, I. *Biophys. J.* **1997**, 72, 2445-2456.

(205) Scholtz, J. M.; Baldwin, R. L. *Annu. Rev. Biophys. Biomol. Struct.* **1992**, *21*, 95-118.

(206) Young, W. S.; Brooks, C. L., III *J. Mol. Biol.* **1996**, *259*, 560-572.

(207) Shirley, W. A.; Brooks, C. L., III *Proteins* **1997**, *28*, 59-71.

(208) Tobias, D. J.; Brooks, C. L., III *Biochemistry* **1991**, *30*, 6059-6070.

(209) Brooks, C. L., III *J. Phys. Chem.* **1996**, *100*, 2546-2549.

(210) Ohkubo, Y. Z.; Brooks, C. L., III *Proc. Natl. Acad. Sci. U.S.A.* **2003**, *100*, 13916-13921.

(211) Gnanakaran, S.; Garcia, A. E. *J. Phys. Chem. B* **2003**, *107*, 12555-12557.

(212) Gnanakaran, S.; Garcia, A. E. *Proteins* **2005**, *59*, 773-782.

(213) Gnanakaran, S.; Hochstrasser, R. M.; Garcia, A. E. *Proc. Natl. Acad. Sci. U.S.A.* **2004**, *101*, 9229-9234.

(214) Hummer, G.; Garcia, A. E.; Garde, S. *Phys. Rev. Lett.* **2000**, *85*, 2637-2640.

(215) Nymeyer, H.; Garcia, A. E. *Proc. Natl. Acad. Sci. U.S.A.* **2003**, *100*, 13934-13939.

(216) Paschek, D.; Gnanakaran, S.; Garcia, A. E. *Proc. Natl. Acad. Sci. U.S.A.* **2005**, *102*, 6765-6770.

(217) Ghosh, T.; Garde, S.; Garcia, A. E. *Biophys. J.* **2003**, *85*, 3187-3193.

(218) Daggett, V.; Levitt, M. *J. Mol. Biol.* **1992**, *223*, 1121-1138.

(219) Doshi, U.; Munoz, V. *Chem. Phys.* **2004**, *307*, 129-136.

(220) Doshi, U. R.; Munoz, V. *J. Phys. Chem. B* **2004**, *108*, 8497-8506.

(221) Munoz, V.; Serrano, L. *J. Mol. Biol.* **1995**, *245*, 297-308.

(222) Sorin, E. J.; Pande, V. S. *Biophys. J.* **2005**, *88*, 2472-2493.

(223) Sorin, E. J.; Pande, V. S. *J. Comp. Chem.* **2005**, *26*, 682-690.

(224) Sorin, E. J.; Rhee, Y. M.; Shirts, M. R.; Pande, V. S. *J. Mol. Biol.* **2006**, *356*, 248-256.

(225) Zagrovic, B.; Jayachandran, G.; Millett, I. S.; Doniach, S.; Pande, V. S. *J. Mol. Biol.* **2005**, *353*, 232-241.

(226) Bertsch, R. A. *In California Institute of Technology, Pasadena, CA, USA.,* **1998**, 190 pp.

(227) Bertsch, R. A.; Vaidehi, N.; Chan, S. I.; Goddard, W. A., III *Proteins* **1998**, *33*, 343-357.

(228) Ferrara, P.; Apostolakis, J.; Caflisch, A. *J. Phys. Chem. B* **2000**, *104*, 5000-5010.

(229) Pande, V. S.; Grosberg, A. Y.; Tanaka, T.; Rokhsar, D. S. *Curr. Opin. Struct. Biol.* **1998**, *8*, 68-79.

(230) Shakhnovich, E. I. *Curr. Opin. Struct. Biol.* **1997**, *7*, 29-40.

(231) Irbaeck, A.; Mohanty, S. *Biophys. J.* **2005**, *88*, 1560-1569.

(232) Doig, A. J. *Biophys. Chem.* **2002**, *101-102*, 281-293.

(233) Doig, A. J.; Errington, N.; Iqbalsyah, T. M. *Protein Folding Handbook* **2005**, *1*, 247-313.

(234) Dobson, C. M.; Sali, A.; Karplus, M. *Angew. Chem. Int. Edit.* **1998**, *37*, 868--893.

(235) Levy, Y.; Jortner, J.; Becker, O. M. *Proc. Natl. Acad. Sci. U.S.A.* **2001**, *98*, 2188-2193.

(236) Nguyen, H. D.; Marchut, A. J.; Hall, C. K. *Protein Sci.* **2004**, *13*, 2909-2924.

(237) Peng, Y.; Hansmann, U. H. E.; Alves, N. A. *J. Chem. Phys.* **2003**, *118*, 2374-2380.

(238) Takano, M.; Nagayama, K.; Suyama, A. *J. Chem. Phys.* **2002**, *116*, 2219-2228.

(239) Takano, M.; Nakamura, H. K.; Nagayama, K.; Suyama, A. *J. Chem. Phys.* **2003**, *118*, 10312-10322.

(240) Takano, M.; Yamato, T.; Higo, J.; Suyama, A.; Nagayama, K. *J. Am. Chem. Soc.* **1999**, *121*, 605-612.

(241) Mortenson, P. N.; Evans, D. A.; Wales, D. J. *J. Chem. Phys.* **2002**, *117*, 1363-1376.

(242) Ulmschneider, J. P.; Jorgensen, W. L. *J. Am. Chem. Soc.* **2004**, *126*, 1849-1857.

(243) Ulmschneider, J. P.; Jorgensen, W. L. *J. Chem. Phys.* **2003**, *118*, 4261-4271.

(244) Tirado-Rives, J.; Maxwell, D. S.; Jorgensen, W. L. *J. Am. Chem. Soc.* **1993**, *115*, 11590-11593.

(245) Tirado-Rives, J.; Jorgensen, W. L. *Biochemistry* **1991**, *30*, 3864-3871.

(246) Hummer, G.; Garcia, A. E.; Garde, S. *Proteins* **2001**, *42*, 77-84.

(247) Mitsutake, A.; Okamoto, Y. *J. Chem. Phys.* **2000**, *112*, 10638-10647.

(248) Samuelson, S.; Martyna, G. J. *J. Phys. Chem. B* **1999**, *103*, 1752-1766.

(249) Hansmann, U. H. E.; Okamoto, Y. *J. Chem. Phys.* **1999**, *110*, 1267-1276.

(250) Wu, X.; Wang, S. *J. Phys. Chem. B* **2001**, *105*, 2227-2235.

(251) Wang, Y.; Kuczera, K. *J. Phys. Chem. B* **1997**, *101*, 5205-5213.

(252) Van Giessen, A. E.; Straub, J. E. *J. Chem. Theory Comput.* **2006**, *2*, 674-684.

(253) Chakrabartty, A.; Baldwin, R. L. *Adv. Prot. Chem.* **1995**, *46*, 141-176.

(254) Chakrabartty, A.; Schellman, J. A.; Baldwin, R. L. *Nature* **1991**, *351*, 586-588.

(255) Arashiro, E.; Drugowich de Felicio, J. R.; Hansmann, U. H. E. *Phys. Rev. E* **2006**, *73*, 040902/040901-040902/040904.

(256) Soto, P.; Mark, A. E. *J. Phys. Chem. B* **2002**, *106*, 12830-12833.

(257) Peng, Y.; Hansmann, U. H. E. *Biophys. J.* **2002**, *82*, 3269-3276.

(258) Smith, A. V.; Hall, C. K. *Proteins* **2001**, *44*, 344-360.

(259) Alves, N. A.; Hansmann, U. H. E. *Physica A* **2001**, *292*, 509-518.

(260) Pellegrini, M.; Gronbech-Jensen, N.; Doniach, S. *Physica A* **1997**, *239*, 244-254.

(261) Klein, C. T.; Mayer, B.; Koehler, G.; Wolschann, P. *Theochem* **1996**, *370*, 33-43.

(262) Hoffmann, D.; Knapp, E.-W. *Eur. Biophys. J.* **1996**, *24*, 387-403.

(263) Scheraga, H. A.; Vila, J. A.; Ripoll, D. R. *Biophys. Chem.* **2002**, *101-102*, 255-265.

(264) Zhang, W.; Lei, H.; Chowdhury, S.; Duan, Y. *J. Phys. Chem. B* **2004**, *108*, 7479-7489.

(265) Rathore, N.; Yan, Q.; de Pablo, J. J. *J. Chem. Phys.* **2004**, *120*, 5781-5788.

(266) Qian, H.; Schellman, J. A. *J. Phys. Chem.* **1992**, *96*, 3987-3994.

(267) Kentsis, A.; Mezei, M.; Gindin, T.; Osman, R. *Proteins* **2004**, *55*, 493-501.

(268) Blanch, E. W.; Morozova-Roche, L. A.; Cochran, D. A. E.; Doig, A. J.; Hecht, L.; Barron, L. D. *J. Mol. Biol.* **2000**, *301*, 553-563.

(269) Chen, K.; Liu, Z.; Kallenbach, N. R. *Proc. Natl. Acad. Sci. U.S.A.* **2004**, *101*, 15352-15357.

(270) Pappu, R. V.; Rose, G. D. *Protein Sci.* **2002**, *11*, 2437-2455.

(271) Sheinerman, F. B.; Brooks, C. L., III *J. Am. Chem. Soc.* **1995**, *117*, 10098-10103.

(272) Sundaralingam, M.; Sekharudu, Y. C. *Science* **1989**, *244*, 1333-1337.

(273) Millhauser, G. L. *Biochemistry* **1995**, *34*, 3873-3877.

(274) Miick, S. M.; Martinez, G. V.; Fiori, W. R.; Todd, A. P.; Millhauser, G. L. *Nature* **1992**, *359*, 653-655.

(275) Fiori, W. R.; Miick, S. M.; Millhauser, G. L. *Biochemistry* **1993**, *32*, 11957-11962.

(276) Martinez, G.; Millhauser, G. *J. Struct. Biol.* **1995**, *114*, 23-27.

(277) Millhauser, G. L.; Stenland, C. J.; Bolin, K. A.; van de Ven, F. J. M. *J. Biomol. NMR* **1996**, *7*, 331-334.

(278) Hanson, P.; Martinez, G.; Millhauser, G.; Formaggio, F.; Crisma, M.; Toniolo, C.; Vita, C. *J. Am. Chem. Soc.* **1996**, *118*, 271-272.

(279) Millhauser, G. L.; Stenland, C. J.; Hanson, P.; Bolin, K. A.; van de Ven, F. J. M. *J. Mol. Biol.* **1997**, *267*, 963-974.

(280) Hanson, P.; Anderson, D. J.; Martinez, G.; Millhauser, G.; Formaggio, F.; Crisma, M.; Toniolo, C.; Vita, C. *Mol. Phys.* **1998**, *95*, 957-966.

(281) Armen, R.; Alonso, D. O. V.; Daggett, V. *Protein Sci.* **2003**, *12*, 1145-1157.

(282) Long, H. W.; Tycko, R. *J. Am. Chem. Soc.* **1998**, *120*, 7039-7048.

(283) Topol, I. A.; Burt, S. K.; Deretey, E.; Tang, T.-H.; Perczel, A.; Rashin, A.; Csizmadia, I. G. *J. Am. Chem. Soc.* **2001**, *123*, 6054-6060.

(284) Podtelezhnikov, A. A.; Wild, D. L. *Proteins* **2005**, *61*, 94-104.

(285) Han, W.-G.; Elstner, M.; Jalkanen, K. J.; Frauenheim, T.; Suhai, S. *Int. J. Quantum Chem.* **2000**, *78*, 459-479.

(286) Lee, K.-H.; Benson, D. R.; Kuczera, K. *Biochemistry* **2000**, *39*, 13737-13747.

(287) Mahadevan, J.; Lee, K.-H.; Kuczera, K. *J. Phys. Chem. B* **2001**, *105*, 1863-1876.

(288) Feig, M.; MacKerell, A. D., Jr.; Brooks, C. L., III *J. Phys. Chem. B* **2003**, *107*, 2831-2836.

(289) Cartailler, J.-P.; Luecke, H. *Structure* **2004**, *12*, 133-144.

(290) Mikhonin, A. V.; Ahmed, Z.; Ianoul, A.; Asher., S. A. *J. Phys. Chem. B* **2004**, *108*, 19020-19028.

(291) Skorobogatiy, M.; Guo, H.; Zuckermann, M. *J. Chem. Phys.* **1998**, *109*, 2528-2535.

(292) Esposito, L.; Vitagliano, L.; Mazzarella, L. *Protein Peptide Lett.* **2002**, *9*, 95-105.

(293) Petrova, T.; Podjarny, A. *Rep. Prog. Phys.* **2004**, *67*, 1565-1605.

(294) Schmidt, A.; Lamzin, V. S. *Curr. Opin. Struc. Biol.* **2002**, *12*, 698-703.

(295) Vrielink, A.; Sampson, N. *Curr. Opin. Struc. Biol.* **2003**, *13*, 709-715.

(296) Kuszewski, J.; Schwieters, C. D.; Garrett, D. S.; Byrd, R. A.; Tjandra, N.; Clore, G. M. *J. Am. Chem. Soc.* **2004**, *126*, 6258-6273.

(297) Tugarinov, V.; Hwang, P. M.; Kay, L. E. *Annu. Rev. Biochem.* **2004**, *73*, 107-146.

(298) Dyson, H. J.; Wright, P. E. *Chem. Rev.* **2004**, *104*, 3607-3622.

(299) Wider, G.; Wuthrich, K. *Curr. Opin. Struc. Biol.* **1999**, *9*, 594-601.

(300) Clore, G. M.; Gronenborn, A. M. *Trends Biotech.* **1998**, *16*, 22-34.

(301) Campbell-Burk, S.; Zhong, S. *Curr. Opin. Biotech.* **1994**, *5*, 346-354.

(302) Bax, A. *Protein Sci.* **2003**, *12*, 1-16.

(303) Billeter, M. *Q. Rev. Biophys.* **1992**, *25*, 325-377.

(304) Bonmatin, J. M.; Genest, M.; Petit, M. C.; Gincel, E.; Simorre, J. P.; Cornet, B.; Gallet, X.; Caille, A.; Labbe, H.; Vovelle, F.; Ptak, M. *Biochimie* **1992**, *74*, 825-836.

(305) Wagner, G.; Hyberts, S.; Peng, J. W. *NMR Proteins* **1993**, 220-257.

(306) Receveur, V.; Garcia, P.; Durand, D.; Vachette, P.; Desmadril, M. *Proteins* **2000**, *38*, 226-238.

(307) Garcia, P.; Serrano, L.; Durand, D.; Rico, M.; Bruix, M. *Protein Sci.* **2001**, *10*, 1100-1112.

(308) Katou, H.; Hoshino, M.; Kamikubo, H.; Batt, C. A.; Goto, Y. *J. Mol. Biol.* **2001**, *310*, 471-484.

(309) Gulotta, M.; Gilmanshin, R.; Buscher, T. C.; Callender, R. H.; Dyer, R. B. *Biochemistry* **2001**, *40*, 5137-5143.

(310) Gulotta, M.; Rogatsky, E.; Callender, R. H.; Dyer, R. B. *Biophys. J.* **2003**, *84*, 1909-1918.

(311) Callender, R.; Dyer, R. B. *Curr. Opin. Struc. Biol.* **2002**, *12*, 628-633.

(312) Nienhaus, K.; Niehnaus, G. U. *Methods Mol. Biol.* **2005**, *305*, 215-241.

(313) Stynes, H. C.; Layo, A.; Smith, R. W. *J. Chem. Educ.* **2004**, *81*, 266-269.

(314) Zhang, J.; Hellwig, P.; Osborne, J. P.; Huang, H.-w.; Moeenne-Loccoz, P.; Konstantinov, A. A.; Gennis, R. B. *Biochemistry* **2001**, *40*, 8548-8556.

(315) Venyaminov, S.; Prendergast, F. G. *Anal. Biochem.* **1997**, *248*, 234-245.

(316) Sreerama, N.; Woody, R. W. *Circular Dichroism (2nd Edition)* **2000**, 601-620.

(317) Woody, R. W.; Koslowski, A. *Biophys. Chem.* **2002**, *101-102*, 535-551.

(318) Woody, R. W. *Monatshefte fuer Chemie* **2005**, *136*, 347-366.

(319) Sabelko, J.; Ervin, J.; Gruebele, M. *J. Phys. Chem. B* **1998**, *102*, 1806-1819.

(320) Porumb, H.; Zargarian, L.; Merad, H.; Maroun, R.; Mauffret, O.; Troalen, F.; Fermandjian, S. *Biochim. Biophys. Acta* **2004**, *1699*, 77-86.

(321) Gast, K.; Damaschun, H.; Misselwitz, R.; Mueller-Frohne, M.; Zirwer, D.; Damaschun, G. *Eur. Biophys. J.* **1994**, *23*, 297-305.

(322) Goldbeck, R. A.; Kim-Shapiro, D. B.; Kliger, D. S. *Annu. Rev. Phys. Chem.* **1997**, *48*, 453-479.

(323) Lewis, J. W.; Goldbeck, R. A.; Kliger, D.S.; Xie, X.; Dunn, R. C.; Simon, J. D. *J. Phys. Chem.* **1992**, *96*, 5243-5254.

(324) Lakowicz, J. R. *J. Biochem. Biophys. Meth.* **1980**, *2*, 91-119.

(325) Kumar, V.; Sharma, V. K.; Kalonia, D. S. *Int. J. Pharmaceut.* **2005**, *294*, 193-199.

(326) Santos, N. C.; Castanho, M. *Trends Applied Spectrosc.* **2002**, *4*, 113-125.

(327) Brown, M. P.; Royer, C. *Curr. Opin. Biotech.* **1997**, *8*, 45-49.

(328) Jiskoot, W.; Hlady, V.; Naleway, J. J.; Herron, J. N. *Pharm. Biotech.* **1995**, *7*, 1-63.

(329) Asher, S. A. *Handbook of Vibrational Spectroscopy*, John Whiley & Sons, Ltd. **2001**, *1*, 557-571.

(330) Asher, S. A.; Ianoul, A.; Mix, G.; Boyden, M. N.; Karnoup, A.; Diem, M.; Schweitzer-Stenner, R. *J. Am. Chem. Soc.* **2001**, *123*, 11775-11781.

(331) Lednev, I. K.; Ermolenkov, V. V.; He, W.; Xu, M. *Anal. Bioanal. Chem.* **2005**, *381*, 431-437.

(332) Chi, Z.; Chen, X. G.; Holtz, J. S. W.; Asher, S. A. *Biochemistry* **1998**, *37*, 2854-2864.

(333) Spiro, T. G.; Grygon, C. A. *J. Mol. Struct.* **1988**, *173*, 79-90.

(334) Spiro, T. G.; Rodgers, K.; Su, C. *Springer Proc. Phys.* **1992**, *68*, 3-5.

(335) Wang, Y.; Purrello, R.; Jordan, T.; Spiro, T. G. *J. Am. Chem. Soc.* **1991**, *113*, 6359-6368.

(336) Copeland, R. A.; Spiro, T. G. *Biochemistry* **1987**, *26*, 2134-2139.

(337) Shashilov, V. A.; Xu, M.; Ermolenkov, V. V.; Lednev, I. K. *J. Quant. Spectrosc. Radiat. Transfer* **2006**, *102*, 46-61.

(338) Chi, Z.; Asher, S. A. *Biochemistry* **1998**, *37*, 2865-2872.

(339) Chi, Z.; Asher, S. A. *J. Phys. Chem. B* **1998**, *102*, 9595-9602.

(340) Harmon, P. A.; Teraoka, J.; Asher, S. A. *J. Am. Chem. Soc.* **1990**, *112*, 8789-8799.

(341) Mikhonin, A. V.; Bykov, S. V.; Myshakina, N. S.; Asher, S. A. *J. Phys. Chem. B* **2006**, *110*, 1928-1943.

(342) Gast, K.; Noeppert, A.; Mueller-Frohne, M.; Zirwer, D.; Damaschun, G. *Eur. Biophys. J.* **1997**, *25*, 211-219.

(343) Clarke, D. T.; Doig, A. J.; Stapley, B. J.; Jones, G. R. *Proc. Natl. Acad. Sci. U.S.A.* **1999**, *96*, 7232-7237.

(344) Chan, C.-K.; Hu, Y.; Takahashi, S.; Rousseau, D. L.; Eaton, W. A.; Hofrichter, J. *Proc. Natl. Acad. Sci. U.S.A.* **1997**, *94*, 1779-1784.

(345) Panick, G.; Herberhold, H.; Sun, Z.; Winter, R. *Spectroscopy* **2003**, *17*, 367-376.

(346) Ma, H.; Gruebele, M. *Abstracts of Papers, 227th ACS National Meeting, Anaheim, CA, United States, March 28-April 1, 2004* **2004**, PHYS-152.

(347) Yamamoto, K.; Mizutani, Y.; Kitagawa, T. *Biophys. J.* **2000**, *79*, 485-495.

(348) Rock, R. S.; Hansen, K. C.; Larsen, R. W.; Chan, S. I. *Chem. Phys.* **2004**, *307*, 201-208.

(349) Mines, G. A.; Pascher, T.; Lee, S. C.; Winkler, J. R.; Gray, H. B. *Chem. Biol.* **1996**, *3*, 491-497.

(350) Kim, J. E.; Pribisko, M. A.; Gray, H. B.; Winkler, J. R. *Inorg. Chem.* **2004**, *43*, 7953-7960.

(351) Raman, C. V. *Nature* **1928**, *121*, 619.

(352) Raman, C. V.; Krishnan, K. S. *Philosophical Magazine (1798-1977)* **1928**, *5*, 498-512.

(353) Raman, C. V.; Krishnan, K. S. *Nature* **1928**, *121*, 711.

(354) Landsberg, G.; Mandelstam, L. *Naturwissenschaften* **1928**, *16*, 557-558.

(355) Landsberg, G.; Mandelstam, L. *Compte Rendus* **1928**, *187*, 109-111.

(356) Ingle, J. D.; Crouch, S. R. *Spectrochemical analysis* **1988**, Prentice-Hall, Inc., a Division of Simon and Schuster, Englewood Cliffs, New Jersey.

(357) Chantry, G. W. *Raman Effect Vol. 1* **1977**, Marcell Dekker, NY, 49-94.

(358) Long, D. A. *Raman Spectroscopy* **1977**, McGraw-Hill, NY.

(359) Tang, J.; Albrecht, A. *Raman Spectroscopy Vol.2 (H.A. Szymanski, ed.)* **1970**, Plenum Press, NY.

(360) Placzek, G. *Rayleigh Scattering and Raman Effect: Radiology Handbook* **1934**, Leipzig.

(361) Boyden, M. N. *In Univ. of Pittsburgh, Pittsburgh, PA, USA,* **2001**, 91 pp.

(362) Robin, M. B. *Higher Excited States of Polyatomic Molecules*; Academic Press: New York **1975**, *Vol. II.*

(363) Momii, R. K.; Urry, D. W. *Macromolecules* **1968**, *1*, 372-373.

(364) Applequist, J. *J. Chem. Phys.* **1979**, *71*, 4332-4338.

(365) Lee, S.-H.; Krimm, S. *Biopolymers* **1998**, *46*, 283-317.

(366) Ozdemir, A.; Lednev, I. K.; Asher, S. A. *Biochemistry* **2002**, *41*, 1893-1896.

(367) Fry, D. C.; Byler, D. M.; Susi, H.; Brown, E. M.; Kuby, S. A.; Mildvan, A. S. *Biochemistry* **1988**, *27*, 3588-3598.

(368) Siedlecka, M.; Goch, G.; Ejchart, A.; Sticht, H.; Bierzynski, A. *Proc. Natl. Acad. Sci. U.S.A.* **1999**, *96*, 903-908.

(369) Overman, S. A.; Thomas, G. J., Jr. *Biochemistry* **1995**, *34*, 5440-5451.

(370) Thomas, G. J., Jr. *Annu. Rev. Biophys. Biomol. Struct.* **1999**, *28*, 1-27.

(371) Tuma, R. *J. Raman Spectrosc.* **2005**, *36*, 307-319.

(372) Fang, C.; Wang, J.; Charnley, A. K.; Barber-Armstrong, W.; Smith, A. B.; Decatur, S. M.; Hochstrasser, R. M. *Chem. Phys. Letters* **2003**, *382*, 586-592.

(373) Fang, C.; Wang, J.; Kim, Y. S.; Charnley, A. K.; Barber-Armstrong, W.; Smith, A. B., III; Decatur, S. M.; Hochstrasser, R. M. *J. Phys. Chem. B* **2004**, *108*, 10415-10427.

(374) Rubtsov, I. V.; Wang, J.; Hochstrasser, R. M. *J. Phys. Chem. A* **2003**, *107*, 3384-3396.

(375) Mix, G.; Schweitzer-Stenner, R.; Asher, S. A. *J. Am. Chem. Soc.* **2000**, *122*, 9028-9029.

(376) Mikhonin, A. V.; Asher, S. A. *J. Phys. Chem. B* **2005**, *109*, 3047-3052.

(377) Topilina, N. I.; Higashiya, S.; Rana, N.; Ermolenkov, V. V.; Kossow, C.; Carlsen, A.; Ngo, S. C.; Wells, C. C.; Eisenbraun, E. T.; Dunn, K. A.; Lednev, I. K.; Geer, R. E.; Kaloyeros, A. E.; Welch, J. T. *Biomacromolecules* **2006**, *7*, 1104-1111.

(378) Xu, M.; Ermolenkov, V. V.; He, W.; Uversky, V. N.; Fredriksen, L.; Lednev, I. K. *Biopolymers* **2005**, *79*, 58-61.

(379) Bykov, S. V.; Lednev, I. K.; Ianoul, A.; Mikhonin, A. V.; Munro, C. H.; Asher, S. A. *Appl. Spectrosc.* **2005**, *59*, 1541-1552.

(380) Overman, S. A.; Thomas, G. J., Jr. *Biochemistry* **1998**, *37*, 5654-5665.

(381) Diem, M.; Lee, O.; Roberts, G. M. *J. Phys. Chem.* **1992**, *96*, 548-554.

(382) Ahmed, Z.; Asher, S. A. *Biochemistry* **2006**, *45*, 9068-9073.

(383) Ahmed, Z.; Beta, I. A.; Mikhonin, A. V.; Asher, S. A. *J. Am. Chem. Soc.* **2005**, *127*, 10943-10950.

2.0 CHAPTER 2. UV RAMAN DEMONSTRATES THAT α-HELICAL POLYALANINE PEPTIDES MELT TO POLYPROLINE II CONFORMATIONS

Work discussed in this chapter is published in *J. Am. Chem. Soc.*, **2004,** *126(27)*, 8433-8440 (Authors: Asher, S. A.; Mikhonin, A. V.; and Bykov, S. V.). We examined the 204 nm UV resonance Raman (UVRR) spectra of the peptide (XAO), which was previously found by Shi et al's NMR study to occur in aqueous solution in a PPII conformation (*Proc. Natl. Acad. Sci. U.S.A.* **2002**, *99*, 9190). The UVRR spectra of XAO are essentially identical to the spectra of small peptides such as A_5 and to the large 21 residue predominantly Ala peptide, AP. We conclude that the non-α-helical conformations of these peptides are dominantly PPII. Thus, AP, which is highly α-helical at room temperature, melts to a PPII conformation. There is no indication of any population of intermediate disordered conformations. We continued our development of methods to relate the Ramachandran Ψ angle to the amide III band frequency. We describe a new method to estimate the Ramachandran Ψ angular distributions from amide III band lineshapes measured in 204 nm UVRR spectra. We used this method to compare the Ψ distributions in XAO, A_5, non-α-helical state of AP and acid denatured apomyoglobin. In addition, we estimated the Ψ angle distributions of peptide bonds which occur in non-α-helix and non-β-sheet conformations in a small library of proteins.

2.1 A NEW PARADIGM IN PROTEIN FOLDING: NON-NATIVE CONFORMATION(S) OF PEPTIDES AND PROTEINS ARE NOT "RANDOM COIL".

The classical view of protein structure and function is that a native protein structure is defined by a single conformation, or a restricted subset of similar conformations, which occur at the minimum (or one of the minima) of the conformational protein energy landscape.[1-7] For many

proteins the native structure is defined as the conformation that an isolated denatured protein evolves into when the chemical environment is altered to favor folding.[8-12] The denatured states are much less defined,[9,13-16] with the likelihood, that numerous states are involved, particular subsets of which are favored by different denaturing environmental conditions. These conformational subsets, as sampled by the peptide bond conformations, are expected to be much smaller than those conformations possible by simply excluding the sterically disallowed peptide bond dihedral angles, which occur in the forbidden portions of the Ramachandran plot.[17] The conformational subspace(s) of the amide bonds of denatured proteins is also expected to be much smaller than the conformational subspace which would remain by additionally excluding all sterically problematic sidechain conformations.[18]

The term "denatured" or "non-native"-state is generally used to denote a variety of protein unfolded states which conformationally differ from that of the biologically active native state. Care is necessary when using these definitions, since unfolded states may have biological function.[19,20] In many cases the denatured structure is expected to have a random secondary structure, where the backbone randomly adopts energetically allowed Ψ and Φ Ramachandran angles, since it has been thought, until recently, that conformational correlations should not exist between adjacent peptide bonds.[21] In this case, for a random coil peptide sequence there would be no correlation in peptide bond conformations between adjacent or distant peptide bonds. It should be mentioned however, that this assumption has been recently questioned.[22-27]

Evidence has recently been presented which indicates that even small peptides have defined solution backbone conformations, and that the "random coil conformation" approximation is invalid even for small peptides such as dialanine.[28,29] These new data have resurrected the early arguments by Tiffany and Krimm[30] that CD spectra indicate a nonrandom secondary structure for poly-glutamic acid and poly-lysine peptides, whose structure was proposed to resemble the poly-proline II type helical structure (PPII-helix, or 3_1-helix). This PPII left-handed backbone helical structure shows Ψ and Φ angles of 145° and -75° respectively, with 3 residues per helical turn.

The unfolded states of other small peptides such as A_3,[31,32] A_7,[33] K_7,[34] and much larger peptides such as poly-L-lysine[35,36], poly-L-glutamic acid[35,36] and poly-L-glutamate[36] and poly-L-aspartate peptides[36] have also been reported to adopt locally ordered PPII-helical conformations.

Evidence for local order has also appeared in VCD studies of high molecular weight poly-L-lys and poly-L-glutamic acid.[37] In addition, researchers have recently presented evidence that the so-called unordered regions of native proteins contain considerable amount of PPII structure.[35,38-40] The recent excellent reviews discussing PPII conformations by Shi et al.[41] and Bochicchio et al.[42] should also be consulted for recent views regarding the importance of the PPII structure. In addition, Blanch et al.[43] recently used Raman Optical Activity to examine melting of lysozymes and a 21 amino acid alanine rich peptide, and found evidence for melting to a PPII conformation.

In this Chapter, we used UV Raman spectroscopy[44,45] to examine the melting of a 21-residue A-based peptide AAAAA(AAARA)$_3$A (AP) which contains three R to confer solubility.[46,47] We find that the melting occurs from an α-helix to a mainly PPII conformation. We find no evidence for a "random coil" conformation. The fact that the melting involves a transition mainly between two defined conformations calls into question the validity of the models[48,49] typically used to model α-helix folding and unfolding. These models assume a large entropic penalty for α-helix nucleation, since they imagine the nucleus requires the conformational constraint of four residues from a high-entropy random coil conformational state in order to begin the growth of longer α-helices. It appears that the α-helix nucleation is not as entropically expensive as proposed, since the conformational change involves transitions between restricted peptide conformational subspaces, between the PPII state(s) to the α-helix-like nucleus. These considerations may dramatically change modeling of the folding and unfolding of α-helices, at least for AP-type peptides.

2.2 EXPERIMENTAL SECTION

2.2.1 Sample preparation

The 21-residue alanine-based peptide AAAAA(AAARA)$_3$A (AP) was prepared (HPLC pure) at the Pittsburgh Peptide Facility by using the solid-state peptide synthesis method. The AP solutions in water contained 1 mg/ml concentrations of AP, and 0.2 M concentrations of sodium

perchlorate, which were used as internal intensity and frequency standards[46,47]. All Raman spectra were normalized to the intensity of the ClO_4^- Raman band (932 cm^{-1}).

A_5 and A_3 peptides were purchased from Bachem Bioscience Inc. (King of Prussia, PA), and used as received. The $A_5 - A_3$ Raman difference spectral measurements utilized identical molar concentrations of A_5 and A_3 (0.34 mg/ml and 0.2 mg/ml, respectively) in solutions containing identical sodium perchlorate concentrations (0.2 M). We normalized the Raman spectra to the intensity of the 932 cm^{-1} perchlorate internal standard band. The $A_5 - A_3$ difference spectra were calculated by subtracting the normalized A_3 spectrum from the normalized A_5 spectrum at each temperature.

The undecapeptide XAO (MW=985) was prepared (HPLC pure) at the Pittsburgh Peptide Facility by using the solid-state peptide synthesis method. The sequence of this peptide is Ac-XXAAAAAAAOO-amide, where all amino acids are in their L form, A is alanine, X is diaminobutyric acid (side chain $CH_2CH_2NH_3^+$), and O is ornithine (side chain $(CH_2)_3NH_3^+$). We used 1 mg/ml solutions of XAO-peptide containing 0.15 M of sodium perchlorate. The UVRR spectra of XAO were also normalized to the ClO_4^- Raman band intensity.

Horse heart metmyoglobin (holoMb) was purchased from Sigma Chemical Co. (St. Louis, MO). ApoMb was made by a 2-butanone extraction of the heme using the procedure of Teale[50], followed by Sephedax-25 gel chromatography. Absorption measurements indicate that >99% of the heme was removed. The apoMb was lyophilized and stored at -20°C. We used 200 μM apoMb solutions (~3 mg/ml) for the steady state Raman measurements. The apoMb sample pH was adjusted to the desired value (pH=1.86) by using HCl. Concentrations were determined from UV absorption spectra by using a molar absorptivity of 14,260 $M^{-1}cm^{-1}$ at 280 nm.[51,52]

2.2.2 Instrumentation

The UV Resonance Raman instrumentation has been described in detail elsewhere.[46,47] A Coherent Infinity Nd:YAG laser produced 355 nm (3^{rd} harmonic) 3 nsec pulses at 100 Hz. This beam was Raman-shifted to 204 nm (5^{th} anti-Stokes) by using a 1 m tube filled with hydrogen (60 psi). A Pellin Broca prism was used to select the 204 nm excitation beam. The Raman scattered light was imaged into a subtractive double spectrometer[53] and the UV light was detected by either a Princeton Instruments solar blind ICCD camera or a Roper Scientific

unintensified, backthinned, liquid nitrogen-cooled CCD camera. All samples were measured in a thermostatted free surface flow stream.

2.3 RESULTS AND DISCUSSION

2.3.1 UV Raman Spectra of PPII XAO Indicate that Melted AP is in a PPII Conformation

Shi et al.[33] carefully measured the temperature dependence of the NMR spectra of XAO peptide, and definitively showed that at 2 °C the structure in water was mainly PPII helix (with no more than 10 % β-strand). The structure remained dominantly PPII helix at 52 °C, with a ~12 % increase in β-strand concentration. We compared the UV resonance Raman spectrum of XAO to the melted form of AP, a 21-amino acid mainly Ala peptide. Fig. 15 shows the 204 nm UV Raman spectra of XAO-peptide between 0 and 80 °C. 204 nm excitation occurs within the $\pi \rightarrow \pi^*$ transitions of the amide peptide bonds.[54] Excitation into these electronic transitions mainly enhances the vibrations of the amide backbone.[55-58]

The XAO UV Raman spectra are essentially invariant with temperature. At 20 °C the spectra[46,47] show the AmI band (~1657 cm^{-1}, mainly C=O stretching of the peptide bond), the AmII band (~1550 cm^{-1}, CN-stretch and NH-bending) and the C_α-H sb doublet (~1388 and 1365 cm^{-1}, a symmetric bending vibration which is enhanced due to coupling with the AmIII vibration). The amide III spectral region is very complex[59-62] and normally is considered to have a number of contributing bands which also derive from CN-stretch and NH-bending as well as other amide coordinates. We described in detail the assignment of these bands,[63] but here only enumerate two of the important amide III-region bands, the $AmIII_2$ (~1302 cm^{-1}) and the $AmIII_3$ (~1244 cm^{-1}) bands.[64]

The frequency of the amide III bands and the resonance Raman enhancement of the C_α-H sb bands depends mainly on the degree of coupling between C_α-H sb and N-H sb motions, which strongly depends on the amide bond Ψ angle.[65] The lowest amide III_3 band frequencies and the strongest mixing were originally expected[65] at Ψ ~ 180°, where the C_α-H and N-H bonds are cis.

In contrast, essentially no mixing occurs for Ψ = -60° (α-helix Ψ-angle), where the C_α-H and N-H bonds are trans.[65]

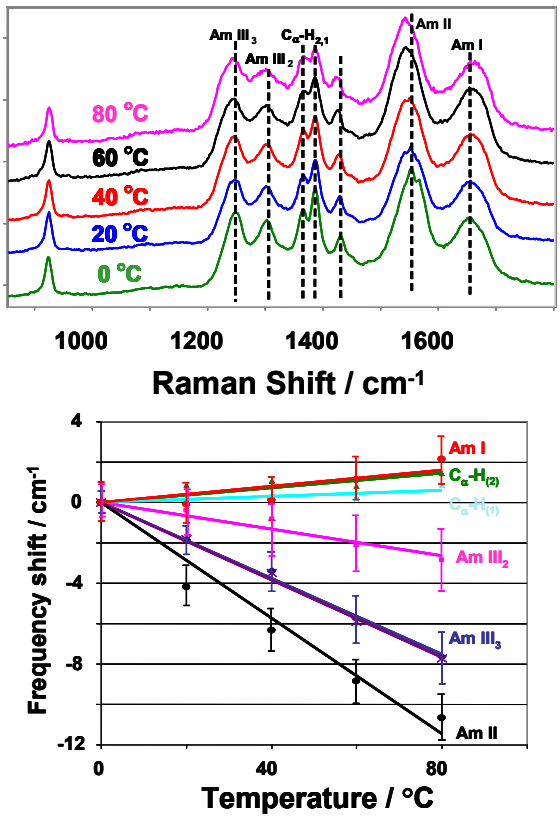

Figure 15. **A)** 204 nm UVRR spectra of PPII-helical XAO-peptide at 0, +20, +40, +60, and +80 °C. **B)** Temperature dependence of PPII-helix UVRR bands. The contribution of the broad water bending band centered at ~1630 cm^{-1} and the sharp O_2 stretching band at 1556 cm^{-1} have been numerically removed.

The low frequency of the amide III bands and the strong enhancement of the C_α-H sb vibration in XAO are fully consistent[65] with the PPII conformation (Ψ ~145°) determined by NMR. However, this low frequency could also be consistent with a β-strand conformation. The lack of a temperature dependence of the UV Raman spectra, except for the small monotonic frequency shifts[46] discussed below in detail, indicates a single, essentially invariant secondary structure conformation.

The band positions and the spectral shape of the XAO UV Raman spectra are very similar to those observed for unfolded state of the ala-based AP-peptide (Fig. 16) and the $A_5 - A_3$ difference spectra.[46] The main difference is that XAO-peptide spectrum shows a decreased $AmIII_3$ frequency (1240 cm^{-1} at +60 °C) and a smaller relative intensity compared to both AP

(1247 cm^{-1} at +62 °C) and $A_5 - A_3$ (1250 cm^{-1} at +50 °C). This frequency shift could result from small differences in the Ψ angles from their normal PPII values of 145°.

Asher et al's study[65] of the Ψ and Φ dependence of the AmIII vibrational frequencies exposed the simple relationship: $\upsilon \sim \upsilon_o + A \sin(\Psi - \delta)$, where υ is the calculated AmIII frequency, υ_o is the AmIII frequency baseline, A is the amplitude of the frequency dependence on Ψ, and δ is the relative phase of the sine curve with respect to Ψ. As discussed below (Eqn. 4) we have fit this relationship to new solution and crystal Raman data and find that this 7 cm^{-1} frequency increase in AP could result from a ~10° increase to Ψ = 155°.

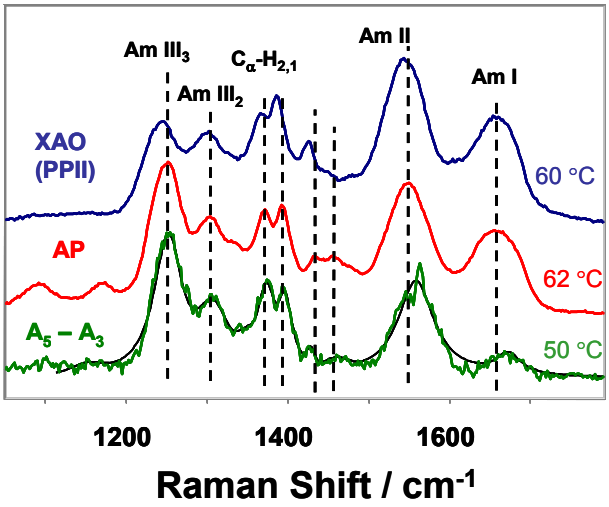

Figure 16. Comparison of 204 nm Raman spectra of predominantly PPII-helical XAO-peptide at +60 °C, to that of non-α-helical AP at +62 °C, and $A_5 - A_3$ at +50 °C.

It is, however, more likely that the spectral differences between AP and XAO derive from the ~50% XAO amide bonds contributed by non-ala amino acids, which are likely to influence the Φ angle as shown by Ianoul et al.[66] This could decrease their $AmIII_3$ frequencies, which would broaden the band and decrease the peak height as observed here. Mirkin & Krimm[67] also demonstrated that the AmIII frequency depends upon both the Ψ- and Φ-angles rather than the Ψ-angle alone.[68]

The temperature dependence of the XAO UV Raman band frequencies (Fig. 15 and Table 4) is essentially identical to that of AP (within experimental precision[46]). The XAO AmII band shows a -0.14 cm^{-1}/K temperature coefficient while the $AmIII_3$ band shows a somewhat

smaller -0.10 cm^{-1}/K coefficient, as shown in Table 4. The C_α-H bending shows no temperature dependence (within experimental error), while the AmI bands show small positive coefficients.

Table 4. Temperature dependence of amide UV Raman bands for different unfolded (non-α-helical) poly-peptides compared to that of PPII-helical XAO-peptide.

	XAO-peptide (>80% PPII-helical), neutral pH		Ala_5 – Ala_3 "random coil", neutral pH		AP, Non-α-helical, neutral pH		Unfolded Apo-Mb pH=1.86 (<20% α-helix)	
	dν/dT	$\nu_{60℃}$, cm^{-1}	dν/dT	$\nu_{50℃}$, cm^{-1}	dν/dT	$\nu_{60℃}$, cm^{-1}	dν/dT	$\nu_{56℃}$, cm^{-1}
AI	0.02 ± ±0.01	1659	0.052± ±0.02	1667	0.052± ±0.02	1659	0.06 ± ±0.01	1671
AII	-0.14± ± 0.01	1545	-0.14 ± ± 0.01	1558	-0.14 ± ± 0.01	1548	-0.17 ± ± 0.04	1550
$C_\alpha H_{(1)}$	0.008± ±0.016	1388	-0.015± ± 0.02	1397	-0.015± ± 0.02	1399	-0.02 ± ± 0.04	1393
$C_\alpha H_{(2)}$	0.018± ±0.017	1365	-0.01 ± ± 0.02	1373	-0.01 ± ± 0.03	1377 broad	N/A	1378 broad
$AIII_2$	-0.03 ± ± 0.02	1300	-0.03 ± ± 0.01	1305	-0.03 ± ± 0.01	1311	-0.05 ± ±0.04	1295
$AIII_3$	-0.10 ± ± 0.02	1241	-0.094± ± 0.018	1250	-0.094± ± 0.018	1247	-0.11 ± ± 0.03	1240

As discussed in detail elsewhere,[69,70] this spectral dependence derives from a weakening of the hydrogen bonding of water to the amide carbonyl and N-H groups. The hydrogen bonding coordinate is anharmonic, which results in an increased water-to-amide hydrogen bond length as the temperature increases (Fig. 17). The consequent decrease in hydrogen bond strength,

increases the contribution of the Fig. 17b resonance form, which would decrease the AmII and AmIII band frequencies and would increase the AmI band frequency, as observed.

The identical amide band frequency temperature dependencies for AP, A_5-A_3 and XAO clearly indicate essentially identical exposures to water and identical backbone hydrogen bonding to water. ***All of these results force us to conclude that non-α-helical AP, and the inner peptide bonds of A_5 occur in PPII-like conformations.*** Although we find that non-α-helical AP occurs in a predominantly PPII-helix conformation, this does not mean that the PPII-helix conformation spans the entire AP length. Rather it is more likely that stretches of PPII-helix occur which are separated by β-turns, for example.

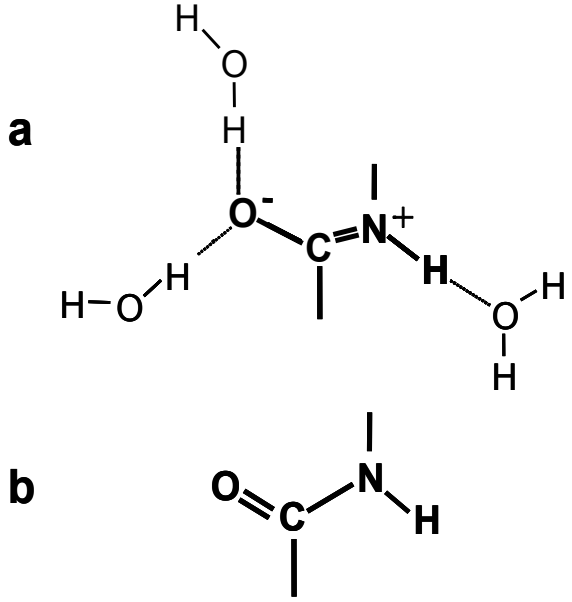

Figure 17. Resonance forms of amide peptide bond. Hydrogen bonding stabilizes resonance form a, which stabilizes C-O single bonding and C=N double bonding.

2.3.2 AP Melts from an α-Helix to a mainly PPII Conformation

The Fig. 18 temperature difference spectra between 60 °C and 0 °C for XAO and non-α-helical AP peptides are very similar. This AP difference spectrum was modeled from Lednev et al's data[46] by numerically removing the α-helix contribution from the 0 °C AP spectrum.

AP is 55% α-helical at 0 °C. The helix melts as the temperature increases. Lednev et al's kinetic measurements[46,47] showed that α-helical AP melts in the ~200-nsec time regime following 3-nsec T-jumps. They found that the transient AP difference spectra at the shortest (~14 nsec) times look identical to the equilibrium temperature difference spectra for the non-α-helical form of AP between the two temperatures (compare Fig. 18 to Fig. 3 of Lednev et al.[47]). Thus, these spectral changes were interpreted to result from the T-induced difference spectra of the "disordered" form of AP, which we can now ascribe to the mainly PPII conformations of a fraction of the AP chains. Only at times >50 nsec do spectral changes appear which indicate melting of α-helices to a conformation which is predominantly PPII. We see no evidence of any additional intermediate conformations. Whatever the reaction pathway, the melting from α-helix to PPII is fast.

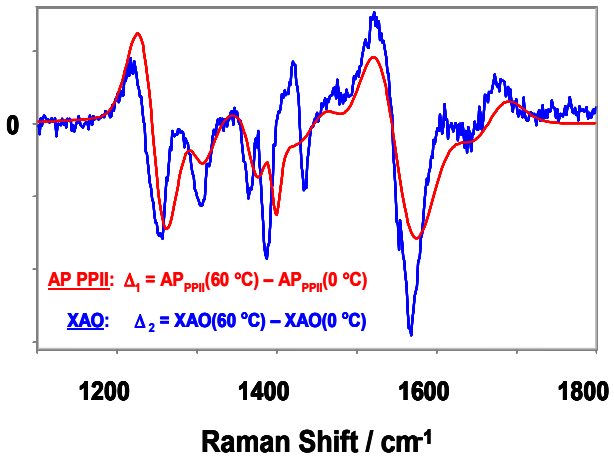

Figure 18. UV Raman difference spectra between +60 °C and 0 °C for the PPII conformation of XAO and that of AP.

2.3.3 Temperature Dependence of Amide Frequencies

Recent studies have also demonstrated that small peptides adopt the PPII structure in solution.[31-33] Fig. 19 shows the temperature dependence of the Raman difference spectra between Ala_5 and Ala_3 (A_5-A_3). This difference spectrum removes the spectral contributions of the penultimate amide bonds and allows us to concentrate on the two central amide bonds of Ala_5. As noted by Lednev et al.[46] these A_5-A_3 spectra are very close to the spectra of non α-helical AP (PPII structure). In fact they show the same temperature dependence of the amide frequencies. This

allows us to conclude that the interior amide bonds of Ala_5 are predominantly in a PPII conformation.

A similar PPII type spectrum can also be obtained from proteins denatured at low pH. For example, Fig. 20 shows the 204 nm UV Raman spectra of apoMb at pH=1.86 and +25 °C (<20% α-helix). Essentially, all α-helices have melted. The unfolded apoMb spectrum is close to that of XAO and AP, suggesting significant population of the PPII conformation in this unfolded protein. However, the amide bands are broad, and the higher frequency $AmIII_3$ shoulder indicates additional contributions from non PPII conformations.

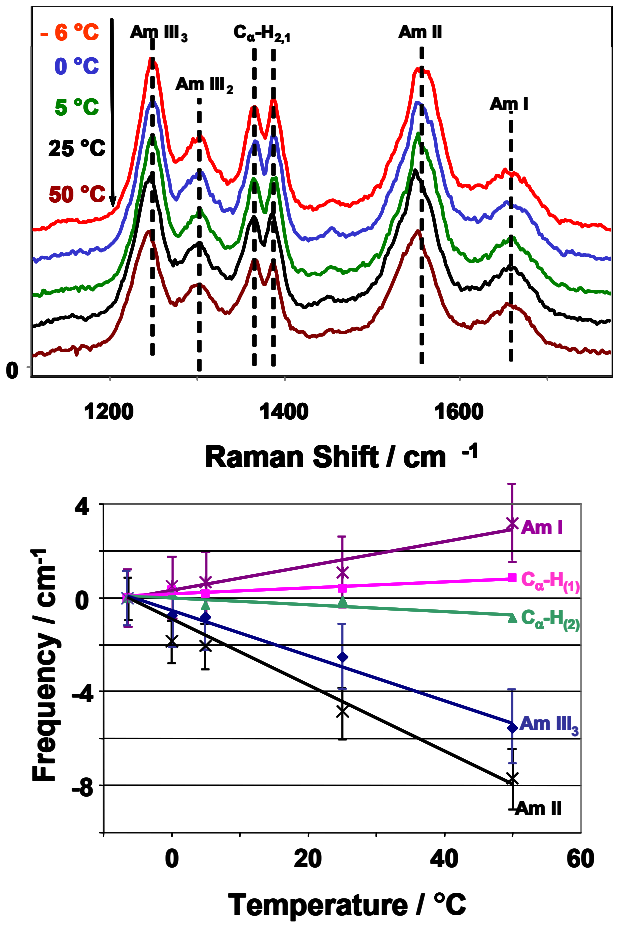

Figure 19. Temperature dependence of $A_5 - A_3$ 204 nm Raman difference spectra and temperature dependence of the $A_5 - A_3$ amide band frequencies.

2.3.4 UVRR Frequency Dependence of Disordered Peptide Bonds of Folded Proteins

The UV Raman spectra of "disordered segments" of folded proteins show little evidence of PPII conformations. Fig. 20 shows the UV Raman basis spectrum of the disordered conformations of the library of native proteins measured by Chi et al.[71] The UV Raman spectra from this protein library were found to have three main factors which completely determined its spectral features, the α-helix, β-sheet and "unordered" forms. Since the conformations of all of these proteins were known from x-ray diffraction, we were able to calculate the basis spectra of the three contributing secondary structure motifs, the α-helix, β-sheet and "unordered" conformations of these folded proteins.

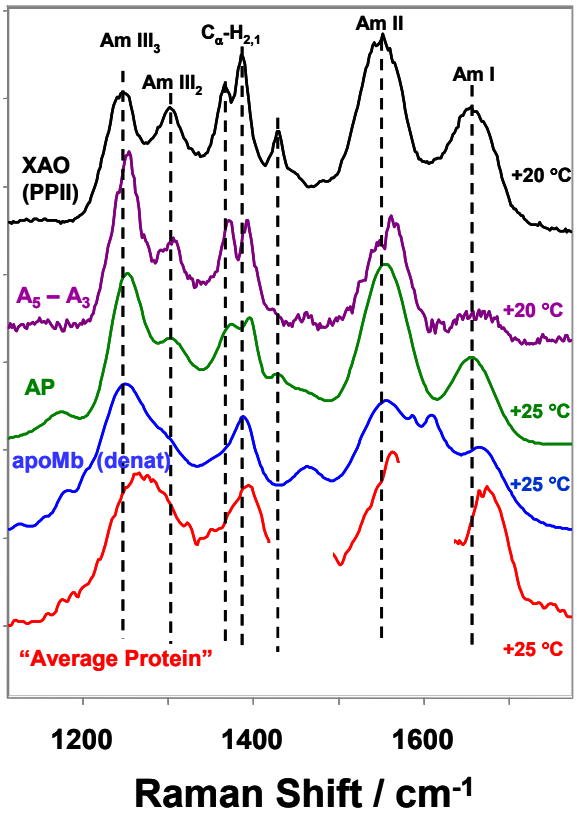

Figure 20. Comparison of 204 nm PPII-helical XAO spectrum (+20 °C) to the spectra of non-α-helical structures for different peptides and proteins: $A_5 - A_3$ (+20 °C), AP (+25 °C), acid denatured apoMb (pH=1.86, +25 °C), "average protein" (+25 °C). The "average protein random coil" spectrum is the average UV Raman spectrum obtained for non-α-helical and non-β-sheet secondary structures in a library of 13 native proteins[71].

The UV Raman basis spectrum of the "disordered" peptide bonds is extremely broad. For example, the AmIII band spans the 1220 – 1320 cm^{-1} spectral region. This frequency span is likely to result from a subset of amide bonds with Ψ and Φ angles spanning a broad region of angles within the Ramachandran dihedral angle plane.

We could use these spectral data to determine the range of Ψ and Φ angles if we knew the homogeneous linewidth of the $AmIII_3$ bands and the dependence of the center frequencies on the Ψ and Φ angles. We can estimate the intrinsic homogeneous linewidth of the bands from UV Raman spectra of crystals of peptides.

2.3.5 Determination of Amide Band Homogeneous Linewidth

Fig. 21 shows the 229 nm Raman spectra of a powder of Gly-Ala-Leu trihydrate crystals grown out of a methanol-water mixture[72] (for which we have also determined a crystal structure). In addition, Fig. 21 shows the Raman spectrum of a powder of Gly-Ala-Leu directly out of the Bachem Company bottle. This powder is claimed by Bachem to result from drying an aqueous solution of Gly-Ala-Leu.

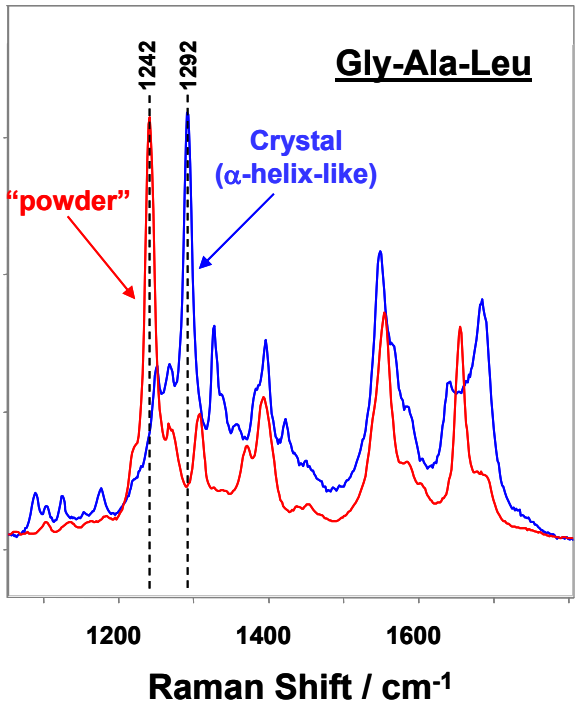

Figure 21. Comparison of 229 nm Raman spectrum of crystal Gly-Ala-Leu · $3H_2O$ ({Ψ,Φ}={-40°,-67°}) to that of "powder" Gly-Ala-Leu

The X-ray diffraction crystal structure[72] of this Gly-Ala-Leu-trihydrate crystal shows that the Ala-Leu peptide bond has α-helix-like Φ and Ψ angles (-67°, -40°). As expected, the Raman spectrum of the trihydrate crystal shows a high-frequency, sharp α-helix-like Am III_3 band at 1292 cm^{-1}. The Gly-Ala-Leu powder from Bachem shows a similar sharp $AmIII_3$ band, which is shifted 50 cm^{-1} to lower frequency. We do not know the peptide structure in this powder. However, the $AmIII_3$ frequency is consistent with a more planar β-strand-like or PPII-like conformation.

Since the trihydrate crystal shows a single well defined hydrogen bonding geometry, the observed Raman bandwidths should be close to that of the homogeneous linewidth of the Raman band (assuming identical dephasing rates in the crystal and in solution). Both the trihydrate crystal and the Bachem powder show $AmIII_3$ bandwidths of 15 cm^{-1} (full width at half height). This bandwidth is significantly larger than our spectral resolution of 6 cm^{-1}. Thus, assuming a Lorentzian bandshape we calculate 7.5 cm^{-1} homogeneous linewidths. The fact that the Bachem powder shows a similar narrow bandwidth indicates that the peptide also occurs in a single well-defined conformation in this powder environment.

2.3.6 Deconvolution of $AmIII_3$ Frequency Distribution for Non-α-helical States of Peptides and Proteins

Given this homogeneous linewidth, we can very roughly estimate the distribution of Ψ angles, by neglecting the dependence of the $AmIII_3$ frequencies on the Φ angle. Previous works by both ourselves and others have shown a much smaller AmIII band frequency dependence on the Φ angle than on the Ψ angle.[65-67] Further, only a very limited region of Φ angles can be populated due to steric constraints. We note that our argument also neglects the unlikely possibility that major contributions occur from Φ angles which occur in the left handed α-helix conformation.

We assume that the inhomogeneously broadened experimentally measured $AmIII_3$ band profile, A(ν) is the sum of M single Lorentzian bands with identical homogeneous linewidths, Γ, with different center frequencies, νe_i :

$$A(\nu) = \pi^{-1} \sum_{i=1}^{M} L_i \cdot \frac{\Gamma^2}{\Gamma^2 + (\nu - \nu e_i)^2} \qquad \textbf{(3)}$$

where L_i is the probability for a band to occur at frequency νe_i.

We deconvoluted the measured XAO, AP, acid denatured apoMb, and average disordered protein spectra into their population distributions of identical 7.5 cm^{-1} Lorentzians. Fig. 22 shows histogram plots of the underlying spectral probability distributions. $A_5 - A_3$ shows the narrowest distribution of frequencies, while the "protein library" shows the broadest. AP is similar to XAO except that it is shifted to higher frequency. Acid denatured apoMb shows a broad range of frequencies, however, it shows a significant maximum around the PPII frequencies.

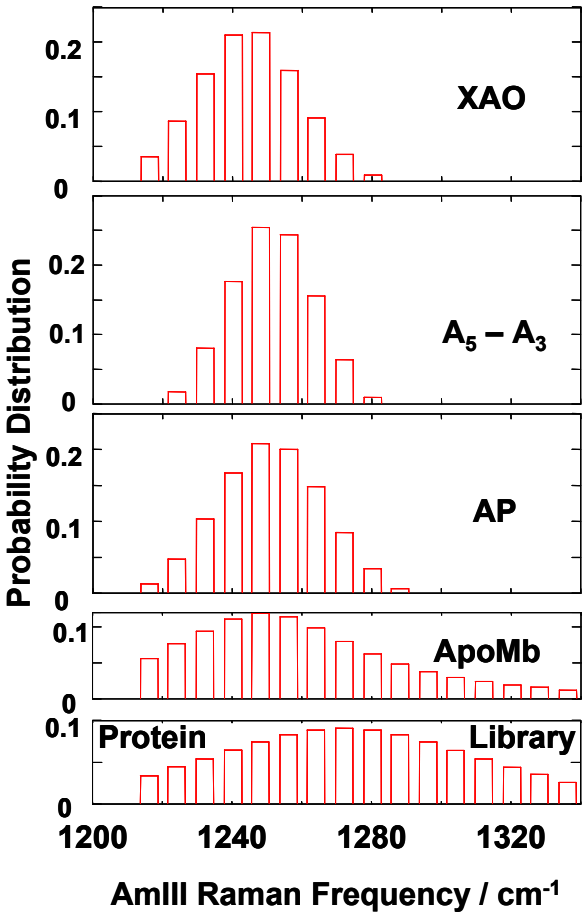

Figure 22. Deconvolution of homogeneously broadened $AmIII_3$ Raman bandshape from Fig. 20 of XAO, $A_5 - A_3$, non-α-helical AP, acid denatured apoMb, and "disordered" protein conformations. The resulting histogram shows the population distribution associated with the plotted $AmIII_3$ frequencies.

These deconvolutions also assume that the Raman cross sections of these bands are independent of frequency (i.e. Ψ angle independent). This is a reasonable assumption, since the only major amide band cross section dependence observed, to date, is for the α-helix

conformation, which appears to result from hypochromic α-helix excitonic interactions by the resonance electronic transitions.[54,55,73-76] This cannot occur here because no extended α-helices contribute, and each amide bond scatters independently.[77,78] The only possible Raman cross section dependence would occur in the presence of a large normal mode composition dependence on the band frequency.

2.3.7 Quantitative Correlation of Ψ and the $AmIII_3$ Frequency

We previously used Gaussian 98W to calculate the Ψ dihedral angle dependence of the amide III frequency of alanine methylamide in vacuum.[65] The frequency dependence was carried out by fixing Ψ at the angles of interest and then optimizing the geometry of the peptide at each angle. The vibrational frequencies were determined for each optimized geometry. We found a sin Ψ dependence: $\upsilon = \upsilon_o + A \sin (\Psi + a)$.

This equation is likely to only roughly estimate the correlation between the $AmIII_3$ frequency and the Ψ angle. However, it appears to capture the physics of the frequency dependence in that it calculates the Ψ angular of the coupling of the $AmIII_3$ vibration with Cα-H bending. It predicts a sinusoidal relationship which correlates with the projection of N-H and Cα-H sb motion. The parameters found from the theoretical fit can be made more predictive for peptides in water by refitting this equation to experimental data for peptide bonds at known Ψ angles. Thus, we fit the expression to three points: the α-helix-like peptide gly-ala-leu-trihydrate with Ψ = -40° and ν_{III3} = 1292 cm^{-1}; the XAO peptide in water in the PPII state with Ψ = 145° and 1242 cm^{-1}; and poly-L-lysine, poly-L-glutamic acid mixture (which forms a β-sheet[69]), with Ψ = 120° and 1227 cm^{-1}. We obtain:

$$\mathbf{\upsilon = 1265\ cm^{-1} - 46.8\ cm^{-1} \sin (\Psi + 5.2°).} \qquad \mathbf{(4)}$$

We can then use the preliminary Eqn. 4, which we will further refine and generalize in Chapter 5, to analyze the Fig. 22 frequency distributions to roughly estimate the Ψ angle distribution of our peptides and proteins (Fig. 23).

We are aware that Mirkin and Krimm[67] calculations show a significant dependence of the AmIII band frequency on the Φ angle. They point out that this dependence will tend to confound a simple correlation relationship such as Eqn. 4, proposed here. However, the Ψ dependence still generally dominates the Ψ, Φ dependence in the allowed regions of Ramachandran plot (see

Chapter 5 for detail). The relationship in Eqn. 4 derives from a theoretical dependence that captures the physics of the coupling of C_α-H and N-H motions, which is then empirically fit to spectral data for particular known conformations. The proposed relationship is likely to span the region of the β-sheet, PPII and α-helical conformations discussed here and lead to rough estimates of Ψ angles. We will further refine and generalize the Eqn. 4 in Chapter 5.

Our approach here is used to estimate the correlation between the AmIII frequency and the Ψ angle. For AP we find Ψ=152 ± 26°. The distribution in Ψ suggests significant population of β-strand conformations. This would be consistent with Sreerama and Woody's molecular dynamics calculation of A_8,[79] which indicated that each amide bond populates both the PPII and β-strand conformations. However, the β-strand was found to be 2-to 3-fold less populated than is the PPII conformation.

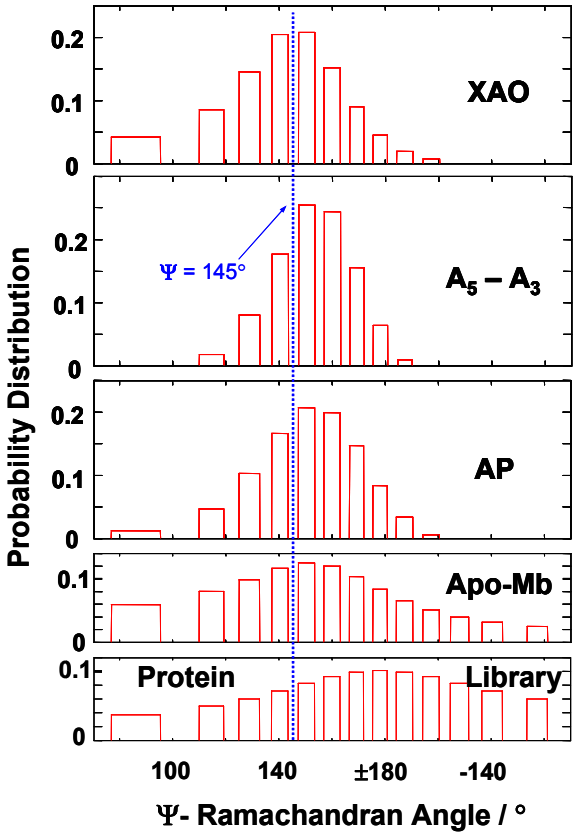

Figure 23. Estimated Ψ-Ramachandran angle distribution of XAO, A_5 – A_3, non-α-helical AP, acid denatured apoMb, and "disordered" state of an "average protein" (from a library of folded proteins)

The Ψ angle distribution found for the non α-helix and non-β-sheet protein library spectrum indicates that a large range of Ψ angles are populated (80° to 180° and –180° to –120°). These include even angles outside the normally allowed range of 40°<Ψ<180° and -180°<Ψ<-160° for unconstrained amide bonds. This large range of amide bonds Ψ angles is expected since the folded protein structures utilize packing constraints to create these unusual dihedral angles.

2.3.8 Transient melting of AP α-helix to PPII

Fig. 24, which was adapted from Fig. 3 of Lednev et al.[47] shows the time dependence of the UVRR spectral changes induced by a T-jump between 4 and 35 °C for AP in water. We can now interpret this data in terms of α-helix→PPII transition, rather than to a random coil conformation. A careful measurement of the frequency of the difference peak finds it identical to that in the steady state spectrum (top) indicating the dominant conformation is to a state with Ψ= 150°, almost certainly PPII.

At short delay times (≤ 40 ns) we only see features, which are due to changes in the temperature dependent hydrogen bonding strength between PPII AP and water. These spectral changes are not associated with α-helix → PPII conformational transition.[47] These features show up immediately after the IR heating pulse, and stay constant until α-helix melting (discussed below) begins at longer delay times (≥ 50 ns) in AP difference spectra. These short delay time spectral changes (Fig. 24) are identical to the difference spectra shown in Fig. 18.

It was shown earlier,[46,47] that the 1236, 1374, 1534, and 1678 cm^{-1} difference spectral features are contributed by the population of AP non-α-helical conformations. We now conclude that these spectral features derive from PPII conformations. The relative contributions of PPII conformations increase in the difference spectra at delay times longer than 40-50 ns. At ~ 400 ns the spectral evolution is complete and the difference spectra becomes identical to all the difference spectra at longer delay times, as well as to steady state difference spectrum between 4 and 35 °C, which can be considered as a difference spectrum with an “infinite” delay time.

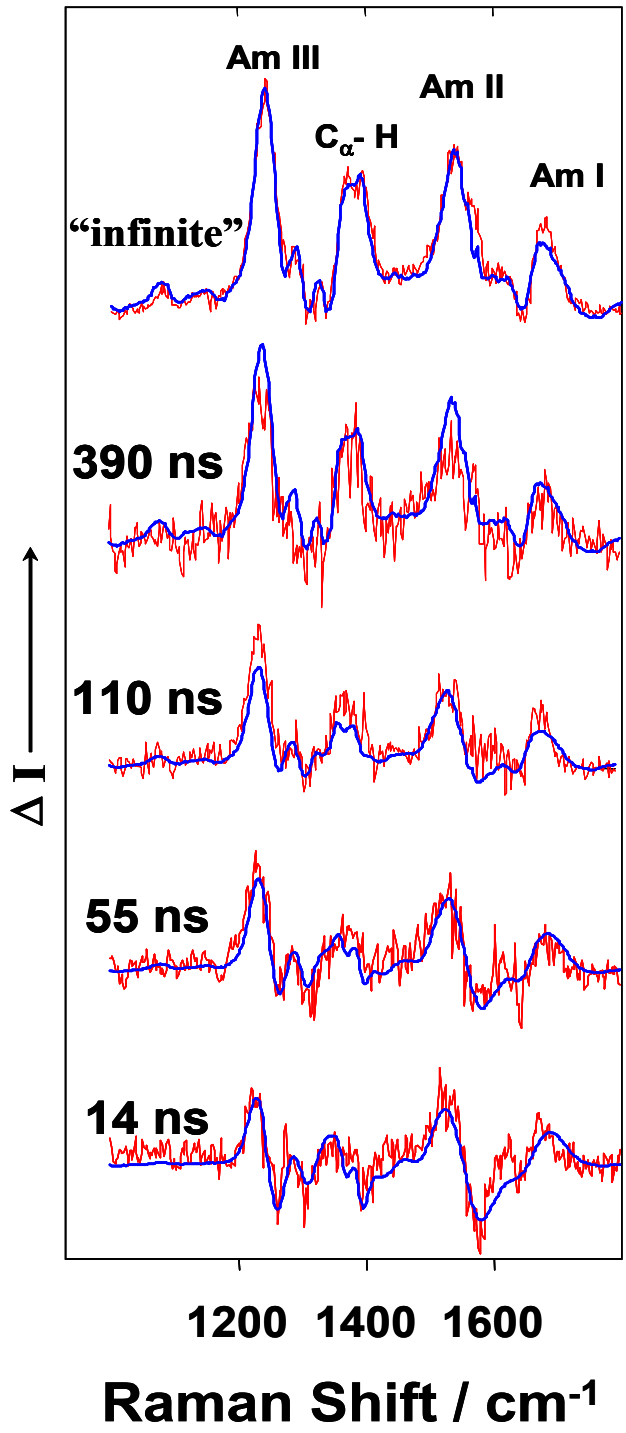

Figure 24. AP UVRR spectrum (top curve) measured in H_2O at 4 °C and transient difference UVRR of AP solution initially at 4 °C at different delay times after T-jump of ~31 °C. The steady state difference UVRR spectrum between 35 and 4 °C is equivalent to the transient difference spectrum at infinite delay time. Adapted from Fig. 3 of Lednev et al.[47]

2.4 CONCLUSIONS

Numerous groups recently demonstrated the occurrence of PPII conformations in large and small peptides. We verified these conclusions for small peptides as well as for a 21 residue, mainly Ala peptide, which exists below room temperature as a mixture of α-helix and PPII helix. AP is mainly in an α-helix conformation at 0 °C and is mainly in a PPII conformation above room temperature. AP undergoes a thermal melting transition between the α-helix and a PPII conformation without any evidence of other significantly populated intermediates. This a distinctly different transition than envisioned by previous theoretical methods which considered a melting transition from an ordered α-helical state to a disordered state.

We developed a method to estimate the Ramanchandran Ψ angle from the AmIII frequency of peptide bonds in water solution (which we will further improve in the Chapter 5 taking into account the hydrogen bonding of a peptide bond). This has allowed us to estimate the Ψ angle distribution in small and large peptides and in acid denatured apoMb. We also estimated the distribution of Ψ angles in disordered regions of folded proteins. As expected, we find population of Ψ angles in the disordered amide bonds of folded proteins that are normally disallowed for unconstrained peptide bonds.

2.5 REFERENCES

(1) Chan, H. S.; Dill, K. A. *Proteins* **1998**, *30*, 2-33.

(2) Dill, K. A. *Biochemistry* **1990**, *29*, 7133-7155.

(3) Pokarowski, P.; Kolinski, A.; Skolnick, J. *Biophys. J.* **2003**, *84*, 1518-1526.

(4) Jewett, A. I.; Pande, V. S.; Plaxco, K. W. *J. Mol. Biol.* **2003**, *326*, 247-253.

(5) Hardin, C.; Eastwood, M. P.; Prentiss, M.; Luthey-Schulten, Z.; Wolynes, P. G. *J. Comp. Chem.* **2002**, *23*, 138-146.

(6) Alm, E.; Baker, D. *Proc. Natl. Acad. Sci. U.S.A.* **1999**, *96*, 11305-11310.

(7) Socci, N. D.; Onucic, J. N.; Wolynes, P. G. *Proteins* **1998**, *32*, 136-158.

(8) Anfinsen, C. B. *Science* **1973**, *181*, 223-230.

(9) Mayor, U.; Guydosh, N. R.; Johnson, C. M.; Grossmann, J. G.; Sato, S.; Jas, G. S.; Freund, S. M. V.; Alonso, D. O. V.; Daggett, V.; Fersht, A. R. *Nature* **2003**, *421*, 863-867.

(10) Myers, J. K.; Oas, T. G. *Annu. Rev. Biochem.* **2002**, *71*, 783-815.

(11) Mirny, L.; Shakhnovich, E. *Annu. Rev. Biophys. Biomol. Struct.* **2001**, *30*, 361-396.

(12) Englander, S. W. *Annu. Rev. Biophys. Biomol. Struct.* **2000**, *29*, 213-238, 213 Plates.

(13) Shortle, D. *Curr. Opin. Struct. Biol.* **1993**, *3*, 66-74.

(14) Daura, X.; Glattli, A.; Gee, P.; Peter, C.; Van Gunsteren, W. F. *Adv. Prot. Chem.* **2002**, *62*, 341-360, 343 plates.

(15) Van Gunsteren, W. F.; Burgi, R.; Peter, C.; Daura, X. *Angew. Chem. Intl. Edition* **2001**, *40*, 352-355.

(16) Fiebig, K. M.; Schwalbe, H.; Buck, M.; Smith, L. J.; Dobson, C. M. *J. Phys. Chem.* **1996**, *100*, 2661-2666.

(17) Ramachandran, G. N.; Sasisekharan, V. *Adv. Prot. Chem.* **1968**, *23*, 283-438.

(18) Shortle, D. *Protein Sci.* **2002**, *11*, 18-26.

(19) Gast, K.; Damaschun, H.; Eckert, K.; Schulze-Forster, K.; Maurer, H. R.; Mueller-Frohne, M.; Zirwer, D.; Czarnecki, J.; Damaschun, G. *Biochemistry* **1995**, *34*, 13211-13218.

(20) Penkett, C. J.; Redfield, C.; Jones, J. A.; Dodd, I.; Hubbard, J.; Smith, R. A.; Smith, L. J.; Dobson, C. M. *Biochemistry* **1998**, *37*, 17054-17067.

(21) Flory, P. J. *Statistical Mechanics of Chain Molecules*, 1969.

(22) Pappu, R. V.; Srinivasan, R.; Rose, G. D. *Proc. Natl. Acad. Sci. U.S.A.* **2000**, *97*, 12565-12570.

(23) Srinivasan, R.; Rose, G. D. *Proc. Natl. Acad. Sci. U.S.A.* **1999**, *96*, 14258-14263.

(24) Marqusee, S.; Robbins, V. H.; Baldwin, R. L. *Proc. Natl. Acad. Sci. U.S.A.* **1989**, *86*, 5286-5290.

(25) Pal, D.; Suhnel, J.; Weiss, M. S. *Angew. Chem., Intl. Edition* **2002**, *41*, 4663-4665.

(26) Watson, J. D.; Milner-White, E. J. *J. Mol. Biol.* **2002**, *315*, 171-182.

(27) Watson, J. D.; Milner-White, E. J. *J. Mol. Biol.* **2002**, *315*, 183-191.

(28) Gnanakaran, S.; Hochstrasser, R. M. *J. Am. Chem. Soc.* **2001**, *123*, 12886-12898.

(29) Schweitzer-Stenner, R.; Eker, F.; Huang, Q.; Griebenow, K.; Mroz, P. A.; Kozlowski, P. M. *J. Phys. Chem. B* **2002**, *106*, 4294-4304.

(30) Tiffany, M. L.; Krimm, S. *Biopolymers* **1968**, *6*, 1379-1382.

(31) Woutersen, S.; Hamm, P. *J. Phys. Chem. B* **2000**, *104*, 11316-11320.

(32) Eker, F.; Cao, X.; Nafie, L.; Schweitzer-Stenner, R. *J. Am. Chem. Soc.* **2002**, *124*, 14330-14341.

(33) Shi, Z.; Olson, C. A.; Rose, G. D.; Baldwin, R. L.; Kallenbach, N. R. *Proc. Natl. Acad. Sci. U.S.A.* **2002**, *99*, 9190-9195.

(34) Rucker, A. L.; Creamer, T. P. *Protein Sci.* **2002**, *11*, 980-985.

(35) Smyth, E.; Syme, C. D.; Blanch, E. W.; Hecht, L.; Vasak, M.; Barron, L. D. *Biopolymers* **2001**, *58*, 138-151.

(36) Woody, R. W. *Adv. Biophys. Chem.* **1992**, *2*, 37-79.

(37) Keiderling, T. A.; Silva, R. A.; Yoder, G.; Dukor, R. K. *Bioorg. & Med. Chem.* **1999**, *7*, 133-141.

(38) Adzhubei, A. A.; Sternberg, M. J. E. *J. Mol. Biol.* **1993**, *229*, 472-493.

(39) Syme, C. D.; Blanch, E. W.; Holt, C.; Jakes, R.; Goedert, M.; Hecht, L.; Barron, L. D. *Eur. J. Biochem.* **2002**, *269*, 148-156.

(40) Sreerama, N.; Woody, R. W. *Biochemistry* **1994**, *33*, 10022-10025.

(41) Shi, Z.; Woody, R. W.; Kallenbach, N. R. *Adv. Prot. Chem.* **2002**, *62*, 163-240.

(42) Bochicchio, B.; Tamburro, A. M. *Chirality* **2002**, *14*, 782-792.

(43) Blanch, E. W.; Morozova-Roche, L. A.; Cochran, D. A. E.; Doig, A. J.; Hecht, L.; Barron, L. D. *J. Mol. Biol.* **2000**, *301*, 553-563.

(44) Asher, S. A. *Anal. Chem.* **1993**, *65*, 59A-66A, 201A-210A.

(45) Asher, S. A. *Handbook of Vibrational Spectroscopy, John Whiley & Sons, Ltd.* **2001**, *1*, 557-571.

(46) Lednev, I. K.; Karnoup, A. S.; Sparrow, M. C.; Asher, S. A. *J. Am. Chem. Soc.* **1999**, *121*, 8074-8086.

(47) Lednev, I. K.; Karnoup, A. S.; Sparrow, M. C.; Asher, S. A. *J. Am. Chem. Soc.* **2001**, *123*, 2388-2392.

(48) Lifson, S.; Roig, A. *J. Chem. Phys.* **1961**, *34*, 1963-1974.

(49) Zimm, B. H.; Bragg, J. K. *J. Chem. Phys.* **1959**, *31*, 526-535.

(50) Teale, F. W. J. *Biochim. Biophys. Acta* **1959**, *35*, 543.

(51) Longworth, J. W. *Excited States Proteins Nucleic Acids* **1971**, 319-484.

(52) Edelhoch, H. *Biochemistry* **1967**, *6*, 1948-1954.

(53) Bykov, S. V.; Lednev, I. K.; Ianoul, A.; Mikhonin, A. V.; Asher, S. A. *Appl. Spectrosc.,* **2005,** In Press

(54) Robin, M. B. *"Higher Excited States of Polyatomic Molecules"; Academic Press: New York* **1975**, *Vol. II*.

(55) Song, S.; Asher, S. A. *J. Am. Chem. Soc.* **1989**, *111*, 4295-4305.

(56) Dudik, J. M.; Johnson, C. R.; Asher, S. A. *J. Phys. Chem.* **1985**, *89*, 3805-3814.

(57) Copeland, R. A.; Spiro, T. G. *Biochemistry* **1987**, *26*, 2134.

(58) Mayne, L. C.; Ziegler, L. D.; Hudson, B. *J. Phys. Chem.* **1985**, *89*, 3395.

(59) Oboodi, M. R.; Alva, C.; Diem, M. *J. Phys. Chem.* **1984**, *88*, 501-505.

(60) Diem, M.; Lee, O.; Roberts, G. M. *J. Phys. Chem.* **1992**, *96*, 548-554.

(61) Lee, S. H.; Krimm, S. *Biopolymers* **1998**, *46*, 283-317.

(62) Overman, S. A.; Thomas, G. J. Jr. *Biochemistry* **1998**, *37*, 5654-5665.

(63) Mikhonin, A. V.; Ahmed, Z.; Ianoul, A.; Asher., S. A. *J. Phys. Chem. B* **2004**, *108*, 19020-19028

(64) *The number scheme used here is consistent with that we use in a paper[63] and Chapter 3 of this thesis, which examines the assignment of all bands in the amide III region of PPII and α-helix peptides. The subscripts enumerate from highest frequency to lowest frequency as typical for vibration mode labeling. Unfortunately, this is the opposite of Diem et al's[60] labeling scheme. Amide III_1 band is not discussed in this paper.*

(65) Asher, S. A.; Ianoul, A.; Mix, G.; Boyden, M. N.; Karnoup, A.; Diem, M.; Schweitzer-Stenner, R. *J. Am. Chem. Soc.* **2001**, *123*, 11775-11781.

(66) Ianoul, A.; Boyden, M. N.; Asher, S. A. *J. Am. Chem. Soc.* **2001**, *123*, 7433-7434.

(67) Mirkin, N. G.; Krimm, S. *J. Phys. Chem. A* **2002**, *106*, 3391-3394.

(68) Lord, R. C. *Appl. Spectrosc.* **1977**, *31*, 187-194.

(69) Mikhonin, A. V.; Bykov, S. B.; Lednev, I. K.; Asher, S. A. *In Preparation* **2004**.

(70) Torii, H.; Tatsumi, T.; Tasumi, M. *J. Raman Spectrosc.* **1998**, *29*, 537-546.

(71) Chi, Z.; Chen, X. G.; Holtz, J. S. W.; Asher, S. A. *Biochemistry* **1998**, *37*, 2854-2864.

(72) Chaturvedi, S.; Go, K.; Parthasarathy, R. *Biopolymers* **1991**, *31*, 397-407.

(73) Schellman, J. A.; Becktel, W. J. *Biopolymers* **1983**, *22*, 171-187.

(74) Momii, R. K.; Urry, D. W. *Macromolecules* **1968**, *1*, 372.

(75) Onari, S. *Jpn. J. Appl. Phys.* **1970**, *9*, 227.

(76) Moffit, W. *Proc. Natl. Acad. Sci. U.S.A.* **1956**, *42*, 736.

(77) Mix, G.; Schweitzer-Stenner, R.; Asher, S. A. *J. Am. Chem. Soc.* **2000**, *122*, 9028-9029.

(78) Mikhonin, A. V.; Asher, S. A. *J. Phys. Chem. B.* **2005**, *109*, 3047-3052.

(79) Sreerama, N.; Woody, R. W. *Proteins* **1999**, *36*, 400-406.

3.0 CHAPTER 3. ASSIGNMENTS AND CONFORMATIONAL DEPENDENCIES OF THE AMIDE III PEPTIDE BACKBONE UV RESONANCE RAMAN BANDS

Work described in this chapter is published in *J. Phys. Chem. B*, **2004**, 108, 19020-19028 (Authors: Mikhonin, A. V.; Ahmed, Z.; Ianoul, A.; and Asher, S. A.). We investigated the assignments and the conformational dependencies of the UV resonance Raman bands of the 21-residue mainly alanine peptide (AP) and its isotopically substituted derivatives in both their α-helical and PPII states. We also examined smaller peptides to correlate conformation, hydrogen bonding and structure. Our vibrational mode analysis confirms the complex nature of the Amide III region, which contains many vibrational modes. We assign these bands by interpreting the isotopically induced frequency shifts, the conformational sensitivity of these bands and their temperature dependence. Our assignments of the amide bands in some cases agree, but in other cases challenge previous assignments by Lee and Krimm (*Biopolymers* **1998**, *46*, 283-317), Overman and Thomas (*Biochemistry* **1998**, *37*, 5654-5665), and Diem et al (*J. Phys. Chem.* **1992**, *96*, 548-554). We see evidence for the partial dehydration of α-helices at elevated temperatures.

3.1 INTRODUCTION

UV Resonance Raman (UVRR) spectroscopy[1] has recently been demonstrated to be a powerful tool for studying the early stages in protein folding.[2-4] The power of the methodology stems from its ability to easily utilize the numerous amide vibrational bands which occur within the 500–2000 cm^{-1} Raman frequency region to probe peptide and protein secondary structure. The amide backbone vibrational frequencies and their normal mode compositions depend sensitively on the peptide backbone secondary structure.[2,3,5-8] For example, the amide III (AmIII) vibrational mode

composition depends sensitively on the peptide bond's Ramachandran dihedral angles.[7-9] This sensitivity of vibrational frequencies to conformation is the basis for the use of vibrational spectroscopy to study molecular structure in general.

The use of vibrational spectroscopy to study protein secondary structure has a long and distinguished history.[10-12] Recent advances in the theory and practice of vibrational spectroscopy indicate that vibrational spectroscopy will continue to evolve more incisive methods to determine peptide and protein structure.[13,14]

Infrared absorption studies generally are limited to examining proteins and peptides in D_2O[13,15,16] to avoid the overwhelming water absorption.[17] IR studies of proteins and peptides in D_2O allow the study of the AmI' and AmII' bands (where the prime designates vibrations from amides which have exchanged their amide NH with deuterium); the AmI' band frequency clearly depends on the protein secondary structure.[13,18-20] Vibrational circular dichroism (VCD) gives additional information on protein and peptide secondary structure.[21-26]

Raman measurements show little interference from water,[10] and thus, the Raman spectra display numerous amide bands including the AmI, AmII, AmIII bands, as well as other backbone bands.[2,5,27-31] In normal Raman spectra excited in the near IR or in the visible spectral region, these bands overlap sidechain bands,[29,32,33] and often only the AmI band is well resolved, although the amide III bands can often also be observed. The AmII band is not observed in the absence of resonance excitation.[34] Raman optical activity (ROA) can give additional insight into the secondary structure due to its sensitivity to backbone conformation.[35-39]

Excitation in the UV enhances numerous Raman bands of the backbone amide peptide bonds.[2,5,30,40-44] These bands include the AmI, AmII and AmIII bands, as well as, a mainly $C_\alpha H$ bending vibration which mixes with the AmIII vibration to a degree which depends on the backbone Ramachandran dihedral angles.[7-9,43,45] This mixing leads to conformationally sensitive UV Raman spectra that can be analyzed to obtain quantitative secondary structure information.[2,5]

The challenge in interpreting the peptide bond vibrational spectra is that there is an incomplete understanding of the amide vibrational modes, in spite of years of excellent experimental and theoretical studies. The spectral region encompassing the "AmIII spectral region" is the least understood; as a result, the normal mode composition of the AmIII bands still remain under intense investigation. For example, Oboodi et al's. Raman[46] and Diem et al's. VCD[47,48] isotopic substitution studies identified at least three "AmIII" bands in alanylalanine and

proposed that these bands originate from mixing between NH in-plane, (N)C_α-H and (C)C_α-H b bending vibrations. Lee and Krimm's[49-51] theoretical and experimental studies of α-helical polyalanine also revealed significant complexity in the AmIII region. Their normal mode analysis proposed contributions of CN-stretch, NH ib, C_α-H b, C_α-C s modes to the observed AmIII region bands. More recently, Overman and Thomas's Raman isotopic substitution studies of α-helical filamentous virus fd demonstrated difficult to reconcile features in the AmIII and C_α-H bending spectral region.[27,33,52] Although they proposed that all of their viral protein "classical AmIII bands" involving CN s and NH b occur only below ~1310 cm^{-1}, they demonstrated that the largest C_α-D substitution isotopic frequency dependencies occurred at ~1345 cm^{-1}!

In our study here we reexamine the UV Raman enhanced amide vibrational bands of the peptide backbone, especially the "amide III vibrations". We should note, that our interpretations of the vibrational spectra are aided by the fact that the amide bonds independently Raman scatter and there is little complication of the spectra by the coupling of vibrational motion between amides.[53,54]

In this study we examine the AmIII region of a 21-residue, mainly ala peptide (AP) and smaller peptides. The AP peptide is an excellent model since we have shown that at temperatures below room temperature, the AP Raman spectra can be described as a sum of the spectra of α-helical and polyproline II (PPII) conformations.[2,9] At temperatures above room temperature, AP is predominantly PPII[2,9]. Time-resolved Raman studies of AP revealed that fast mono-exponential α-helix melting occurs with a relaxation time of about 200 ns.[2,3] Melting from the α-helix to the PPII state spectrally appears to be a two-state process without any evidence of significantly populated intermediate states.[2,3,9] We originally thought that the AP unfolded state was a disordered random coil state.[2,3] However, we recently demonstrated that it is predominantly a PPII helix.[9]

In this work, we examine the assignments of UVRR backbone amide bands of AP in both its α-helical and PPII states by using isotopic substitutions that dramatically change the amide group normal mode composition, by using resonance Raman enhancement of these bands, and by using the temperature dependence of the amide band frequencies of each conformational state, which gives information on the contribution of N-H bending, CN stretching, and C=O stretching to these vibrations.

3.2 EXPERIMENTAL SECTION

3.2.1 Sample Preparation.

The 21-residue alanine-based peptide AAAAA(AAARA)$_3$A (AP) was prepared (HPLC pure) at the Pittsburgh Peptide Facility by using the solid-state peptide synthesis method. All AP samples contained 1 mg/ml AP and included 0.2 M sodium perchlorate as an internal standard.
The 21-residue alanine-based AdP peptide of sequence **AAAAAAAA**RAAAAR**AAAA**R**AA** (where **A** is L-alanine (2,3,3,3 – D_4)), R is L-arginine, and A is normal abundance L-alanine) was prepared (HPLC pure) at the Pittsburgh Peptide Facility and at Anaspec Corp. (San Jose, CA) using the solid-state peptide synthesis method. AdP is a perdeuterated AP peptide, except for the R residues and the central A_{10}-A_{13} residues; essentially all but the internal six residues R_9AAAAR_{14} are perdeuterated (except for R_{19}). All AdP samples contained 0.5 mg/ml AdP and included 0.15 M of sodium perchlorate. All Raman spectra were normalized to the intensity of the 932 cm^{-1} ClO_4^- Raman band. Prior to the UVRR measurements, the AP and AdP in D_2O solutions were kept at +62 °C for 5 min to ensure complete N-deuteration.

Short poly-alanine peptides A_n (n = 2, 3, … , 6) as well as Ala-Asp, Val-Lys di-peptides were purchased from Bachem Bioscience Inc. (King of Prussia, PA), and used as received in water solutions. We utilized peptide concentrations in water between 0.15 – 5 mg/ml. Sodium perchlorate (0.1 – 0.15 M) was used in each solution as an internal standard.

Ala-Asp, Val-Lys and Ala-Ala crystals were prepared by growing them directly from water solution. All crystal structures and Ψ and Φ dihedral angles were obtained from X-ray diffraction measurements at the University of Pittsburgh and/or from literature X-ray diffraction studies. N-methyl-acetamide (NMA, Aldrich) concentrations in both water and D_2O were ~0.033 M (5 ml of NMA in 20 ml of water/D_2O).

3.2.2 Instrumentation.

The UV Resonance Raman instrumentation has been described in detail elsewhere.[2,3] A Coherent Infinity Nd:YAG laser produced 355 nm (3rd harmonic) 3 nsec pulses at 100 Hz. This beam was

Raman shifted to 204 nm (5th anti-Stokes) by using a 1 m tube filled with hydrogen (60 psi). A Pellin Broca prism was used to select the 204 nm excitation beam. The Raman scattered light was imaged into a subtractive double spectrograph and the UV light was detected by either a Princeton Instruments solar blind ICCD camera or a Roper Scientific unintensified liquid nitrogen cooled CCD camera. All samples were measured in a thermostatted free surface flow stream.

UVRR powder crystal spectra, as well as, some solution spectra of short peptides were measured by using the 229 nm line of a CW doubled Ar^+ laser. The scattered light was collected by Spex Triplemate spectrograph coupled to a Princeton Instruments solar blind ICCD camera.

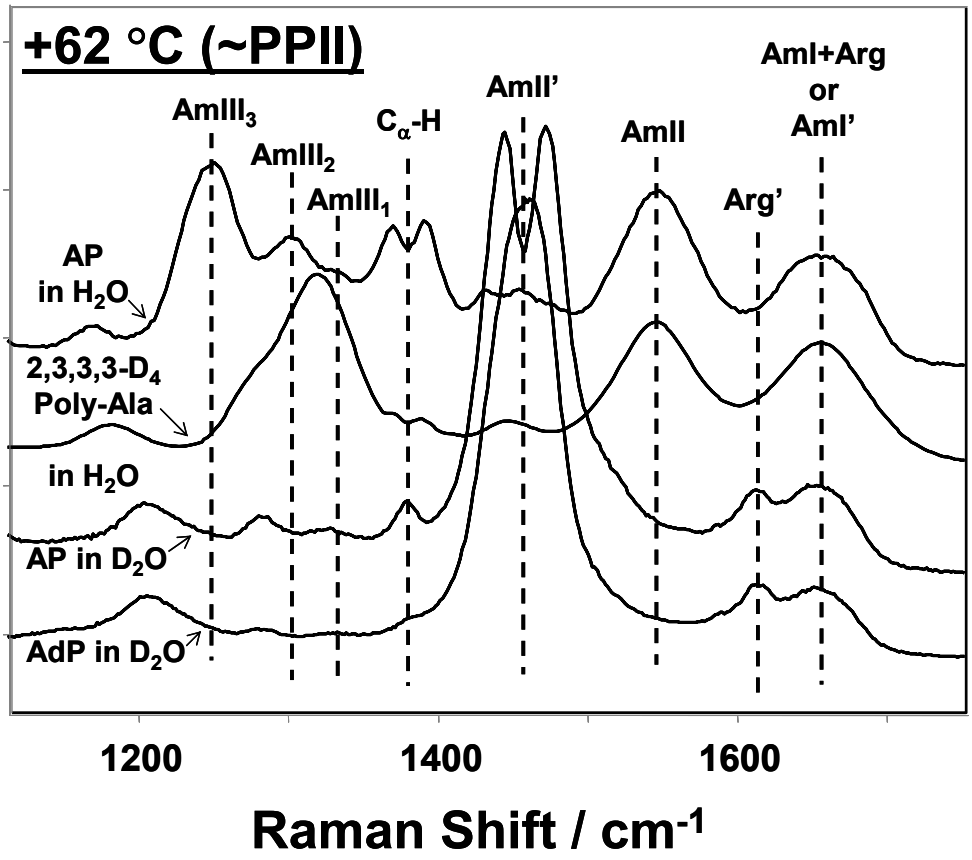

Figure 25. 204 nm UVRR spectra (at 62 °C) of AP PPII in water (red). At this temperature AP is fully in the PPII conformation. b) 2,3,3,3-deuterated poly-alanine PPII in water (blue). This is a calculated spectrum where the contribution of nondeuterated residues were numerically subtracted, c) AP PPII in D_2O. At this temperature AP is fully in the PPII conformation. d) 2,3,3,3-deuterated poly-alanine PPII in D_2O (black). This is a calculated spectrum where the contribution of nondeuterated residues were numerically subtracted.

3.3 RESULTS AND DISCUSSION

3.3.1 Assignment of the Amide III Region Bands (1230 cm^{-1} – 1410 cm^{-1}) of AP in its PPII Conformation.

Fig. 25 shows the 204 nm excited UV resonance Raman (UVRR) spectra[55] of the PPII conformation of AP in H_2O and D_2O, as well as, the calculated spectrum of the PPII conformation of an isotopically substituted AP where 14 ala were perdeuterated. We designate the intense **1245 cm^{-1} band of the PPII conformation of AP** in water as the "classical" **AmIII band** because it shows the largest dependence upon peptide bond conformational changes (vide infra).

This band, which disappears upon N-deuteration, also shows the large -0.15 cm^{-1}/°C frequency temperature dependence typical for the AmIII and AmII bands of non-α helical and non-β-sheet peptides, and simple amides such as N-methylacetamide (NMA, Fig. 26). This temperature coefficient of -0.15 cm^{-1} is higher than the -0.1 cm^{-1} temperature reported earlier by Lednev et al.[2] for $A_5 - A_3$. We measured the AP temperature coefficient from high S/N spectra at +49 °C and +65 °C.

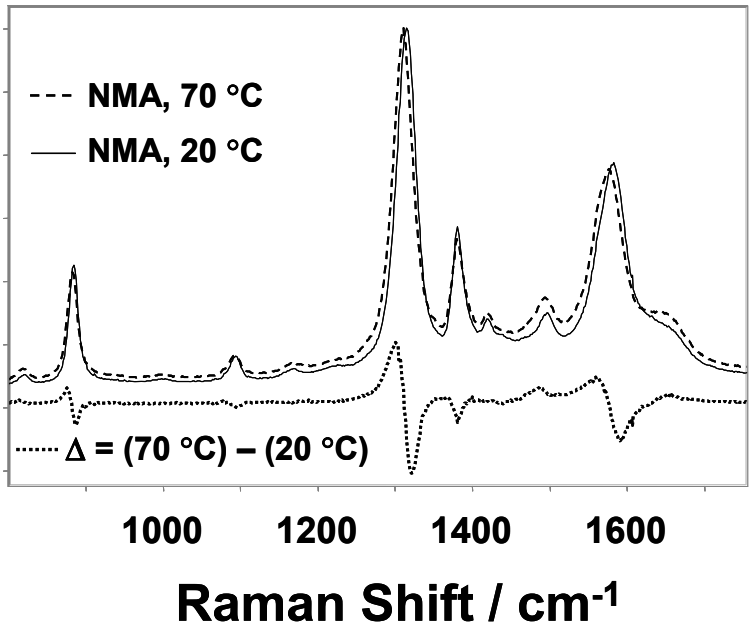

Figure 26. Temperature dependence of the 204 nm UVRR spectra of N-methylacetamide and their 70 °C – 20 °C difference spectrum.

For NMA the AmII and III bands shift by -0.11 and –0.09 cm^{-1}/°C, while the AmI band shifts up by a much smaller amount. This temperature dependence derives from the decrease in hydrogen bonding by water as the temperature increases.[56,57] The mode frequencies decrease as the weakened water hydrogen bonding decreases the amide N-H bending and the C-N stretching force constants.[9,56,58]

This conclusion is evident from the temperature dependence of N-deuterated NMA (NMAD). The substitution of the much heavier N-D decouples N-D bending from C-N stretching, and we have almost a pure C-N stretch which appears as a Fermi resonance doublet[59] at ~1500 cm^{-1} (Fig. 27).

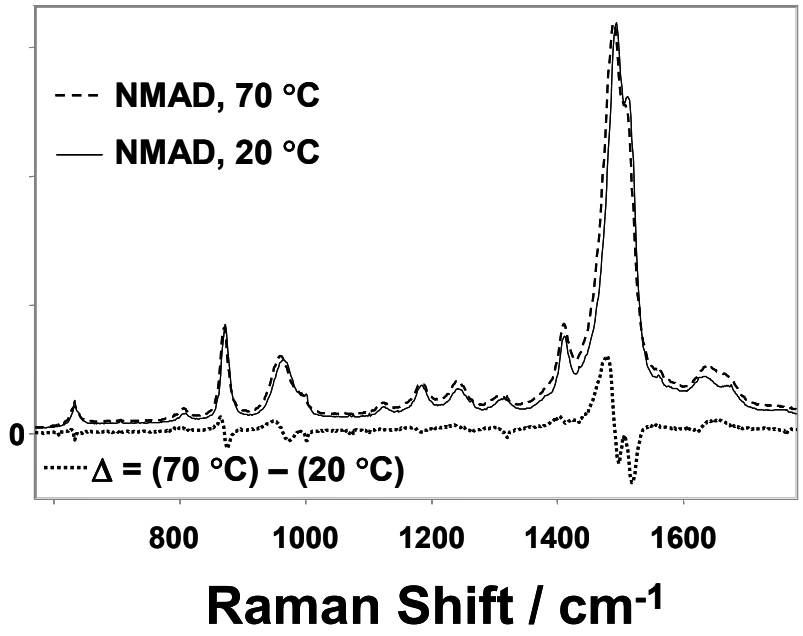

Figure 27. 204 nm excited UVRR spectra temperature dependence of NMAD showing the large downshift of the 965 cm^{-1} AmIII' band and the smaller downshift of the AmII' doublet. The AmI' band slightly upshifts and changes bandshape.

We find that changes in water hydrogen bonding impact the N-D bend force constant more than the C-N stretch force constant; NMAD shows a smaller, -0.07 cm^{-1}/°C temperature dependence of the mainly C-N stretching AmII' band, compared to the -0.11 cm^{-1}/°C frequency decrease in the N-D bending dominated NMAD AmIII' band at 965 cm^{-1} (Fig. 27). If an analogous pure N-H bending mode occurred at ~1400 cm^{-1}, it would show a significantly larger temperature dependent frequency shift of ~ -0.16 cm^{-1}/°C.

This result indicates that the change in water hydrogen bonding impacts the N-H bending coordinate motions significantly more than the C-N stretching coordinates. The C_α-H bending bands show no temperature dependence, while the C=O stretching dominated AmI bands of peptides and NMA show only a small positive frequency dependence on temperature. Small anhydrous peptide crystals show a negligible temperature dependence (data not shown).

Thus, a significant temperature dependence signals significant contributions of N-H bending and C-N stretching to a Raman band. From this, we conclude that the 1245 cm^{-1} PPII AP band in water contains a significant contribution of NH ib and C-N stretching. Thus, the 1245 cm^{-1} PPII AP band can be clearly assigned to the "classical AmIII vibration".

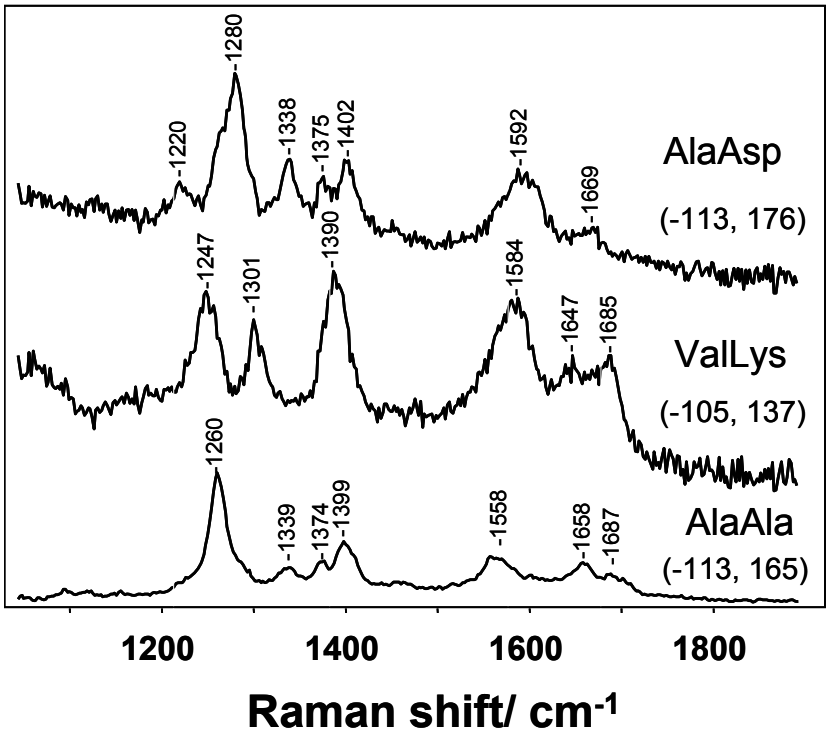

Figure 28. 229 nm excited UVRR spectra of dipeptide crystal powders. Also shown are the Φ and Ψ dihedral angles obtained from the x-ray crystal structures.

2,3,3,3-deuteration of the ala sidechains and C_α positions shifts the 1245 cm^{-1} PPII AP band to 1320 cm^{-1} (Fig. 25). The 1320 cm^{-1} band shows a significant, but somewhat smaller, temperature dependence (-0.7 cm^{-1}/°C) than the 1245 cm^{-1} band. This band also disappears on NH deuteration. Thus, this vibration contains significant fractions of NH ib and C-N stretching. The main difference is that this vibration no longer contains C_αH bending. This 81 cm^{-1} frequency shift on deuteration is heartwarmingly close to that expected from the relationship

proposed by Asher et al.[7,9] which correlates the AmIII band frequency to the extent of AmIII and C_α-H sb coupling (υ = 1265 cm^{-1} - **46.8 cm^{-1}** sin (Ψ + 5.2°))**.**

The **1303 cm^{-1} and 1337 cm^{-1}** bands of PPII AP in water disappear upon N-D deuteration, which suggests significant contributions from NH bending. However, this is contradicted by the fact that the 1303 cm^{-1} and 1337 cm^{-1} bands show only a small temperature dependence. The much weaker bands at 1284 cm^{-1} and 1328 cm^{-1}, which occur in D_2O, could possibly be remnants of the 1303 cm^{-1} and 1337 cm^{-1} bands if the new modes in D_2O lost contributions of C-N, C=O, C-C and N-C motions that gave rise to their original resonance Raman enhancements.

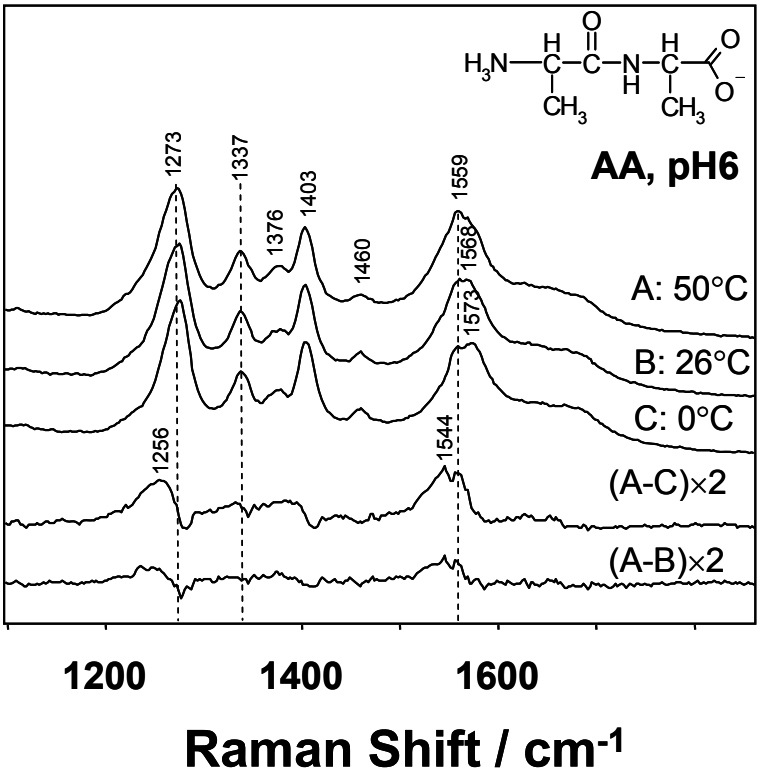

Figure 29. Temperature dependence of the 229 nm, UVRR spectra of AA in water. Power- 5 mW, sample concentration 5 mg/ml. Spectral resolution 8 cm^{-1}.

A more likely explanation is that the existence of the 1303 cm^{-1} and 1337 cm^{-1} normal modes of PPII AP depend sensitively on their N-H contributions. The removal of the N-H bending component could alter their vibrational mode compositions sufficiently that the resulting modes shift outside the 1250 – 1400 cm^{-1} region.

Dipeptides such as AA, AD and VK also show bands at these frequencies (1300 cm^{-1} and 1340 cm^{-1}), which often appear overlapped either in solution on in crystals, as is evident from the resonance Raman spectra of crystals of dipeptides shown in Fig. 28, along with their Φ and Ψ dihedral angles determined from their crystal structures. Ala-asp and ala-ala, which have β-strand-like Ψ angles show a ~1338 cm^{-1} band, while the PPII-like Ψ = 137° of val-lys shows only a 1301 cm^{-1} band. We assume the 1305 cm^{-1} and ~1338 cm^{-1} bands have similar origins to those of PPII AP. From their small temperature dependence (Fig. 29) and their large conformational dependence, we assign these bands to vibrations mainly involving C-C_α stretching mixed with C_αH bending.

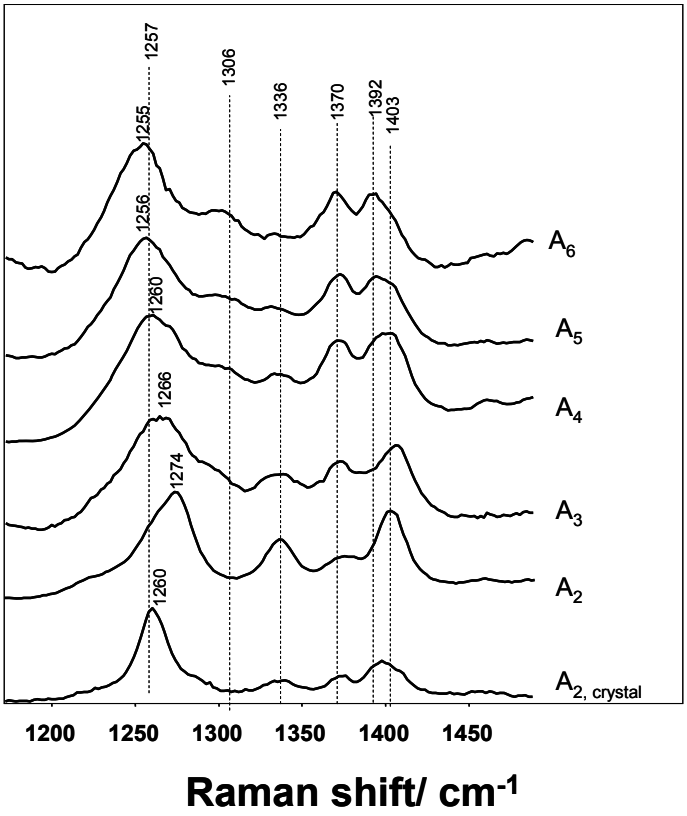

Figure 30. 204 nm UVRR spectra of different poly-ala in water and the 229 nm UVRR of A_2 crystal powder.

Our assignment appears to contradict that of Diem and coworkers[48] who "unequivocally" assigned the 1336 cm^{-1} band in ala-ala to an unperturbed NH deformation motion. The future will further illuminate the assignments of this complex spectral region.

Fig. 30 shows the dependence of the 204 nm UVRR spectra of increasingly long alanine peptides. Ala-ala shows a much stronger **1337 cm^{-1}** band than occurs in the larger peptides; the

decreased intensity observed for the **1337 cm^{-1}** band in the ala-ala crystals may be due to its preresonance excitation at 229 nm, to the red of the amide $\pi \rightarrow \pi^*$ transition.

The relative intensity of the **1337 cm^{-1}** band smoothly decreases as the peptide length increases to A_6 (Fig. 30). The various difference spectra between these peptides shown in Fig. 31 display no feature close to 1337 cm^{-1} for peptides larger than ala_3. Thus, the existence of a small peak in AP at this frequency at elevated temperatures is quite surprising. This 1337 cm^{-1} peak clearly derives from AP, which is predominantly PPII at this temperature. It does not derive from small peptide fragments, since HPLC-MS analysis of AP samples clearly demonstrate the absence of significant hydrolysis or photolysis to smaller fragments. Temperature difference spectra between 50 and 80 °C show a small intensity increase and broadening of this band.

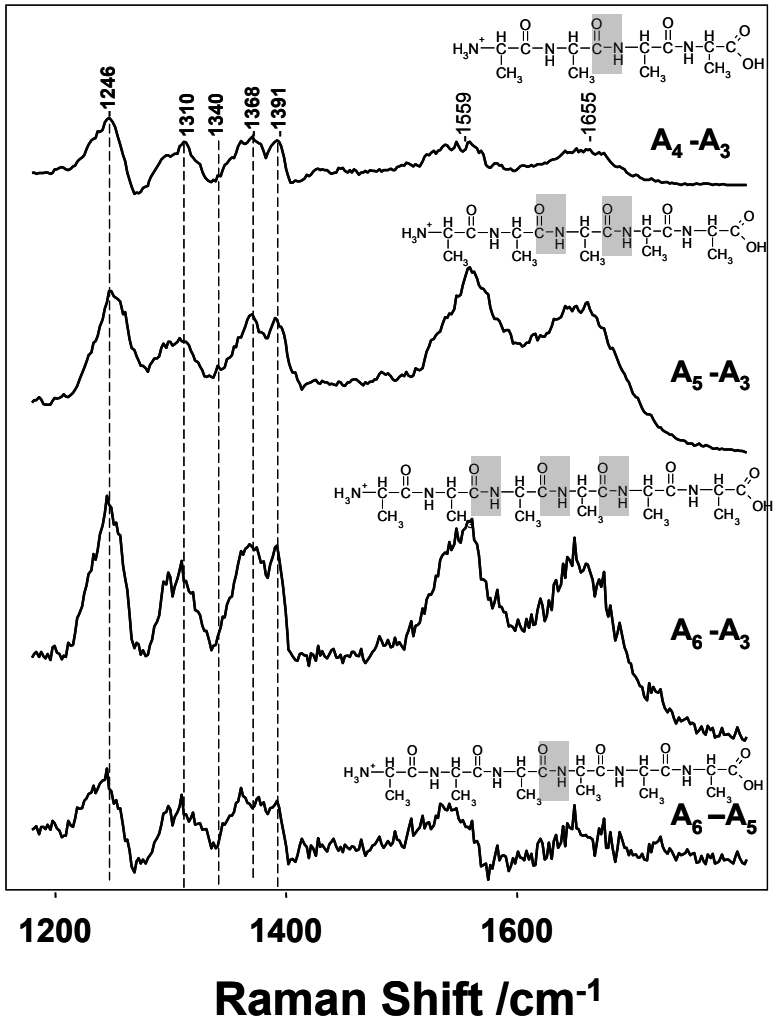

Figure 31. 204 nm UVRR difference spectra between different poly-ala in water.

This band must signal a minority population of some conformation of AP. It is impossible at this point to determine the nature of this conformation solely from the spectra since the 1337 cm^{-1} band appears both in β-strand and α-helix-like conformations. We would need to resolve whether the other bands which are signatory of non PPII conformations are also present in the underlying the spectra. It is most likely, however, that this small band derives from a small β-strand contribution, in view of the known occurrence of minor β-strand contributions to the mainly PPII conformation of the alanine rich XAO peptide.[60]

3.3.2 Assignment of the Amide I Region Bands of AP in its PPII Conformation.

The N-D PPII state of AP and AdP in D_2O both show 2 bands in the AmI' region at ~1614 cm^{-1} and ~1660 cm^{-1} (Fig. 25). The 1660 cm^{-1} band shows the expected AmI band's temperature dependence, in which it slightly upshifts in frequency as the temperature increases. In contrast the 1614 cm^{-1} band shows negligible temperature dependence. As shown below (Chapter 4, Fig. 42), the 1614 cm^{-1} band derives from an arg sidechain vibration, while the ~1660 cm^{-1} band is the AmI' band.

3.3.3 Assignment of the Amide III Region Bands of AP in the α-Helical Conformation.

Fig. 32 shows the calculated 204 nm UVRR spectra of α-helical AP, and of its perdeuterated derivative in both water and D_2O. These α-helical spectra were calculated by removing contributions from PPII conformations, and in the cases of the perdeuterated derivatives, from protonated amino acids in the chain. The details are described in the figure caption.

The UVRR spectra of α-helical AP displays a triplet of bands at 1261 ($AmIII_3$), 1303 ($AmIII_2$), and 1337 cm^{-1} ($AmIII_1$) in the amide III region. We should caution that there is no implication in this labeling scheme that the $AmIII_i$ bands of the α-helix correspond to the same labeled bands of the PPII conformation.

The temperature dependence of the entire α-helix spectrum is negligibly small below 10 °C (Fig. 33), as originally noted by Lednev et al.[2,3,61-63] However, at temperatures above 20 °C the spectrum shows a surprising downshift for the $AmIII_3$ band which is accompanied by an AmI

bandshape change and the appearance of an additional, AmI_1 band (Fig. 34). In Chapter 8, we explain the $AmIII_3$ profile change in terms of pre-melting of water-mediated α-helical defects, such as π-bulges and 3_{10}-helices. The decreased S/N of the higher temperature α-helix spectra displayed in Fig. 33 is due to the decreased α-helical fractions of AP at +20 and +30 °C, compared to those[2,3,61-63] at -3.5, 0, and +10 °C.

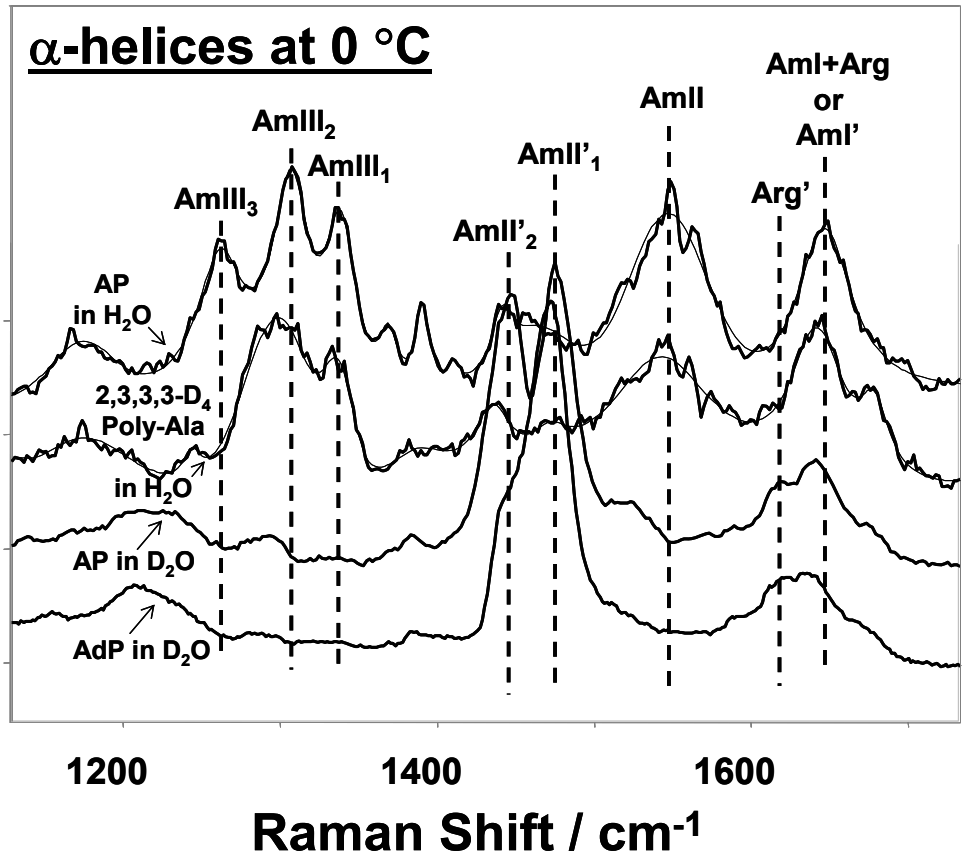

Figure 32. Calculated 204 nm UVRR α-helical spectra of AP and its isotopically substituted derivatives at 0 °C: a) α-helical AP in water. This spectrum was obtained by subtracting the 0 °C calculated AP PPII spectrum from the measured 0 °C AP spectrum (~45% PPII); b) 2,3,3,3-deuterated poly-L-alanine α-helix in water where the contribution from the protonated amides was numerically removed. This spectrum was obtained by subtracting the calculated 0 °C AdP PPII spectrum from the measured 0 °C AdP spectrum followed by subtraction of appropriate amount of 0 °C AP α-helix spectrum; c) α-helical AP in D_2O. This spectrum was obtained by subtracting the 0 °C AP PPII spectrum from the experimental 0 °C AP spectrum (~45% PPII); d) α-helical AdP in D_2O. This spectrum was obtained by subtracting the 0 °C AdP PPII spectrum from the experimental 0 °C AdP spectrum (~45% PPII). Note that AdP sequence contains fourteen 2,3,3,3-deuterated ala, 4 non-deuterated ala and 3 non-deuterated arg.

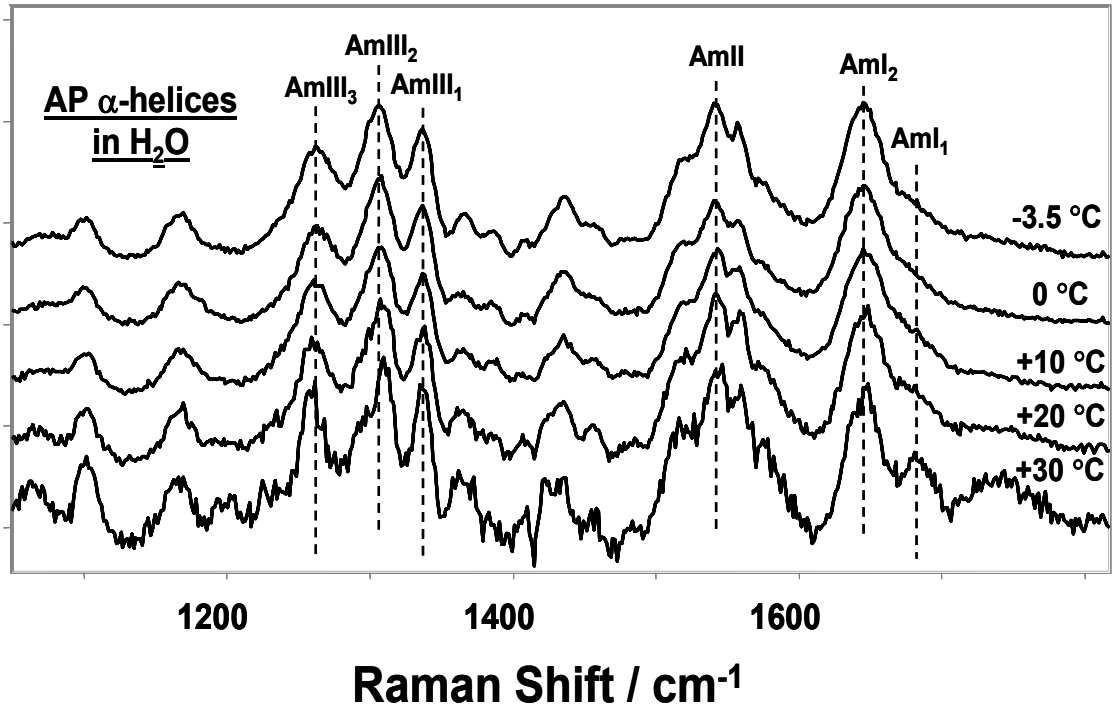

Figure 33. Calculated temperature dependence of 204 nm UVRR spectra of α-helical AP in water. The spectra were calculated by subtracting the appropriate amount of PPII AP spectrum from the measured spectrum at the corresponding temperature. The low S/N of the AmII band results from the incomplete subtraction of the Raman band of O_2.

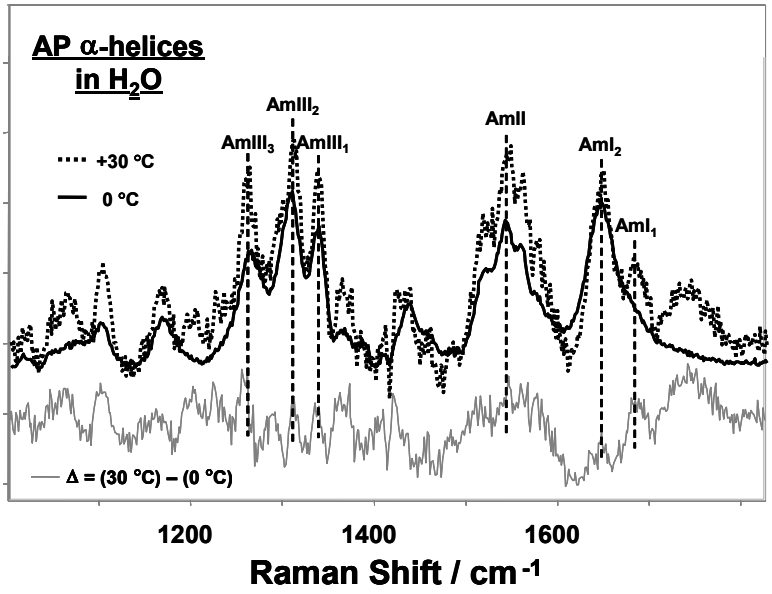

Figure 34. UVRR spectra of α-helical AP at 0 and 30 °C and their difference specrtrum showing the downshift of $AmIII_3$ and the appearance of a higher frequency AmI_1 band.

We suggest that these spectral changes result from an α-helix hydration change at higher temperatures. The polyala α-helix should be well hydrated by water.[56,58,64-68] The temperature increase should decrease the extent of hydration of a fraction of the α-helical peptide bonds due to the decrease in the water-peptide hydrogen bonding strength.[58,68] This then shifts those bands with significant N-H b and C-N s to lower frequency and shifts the AmI band to higher frequency. The new AmI_1 band is shifted to 1682 cm^{-1}, which may be a signature of a nonhydrated helix.

Obviously, our spectral changes are discontinuous, and a transition appears around 20 °C, yielding a partially "dehydrated" helix. Possibly, these dehydrated helix segments are an intermediate in the α-helix to PPII conformational transition. The dehydrated helical segments may have an increased propensity to evolve into the PPII form, because temperature increase raises the free energy of partially "dehydrated" α-helical segments above that of the PPII conformation.

Whatever the case, we conclude that the $AmIII_3$ band contains a large amount of N-H bending. Therefore, we label the **1261 cm^{-1} band as the "classical AmIII band"**.

This triplet of bands disappears upon N-deuteration (Fig. 32), leaving only a very weak ~1293 cm^{-1} band. The spectral intensities can be referenced to a constant AmI band intensity, since the AmI cross sections change little with temperature, conformation or isotopic substitution.

The AmII' doublet of AP in D_2O is replaced by a singlet in the perdeuterated derivative AdP in D_2O because of a loss of the Fermi resonance between CN s and CH_3 bending.[59] However, the AdP spectrum still shows some remnant of the doublet due to the contribution of the AmII' doublet from the 4 non-perdeuterated ala residues.

The largest change that occurs upon the perdeuteration of α-helical AP is the disappearance of the $AmIII_3$ band which leaves behind a doublet spectral contour (Fig. 32). We attempted to determine whether the $AmIII_3$ band disappeared or whether it shifted underneath the doublet. Unfortunately, the Fig. 35 deconvolution attempt does not by itself definitively resolve whether two or three bands underlie the broad doublet contour of perdeuterated α-helical AP. The contour can be fit by two bands if the lower frequency band is allowed to have a >50 cm^{-1} bandwidth. However, a more likely conclusion is that a triplet of ~30 cm^{-1} bandwidth bands at

1284, 1308, and 1335 cm^{-1} underlie this contour; the 50 cm^{-1} bandwidth appears unphysically large.

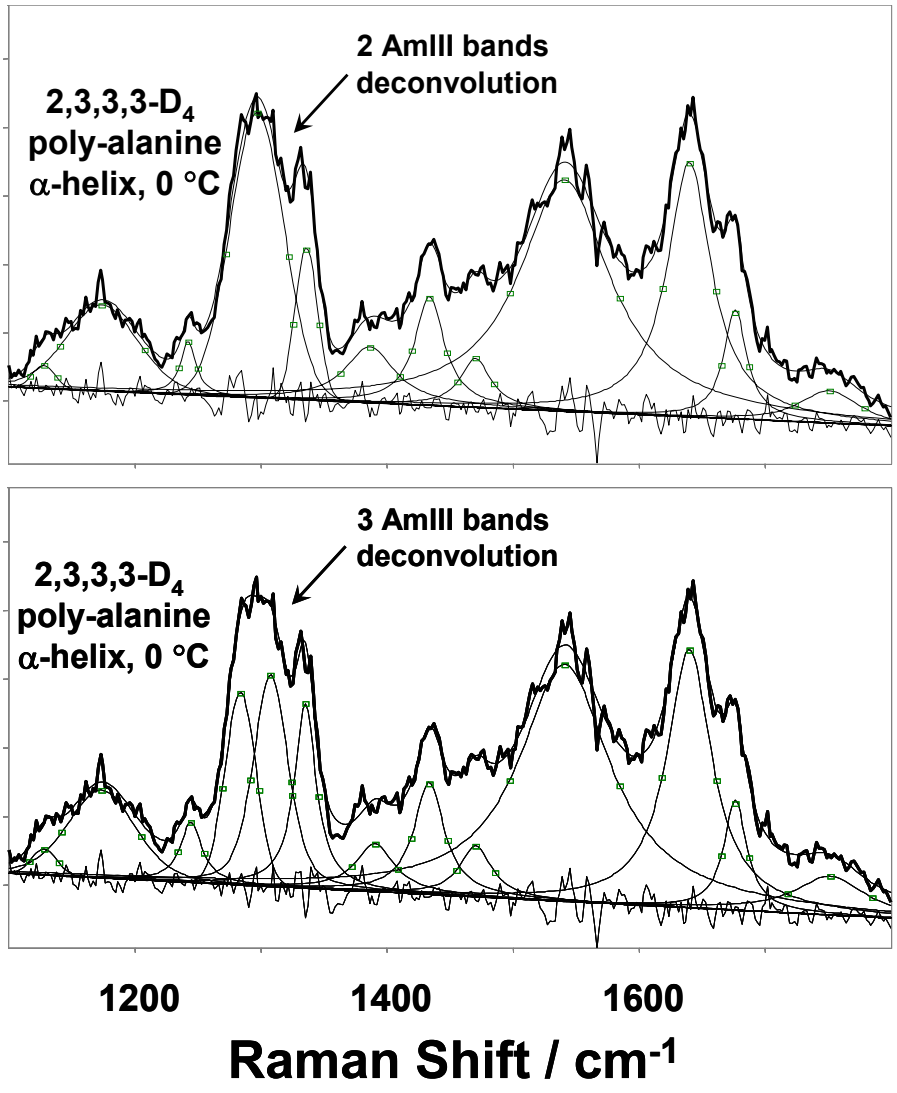

Figure 35. Attempts to deconvolute the ala perdeuterated α-helix AP AmIII region into a doublet and triplet of underlying bands using GRAMS software.

Some shift of the $AmIII_3$ band to higher frequency upon C_α deuteration is consistent with the expectation[7] that the AmIII band frequency depends on coupling between N-H and $C_\alpha H$ motions of two essentially degenerate vibrations. However, because the C_α-H and N-H bonds are trans in the α-helix conformation we expect only a small shift. It should be noted, however the $AmIII_3$ band might also contain contributions of other components of C_α-H motion, whose

removal might cause a frequency upshift, resulting in the overlap of the original $AmIII_1$ and $AmIII_2$ bands with the $AmIII_3$ band blueshifted to ~1326 cm^{-1}.

In contrast, we conclude that the $AmIII_3$ band disappears, if we consider the resonance Raman intensities and expect that the integrated Raman cross section would be conserved if the $AmIII_3$ band shifts into the doublet contour. We utilized the measured intensity ratio of the AmIII band envelope relative to the AmI band(s) to determine whether the doublet envelope contains the $AmIII_3$ band. We assume that that the resonance Raman enhancement of these Raman bands derive from their C-N s, C=O s, C_α-CO s and N-C s motions.[59] Our analysis requires that isotopic substitution does not perturb the electronic transitions, and that the loss of $C_\alpha H$ bending does not change the Raman intensities. If the $AmIII_3$ band shifts underneath the doublet contour, the integrated intensity within the contour, relative to that of the AmI band (whose intensity remains relatively constant) would remain identical to that of natural abundance α-helical AP. In contrast, the ratio decreases almost 2-fold in the perdeuterated derivative, suggesting that the band disappears. Thus, we are unable to come to a definitive conclusion of what happens to the $AmIII_3$ band in the deuterated derivative.

Thus, we assign the **1261 cm^{-1}** band to the classical AmIII of an α-helix conformation, which as pointed out by Lee and Krimm involve CN s and NH b motions. It may also contain some C_α-C s**.**

We assign the **1306 cm^{-1}** band of natural abundance α-helical AP to a vibration which involves mainly C-C and N-C stretching since this band shows little temperature dependence and may be slightly affected by hydration (Fig. 33). This band is not conformationally sensitive since it shows up in both the α-helix (~1306 cm^{-1}) and the PPII (~1303 cm^{-1}) conformations (Figs. 25, 33 and 36). The assignments of the other bands are indicated above.

We should note the recent results of Overman et al.[27] who examined the impact of ala C_α-D substitution on normal Raman α-helical virus coat proteins. Upon replacement of C_α-H they observe that a 1345 cm^{-1} band shifts to 1296 cm^{-1}. This behavior is almost exactly the opposite of what we observe. Barron et al.[69-71] also have observed a hydrated α-helix band at ~1345 cm^{-1} with visible excitation ROA. We see no hydration dependence for our 1337 cm^{-1} band. Thus, we conclude that their hydrated~1345 cm^{-1} α-helix band is not enhanced upon 204 nm resonance excitation.

3.3.4 Assignment of Other Amide Bands of AP in the α-Helical Conformation.

The intensity of the 1380 cm^{-1} band of α-helical AP in D_2O decreases significantly in AdP in D_2O (Fig. 25 and 32). This observation is completely consistent with the assignment of this band to mainly CH_3 sb mode of ala side chain by Lee and Krimm,[49] since AdP contains only 4 non-perdeuterated ala while the AP contains 18 non-perdeuterated ala.

The 1614 cm^{-1} band, which shows up in the UVRR spectra of both α-helical and PPII states of AP and AdP in D_2O (Fig. 25 and 32) cannot be assigned to the AmI' band, because it is not conformationally sensitive, and it does not show the temperature dependence typical of the AmI bands. We assign this band to an arginine side chain CN s mode based on Fig. 42 of Chapter 4. The observed 1630 cm^{-1} arg band in water downshifts in D_2O.

Tables 5 and 6 summarize the spectroscopic information used to assign the amide III region of the PPII and α-helical conformations of AP.

Table 5. Assignments, Isotopic and Temperature Dependencies of Amide III Region UV Raman Bands of the PPII Conformation of AP.

UVRR Band Assignment	**Conformational Dependence**	**NH / ND substitution**	**C_α-D Substitution**	**T dependence**	**Included Atomic Motions**	**Excluded Atomic Motions**
1245 cm^{-1} "Classical amide III"	Most sensitive to conformation "	Disappears with AmIII' band appearing at ~950 – 1000 cm^{-1}	Shifts to 1326 cm^{-1} (NH b and CN s)	Large T-dependence	NH b coupled to C_α-H b and CN stretch	None
1303 cm^{-1}	No?	disappears	Transforms to shoulder at 1278 cm^{-1}?	moderate T-dependence	Stretches of heavy atoms, C_α-C s, NC s, CN s + some C_α-H b	NH b
1337 cm^{-1}	Originates from extended β-strand-like conformation?	disappears	Hidden under the broad ~1326 cm^{-1} envelope?	Small T-dependence	C_α-C s and NC s	NH b CN s
1370 cm^{-1}	Most sensitive to conformation	disappears	disappears	No T-dependence	C_α-H b, C_α-C s, CH_3 umbrella. Maybe small amount of C-N s	NH b
1394 cm^{-1}	Most sensitive to conformation	disappears	disappears	No T-dependence	C_α-H b, C_α-C s Maybe small amount of C-N s	NH b

Table 6. Assignments and Isotopic and Temperature Dependence of Amide III Region UV Raman Bands of the α-helical Conformation of AP.

Band Assignment	Conformational Dependence	NH / ND substitution	C_α-D, and CD_3 Substitution	T-dependence	Hydration Dependence	Included Atomic Motions	Excluded Atomic Motions
1261 cm^{-1} "Classical amide III"	Most sensitive to conformation ?	Disappears with AmIII' band appearing at ~950 – 1000 cm^{-1}	??? (see text)	Strong T-dependence (at T > +10 °C)	Most sensitive to hydration	NH b and CN s and maybe C_α-C b	None
1306 cm^{-1}	Not sensitive	disappears	Either shifts to ~1284 cm^{-1} or remains at ~1308 cm^{-1}	Small T-dependence	Only slightly influenced by hydration	C_α-C s and NC s maybe some and small amount of CN s	NH b, and maybe C_α-H b,
1337 cm^{-1}	Not sensitive ?	disappears	Remains at the same position?	No	No	C_α-C s, NC s maybe small amount of CN s	NH b, C_α-H b,

3.3.5 Comparison Between UVRR Spectra of α-Helical and PPII Conformations of AP and AdP.

Fig. 36 compares the UVRR spectra of the α-helix and PPII conformations of AP. As earlier found by Chi et al.[5] the intense PPII ~1245 cm^{-1} $AmIII_3$ band and the intense ~1400 cm^{-1} C_α-H sb band (called incorrectly random coil[2,3,61-63]) dramatically decrease in intensity in the α-helix conformation, and are replaced by a broad envelope of bands centered at ~1300 cm^{-1}. The ~1400 C_α-H sb band contour in PPII disappears completely and is replaced by a weak band ~1390 cm^{-1}

due to the methyl umbrella mode. The intensity of the PPII AmII band decreases by more than 2-fold, while its frequency downshifts by ~12 cm^{-1} in the α-helix. The peak height intensity of the AmI band remains essentially constant, while its frequency downshifts by ~13 cm^{-1}.

The decrease in intensity results from a decrease in the oscillator strength of the amide $\pi \rightarrow \pi^*$ transition due to excitonic interactions in the α-helical conformation.[40,72-76] This is clearly evident in the Fig. 37 comparison between the α-helix and PPII UVRR spectra of AP and AdP in D_2O. Resonance Raman enhancement is dominated by the AmII' band which is mainly C-N s.[59] The intensity of the AmI' band stays constant while the integrated intensity of the AmII' band of the α-helix conformation decreases by more than 2-fold for AP and AdP. In contrast, the Fig. 38 AmII' comparison between AP and AdP conformations show that the enhancement remains relatively constant even though AdP residues are deuterated. The small AmII' enhancement decrease in PPII AP is made up by small enhancement increases for the AmIII' band as well as other small bands. For the α-helix, essentially identically enhanced AmII' bands occur.

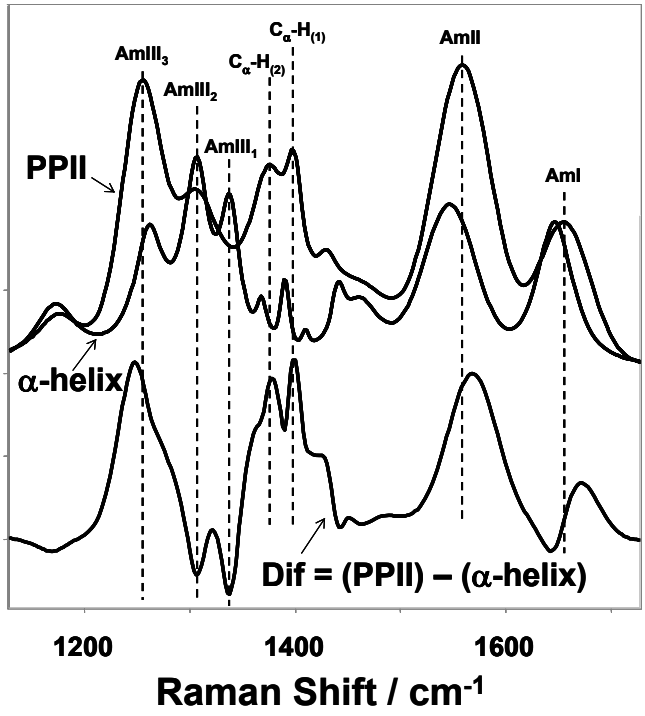

Figure 36. Comparison of the 204 nm calculated UVRR spectra of the α-helix and PPII conformations of AP at 0 °C and their difference spectrum.

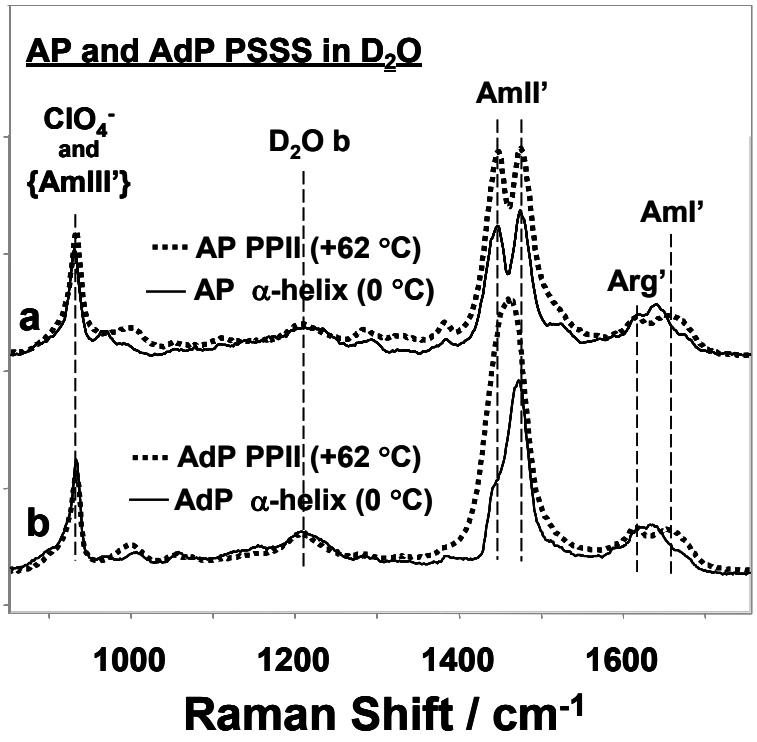

Figure 37. Comparison between measured PPII and calculated α-helix AP and AdP in D_2O UVRR spectra.

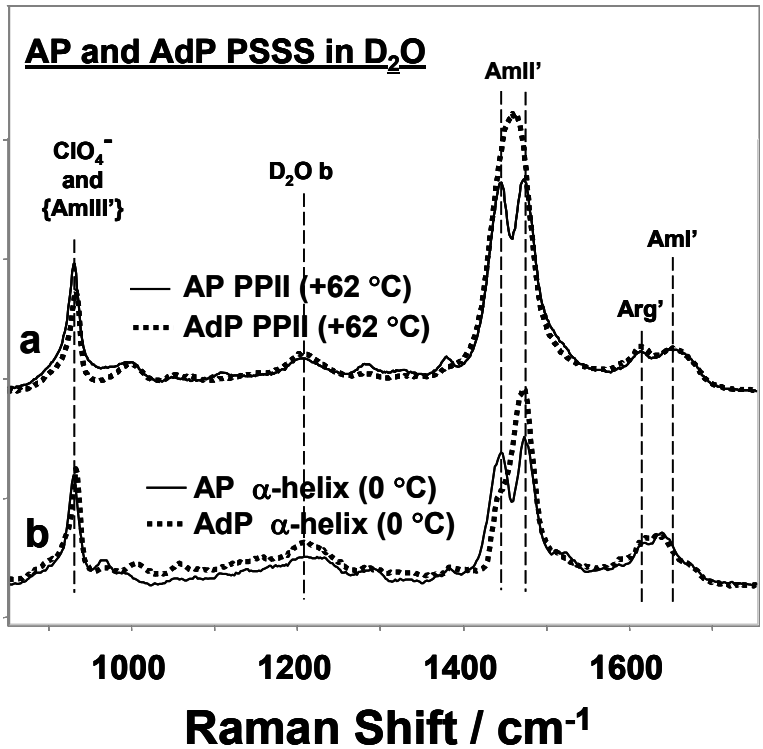

Figure 38. Comparison of measured PPII and calculated α-helix AP and AdP in D_2O UVRR spectra.

The Fig. 36 UVRR spectra display the significant spectral changes which occur between the PPII and α-helix conformations of natural abundance AP in H_2O. The maximum changes occur in the Amide III spectral region. It is not possible to assign bands of the PPII and α-helix conformations to similar vibrations, but the $AmIII_3$ vibrations of both conformations seem to have both N-H b and C-N s contributions. For example, the ~1245 cm^{-1} $AmIII_3$ band of PPII has significant N-H bending and C-N s as evident from the -0.15 cm^{-1} / ºC temperature coefficient. Similarly, the α-helix $AmIII_3$ band shows a -0.15 cm^{-1} / ºC temperature coefficient between 10 and 30 ºC (while showing no temperature dependence below 10 ºC). This agrees well with Lee and Krimm[50] who calculate a band at 1263 cm^{-1} which is dominated by N-H bending, which also contains a large component of C-N s which gives rise to enhancement.

The bands labeled $AmIII_1$ and $AmIII_2$ of PPII and α-helical conformations significantly differ. Perhaps this point is most succinctly shown by the differences between the calculated UVRR spectra of PPII and α-helix conformations of fully perdeuterated AP (Fig. 39). Even though deuteration has removed coupling with the $C_\alpha H$ b, significant differences occur in the Amide III region, in addition to the hypochromic α-helix spectral intensity decrease.

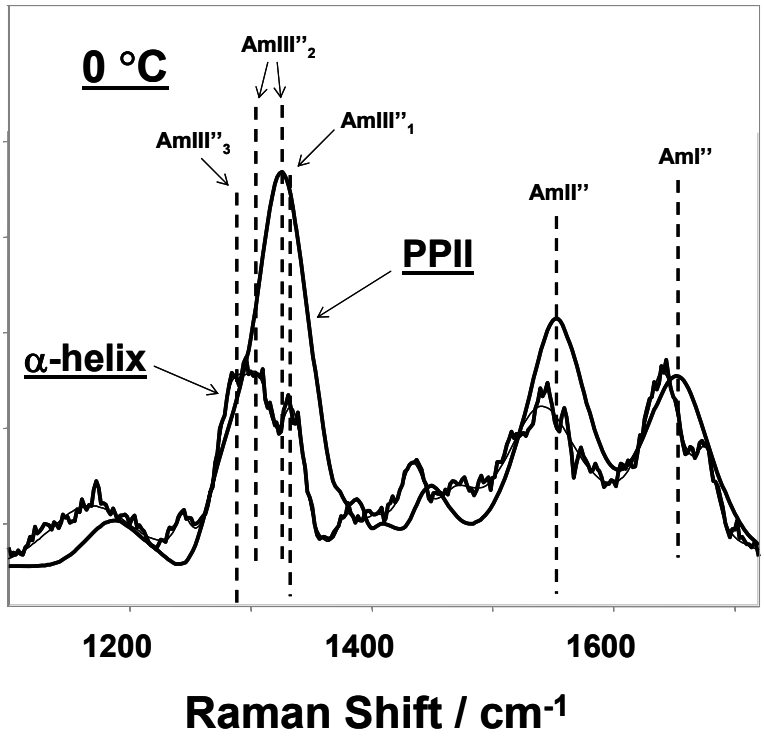

Figure 39. Comparison of calculated UVRR spectra of PPII and α-helix of fully 2,3,3,3-D_4 deuterated A_{21}

This investigation of the melting of AP from the α-helix to PPII conformations indicates that the melting can be quantitated by the characteristic difference spectra displayed in Fig. 36. Obviously, these difference spectra will change at different temperatures due to the temperature dependence of the basis spectra.

Although we expect that the other α-helix peptide conformations will show qualitatively similar spectra, we expect to also see significant differences, due to the fact that sidechains differ, the environments differ, and the α-helix exposure to solvent and its resulting hydration may differ.[56,58,68] This is clearly evident in the Fig. 40 UVRR spectral temperature dependence of the mainly α-helical apoMb. The contributions from the unordered states of apoMb were numerically removed by subtracting the acid denatured apoMb spectra from the neutral pH apoMb spectra. The resulting overlapped AmIII triplet contour α-helix apoMb spectra shows little temperature dependence even up to 56 °C.

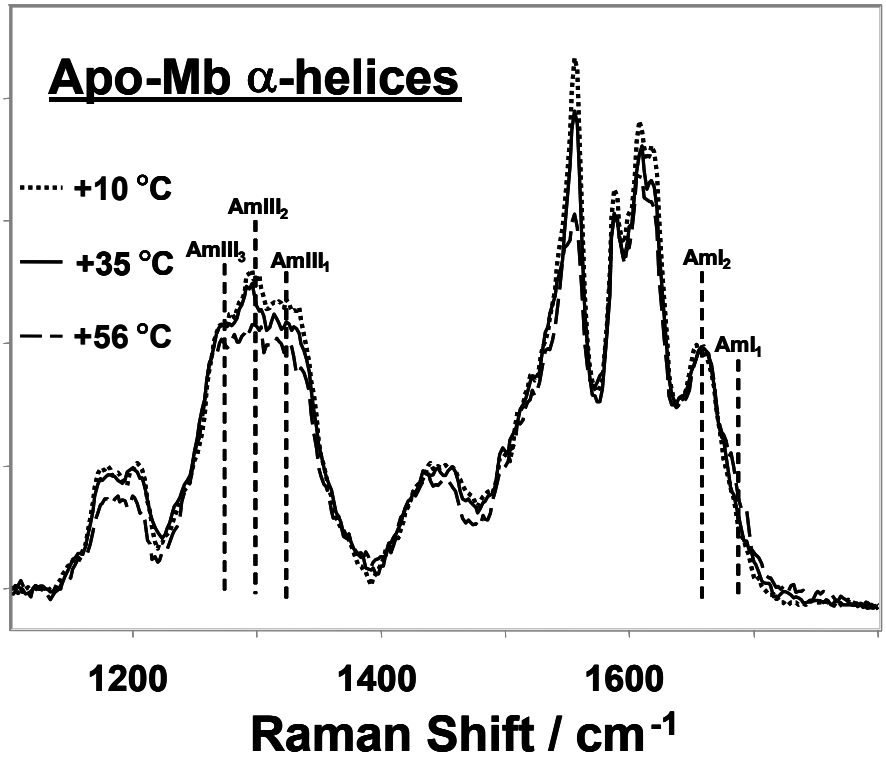

Figure 40. Temperature dependence of the UVRR spectra of apoMb α-helices. Non-α-helical spectral contributions were removed by subtracting pH=1.86 unordered apoMb spectra.

The spectral temperature changes observed are significantly smaller than in α-helical AP (at T > +10 °C). The largest change is the blue shift of the AmI band high frequency edge which shows up at the highest temperatures. Obviously, the apoMb α-helices are much more stable and show much less hydration changes than are observed for AP which is monomeric and fully water exposed.

Careful UV Raman studies of proteins may be able to monitor subtle effects such as helix hydration changes, in addition to being able to monitor the larger conformational changes.

3.4 CONCLUSIONS

We have reexamined in detail the assignment of the amide III region of the PPII and α-helix conformations of peptides and proteins using UV Raman spectra of a mainly polyala peptide. Many of our assignments agree with previous studies, while others challenge the conventional understanding. The conformational dependence of the UVRR spectra make this methodology a sensitive probe of protein and peptide secondary structure. We appear to see spectral signatures of α-helix hydration changes with temperature.

3.5 REFERENCES

(1) Asher, S. A. *Handbook of Vibrational Spectroscopy, John Whiley & Sons, Ltd.* **2001**, *1*, 557.

(2) Lednev, I. K.; Karnoup, A. S.; Sparrow, M. C.; Asher, S. A. *J. Am. Chem. Soc.* **1999**, *121*, 8074.

(3) Lednev, I. K.; Karnoup, A. S.; Sparrow, M. C.; Asher, S. A. *J. Am. Chem. Soc.* **2001**, *123*, 2388.

(4) Gruebele, M. *Annu. Rev. Phys. Chem.* **1999**, *50*, 485.

(5) Chi, Z.; Chen, X. G.; Holtz, J. S. W.; Asher, S. A. *Biochemistry* **1998**, *37*, 2854.

(6) Schweitzer-Stenner, R. *J. Raman Spectrosc.* **2001**, *32*, 711.

(7) Asher, S. A.; Ianoul, A.; Mix, G.; Boyden, M. N.; Karnoup, A.; Diem, M.; Schweitzer-Stenner, R. *J. Am. Chem. Soc.* **2001**, *123*, 11775.

(8) Ianoul, A.; Boyden, M. N.; Asher, S. A. *J. Am. Chem. Soc.* **2001**, *123*, 7433.

(9) Asher, S. A.; Mikhonin, A. V.; Bykov, S. B. *J. Am. Chem. Soc.* **2004**, *126*, 8433.

(10) Badger, R. M. *Annu. Rev. Phys. Chem.* **1955**, *6*, 217.

(11) Chen, M. C.; Lord, R. C. *J. Am. Chem. Soc.* **1974**, *96*, 4750.

(12) Chen, M. C.; Lord, R. C.; Mendelsohn, R. *Biochim. Biophys. Acta* **1973**, *328*, 252.

(13) Hamm, P.; Lim, M.; DeGrado, W. F.; Hochstrasser, R. M. *Proc. Natl. Acad. Sci. U.S.A.* **1999**, *96*, 2036.

(14) Chen, Z.; Shen, Y. R.; Somorjai, G. A. *Annu. Rev. Phys. Chem.* **2002**, *53*, 437.

(15) Woutersen, S.; Hamm, P. *J. Chem. Phys.* **2001**, *114*, 2727.

(16) Speare, J. O.; Rush, T. S., III. *Biopolymers* **2003**, *72*, 193.

(17) Venyaminov, S.; Prendergast, F. G. *Anal. Biochem.* **1997**, *248*, 234.

(18) Torrecillas, A.; Corbalan-Garcia, S.; Gomez-Fernandez, J. C. *Biochemistry* **2004**, *43*, 2332.

(19) Wu, Y.; Murayama, K.; Ozaki, Y. *J. Phys. Chem. B* **2001**, *105*, 6251.

(20) Prestrelski, S. J.; Byler, D. M.; Thompson, M. P. *Intl. J. of Pep & Prot. Research* **1991**, *37*, 508.

(21) Keiderling, T. A. *Curr. Opin. Chem. Biol.* **2002**, *6*, 682.

(22) Keiderling, T. A. *Circular Dichroism (2nd Edition)* **2000**, 621.

(23) Tanaka, T.; Inoue, K.; Kodama, T.; Kyogoku, Y.; Hayakawa, T.; Sugeta, H. *Biopolymers* **2001**, *62*, 228.

(24) Wang, F.; Polavarapu, P. L. *J. Phys. Chem. B* **2001**, *105*, 7857.

(25) Baello, B. I.; Pancoska, P.; Keiderling, T. A. *Anal. Biochem.* **1997**, *250*, 212.

(26) Kocak, A.; Luque, R.; Diem, M. *Biopolymers* **1998**, *46*, 455.

(27) Overman, S. A.; Thomas, G. J., Jr. *Biochemistry* **1998**, *37*, 5654.

(28) Mizuno, A.; Fujii, N.; Akaboshi, M.; Momose, Y.; Shimo-oka, T. *Japanese J. of Ophthalmology* **2000**, *44*, 354.

(29) Colaianni, S. E. M.; Aubard, J.; Hansen, S. H.; Nielsen, O. F. *Vibrational Spectrosc.* **1995**, *9*, 111.

(30) Copeland, R. A.; Spiro, T. G. *Biochemistry* **1987**, *26*, 2134.

(31) Sane, S. U.; Cramer, S. M.; Przybycien, T. M. *Anal. Biochem.* **1999**, *269*, 255.

(32) Overman, S. A.; Thomas, G. J., Jr. *Biochemistry* **1995**, *34*, 5440.

(33) Overman, S. A.; Thomas, G. J., Jr. *Biochemistry* **1999**, *38*, 4018.

(34) Dudik, J. M.; Johnson, C. R.; Asher, S. A. *J. Phys. Chem.* **1985**, *89*, 3805.

(35) Wilson, G.; Hecht, L.; Barron, L. D. *Biochemistry* **1996**, *35*, 12518.

(36) McColl, I. H.; Blanch, E. W.; Gill, A. C.; Rhie, A. G. O.; Ritchie, M. A.; Hecht, L.; Nielsen, K.; Barron, L. D. *J. Am. Chem. Soc.* **2003**, *125*, 10019.

(37) McColl, I. H.; Blanch, E. W.; Hecht, L.; Kallenbach, N. R.; Barron, L. D. *J. Am. Chem. Soc.* **2004**, *126*, 5076.

(38) Nafie, L. A.; Yu, G.-S.; Freedman, T. B. *Vibrational Spectrosc.* **1995**, *8*, 231.

(39) Yu, G.-S.; Freedman, T. B.; Nafie, L. A.; Deng, Z.; Polavarapu, P. L. *J. Phys. Chem.* **1995**, *99*, 835.

(40) Song, S.; Asher, S. A. *J. Am. Chem. Soc.* **1989**, *111*, 4295.

(41) Wang, Y.; Purrello, R.; Georgiou, S.; Spiro, T. G. *J. Am. Chem. Soc.* **1991**, *113*, 6368.

(42) Wang, Y.; Purrello, R.; Spiro, T. G. *J. Am. Chem. Soc.* **1989**, *111*, 8274.

(43) Jordan, T.; Spiro, T. G. *J. Raman Spectrosc.* **1994**, *25*, 537.

(44) Jordan, T.; Mukerji, I.; Wang, Y.; Spiro, T. G. *J. Mol. Struct.* **1996**, *379*, 51.

(45) Mirkin, N. G.; Krimm, S. *J. Phys. Chem. A* **2002**, *106*, 3391.

(46) Oboodi, M. R.; Alva, C.; Diem, M. *J. Phys. Chem.* **1984**, *88*, 501.

(47) Diem, M.; Polavarapu, P. L.; Oboodi, M.; Nafie, L. A. *J. Am. Chem. Soc.* **1982**, *104*, 3329.

(48) Diem, M.; Lee, O.; Roberts, G. M. *J. Phys. Chem.* **1992**, *96*, 548.

(49) Lee, S.-H.; Krimm, S. *Biopolymers* **1998**, *46*, 283.

(50) Lee, S.-H.; Krimm, S. *Chem. Phys.* **1998**, *230*, 277.

(51) Lee, S.-H.; Krimm, S. *J. Raman Spectrosc.* **1998**, *29*, 73.

(52) Overman, S. A.; Thomas, G. J., Jr. *J. Raman Spectrosc.* **1998**, *29*, 23.

(53) Mix, G.; Schweitzer-Stenner, R.; Asher, S. A. *J. Am. Chem. Soc.* **2000**, *122*, 9028.

(54) Mikhonin, A. V.; Asher, S. A. *J. Phys. Chem. B.*, **2005,** *109 (7)*, 3047-3052

(55) Note: We apologize for reversing the labeling scheme pioneered by Diem et al. (Ref 48), but find it more logically consistent with the normal vibrational numbering scheme which numerates bands in the order of highest to lowest frequencies.

(56) Manas, E. S.; Getahun, Z.; Wright, W. W.; DeGrado, W. F.; Vanderkooi, J. M. *J. Am. Chem. Soc.* **2000**, *122*, 9883.

(57) Wernet, P., Nordlund, D., Bergmann, Carvalleri, M.,Odelius, M., Ogasawara, H., Naslund, L. A., Hirsch, T. K., Ojamae, L., Glatzel, P., Pettersson, L. G. M , Nilsson, A. *Science* **2004**, *304*, 995.

(58) Walsh, S. T. R.; Cheng, R. P.; Wright, W. W.; Alonzo, D., O. V; Daggett, V.; Vanderkooi, J. M.; DeGrado, W. F. *Protein Sci.* **2003**, *12*, 520.

(59) Chen, X. G.; Asher, S. A.; Schweitzer-Stenner, R.; Mirkin, N. G.; Krimm, S. *J. Am. Chem. Soc.* **1995**, *117*, 2884.

(60) Shi, Z.; Olson, C. A.; Rose, G. D.; Baldwin, R. L.; Kallenbach, N. R. Proc. Natl. Acad. Sci. U.S.A. **2002**, 99, 9190.

(61) Lednev, I. K.; Karnoup, A. S.; Sparrow, M. C.; Asher, S. A. *Spectroscopy of Biological Molecules: New Directions, European Conference on the Spectroscopy of Biological Molecules, 8th, Enschede, Netherlands, Aug. 29-Sept. 2,* **1999**, 11.

(62) Lednev, I. K.; Karnoup, A. S.; Sparrow, M. C.; Asher, S. A. *J. Am. Chem. Soc.* **1999**, *121*, 4076.

(63) Lednev, I. K.; Karnoup, A. S.; Sparrow, M. C.; Asher, S. A. *Book of Abstracts, 219th ACS National Meeting, San Francisco, CA, March 26-30,* **2000**, PHYS.

(64) Ghosh, T.; Garde, S.; Garcia, A. E. *Biophys. J.* **2003**, *85*, 3187.

(65) Demmel, F.; Doster, W.; Petry, W.; Schulte, A. *Eur.Biophys. J.* **1997**, *26*, 327.

(66) Gerstein, M.; Lynden-Bell, R. M. *J. Phys. Chem.* **1993**, *97*, 2991.

(67) Gerstein, M.; Lynden-Bell, R. M. *J. Phys. Chem.* **1993**, *97*, 2982.

(68) Garcia, A. E. *Polymer* **2004**, *45*, 669.

(69) Blanch, E. W.; Bell, A. F.; Hecht, L.; Day, L. A.; Barron, L. D. *J. Mol. Biol.* **1999**, *290*, 1.

(70) Blanch, E. W.; Kasarda, D. D.; Hecht, L.; Nielsen, K.; Barron, L. D. *Biochemistry* **2003**, *42*, 5665.

(71) Blanch, E. W.; Robinson, D. J.; Hecht, L.; Syme, C. D.; Nielsen, K.; Barron, L. D. *Journal of General Virology* **2002**, *83*, 241.

(72) Robin, M. B. *"Higher Excited States of Polyatomic Molecules"*; Academic Press: New York **1975**, Vol. II.

(73) Schellman, J. A.; Becktel, W. J. *Biopolymers* **1983**, *22*, 171.

(74) Momii, R. K.; Urry, D. W. *Macromolecules* **1968**, *1*, 372.

(75) Onari, S. *Jpn. J. Appl. Phys.* **1970**, *9*, 227.

(76) Moffit, W. *Proc. Natl. Acad. Sci. U.S.A.* **1956**, *42*, 736.

4.0 CHAPTER 4. UNCOUPLED PEPTIDE BOND VIBRATIONS IN α-HELICAL AND POLYPROLINE II CONFORMATIONS OF POLYALANINE PEPTIDES

Work described in this Chapter is published in *J. Phys. Chem. B.*, **2005,** *109*, 3047-3052 (Authors: Mikhonin, A. V.; and Asher, S. A.). We examined the 204 nm UV resonance Raman (UVRR) spectra of the polyproline II (PPII) and α-helical states of a 21-residue mainly alanine peptide (AP) in different H_2O/D_2O mixtures. Our hypothesis is that, if the amide backbone vibrations are coupled then partial deuteration of the amide N will perturb the amide frequencies and Raman cross sections since the coupling will be interrupted; the spectra of the partially deuterated derivatives will not simply be the sum of the fully protonated and deuterated peptides. We find that the UVRR spectra of the AmIII and AmII' bands of both the PPII conformation and the α-helical conformation (and also the PPII AmI, AmI', and AmII bands) can be exactly modeled as the linear sum of the fully N-H protonated and N-D deuterated peptides. Negligible coupling occurs for these vibrations between adjacent peptide bonds. Thus, we conclude that these peptide bond Raman bands can be considered as being independently Raman scattered by the individual peptide bonds. This dramatically simplifies the use of these vibrational bands in IR and Raman studies of peptide and protein structure. In contrast, the AmI and AmI' bands of the α-helical conformation cannot be well modeled as a linear sum of the fully N-H protonated and N-D deuterated derivatives. These bands show evidence of coupling between adjacent peptide bond vibrations. Care must be taken in utilizing the AmI and AmI' bands for monitoring α-helical conformations since these bands are likely to change as the α-helical length changes and the backbone conformation is perturbed

4.1 INTRODUCTION

Vibrational spectroscopy[1-25] is a very powerful tool for studying peptide and protein structure. The utility of vibrational spectroscopic methods derive from their inherently high resolution. In addition, these methods are uniquely powerful since they can be used kinetically to examine short time (nsec, psec, and fsec) dynamics.[26-37] UV resonance Raman (UVRR) spectroscopy[4-7,27,28] is an especially powerful approach since it can be used to selectively excite within the amide backbone $\pi \rightarrow \pi^*$ transition[38] in order to selectively examine numerous amide vibrations.[39-42] In addition, it shows little interference from the vibrations of the ubiquitous solvent water,[27,43] in contrast to IR absorption based methods.[44]

We recently demonstrated that UVRR spectroscopy is the most powerful method to determine secondary structure of proteins and peptides in dilute solutions.[6,27,45] The method utilizes the unique UVRR spectral signatures of each of the protein secondary structure motifs.[6] The intrinsic assumption is that the basis spectra of each motif can be linearly added to fit the observed spectra and that the linear weighting factors give the relative abundancies of each motif.

The use of this approximation could be problematic. For example, it is clear that the Raman cross section of the α-helix conformation is relatively small due to the dependence of the Raman cross sections on the molar absorptivity of the peptide bond electronic transitions.[39] It is well known that the amide backbone $\pi \rightarrow \pi^*$ transitions suffer hypochromism due to excitonic interactions.[38,39,46-49] This causes hypochromism in the resonance Raman cross sections. Thus, the Raman spectra of an amide bond with α-helical Φ and Ψ angles, but not in an α-helix will display the identical spectrum as a peptide bond within a long α-helix.[7] However, the long α-helix peptide bond Raman cross sections will be smaller due to hypochromism.[50] The α-helical Raman intensities increase as the helix length shortens, exactly the opposite behavior seen for CD α-helical molar ellipticities. In fact, the CD molar ellipticity vanishes for short helices.[45,51,52]

The intrinsic assumption utilized in many vibrational spectroscopic studies: that the measured spectra derive from the linear summation of spectra contributed by the individual peptide bonds. This assumption ignores the possibility of coupling of the vibrational motion of adjacent peptides. This assumption is used even though there are numerous reports that indicate coupling of the amide I (AmI) bands of peptides.[36,53-59]

The nature of amide vibrations is very complex[50,60-65] and not yet fully understood. The vibrations of a peptide group involve atomic motions such as CO stretching (CO s), CN stretching (CN s), C_α-C stretching (C_α-C s), NH bending (NH b), C_α-H bending (C_α-H b). The individual vibrational modes of adjacent peptide bonds could strongly couple to each other, to form complex collective vibrations. This coupling could occur as a result of through-bond interactions between adjacent amide groups,[54,58,59] through hydrogen bond interactions,[58] and/or through the interactions between the oscillating electronic charge densities of adjacent peptide groups. The latter interactions can be expressed either in terms of a relatively simple transient dipole coupling model (TDC),[55-57,59] or in terms of a somewhat more complex transient charge model (TCM).[13,54,55] TDC is expected to have the greatest impact on vibrations with large dipole moment changes. As expected, there are examples of coupling between the AmI modes peptide groups due to their large dipole moment changes.[36,53-59]

In a previous investigation[66] we attempted to examine the coupling between adjacent peptide bonds by investigating the UVRR spectra of two linked amides in mixed H_2O/D_2O solutions. Deuteration of the amide N (N-D) dramatically perturbs the amide vibrational modes. The experiment probed whether deuteration of one amide perturbed the vibrational modes of the linked amide. In the case studied we clearly demonstrated independent AmIII, AmII and AmII' vibrations in this small peptide. Unfortunately we were unable to come to a definitive conclusion for the AmI bands due to their weak intensities.[66]

In the work here we examine the same issue in a 21 residue mainly ala peptide AP which is ~50 % α-helix at 0 °C[27,28] and melts to a polyproline II (PPII) conformation at higher temperatures.[67] We already examined the UVRR spectra and the normal modes of this peptide in both its α-helical and PPII states in detail.[50] We demonstrated that, as in the amide functional group, N-deuteration of a peptide bond dramatically changes the normal mode composition of the peptide bond vibrations due to the decoupling of CN s and NH b motion.[60,68] This gives rise to completely differentiable spectra of the N-H and N-D peptide bonds, which permits us to monitor spectral changes due to the deuteration of adjacent peptide bonds. We searched for evidence of perturbation of the spectra due to adjacent peptide bond deuteration. As shown below we see no evidence for coupling of the amide vibrations, except for the lone case of the AmI/AmI' vibrations of the α-helix conformation of AP. This indicates that in most cases vibrational spectra can be simply interpreted as the linear sum of the spectra of the individual

peptide bonds. This result increases the utility of vibrational spectroscopic methods for studying protein structure and function.

4.2 EXPERIMENTAL SECTION

4.2.1 Sample Preparation.

The 21-residue ala-based peptide AAAAA(AAARA)$_3$A (AP) was prepared (HPLC pure) at the Pittsburgh Peptide Facility by using the solid-state peptide synthesis method. The AP H_2O/D_2O mixtures contained 1 mg/ml AP and 0.2 M sodium perchlorate. All Raman spectra were normalized to the intensity of the ClO_4^- internal standard Raman band (932 cm^{-1}).

To ensure the random deuteration of the peptide groups along the AP chain in its α-helical state, all the AP solutions in H_2O/D_2O mixtures were held at +62 °C for 5 min prior to lowering the temperature to form the α-helix conformations. At 62 °C AP exists predominantly in a highly water exposed PPII conformation, which ensures fast and random H/D exchange of the amide nitrogens. All UVRR measurements were cycled through the temperature sequence: 0, +50, +62, 0 °C.

L-arginine was purchased from Sigma Chemical (St. Louis, MO) and used as received. All the arg solutions in H_2O/D_2O mixtures contained 5 mg/ml concentrations of arg, and 0.5 M concentrations of sodium perchlorate.

4.2.2 Instrumentation

The UV resonance Raman instrumentation has been described in detail elsewhere.[27,28] A Coherent Infinity Nd:YAG laser produced 355 nm (3rd harmonic) 3 nsec pulses at 100 Hz. This beam was Raman shifted to 204 nm (5th anti-Stokes) by using a 1 m tube filled with hydrogen (60 psi). A Pellin Broca prism was used to select the 204 nm excitation beam. The Raman scattered light was imaged into a subtractive double spectrometer[69] and the UV light was

detected by a Roper Scientific nitrogen cooled CCD camera. All samples were measured in a thermostatted free surface flow stream.

4.3 RESULTS AND DISCUSSION

AP is >50% α-helical at 0 °C and melts as the temperature increases to 30 °C.[27] The unfolded state of AP peptide was initially assumed to be disordered or in a random coil state.[27,28,70] However, we recently demonstrated that the AP α-helix melts to a predominantly polyproline II (PPII) conformation.[67] The kinetic studies[27,28,70] reveal fast (~200 ns) α-helix melting to the PPII-state without any significantly populated intermediates.

4.3.1 AP PPII bands in pure H_2O.

204 nm excitation occurs within the π→π* electronic transitions of the amide backbone,[38] which enhances the backbone amide bond vibrational modes.[39-42] UVRR spectra of the AP PPII-state in water at +62 °C (Fig. 41) show an AmI band at 1660 cm^{-1} (mainly CO stretching), the AmII band at 1558 cm^{-1} (mainly CN s and NH b) and the C_α-H b doublet (with a contribution from the CH_3-umbrella mode) at 1370 and 1394 cm^{-1}. The C_α-H b bands are resonancely enhanced only in PPII-like and β-sheet-like conformations and do not appear in the α-helix conformation.[6,7,50,67,71] Our recent study of the AmIII region[50] has demonstrated the complex origin of these bands which involve CN s and NH b coupled to C-C_α s and C_α-H b motions.[7,50] The 1245 cm^{-1} ($AmIII_3$) band,[50] which is assigned to the "classic" AmIII band shows dominating contributions from NH bending and C-N stretching. The 1303 cm^{-1} ($AmIII_2$) band derives mainly from C-C_α stretching mixed with C_αH bending, with possibly a small contribution from CN stretching.[50] The weak $AmIII_1$ band at 1336 cm^{-1} was suggested[50] to result from a minor β-strand conformation of AP. In this case the band would contain contributions from mainly C_α-C s and N-C s.

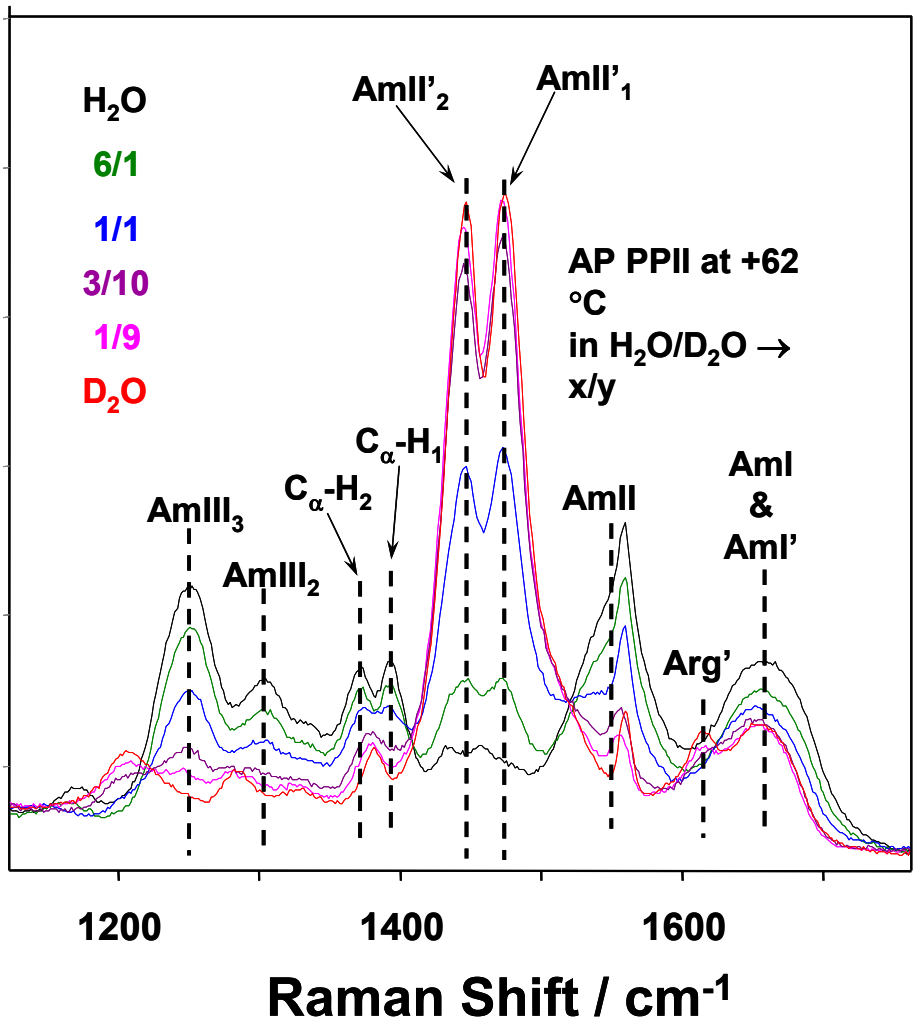

Figure 41. 204 nm UVRR spectra of AP PPII-state in different H_2O/D_2O mixtures at +62 °C. Neither H_2O nor D_2O Raman spectra were subtracted. The O_2 stretching contribution (sharp band at ~1555 cm^{-1}, overlapping the AmII band) was not removed.

4.3.2 AP PPII bands in pure D_2O.

The 204 nm UVRR spectrum of PPII AP in pure D_2O at 62 °C (Fig. 41) shows a dominating Am II' doublet at 1444 and 1476 cm^{-1} due to the exchange of the peptide bonds to form the N-D derivatives. In the N-D derivative the ND b is decoupled from the CN s. This doublet derives from the resonance coupling of an almost pure CN s vibration with a CH_3 asymmetric bending vibration.[28,50,60,72] This coupling disappears[50] upon substitution of natural abundance ala by perdeuterated 2,3,3,3-D_4 ala to form the deuterated derivative AdP.

AP in D_2O also shows a doublet in the AmI' region, with bands at 1614 cm^{-1} and 1660 cm^{-1} (Fig. 41). We recently demonstrated that the 1660 cm^{-1} band is the AmI' vibration,[50] while the ~1614 cm^{-1} band results from arg side chain vibration(s) (Fig. 42), as discussed in detail below. The protonated ala sidechains in D_2O give rise to a small band at ~1380 cm^{-1} from the CH_3 umbrella mode.[50,60] Thus, N-D deuteration of AP in D_2O results in the loss of the $AmIII_3$, $AmIII_2$, the weak $AmIII_1$ and the AmII bands, which are replaced by the dominating AmII' doublet. Small frequency shifts occur between the AmI and AmI' bands. Thus, we can separately monitor the spectral features of protonated and deuterated peptide groups since most strong bands do not overlap.

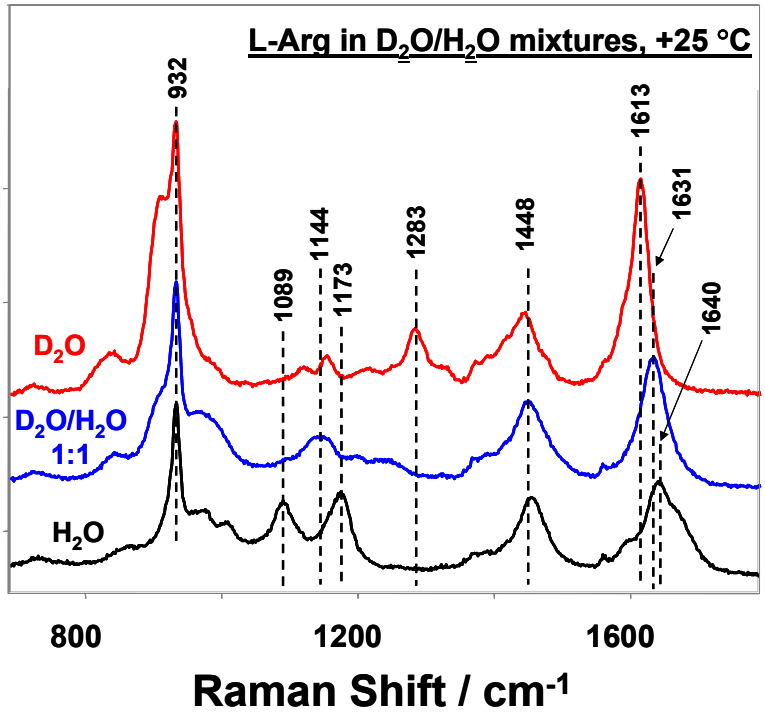

Figure 42. 204 nm UVRR spectra of L-arg (5 mg/ml) in pure D_2O, pure H_2O and in a H_2O/D_2O mixture (1:1) at +25 °C. The ~1640 cm^{-1} band in H_2O shifts to ~1613 cm^{-1} in D_2O.

4.3.3 AP PPII bands in H_2O/D_2O mixtures.

We can examine the UVRR spectra of PPII AP in mixed H_2O/D_2O solutions to determine whether there is coupling of the amide vibrations between peptide bonds. The hypothesis is, that if coupling occurs between protonated segments, random deuteration will break this coupling and cause changes in the coupled normal modes and shifts in the vibrational frequencies. This

will result in an inability to model the spectra of randomly deuterated AP simply as the weighted sums of AP in pure H_2O and D_2O. Obviously, if coupling is absent then we can treat the Raman scattering from PPII conformations as independent scattering from individual peptide bonds. Our earlier study of two linked amides concluded that there was no coupling between adjacent peptide groups in that small peptide(s).[66]

The rate of H/D exchange at the amide nitrogen depends mainly on the peptide/protein conformation as well as on the pH/pD value.[73-75] Exposed amino acid residues at neutral pH's exchange fast, while the rates for buried amino acid residues in native state may be reduced by factors as large as 10^8 relative to the same residues in unfolded state.[76]

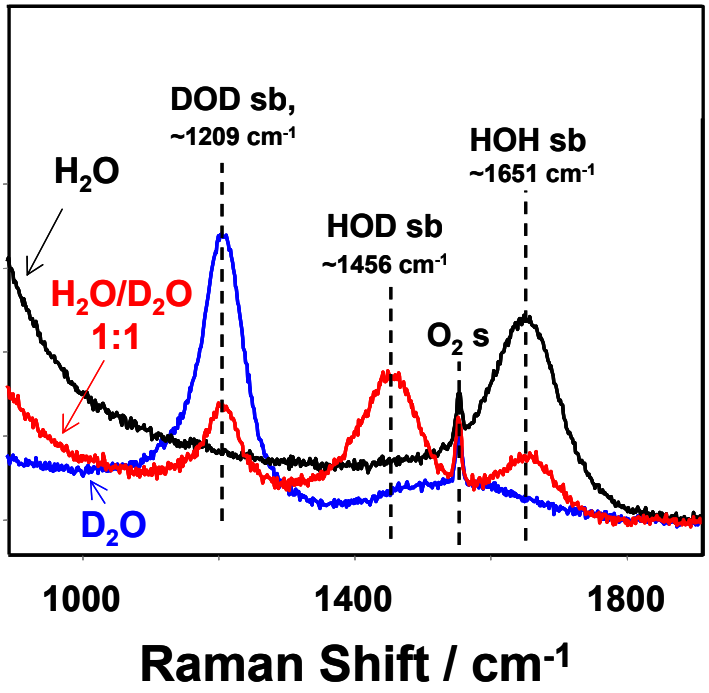

Figure 43. 204 nm UVRR spectra of pure H_2O, pure D_2O, and 1:1 H_2O/D_2O mixture. Spectra clearly shows that 1:1 mixture consists of 25% H_2O, 50% HOD, and 25% D_2O. Note: the contribution from atmospheric oxygen (O_2 s) has not been removed.

Since the PPII state of AP is highly exposed to H_2O and/or D_2O, and/or H_2O/D_2O, the H/D exchange at the amide nitrogen will be complete at neutral pH/pD values within min, as we confirmed by our spectral measurements. Thus, we have complete statistical exchange of H and D, and the numbers of both N-protonated and N-deuterated amide groups is simply proportional to the relative concentrations of H_2O and D_2O.

Fig. 41 shows AP PPII spectra taken at +62 °C in various mixtures. Though water, D_2O, and HOD contributions are not subtracted from these UVRR spectra their relative contributions for AP concentration of 1 mg/ml are low. The broad H_2O OH bending band at ~1651 cm^{-1} contributes only to the AmI region, while the broad D_2O OD bending band at ~1209 cm^{-1} does not overlap any band in the 1240 – 1670 cm^{-1} region of interest. However, the HOD bending band, in D_2O/H_2O mixtures at ~1456 cm^{-1}, may overlap the AmII' band (Fig. 43).

In contrast, the arg sidechain bands complicate the AmI spectral region (Fig. 42). For example, the ~1640 cm^{-1} arg band in water downshifts to ~1614 cm^{-1} in D_2O. There is also an arg band at ~1450 cm^{-1} which overlaps the AmII' doublet. However, the AmII and AmIII regions are free from any overlap from arg, H_2O, HOD and D_2O vibrations.

The Fig. 41 spectra show that the AmIII and AmII band intensities are proportional to the relative concentration of H in the H_2O/D_2O mixtures, while the AmII' band intensity is proportional to a relative concentration of D. There are no obvious changes in spectral bandshapes as the relative H_2O and D_2O concentrations change. No new bands appear.

Fig. 44 compares the experimentally measured AP PPII spectrum in a 1:1 H_2O/D_2O mixture at +62 °C to the equally weighted sum of the AP PPII spectra in pure water and AP PPII in pure D_2O at +62 °C. In Fig. 44 we digitally removed the spectral contributions from H_2O, HOD, D_2O, as well as from arg sidechains. Fig. 44 clearly shows no evidence of spectral differences between the mixed and pure H_2O/D_2O spectra; the entire 1:1 H_2O/D_2O spectrum is modeled well by linearly summing AP spectra in pure H_2O and D_2O.

This observation is not particularly surprising for the AmII, II' and III vibrations since they have modest dipole moments and would not couple well through a transition dipole coupling mechanism.[55-57,59] However, the lack of coupling for the AmI vibration may be surprising in view of the Hochstrasser group's recent 2-D IR spectral observation of AmI coupling in an α-helical peptide.[53,54] There is no real conflict here since our PPII structure is quite different; the carbonyls are not coparallel and the PPII structure does not have intrapeptide hydrogen bonds. Further, because of their relative orientation and because the through space distance between carbonyls is longer in the PPII structure compared to that in the α-helix, we expect a decreased transition dipole coupling in the PPII conformation compared to that in the α-helix conformation.[55,56]

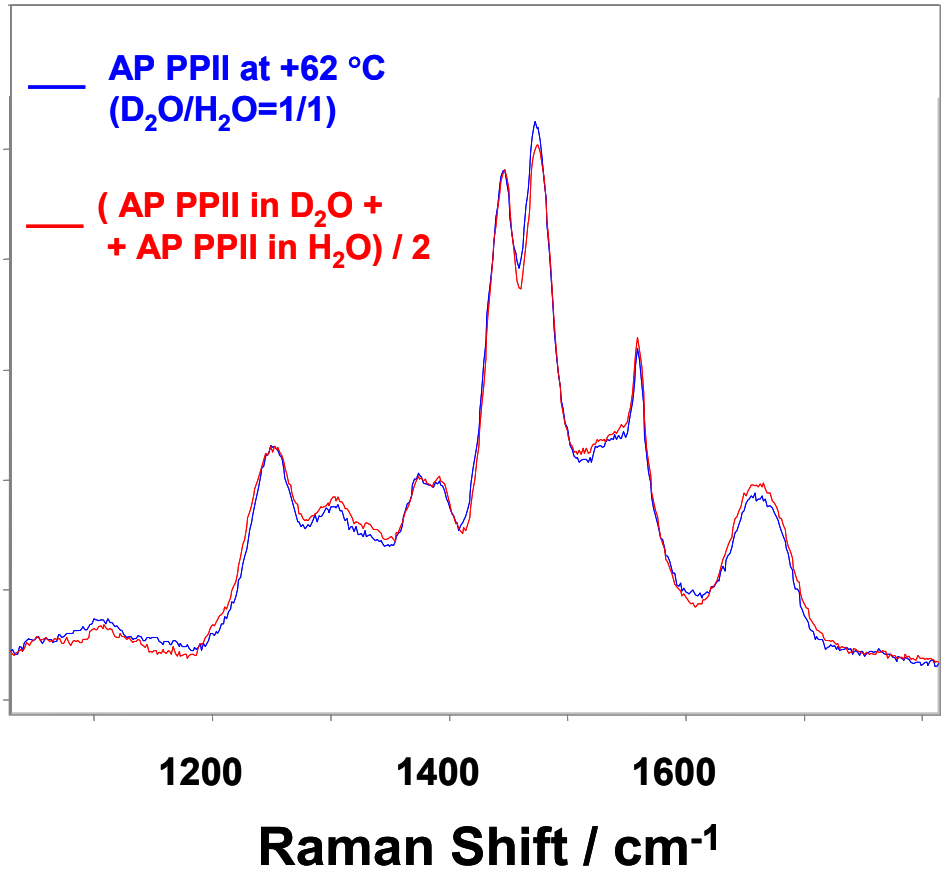

Figure 44. 204 nm UVRR spectra of the AP PPII state in a D_2O/water mixture (1:1) at +62 °C can be modeled well by the sum of spectra of AP PPII in pure water and AP PPII in pure D_2O. Note that the contributions of the arg sidechain in D_2O, H_2O and in H_2O/D_2O were digitally removed, as were the D_2O, H_2O, and HOD spectral contributions.

Deuteration dramatically changes the amide normal modes,[28,50,60] where the UVRR AmIII and AmII bands disappear and are replaced by an AmII' band which contains a large amount of CN s. In a 1:1 mixed H_2O/D_2O solution, 75 % of the N-H (N-D) derivatives possess an adjacent N-D (N-H) peptide bond, while in the 6:1 mixture only 36.7% of the N-H (N-D) have at least one adjacent N-D (N-H) (Table 7). **Thus we can clearly conclude that coupling between the identical vibrations of adjacent peptide groups (namely AmI, II, III, II' and I') does not occur *in the AP PPII conformation and each peptide bond vibrates independently from its neighbors.*** Alternatively, we would conclude that coupling results in insignificant spectral changes in either intensity or frequency.

Table 7. Population of protonation/deuteration states of three adjacent peptide bonds in different D_2O/H_2O mixtures.

H_2O/D_2O ratio	Population Fraction of Pure Protonation or Deuteration States, %			Population Fractionof Mixed Protonation and Deuteration States, %						
	HHH	DDD	**Total**	HHD	DHH	DHD	DDH	HDD	HDH	**Total**
6:1	63	0.29	**63.3**	10.5	10.5	1.7	1.7	1.7	10.5	**36.7**
1:1	12.5	12.5	**25**	12.5	12.5	12.5	12.5	12.5	12.5	**75**
3:10	1.2	45.5	**46.7**	4.1	4.1	13.7	13.7	13.7	4.1	**53.3**
1:9	0.1	72.9	**73**	0.9	0.9	8.1	8.1	8.1	0.9	**27**

4.3.4 Calculation of AP α-helical UVRR spectra in different H_2O/D_2O mixtures.

It is not possible to prepare pure α-helical conformation samples of AP. Even low temperature samples are a mixture of α-helical and PPII AP conformations. We calculated the pure AP α-helical spectra by numerically removing the PPII spectral contribution. This is straightforward since we previously characterized the AP PPII spectrum in pure water and pure D_2O[27,28,50,67] and determined the temperature dependence of the PPII amide bands between -5.5 °C to 80 °C. Thus, we calculate the AP α-helix spectra at 0 °C from the relationship:

$$\mathbf{S_\alpha(0\ °C) = [S_{obs}(0\ °C) - (1\text{-}f_\alpha)*S_{PII}(0\ °C)] / f_\alpha} \qquad \mathbf{(5)}$$

where $S_\alpha(0\ °C)$ is the calculated AP α-helix spectrum, $S_{obs}(0\ °C)$ is the observed AP spectrum, and $S_{PII}(0\ °C)$ is the calculated AP PPII spectrum, all at T=0 °C in a specific H_2O/D_2O mixture. f_α=0.55 is the α-helix fraction of AP at 0 °C determined by Lednev et al.[27] Fig. 45 shows an example of the decomposition of the T = 0 °C AP spectrum in H_2O/D_2O (1:1) into its α-helix and PPII components, while Fig. 46 compares the calculated α-helix spectra of six different H_2O/D_2O mixtures ranging from pure water to pure D_2O.

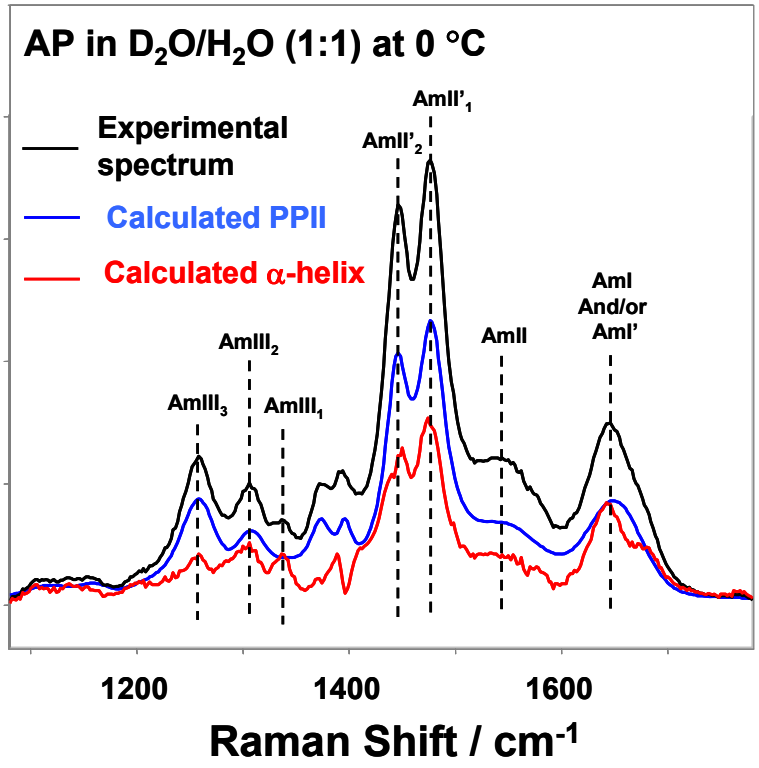

Figure 45. Example of decomposition of 204 nm UVRR spectra of AP into its PPII and α-helical components in a H_2O/D_2O mixture (1:1) at 0 °C. The PPII spectrum at 0 °C was calculated from the experimental AP PPII spectrum at +50 °C utilizing the measured temperature dependence of its UVRR bands. The α-helix spectrum at 0 °C was calculated by subtracting the calculated 0 °C PPII UVRR spectrum from the 0 °C experimental UVRR spectrum using the Eqn. 5. Note: arg, water, DOD, and D_2O contributions were not subtracted.

4.3.5 AP α-helix bands in pure water.

We recently examined the assignment of the UVRR bands of α-helical AP in water in detail.[50] The AmI band occurs at ~1646 cm^{-1}, while the AmII band occurs at 1547 cm^{-1} (Fig. 46). The AmI and AmII bands of the α-helix are 13 cm^{-1} and 11 cm^{-1} downshifted compared to those of the PPII conformation.[50] In addition, the AP α-helix, N-H amide bond AmIII region shows a characteristic triplet of bands between 1250 and 1350 cm^{-1}, which are denoted as $AmIII_3$ (~1261 cm^{-1}), $AmIII_2$ (~1306 cm^{-1}) and $AmIII_1$ (~1337 cm^{-1}).[50] The normal mode composition of these bands is complicated; the vibrations were shown to involve different combinations of NH ib, CN s, NC s, C_α-H b, and C_α-C s.[50] The shape of AmIII band envelope dramatically changes between the PPII and α-helix conformations (See Fig. 12 of Mikhonin et al.[50] or Fig. 36 of Chapter 3). It

was also shown that the $AmIII_3$ band frequency is very sensitive to the Ψ dihedral angle, which specifies the backbone secondary structure,[7,67] due to the Ψ dependence of the coupling between NH b and C_α-H b vibrations. NH b was shown to be highly mixed with C_α-H b at Ψ ~ 120° (β-strand-like or PPII-like), but almost free from this mixing at Ψ = -60° (α-helix-like Ψ-angle). The AmIII band envelope suffers a large relative intensity decrease upon α-helix formation (See Fig. 12 of Mikhonin et al.[50] or Fig. 36 of Chapter 3) due to the hypochromism due to α-helix excitonic interactions.[38,39,46-49]

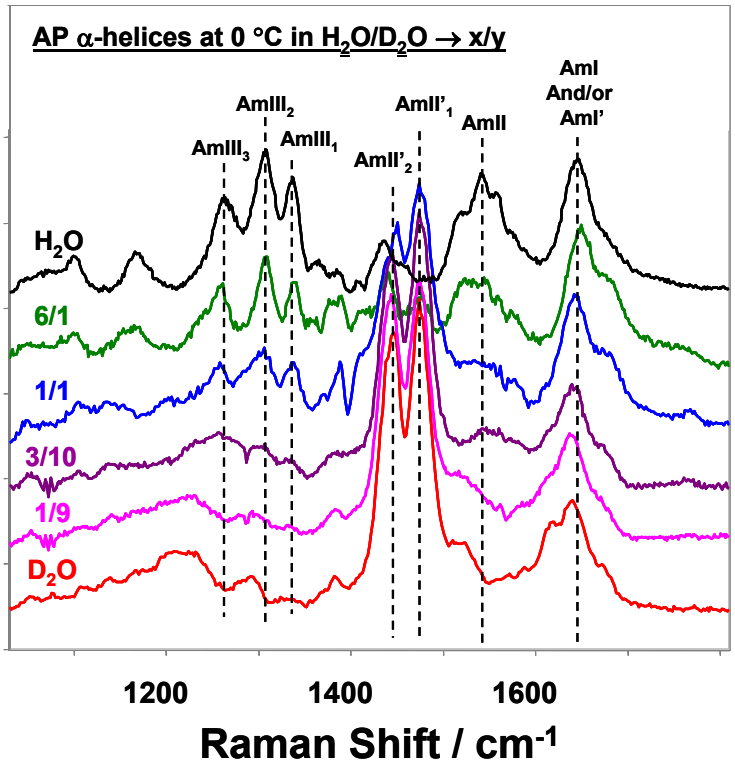

Figure 46. UVRR spectra of AP α-helices calculated at 0 °C in different H_2O/D_2O mixtures using the Eqn. 5. Note: arg, water, DOD, and D_2O contributions are not subtracted.

4.3.6 AP α-helix bands in pure D_2O.

N-deuteration also dramatically affects the AP α-helix UVRR spetra (Fig. 46). The decoupling of ND b from CN s and C_α-H b again leads to a dominating enhancement of the AmII' band, where CN s motion is resonancely coupled with one of the components of the CH_3 bending

mode.[28,50,60,72] Though the AmII' band of the AP α-helix is only slightly downshifted compared to the AmII' band of the AP PPII, it shows a ~2-fold intensity loss[50] due to the α-helix excitonic interactions.[38,39,46-49]

The AmI' band, which occurs in α-helical AP at 1639 cm^{-1}, shows no significant change in relative intensity compared to that of AmI' band of AP PPII. However the frequency of the AmI' band downshifts ~20 cm^{-1} upon α-helix formation. The AmIII' bands, which are almost pure N-D b, are weak and occur between 900 – 1000 cm^{-1} (not shown).

4.3.7 Coupling of AP α-helical amide bond vibrations.

We can determine whether coupling occurs between amide vibrations in adjacent α-helical bonds in AP by testing whether the UVRR spectra of mixed H_2O/D_2O mixtures can be modeled as the sum of α-helical spectra of AP in pure H_2O and D_2O. We can easily and independently monitor the N-H and N-D AmIII and AmII' bands since they do not significantly overlap with themselves nor with water or D_2O. Even though the ~1450 cm^{-1} arg sidechain, as well as the ~1456 cm^{-1} HOD bands overlap the AmII' band, they are too weak to significantly interfere (Figs. 42 and 43).

Fig. 46 shows that the intensity in the AmIII and AmII regions in the N-H α-helix UVRR spectra smoothly decrease as the concentration of D_2O increases. In contrast, the AmI region shows discontinuous changes such as the appearance of a high frequency AmI shoulder at ~1675 cm^{-1}. The low frequency AmI'shoulder at ~1614 cm^{-1} simply results from an arg sidechain band downshifted in D_2O to ~1613 cm^{-1} from its ~1640 cm^{-1} value in H_2O (Fig. 42).

Fig. 47 clearly shows the AmIII and AmII' regions of α-helical AP can be satisfactory modeled as the sum of spectra of α-helical AP in pure H_2O and D_2O. The situation is difficult to resolve for the AmII N-H α-helix region since it is plagued by overlapping bands from atmospheric oxygen, arg and HOD, which make the results unreliable.

In contrast, it is clear that the AmI/AmI' region cannot be modeled as the weighted sum of individual α-helices in pure water and pure D_2O. **We, thus, find evidence of adjacent peptide coupling in the AmI/AmI' region of α-helical AP.** The high frequency shoulder at ~1675 cm^{-1} derives from a band contributed by the N-H peptide bonds (Fig. 46), which is not,

however, present in pure H_2O (Fig. 43). It is a collective vibrational frequency which is not observed in the absense of partial deuteration.

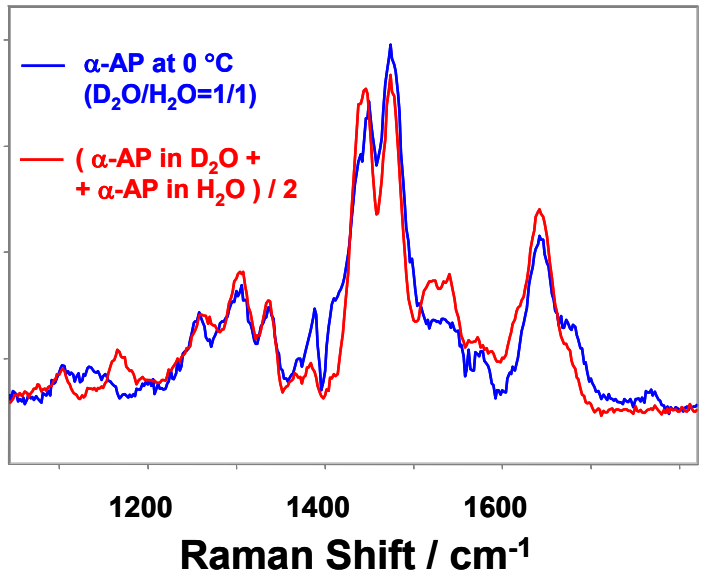

Figure 47. 204 nm calculated UVRR spectra of AP α-helix in 1:1 D_2O/water mixture at 0 °C. The AmIII and AmII' regions are well modeled by the sum of the AP α-helix in pure H_2O and AP α-helix in pure D_2O. We attempted to digitally remove overlapping bands from arg in D_2O, H_2O, and H_2O/D_2O contributions as well as D_2O, H_2O, and HOD. The AmII band fitting is unreliable because of the overlapping contributions of these bands to the AmII region and the contribution from atmospheric oxygen. The spectral differences in the AmI/AmI' region clearly indicate vibrational coupling between adjacent peptides in this α-helix conformation.

Our observation of coupling of the AmI/AmI' bands of α-helical AP is consistent with Hochstrasser's group's[53,54] recent demonstration of coupling between the AmI' bands of α-helical peptides. These studies were accomplished by ultrafast, transient 2-D IR studies of $^{13}C=^{18}O$ isotopically edited peptides.

The lack of coupling of the amide vibrations in the PPII conformation, and the lack of coupling of the AmIII, AmII' (and probably AmII) bands in the α-helix conformation, is important since it makes these bands very straightforward indicators of the conformation of peptides and proteins. The UVRR spectra can be assumed to result from the independent Raman scattering of different peptide bonds. Obfuscation of spectral interpretations of conformational changes will not result from alterations in the characteristic basis spectra as the peptide or protein adopts different conformations. This promises to make vibrational spectroscopy of even higher

utility for protein structural studies. This is especially important because it increases the utility of kinetic vibrational spectroscopy to elucidatethe initial steps in protein folding.[26-33]

4.4 CONCLUSIONS

UV Raman studies of α-helical and PPII conformations of AP in mixed H_2O and D_2O samples show that the AmIII (PPII and α-helix), AmII (PPII) and AmII' (PPII and α-helix) bands can be modeled as being independently Raman scattered by the individual peptide bonds. Negligible coupling occurs for these vibrations between the adjacent peptide bonds. This dramatically simplifies the use of vibrational spectral modeling to elucidate peptide and protein structure. The AmI and AmI' vibrations of PPII also show no evidence of coupling between adjacent peptide bonds. In contrast, the AmI and AmI' bands of the α-helical conformation clearly indicate the occurrence of interamide coupling. The interamide coupling in the α-helix is probably the result of the proximity of the amide C=O groups to one another, the fact that they are oriented parallel to one another, and because the C=O of different amides are linked through interamide hydrogen bonding.

4.5 REFERENCES

(1) Barth, A.; Zscherp, C. *Q. Rev. Biophys.* **2002**, *35*, 369.

(2) Vogel, R.; Siebert, F. *Curr. Opin. Struct. Biol.* **2000**, *4*, 518.

(3) Vass, E.; Hollosi, M.; Besson, F.; Buchet, R. *Chem. Rev.* **2003**, *103*, 1917.

(4) Asher, S. A. *Handbook of Vibrational Spectroscopy, John Whiley & Sons, Ltd.* **2001**, *1*, 557.

(5) Asher, S. A. *Anal. Chem.* **1993**, *65*, 59A.

(6) Chi, Z.; Chen, X. G.; Holtz, J. S. W.; Asher, S. A. *Biochemistry* **1998**, *37*, 2854.

(7) Asher, S. A.; Ianoul, A.; Mix, G.; Boyden, M. N.; Karnoup, A.; Diem, M.; Schweitzer-Stenner, R. *J. Am. Chem. Soc.* **2001**, *123*, 11775.

(8) Barron, L. D.; Blanch, E. W.; McColl, I. H.; Syme, C. D.; Hecht, L.; Nielsen, K. *Spectroscopy* **2003**, *17*, 101.

(9) Nafie, L. A.; Yu, G.-S.; Freedman, T. B. *Vibrational Spectrosc.* **1995**, *8*, 231.

(10) Diem, M. *Spectroscopy* **1995**, *10*, 38.

(11) Keiderling, T. A. *Curr. Opin. Chem. Biol.* **2002**, *6*, 682.

(12) Keiderling, T. A. *Circular Dichroism (2nd Edition)* **2000**, 621.

(13) Hamm, P.; Lim, M.; DeGrado, W. F.; Hochstrasser, R. M. *Proc. Natl. Acad. Sci. U.S.A.* **1999**, *96*, 2036.

(14) Woutersen, S.; Hamm, P. *J. Chem. Phys.* **2001**, *114*, 2727.

(15) Speare, J. O.; Rush, T. S., III. *Biopolymers* **2003**, *72*, 193.

(16) Torrecillas, A.; Corbalan-Garcia, S.; Gomez-Fernandez, J. C. *Biochemistry* **2004**, *43*, 2332.

(17) Wu, Y.; Murayama, K.; Ozaki, Y. *J. Phys. Chem. B* **2001**, *105*, 6251.

(18) Prestrelski, S. J.; Byler, D. M.; Thompson, M. P. *Intl. J. of Pep & Prot. Research* **1991**, *37*, 508.

(19) Tanaka, T.; Inoue, K.; Kodama, T.; Kyogoku, Y.; Hayakawa, T.; Sugeta, H. *Biopolymers* **2001**, *62*, 228.

(20) Wang, F.; Polavarapu, P. L. *J. Phys. Chem. B* **2001**, *105*, 7857.

(21) Baello, B. I.; Pancoska, P.; Keiderling, T. A. *Anal. Biochem.* **2000**, *280*, 46.

(22) Baello, B. I.; Pancoska, P.; Keiderling, T. A. *Anal. Biochem.* **1997**, *250*, 212.

(23) Kocak, A.; Luque, R.; Diem, M. *Biopolymers* **1998**, *46*, 455.

(24) Wilson, G.; Hecht, L.; Barron, L. D. *Biochemistry* **1996**, *35*, 12518.

(25) McColl, I. H.; Blanch, E. W.; Gill, A. C.; Rhie, A. G. O.; Ritchie, M. A.; Hecht, L.; Nielsen, K.; Barron, L. D. *J. Am. Chem. Soc.* **2003**, *125*, 10019.

(26) Callender, R.; Dyer, R. B. *Curr. Opin. Struct. Biol.* **2002**, *12*, 628.

(27) Lednev, I. K.; Karnoup, A. S.; Sparrow, M. C.; Asher, S. A. *J. Am. Chem. Soc.* **1999**, *121*, 8074.

(28) Lednev, I. K.; Karnoup, A. S.; Sparrow, M. C.; Asher, S. A. *J. Am. Chem. Soc.* **2001**, *123*, 2388.

(29) Gulotta, M.; Gilmanshin, R.; Buscher, T. C.; Callender, R. H.; Dyer, R. B. *Biochemistry* **2001**, *40*, 5137.

(30) Gulotta, M.; Rogatsky, E.; Callender, R. H.; Dyer, R. B. *Biophys. J.* **2003**, *84*, 1909.

(31) Gilmanshin, R.; Gulotta, M.; Dyer, R. B.; Callender, R. H. *Biochemistry* **2001**, *40*, 5127.

(32) Yamamoto, K.; Mizutani, Y.; Kitagawa, T. *Biophys. J.* **2000**, *79*, 485.

(33) Wang, J.; El-Sayed, M. A. *Biophys. J.* **1999**, *76*, 2777.

(34) Rubtsov, I. V.; Wang, J.; Hochstrasser, R. M. *J. Phys. Chem. A* **2003**, *107*, 3384.

(35) Kubo, M.; Shiomitsu, E.; Odai, K.; Sugimoto, T.; Suzuki, H.; Ito, E. *Proteins* **2004**, *54*, 231.

(36) Hamm, P.; Lim, M.; Hochstrasser, R. M. *J. Phys. Chem. B* **1998**, *102*, 6123.

(37) Vos, M. H.; Martin, J.-L. *Biochim. Biophys. Acta* **1999**, *1411*, 1.

(38) Robin, M. B. *"Higher Excited States of Polyatomic Molecules"; Academic Press: New York* **1975**, *Vol. II*.

(39) Song, S.; Asher, S. A. *J. Am. Chem. Soc.* **1989**, *111*, 4295.

(40) Dudik, J. M.; Johnson, C. R.; Asher, S. A. *J. Phys. Chem.* **1985**, *89*, 3805.

(41) Copeland, R. A.; Spiro, T. G. *Biochemistry* **1987**, *26*, 2134.

(42) Mayne, L. C.; Ziegler, L. D.; Hudson, B. *J. Phys. Chem.* **1985**, *89*, 3395.

(43) Badger, R. M. *Annu. Rev. Phys. Chem.* **1955**, *6*, 217.

(44) Venyaminov, S.; Prendergast, F. G. *Anal. Biochem.* **1997**, *248*, 234.

(45) Ozdemir, A.; Lednev, I. K.; Asher, S. A. *Biochemistry* **2002**, *41*, 1893.

(46) Schellman, J. A.; Becktel, W. J. *Biopolymers* **1983**, *22*, 171.

(47) Momii, R. K.; Urry, D. W. *Macromolecules* **1968**, *1*, 372.

(48) Onari, S. *Jpn. J. Appl. Phys.* **1970**, *9*, 227.

(49) Moffit, W. *Proc. Natl. Acad. Sci. U.S.A.* **1956**, *42*, 736.

(50) Mikhonin, A. V.; Ahmed, Z.; Ianoul, A.; Asher, S. A. *J. Phys. Chem. B* **2004**, *108*, 19020.

(51) Fry, D. C.; Byler, D. M.; Susi, H.; Brown, E. M.; Kuby, S. A.; Mildvan, A. S. *Biochemistry* **1988**, *27*, 3588.

(52) Siedlecka, M.; Goch, G.; Ejchart, A.; Sticht, H.; Bierzynski, A. *Proc. Natl. Acad. Sci. U.S.A.* **1999**, *96*, 903.

(53) Fang, C.; Wang, J.; Charnley, A. K.; Barber-Armstrong, W.; Smith, A. B.; Decatur, S. M.; Hochstrasser, R. M. *Chemical Physics Letters* **2003**, *382*, 586.

(54) Fang, C.; Wang, J.; Kim, Y. S.; Charnley, A. K.; Barber-Armstrong, W.; Smith, A. B., III; Decatur, S. M.; Hochstrasser, R. M. *J. Phys. Chem.*, ACS ASAP.

(55) Hamm, P.; Woutersen, S. *Bull. Chem. Soc. Jpn.* **2002**, *75*, 985.

(56) Krimm, S.; Abe, Y. *Proc. Natl. Acad. Sci. U.S.A.* **1972**, *69*, 2788.

(57) Lee, S.-H.; Krimm, S. *Chem. Phys.* **1998**, *230*, 277.

(58) Kobko, N.; Dannenberg, J. J. *J. Phys. Chem. A* **2003**, *107*, 6688.

(59) Torii, H.; Tasumi, M. *J. Raman Spectrosc.* **1998**, *29*, 81.

(60) Lee, S.-H.; Krimm, S. *Biopolymers* **1998**, *46*, 283.

(61) Diem, M.; Lee, O.; Roberts, G. M. *J. Phys. Chem.* **1992**, *96*, 548.

(62) Diem, M.; Polavarapu, P. L.; Oboodi, M.; Nafie, L. A. *J. Am. Chem. Soc.* **1982**, *104*, 3329.

(63) Oboodi, M. R.; Alva, C.; Diem, M. *J. Phys. Chem.* **1984**, *88*, 501.

(64) Mirkin, N. G.; Krimm, S. *J. Mol. Structure* **1996**, *377*, 219.

(65) Chen, X. G.; Schweitzer-Stenner, R.; Asher, S. A.; Mirkin, N. G.; Krimm, S. *J. Phys. Chem.* **1995**, *99*, 3074.

(66) Mix, G.; Schweitzer-Stenner, R.; Asher, S. A. *J. Am. Chem. Soc.* **2000**, *122*, 9028.

(67) Asher, S. A.; Mikhonin, A. V.; Bykov, S. V. *J. Am. Chem. Soc.* **2004**, *126*, 8433.

(68) Chen, X. G.; Asher, S. A.; Schweitzer-Stenner, R.; Mirkin, N. G.; Krimm, S. *J. Am. Chem. Soc.* **1995**, *117*, 2884.

(69) Bykov, S. V.; Lednev, I. K.; Ianoul, A.; Mikhonin, A. V.; Asher, S. A. *Appl. Spectrosc.,* **2005,** *In Press*

(70) Lednev, I. K.; Karnoup, A. S.; Sparrow, M. C.; Asher, S. A. *J. Am. Chem. Soc.* **1999**, *121*, 4076.

(71) Wang, Y.; Purrello, R.; Jordan, T.; Spiro, T. G. *J. Am. Chem. Soc.* **1991**, *113*, 6359.

(72) Rabolt, J. F.; Moore, W. H.; Krimm, S. *Macromolecules* **1977**, *10*, 1065.

(73) Englander, S. W. *Annu. Rev. Biophys. Biomol. Struct.* **2000**, *29*, 213.

(74) Dempsey, C. E. *Progress in NMR Spectroscopy* **2001**, *39*, 135.

(75) Li, R.; Woodward, C. *Prot. Sci.* **1999**, *8*, 1571.

(76) Dharmasiri, K.; Smith, D. L. *Analytical Chem.* **1996**, *68*, 2340.

5.0 CHAPTER 5. PEPTIDE SECONDARY STRUCTURE FOLDING REACTION COORDINATE: CORRELATION BETWEEN UV RAMAN AMIDE III FREQUENCY, Ψ RAMACHANDRAN ANGLE AND HYDROGEN BONDING

Work described in this chapter is published in *J. Phys. Chem. B.*, **2006,** *110 (4)*, 1928-1943 (Authors: Mikhonin, A. V., Bykov, S. V.; Myshakina, N. S.; and Asher, S. A.). We used UVRR spectroscopy to quantitatively correlate the peptide bond $AmIII_3$ frequency to its Ψ Ramachandran angle and to the number and types of amide hydrogen bonds at different temperatures. This information allows us to develop a family of relationships to directly estimate the Ψ Ramachandran angle from measured UVRR $AmIII_3$ frequencies for peptide bonds (PB) with known hydrogen bonding (HB). These relationships ignore the more modest Φ Ramachandran angle dependence, and allow to determine the Ψ angle with a standard error of ±8°, if HB state of a PB is known. This is normally the case if a known secondary structure motif is studied. Further, if HB state of a PB in water is unknown, the extreme alterations in such a state could additionally bias the Ψ angle by ±6°. The resulting ability to measure Ψ spectroscopically will enable new incisive protein conformational studies, especially in the field of protein folding. This is because any attempt to understand reaction mechanisms, requires elucidation of the relevant reaction coordinate(s). The Ψ angle is precisely the reaction coordinate that determines secondary structure changes. As shown elsewhere (Mikhonin et al., *J. Am. Chem. Soc.* **2005**, *127*, 7712), this correlation can be used to determine portions of the energy landscape along the Ψ reaction coordinate.

5.1 INTRODUCTION

The various techniques of molecular spectroscopy constitute the toolset used by scientists for investigating molecular conformations and reaction mechanisms. These various spectroscopic techniques require quantitative correlations between the spectral parameters measured and the molecular conformational parameters. NMR, and especially multi-dimensional NMR techniques are certainly the most powerful spectroscopic methods for solution studies.[1-13] The origin of the power of NMR derives from its ultrahigh spectral resolutions and because the important spin interactions can be accurately modeled in terms of distances between atoms. The NMR techniques are certainly the gold standard methods for studying systems at high concentrations where the dynamical questions probed are slower than the μsec time scale.[14,15]

In contrast, optical spectroscopic methods are used for lower concentration samples and for systems controlled by faster dynamics. For example, vibrational spectroscopic techniques can often be easily applied to studying low concentrations of species,[16-21] as well as to probe both very fast (fsec) and very slow processes.[22-34] Unfortunately, the resulting vibrational spectroscopic information cannot as easily be interpreted to obtain quantitative information on molecular conformation.[35] Although it is possible to calculate normal modes of large molecules in vacuum, the uncertainties in these calculated frequencies and their assignments in the condensed phase prevent interpreting these results in terms of the molecular geometry present in the condensed phase. In general, the vibrational spectra are interpreted through indirect empirical arguments. It is unusual to be able to interpret vibrational spectra quantitatively by correlating measured vibrational spectral parameters to bond lengths, angles etc.[36,37]

In the work here we have determined the frequency dependence of the Amide III (AmIII) band observed in the ~200 nm UVRR spectra of peptides and proteins on the Ψ Ramachandran angle, which largely defines the peptide bond secondary structure.[22,38,39] The understanding of the dependence of the AmIII band on the Ψ Ramachandran angle has a long and distinguished history; almost 30 years ago Lord proposed that the AmIII band correlates with the peptide secondary structure.[40] During the succeeding years numerous investigators have used this band to determine protein and peptide secondary structure.[38,39,41-58]

Recently Asher et al.[47] theoretically examined the dependence of the AmIII band on the Ψ angle, and discovered that this dependence resulted from coupling between the peptide bond

N-H and C_α-H in-plane bends. They found that this coupling varied sinusoidally with Ψ angle. They also discovered that there was much less dependence of the AmIII band on the Φ Ramachandran angle.[47,59] They also carefully examined[42] the amide III region of peptides and proteins and assigned a number of the bands in this region. They assigned one band in this spectral region, the $AmIII_3$ band to the vibration whose frequency varies with the Ψ angle.[43,60] Further, they also recently showed that this Raman band derives from independent contributions from individual peptide bonds in the peptide and protein; there is no evidence of coupling of this vibration between adjacent peptide bonds,[61,62] unlike the commonly used AmI band.[61,63]

These observations are important because they indicate that the $AmIII_3$ band may be uniquely useful in peptide and protein conformational studies. This band is easily observed because it is strongly enhanced by resonance excitation in the peptide bond ~200 nm $\pi\rightarrow\pi^*$ transitions.[39,64-66] Further, we showed that this band can be selectively measured for a single peptide bond by isotope editing the peptide or protein by replacing the C_α-H by C_α-D.[42,47,67,68] The high S/N difference spectrum directly displays the $AmIII_3$ frequency.

In the work here we carefully examined the dependence of this $AmIII_3$ frequency on hydrogen bonding (HB), in order to separate the HB dependence from the Ψ angle dependence. This allows us to propose a family of relationships which can be used to determine the Ψ angle directly from the measured $AmIII_3$ frequency with a typical accuracy of ±8°, assuming a known HB state (however, see discussion below).

We are optimistic that these relationships will be very useful for protein conformational studies, especially in the field of protein folding. This is because any attempt to understand reaction mechanisms, such as, for example protein folding, requires elucidation of the relevant reaction coordinate(s). The Ψ angle is precisely the reaction coordinate that determines secondary structure changes. As shown elsewhere[60] the correlation we propose can be used to experimentally determine features of the energy landscape along this Ψ reaction coordinate. Such an experimental insight into a protein conformation and energy landscape is crucially needed, since there are still a lot of unresolved questions regarding the theoretical modeling of protein folding in spite of remarkable recent achievments.[69-71]

5.2 EXPERIMENTAL SECTION

5.2.1 Sample preparation

N-methylacetamide (>99% pure) was purchased from Sigma Chemicals (St. Louis, MO) and used as received without any further purification. Neat liquid NMA (~13 M) as well as 0.13 M NMA in water solutions were used.

As described elsewhere,[43] the 21-residue alanine-based peptide AAAAA(AAARA)$_3$A (AP) was prepared (HPLC pure) at the Pittsburgh Peptide Facility by using the solid-state peptide synthesis method. The AP solutions in water contained 1 mg/ml concentrations of AP, and 0.2 M concentrations of sodium perchlorate, which was used as an internal intensity and frequency standard.[22,29] All Raman spectra were normalized to the intensity of the ClO_4^- Raman band (932 cm^{-1}).

The undecapeptide XAO (MW=985) was prepared (HPLC pure) at the Pittsburgh Peptide Facility by using the solid-state peptide synthesis method. The sequence of this peptide is Ac-XXAAAAAAAOO-amide, where all amino acids are in their L form, A is alanine, X is diaminobutyric acid (side chain $CH_2CH_2NH_3^+$), and O is ornithine (side chain $(CH_2)_3NH_3^+$). We used 1 mg/ml solutions of XAO-peptide containing 0.15 M of sodium perchlorate. The UVRR spectra of XAO were also normalized to the ClO_4^- Raman band intensity.

As described elsewhere,[60] poly-L-lysine HCl (PLL, MW_{vis}=28,500, MW_{LALLS}=20,200) and the sodium salt of poly-L-glutamic acid (PGA, MW_{vis} =17,000, MW_{mALLS}=8853) were purchased from Sigma Chemical, and used as received. Solution spectra of PLL and PGA were measured at pH=2 and pH=9, respectively, to ensure the absence of α-helix contributions. The mixed PLL and PGA neutral pH sample solutions contained identical concentrations of lysine and glutamic acid residues. These samples were freshly prepared before the Raman measurements. The total peptide concentrations were kept below 0.3 mg/ml to avoid gel formation.

5.2.2 UV resonance Raman instrumentation

The Raman instrumentation has been described in detail elsewhere.[22,72] A Coherent Infinity Nd:YAG laser produced 355 nm (3rd harmonic) 3 nsec pulses at 100 Hz. This beam was Raman shifted to 204 nm (5th anti-Stokes) by using a 1 m tube filled with hydrogen (60 psi). A Pellin Broca prism was used to select the 204 nm excitation beam. The Raman scattered light was imaged into a subtractive double spectrometer[72] and the UV light was detected by a Princeton Instruments solar blind ICCD camera or a Roper Scientific UV CCD camera. All samples were measured in a thermostatted free surface flow stream.

5.3 RESULTS AND DISCUSSION

5.3.1 Dependence of $AmIII_3$ Frequency on Ramachandran Angles and Hydrogen Bonding

The amide III (AmIII) band region is complex. We recently examined this spectral region in detail and identified a band, which we call $AmIII_3$ and which is most sensitive to the peptide bond conformation.[42] As briefly discussed in the introduction, the peptide bond (PB) $AmIII_3$ frequency depends upon its secondary structure which is defined by its Ψ and Φ Ramachandran angles.[43,47,59,73] The $AmIII_3$ frequency also depends on whether the PB hydrogen bonds (HB) to water (***$HB_{P\text{-}W}$***),[74-77] or to other PBs (***$HB_{P\text{-}P}$***).[77-81] Although there is a modest Φ angle $AmIII_3$ frequency dependence, our studies to date show that the Ψ dependence dominates.[43,47,59] We discuss the relative Ψ and Φ angular dependencies in detail below. In addition, PB HB to water leads to a characteristic temperature dependence[22,29,42,43] that derives from anharmonicities[25,82-87] in the PB and water HB potential functions (see Appendix A for detail). Thus, we write:

$$\nu_{III3} = \nu_{III3}\left(\psi, \phi, HB_{P-P}, \ HB_{P-W}, T\right) \qquad \textbf{(6)}$$

5.3.2 $AmIII_3$ Frequency Dependence on Coupling Between C_α-H and N-H Bending Motions

We showed earlier that the conformational sensitivity of the $AmIII_3$ band derives from coupling between the N-H and C_α-H bending motions.[47] For example, for β-strand-like Ψ and Φ Ramachandran angles the N-H and C_α-H bonds are approximately cis (Fig. 48), which gives rise to strong N-H to C_α-H bend coupling. In contrast, for α-helix-like Ψ and Φ Ramachandran angles the N-H and C_α-H bonds are approximately trans (Fig. 48), and the N-H to C_α-H coupling disappears. The stronger the coupling, the lower the $AmIII_3$ frequency, as explained in detail elsewhere.[47]

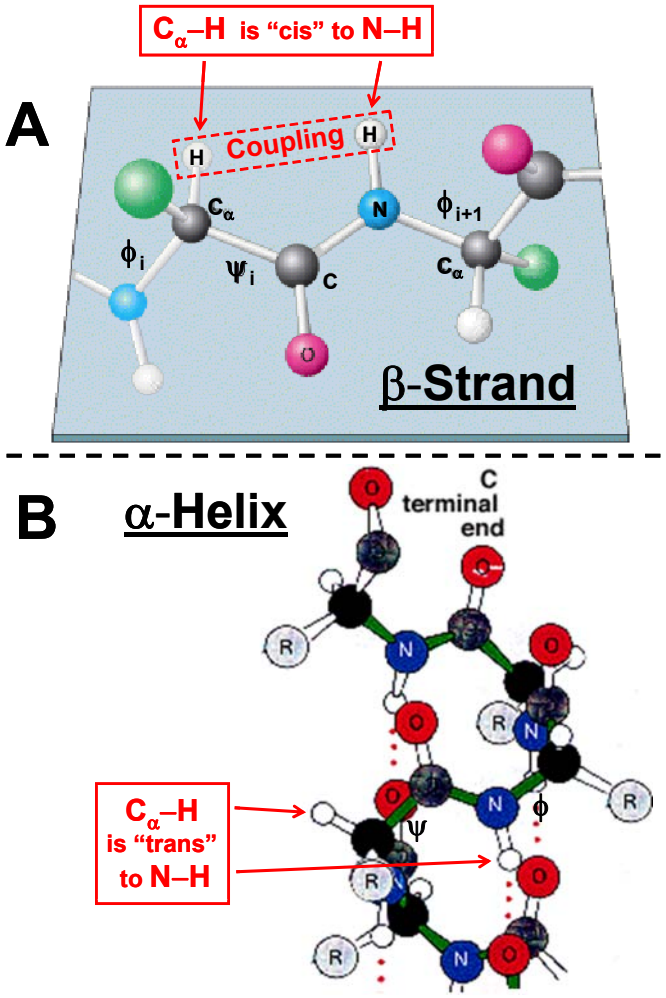

Figure 48. Model of a polypeptide chain (A) at β-strand-like, and (B) at α-helix-like Ψ and Φ Ramachandran angles. The distance between C_α-H and N-H hydrogens depends on the Ψ Ramachandran angle.

This coupling between the N-H and C_α-H bending motions can be completely removed by C_α-D isotopic substitution because of the dramatically lowered C-D bending frequency. Ala-ala (AA) in water exists in a PPII-like conformation with Ψ and Φ angles of 132° and −67°, respectively.[88] The N-H and C_α-H bending motions strongly couple. C_α-D isotopic substitution in AA[47] results in a 68 cm^{-1} upshift of the $AmIII_3$ band frequency from 1270 to 1338 cm^{-1}. This occurs because of the loss of this strong coupling between the N-H and C_α-H bending motions. This shift upon C_α deuteration is also observed in the 21-residue mainly ala peptide (AP). Natural abundance AP in its unfolded state (essentially PPII, Ψ≈145°, Φ≈–75°) shows the $AmIII_3$ band at 1252 cm^{-1} (at 0 °C).[42,43] 2,3,3,3-D_4 isotopic substitution (C_α-D, CD_3) results in a ~74 cm^{-1} upshift of the $AmIII_3$ band to ~1326 cm^{-1}.[42]

The extreme lowest frequency experimental value observed to date for the $AmIII_3$ frequency of 1227 cm^{-1} occurs in anti-parallel β-sheet PB in water (Ψ≈135°, Φ≈–139°) formed by PLL and PGA mixtures. Thus, it appears that the $AmIII_3$ frequency can be shifted by a maximum of ~100 cm^{-1} due to this coupling of C_α-H and N-H bending motions.

The physical origin of this Ψ angle $AmIII_3$ frequency dependence is that the hydrogen van der Waals radii in the C_α-H and N-H bonds are in contact for positive Ψ angles (Fig. 48), and the distance between the two H atoms shows a sinusoidal angular dependence. The coupling of these bending motions increases with the proximity of the hydrogen atoms. The coupling of bending motion causes a splitting of the vibrations into a high and low frequency component, the $AmIII_3$ band and an anomalously enhanced C_α-H bending band which contains additional motions such as CO-N stretching.

5.3.3 Relative Impact of the Ψ and Φ Ramachandran Angles on the $AmIII_3$ Frequency

Although, the projections of the N-H and C_α-H bending motions on each other (and as a result the degree of coupling between them) depend upon *both* the Ψ and Φ Ramachandran angles, an examination of a model of a peptide bond (Fig. 48), clearly shows that for the allowed regions of the Ramachandran plot only the Ψ angle directly alters the distance between the two hydrogens, while the Φ angle has little direct impact. Thus, for steric reasons alone we expect little influence on the $AmIII_3$ frequency due to variations in the Φ angle.

Asher et al.[47] theoretically investigated the Ψ angular dependence of $AmIII_3$ frequency in isolated alanine methylamide (AMA). AMA geometry was optimized at fixed Ψ angles using Gaussian 98W, and then the vibrational frequencies were calculated. This approach revealed the strong dependence of the AmIII frequency on the Ψ Ramachandran angle with a ~61 cm^{-1} total span of calculated AmIII frequencies (~74 cm^{-1} span from sinusoidal fit of these calculated data points, Fig. 49).

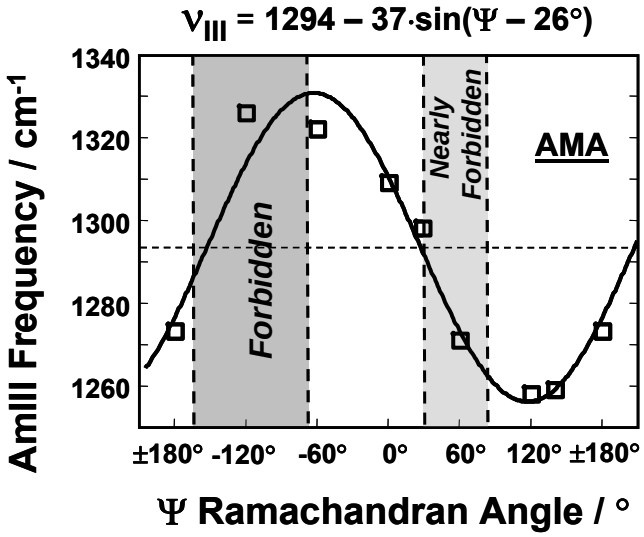

Figure 49. Black boxes (□): AmIII frequencies for isolated alanine methylamide (AMA) at fixed Ψ angles but with all the other parameters optimized, calculated by Gaussian 98W (see Asher et al.[47] for detail). Black line (—): fit of calculated points using the Eqn. 8 (see text for detail). Note: Grey regions show the forbidden and/or nearly forbidden Ψ Ramachandran angles based on recent Ramachandran plots.[90-92]

Mirkin and Krimm[73] theoretically examined the Ψ and Φ frequency dependence of the AmIII band of "alanine dipeptide" (N-acetyl-L-alanine-N-methylamide). They concentrated on peptide bond 2, whose frequencies were close to those measured experimentally. Although Mirkin and Krimm claim in their conclusions, that AmIII frequency shows strong dependence on both Ψ and Φ Ramachandran angles, we note that the impact of changes in the Φ angle is relatively modest if we only include the allowed regions of the Ramachandran plot (Fig. 50).

In the allowed regions of Ramachandran plot, Mirkin and Krimm[73] calculated a 25-40 cm^{-1} AmIII frequency span over the allowed Ψ angles for fixed Φ angles (Figs. 50 and 51). This 25-40 cm^{-1} Ψ angular frequency variation is somewhat lower, than the 61 cm^{-1} span we[47] estimated for AMA. However, it is ~3-fold greater than the 6-16 cm^{-1} AmIII frequency

dependence calculated for the Φ angular dependence for fixed Ψ angles over the allowed regions of the Ramachandran plot (Figs. 50 and 51).

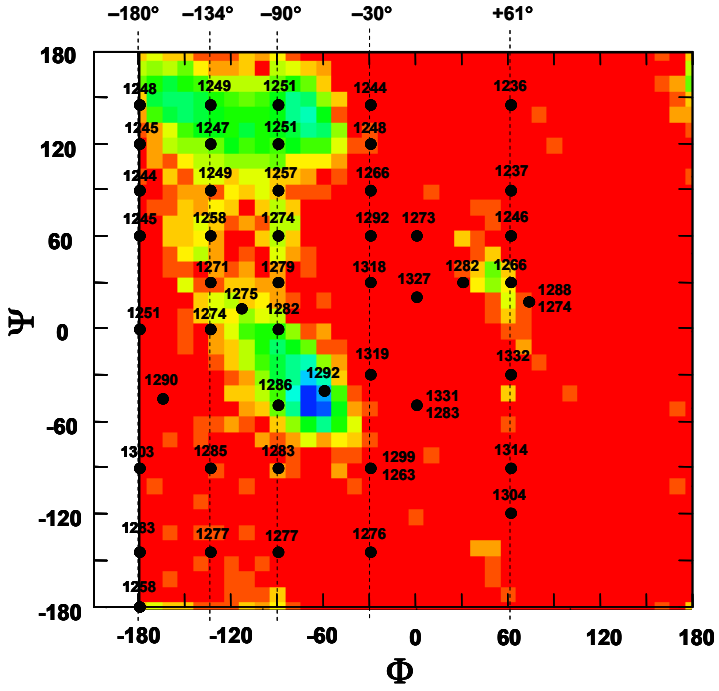

Figure 50. This AmIII vibrational frequency map for peptide group 2 of the alanine dipeptide is adapted from a figure by Mirkin and Krimm's.[73] This map is overlaid with the recent Ramachandran plot for ala (obtained from http://alpha2.bmc.uu.se/gerard/rama/ramarev.html). The results show that over the allowed regions of Ramachandran plot the AmIII band shows a 3-fold greater frequency dependence on the Ψ angle than on the Φ angle.

In addition, the largest 16 cm^{-1} span in the AmIII frequency with Φ angle occurs in an almost forbidden region of the Ramachandran plot in between the β-sheet and α-helical regions (at Φ angles of –134° and –90° and Ψ angle of 60°, Figs. 50 and 51). In contrast, in the α-helical region of Ramachandran plot the AmIII frequency of alanine dipeptide shows no more than 8 cm^{-1} Φ angular span, while in β-strand region of Ramachandran plot the AmIII frequency shows no more than 6 cm^{-1} Φ dependence (Fig. 50).

Fig. 51, which shows Mirkin and Krimm's[73] Ψ angular dependence of peptide bond 2 alanine dipeptide AmIII frequency at fixed Φ angles, emphasizes the dominance of the Ψ angular dependence in the allowed regions of Ramachandran plot (Fig. 50). Fig. 51 indicates that

in most of the β-strand region of Ramachandran plot (Ψ=120 - 180°) there is essentially a negligible dependence of the AmIII frequency on the Φ angle.

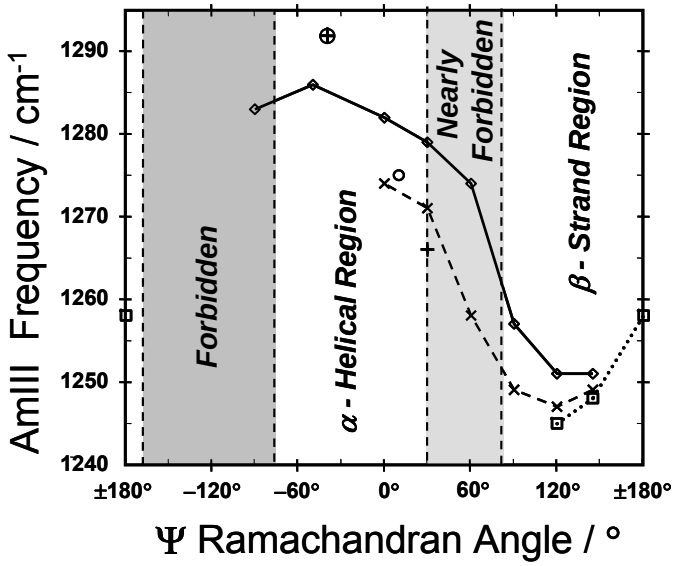

Figure 51. Ψ angular dependence of Mirkin and Krimm's[73] alanine-dipeptide AmIII frequencies at fixed Φ angles in the allowed regions of recent Ramachandran plot for ala (Fig. 50, obtained from http://alpha2.bmc.uu.se/gerard/rama/ramarev.html): (□) at Φ=±180°; (×) at Φ=–134°; (O) at Φ=–115°; (◊) at Φ=–90°; (⊕) at Φ=–60°; (+) at Φ=+61.° Note: Grey regions show the forbidden and/or nearly forbidden Ψ Ramachandran angles.

Ianoul et al.'s[59] combined experimental and theoretical studies of Ac-X-OCH_3 (X=Val, Ile, Leu, Lys, Ala) revealed a 9 cm^{-1} $AmIII_3$ frequency shift upon an 18° increase of the Φ Ramachandran angle from –96 to –78°. In addition, Ianoul et al. also performed theoretical calculations for Ala-Ala at a fixed α-helix-like Ψ angle of –21° and calculated only a 3 cm^{-1} $AmIII_3$ frequency upshift upon the 20° increase of Φ angle from –95° to –75°. Thus, Ianoul et al. never observed more than 9 cm^{-1} shift of $AmIII_3$ frequency due to variation of Φ Ramachandran angle.

In addition, we recently[60] measured the UVRR $AmIII_3$ frequencies of two different secondary structure conformations in aqueous solutions with very similar Φ angles, but very different Ψ angles. Specifically, an equimolar mixture of PLL and PGA forms an anti-parallel β-sheet[60] (Ψ≈135°, Φ≈–139°), which shows an $AmIII_3$ frequency at 1227 cm^{-1}. In contrast individual PLL and PGA samples form extended 2.5_1-helices[60] (Ψ≈170°, Φ≈–130°), which show $AmIII_3$ frequencies at ~1271 cm^{-1}. Figs. 50 and 51 demonstrate that the entire frequency shift

derives from changes in the Ψ Ramachandran angle alone; the 35° increase in the Ψ angle is mainly responsible for the large 44 cm^{-1} $AmIII_3$ frequency upshift. As discussed in detail in the Appendix A, the difference in peptide HB in this case also has a minor impact on the $AmIII_3$ frequency difference.

To summarize, the total Φ angular span of the $AmIII_3$ frequencies appears experimentally[59] to be no more than 9 cm^{-1}, and no more than 16 cm^{-1} in the allowed regions of Ramachandran plot from theoretical calculations.[73] In contrast, Ψ angular span was observed to be as high as 44 cm^{-1} from the experiment (see above), and as high as 61 cm^{-1} from theoretical calculations[47] over the allowed region of Ramachandran plot (Fig. 49). We will show below that the Ψ Ramachandran angular span of the $AmIII_3$ frequency can be as high as 80 cm^{-1} in the allowed regions of Ramachandran plot (Fig. 52).

Thus, we conclude that **Ψ Ramachandran angular dependence of the $AmIII_3$ frequency dominates the Φ angular dependence in the allowed regions of Ramachandran plot!!!**

If we totally neglect the Φ angular dependence of $AmIII_3$ frequency, this could enable an error in the Ψ dependent $AmIII_3$ frequency of no more than ±8 cm^{-1} (since the total Φ angular span of $AmIII_3$ frequencies no higher than 16 cm^{-1}, Fig. 50). Thus, we can rewrite Eqn. 6:

$$\nu_{III3}(\psi, \phi, HB_{P-P}, HB_{P-W}, T) \cong \nu_{III3}(\psi, HB_{P-P}, HB_{P-W}, T) \quad \textbf{(7)}$$

It was already mentioned that the $AmIII_3$ frequency dependence on the Ψ Ramachandran angle results from the Ψ angular dependence of coupling between the N-H and C_α-H bending motions.[47] Our theoretical calculations of alanine methylamide (AMA) in vacuum[47] showed that the extent of this coupling depends on the projections of these motions onto one another, and that this dependence results in a sinusoidal-like $AmIII_3$ frequency dependence for a non-HB PB:

$$\nu_{III3}(\psi) \cong \nu_0 - A \cdot \sin(\psi - \alpha_0) \quad \textbf{(8)}$$

Further, we assume that the $AmIII_3$ frequency dependencies on its Ψ Ramachandran angle and on its HB are independent. Thus, we can rewrite Eqn. 7:

$$\nu_{III3}(\psi, HB_{P-P}, HB_{P-W}, T) \cong \{\nu_0 - A \cdot \sin(\psi - \alpha_0)\} + \Delta\nu_{III3}(HB_{P-P}, HB_{P-W}, T) \quad \textbf{(9)}$$

where $\Delta\nu_{III3}(HB_{P\text{-}P}, HB_{P\text{-}W}, T)$ is the $AmIII_3$ frequency shift due to HB of the PB N-H and/or C=O groups.

Formation of PB-*water* and PB-PB HBs upshift the $AmIII_3$ frequency, in part, due to the resulting increased C(O)=N double bond character.[75,76] The magnitude of this $AmIII_3$ frequency upshift depends on whether C=O and/or N-H sites HB, and whether these HB occur to water or to other PB. The Appendix A below details our determinations of the $AmIII_3$ frequency shifts due to HB for all the common PB conformations and HB patterns. These considerations allow us to write three families of equations 10, 11A-D, and 12A-C which display the dependence of the $AmIII_3$ frequency on the Ψ angle, on the PB HB and on temperature. **These relationships and Figs. 52-54 can be used to determine the Ψ angle of a particular PB from its experimentally determined $AmIII_3$ frequency, given its known HB state with an error as discussed below.** In addition, we also developed the "average" Eqn. 11E, if the HB state of a PB in water is unknown.

Determining these correlations between the $AmIII_3$ frequency and PB HB requires detailed considerations of the many HB states (see Appendix A). In order to make the results of our study easily accessible to the reader we first discuss the conclusions. We leave the discussion of the detailed considerations of the different HB patterns to a lengthy Appendix A, which must be examined in order to judge the reliability of our conclusions.

The relationships given below by equations 10 (for non-HB PB in vacuum), 11A-E (PB in aqueous solutions), and 12A-C (PB in the absence of water) are shown in Figs 52, 53 and 54, respectively.

5.3.4 Correlation between $AmIII_3$ Frequency and Ψ Ramachandran Angle in the Absence of HB

We measured the UVRR $AmIII_3$ frequencies for the AP α-helix[42,89] (~1263 cm^{-1}, 0 °C), XAO PPII[42,43] (1247 cm^{-1}, 0 °C), PLL and PGA 2.5_1-helix[60] (~1271 cm^{-1}, 0 °C), and PLL-PGA mixture anti-parallel β-sheet[60] (~1227 cm^{-1}, 0 °C) conformations of different polypeptides in aqueous solutions. Each of these conformations has known Ramachandran angles (Table 8).

Table 8. Dependence of $AmIII_3$ frequencies on hydrogen bonding (HB) for different secondary structures at 20 °C (unless stated otherwise) under conditions specified

	$AmIII_3$ frequency without any PB-PB and PB-*water* HB (in vacuum)	$AmIII_3$ frequency with PB-PB HB, but without PB-*water* HB	$AmIII_3$ frequency in water, but without any PB-PB HB	$AmIII_3$ frequency both in water and with PB-PB HB
PPII (Ψ=145°, Φ= –75°)	1183 cm^{-1}	N/A	***1247 cm^{-1}**	N/A
2.5_1-helix (Ψ=170°, Φ= –130°)	1207 cm^{-1}	N/A	***1271 cm^{-1}**	N/A
α-helix Internal residues (Ψ=–47°, Φ= –57°)	1211 cm^{-1}	***1258 cm^{-1}**	N/A	***1263 cm^{-1}**
α-helix three terminal residues on C-terminus site (Ψ=–47°, Φ= –57°)	1211 cm^{-1}	1246 cm^{-1}	N/A	1266 cm^{-1}
α-helix three terminal residues on N-terminus site (Ψ=–47°, Φ= –57°)	1211 cm^{-1}	1223 cm^{-1}	N/A	1272 cm^{-1}
Anti-‖ β-sheet All residues, which are two end-on PB-PB H-bonded (see text) (Ψ=135°, Φ= –139°)	1175 cm^{-1}	1222 cm^{-1}	N/A	***1227 cm^{-1}**
Anti-‖ β-sheet residues from exterior strands (see text) (Ψ=135°, Φ= –139°)	1175 cm^{-1} 1175 cm^{-1}	1210 cm^{-1} 1184 cm^{-1}	N/A N/A	1230 cm^{-1} 1236 cm^{-1}

*****Measured experimentally. The Appendix A describes these frequency assignments in detail

We can calculate the $AmIII_3$ frequencies that would result from the above peptide conformations in the fictitious case where the PB did not partake in any HB at all. This would be done by subtracting the HB-induced $AmIII_3$ frequency shifts (Table 9), determined in the Appendix A, from the experimentally measured $AmIII_3$ frequencies in aqueous solutions (Table 8). The resulting $AmIII_3$ frequencies for non-HB PB at corresponding Ψ Ramachandran angles are shown in the second column of Table 8. Removal of this HB dependence then allows us to refine our theoretically calculated frequency dependence of the $AmIII_3$ band on the Ψ angle dependent coupling between N-H and C_α-H bends (Eqn. 8).

Table 9. $AmIII_3$ Frequency Upshifts for Different Peptide Secondary Structures Due to PB-*water* and PB-PB HB at 0 °C with respect to non-HB PB in vacuum

Secondary Structure	$AmIII_3$ frequency upshift due to PB-*water* HB at specific sites,[a] cm^{-1}					$AmIII_3$ frequency upshift due to PB-PB HB at specific sites,[a] cm^{-1}			Total $AmIII_3$ frequency upshift due to HB, cm^{-1}
	$\Delta\nu^A$	$\Delta\nu^B$	$\Delta\nu^C$	$\Delta\nu^{D,D*}$	**Total**	$\Delta\nu^E$	$\Delta\nu^F$	**Total**	
PPII	15	33	16	N/A	64	N/A	N/A	N/A	64
2.5_1-Helix	15	33	16	N/A	64	N/A	N/A	N/A	64
Extended β-strand	15	33	16	N/A	64	N/A	N/A	N/A	64
AP solid state α-helix (dehydrated)	N/A	N/A	N/A	N/A	N/A	35	12	47	47
AP α-helix in water	N/A	N/A	N/A	5	5	35	12	47	52
PLL-PGA mixture anti-|| β-sheet	N/A	N/A	N/A	5	5	35	12	47	52

[a] See Figures 80, and 85-87 and text of the Appendix A for detail.

By fitting the above 4 "non-HB" data points to Eqn. 8, we obtain the following semi-empirical relationship, which relates the $AmIII_3$ frequency to the Ψ Ramachandran angle dependent coupling between N-H and C_α-H bending motions:

$$\nu_{III3}(\psi) = [1192\ cm^{-1} - 54\ cm^{-1} \cdot \sin(\psi + 26^0)] \quad \textbf{(10)}$$

Figure 52 shows the dependence of the $AmIII_3$ frequency on the Ψ angle as predicted by Eqn. 10. The grey regions in Fig. 52 (as well as in Figs. 53 and 54) show the sterically forbidden Ψ Ramachandran angles based on revised Ramachandran map for non-Gly, non-Pro, and non-pre-Pro residues.[90-92]

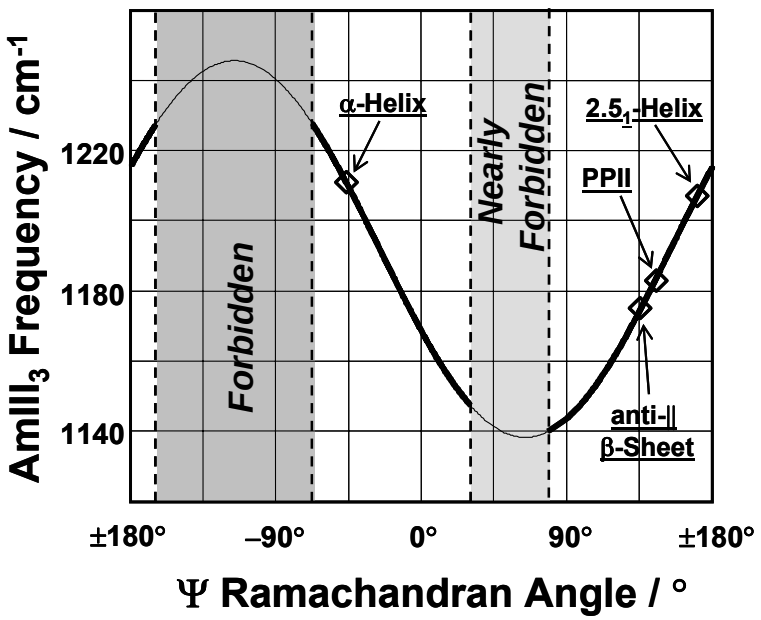

Figure 52. Refinement of correlation between $AmIII_3$ frequency and Ψ Ramachandran angle for non-HB PB, which reflects only coupling between N-H and C_α-H bending motions, as predicted earlier for AMA.[47] A) (◊) show the $AmIII_3$ frequencies, where the HB-induced frequency upshifts were subtracted from the experimentally measured values (see Appendix A). B) Black curve shows the best fit of these data (Eqn. 10). Note: Grey regions show the sterically forbidden/nearly forbidden Ψ Ramachandran angles based on recent Ramachandran plots for non-Gly, non-Pro, and non-pre-Pro residues.[90-92]

5.3.5 Correlation of $AmIII_3$ Frequency and Ψ Ramachandran Angle for PB Fully Exposed to Water: PPII, 2.5_1-Helix and Extended β-strand

PB fully exposed to water, such as in the PPII, 2.5_1-helix and extended β-strand-like conformations, will HB to three waters/water clusters at sites A, B, C (Appendix A, Fig. 80). As discussed in the Appendix A, this results in an $AmIII_3$ frequency upshift of 64 cm^{-1} (at T=0 ºC) compared to that predicted by the Eqn. 10. In addition, the $AmIII_3$ frequency will show a temperature dependence for these conformations[42,43,60] because the strength of the PB-*water* HB decreases as the temperature increases (see Eqns. 43-45 of the Appendix A). Thus, we can write:

$$\nu_{III3}^{EXT}(\psi, T, HB) = [1256\ cm^{-1} - 54\ cm^{-1} \cdot \sin(\psi + 26^0)] - 0.11 \cdot \frac{cm^{-1}}{^{O}C} \cdot (T - T_0)\} \quad \textbf{(11A)}$$

where T_0=0 °C

The blue curve in Fig. 53 shows the dependence of the $AmIII_3$ frequency on Ψ angle as predicted by Eqn. 11A at T=0 ºC for these water-exposed conformations. The experimentally observed $AmIII_3$ frequencies of the XAO PPII (0 °C) and PLL or PGA 2.5_1-helix (0 °C) lie on this curve.

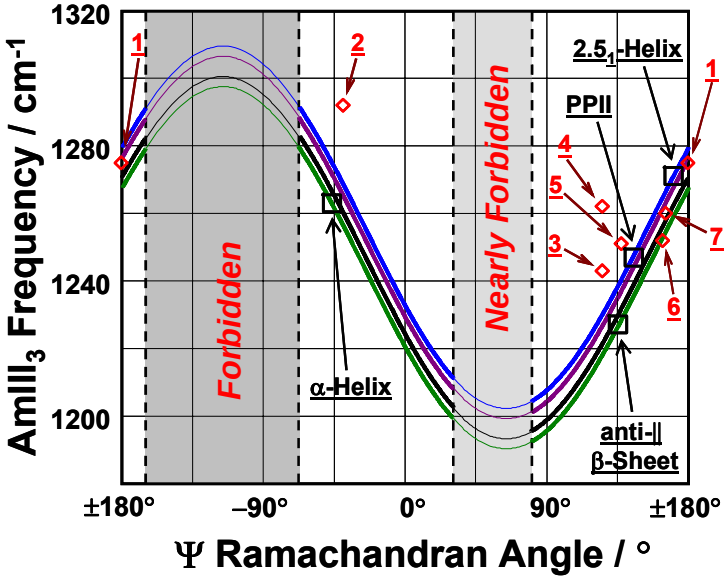

Figure 53. Correlation between $AmIII_3$ frequency, HB pattern, and Ψ Ramachandran angle. (□) measured $AmIII_3$ frequencies of α-helix, antiparallel β-sheet, PPII and 2.5_1 helix in aqueous solutions; (◊) measured $AmIII_3$ frequencies of peptide crystals, plotted against their Ψ Ramachandran angles: 1–Ala-Asp; 2–Gly-Ala-Leu•$3H_2O$; 3–Val-Glu; 4–Ala-Ser; 5–Val-Lys; 6–Ser-Ala; 7–Ala-Ala; Blue curve theoretically predicted correlation (Eqn. 11A) for PB, which are fully exposed and fully HB to water (PPII, 2.5_1-Helix, extended β-strand); Green curve theoretically predicted correlation (Eqn. 11B) for PB, for two end-on PB-PB HB (infinite α-helix, interior strands of β-sheet); Magenta curve theoretically predicted correlation (Eqn. 11C) for PB where only the C=O group has a PB-PB HB (example: three α-helix N-terminal PB, half of PB of the exterior strands of a β-sheet; Black curve theoretically predicted correlation (Eqn. 11D) for PB with just their N-H group PB-PB HB (example: three α-helix C-terminal PB, the other half of PB of exterior strands of β-sheet).

5.3.6 Correlation of $AmIII_3$ Frequency and Ψ Ramachandran Angle for Two-End-On PB-PB HB: Infinite α-Helix, Interior Strands of β-Sheet in Water

Each PB in infinitely long α-helices and in interior strands of multi-stranded β-sheets in aqueous solutions (Appendix A, Figs. 84 and 85), will partake in two-end-on PB-PB HB at sites E and F. In the Appendix A we show that in this case the $AmIII_3$ frequency upshifts by 47 cm^{-1} for α-

helix and β-sheet due to PB-PB HB (Table 9, Fig. 85). It upshifts an additional 5 cm^{-1} in both α-helices and β-sheets due to an additional PB-water HB producing a total HB-induced upshift of 52 cm^{-1} (Table 9, Fig. 85). In addition, there is essentially no temperature dependence for the $AmIII_3$ frequency for the long α-helix[42,89] and multi-stranded β-sheet[60] conformations (see Appendix A, Eqn. 46). Thus, we include a 52 cm^{-1} HB-induced shift to Eqn. 10 and write:

$$\nu_{III3}^{i\alpha}(\psi, T_0, HB) = [1244\ cm^{-1} - 54\ cm^{-1} \cdot \sin(\psi + 26^0)] \qquad \textbf{(11B)}$$

The green curve in Fig. 53 shows the predicted Eqn. 11B behavior. The experimentally observed $AmIII_3$ frequencies of the AP α-helix and the PLL-PGA antiparallel β-sheet conformations (dominated by interior strands) lie on this curve.

5.3.7 Correlation of $AmIII_3$ Frequency and Ψ Ramachandran Angle for PB Where only the C=O Group Participates in PB-PB HB: Three N-Terminal α-Helix PB, Half of PB of Exterior Strands of β-Sheet in Water

The three N-terminal PBs of α- helices and half of the PBs of exterior strands of β-sheets (Appendix A, Figs. 84 and 86) will have just their C=O groups HB to PB (with possibly an additional C=O HB to water). In contrast, their N-H groups will HB to water clusters. In the Appendix A (Fig. 86) we estimate that the $AmIII_3$ upshift is 61 cm^{-1} (with respect to the same PB, which does not partake in any HB). As discussed in the Appendix A, we expect a smaller temperature dependence (see discussion below the Eqn. 47 in the Appendix A) than for the fully water HB PB. Thus, we can write:

$$\nu_{III3}^{e\alpha 1,\ e\beta 1}(\psi, T, HB) = [1253 cm^{-1} - 54 cm^{-1} \cdot \sin(\psi + 26^0)] - 0.08 \cdot \frac{cm^{-1}}{^{O}C} \cdot (T - T_0) \qquad \textbf{(11C)}$$

The magenta curve in Fig. 53 shows the behavior of Eqn. 11C at T=0 °C. We do not, at present, have any experimentally measured data points for peptides with the HB patterns considered in Eqn. 11C. However, experimentally measured UVRR spectra of double-stranded β-sheet and/or short α-helices must contain contributions from such HB conformations.

5.3.8 Correlation of $AmIII_3$ Frequency and Ψ Ramachandran Angle for PB in Which only the N-H Group Participates in PB-PB HB: Three C-Terminal α-Helix PB, Other Half of PB of Exterior Strands of β-Sheet in Water

The three C-terminal PBs of α-helices and the other half of the PBs of the exterior strands of β-sheet (Appendix A, Figs. 84 and 87) will have just their N-H groups HB to another PB at site E, while their C=O groups will be HB to water at sites A and C. In the Appendix A we estimate that in this case the HB-induced $AmIII_3$ upshift is 55 cm^{-1} (Appendix A, Fig. 87). In addition, we estimate the temperature dependence to be half that of the PPII conformation (discussion below Eqn. 47 in Appendix A). Thus, we can add 55 cm^{-1} HB-induced upshift as well as the temperature-dependent term to Eqn. 10 and write:

$$\nu_{III3}^{e\alpha 2,\ e\beta 2}(\psi, T, HB) = [1247cm^{-1} - 54cm^{-1} \cdot \sin(\psi + 26^0)] - 0.05 \cdot \frac{cm^{-1}}{^{O}C} \cdot (T - T_0) \quad \textbf{(11D)}$$

The black curve in Fig. 53 shows the behavior of Eqn. 11D. We do not, at present, have any experimentally measured data points for peptides with the HB patterns considered in Eqn. 11D. However, experimentally measured UVRR spectra of double-stranded β-sheet and/or short α-helices will contain contributions from these HB conformations.

5.3.9 Correlation of $AmIII_3$ Frequency and Ψ Angle for a PB in Water If Its HB State is Unknown

If the HB state of a PB in aqueous solution is unknown, we suggest the use of equation 11E, which is the "average" of Eqns 11A-D. This will minimize the error in determination of the Ψ Ramachandran angle and will allow the estimation of the Ψ angle with the error bounds discussed below.

$$\nu_{III3}^{EXT}(\psi, T, HB) = [1250\ cm^{-1} - 54\ cm^{-1} \cdot \sin(\psi + 26^0)] - 0.06 \cdot \frac{cm^{-1}}{^{O}C} \cdot (T - T_0)\} \quad \textbf{(11E)}$$

5.3.10 Correlation Between $AmIII_3$ Frequency and Ψ Ramachandran Angle in Peptide Crystals

Figs. 53 and 54 show the correlation of the previously measured[42] $AmIII_3$ frequencies and the Ramachandran Ψ angles for crystal powders of the three anhydrous dipeptides Val-Lys, Ala-Ala, and Ala-Asp, and three new anhydrous dipeptides Ser-Ala, Val-Glu, and Ala-Ser, as well as for a hydrated crystal[43] powder of Gly-Ala-Leu•$3H_2O$ (GAL). The structures of these peptides are known from single-crystal x-ray diffraction measurements.[93-99] We grew the crystal powders and measured the lattice constants using powder pattern x-ray diffraction. If our lattice constants matched that of known crystal structures confirmed, we assumed these published crystal structures Ψ and Φ Ramachandran angles (Table 10).

Table 10. UVRR $AmIII_3$ Frequencies and x-ray Ψ and Φ Ramachandran angles for peptide crystals

	$AmIII_3$ Frequency, cm^{-1}	Ψ angle, °	Φ angle, °
Gly-Ala-Leu•$3H_2O$	1292	–40	–67
Ala-Ser (anhydrous)	1262	125	–157
Val-Glu (anhydrous)	1243	125	–82
Val-Lys (anhydrous)	1251	137	–105
Ser-Ala (anhydrous)	1252	163	–80
Ala-Ala (anhydrous)	1260	165	–113
Ala-Asp (anhydrous)	1275	179	–113

Figs. 53 and 54 show that the crystal data appear to roughly follow the sinusoidal relationship between the $AmIII_3$ frequency and the Ramachandran angle (see red dashed curve in Fig. 54); however, the crystal data are systematically upshifted. This upshift is largest when comparing the data to the green, black and magenta theoretical curves in Fig. 54, where the curves model PB-PB HB in the absence of water. The systematic upshifts in the crystal frequencies almost certainly result from the different types, numbers, and increased strengths of HB in these peptide crystals. Specifically, in these di- and tripeptide crystals,[93-99] N-H groups of

PB usually HB to carboxylates instead of carbonyls (as in longer peptides), while C=O groups of PB usually HB to N-H_3^+ groups instead of N-H groups (as in longer peptides). In spite of sharing many common features, the HB patterns of these peptide crystals differ from each other. Thus, some scatter of $AmIII_3$ frequencies in these crystals (Figs. 53 and 54) probably occurs due to these differences in HB. We are presently attempting to understand these affects in detail, but for the moment we only use these data to further indicate the veracity of our correlations.

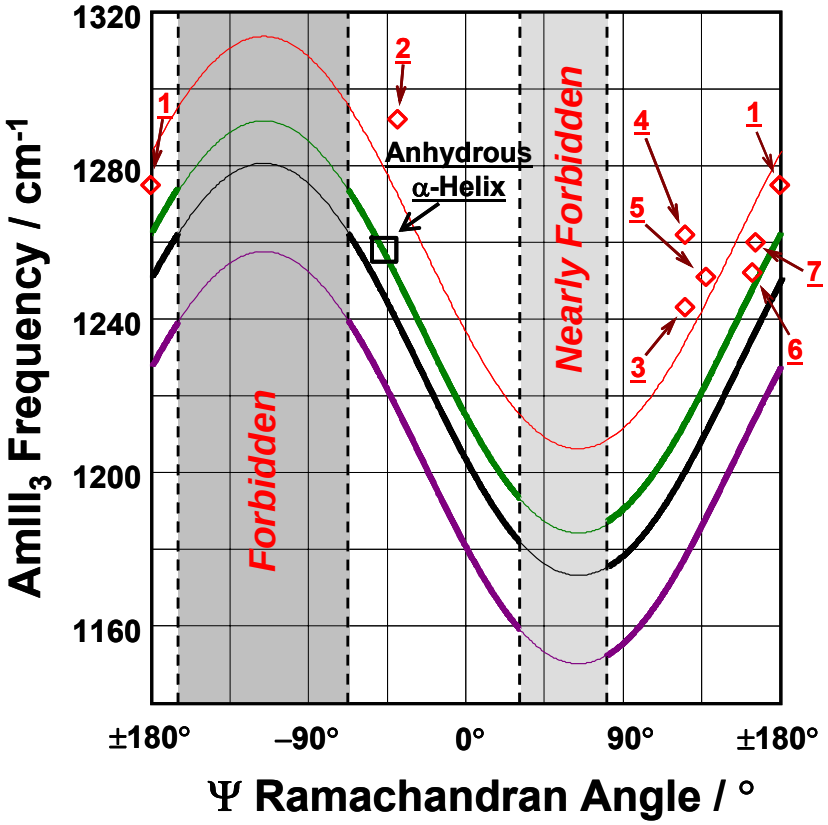

Figure 54. Correlation between $AmIII_3$ frequency, HB pattern, and Ψ Ramachandran angle for lyophilized anhydrous peptides. (□) is measured $AmIII_3$ frequencies of anhydrous AP α-helix; (◊) are measured $AmIII_3$ frequencies of peptide crystals, plotted against their Ψ Ramachandran angles: 1–Ala-Asp; 2–Gly-Ala-Leu·•$3H_2O$; 3–Val-Glu; 4–Ala-Ser; 5–Val-Lys; 6–Ser-Ala; 7–Ala-Ala; Green curve is theoretically predicted correlation (Eqn. 12A) for anhydrous PB with two end-on PB-PB HB (infinite α-helix, interior strands of β-sheet); Magenta curve is theoretically predicted correlation (Eqn. 12B) for anhydrous PB where only the C=O group has a PB-PB HB (example: three N-terminal PB of anhydrous α-helix, half of PB of the exterior strands of an anhydrous β-sheet); Black curve is theoretically predicted correlation (Eqn. 12C) for anhydrous PB with just their N-H group PB-PB HB (example: three C-terminal PB of anhydrous α-helix, the other half of PB of exterior strands of anhydrous β-sheet).

5.3.11 Anhydrous α-helical and β-sheet Conformations

If we dehydrate a two-end-on PB-PB HB α-helical conformation, we will see a 5 cm^{-1} $AmIII_3$ frequency downshift due to the loss of hydrogen bonding to the normally present sheath of water.[89] In this case we can subtract out 5 cm^{-1} from the Eqn. 11B and write the Eqn. 12A (see also Fig. 85 of Appendix A):

$$\nu_{III3}^{i\alpha,\,i\beta}(\psi, T_0, HB) = [1239\ cm^{-1} - 54\ cm^{-1} \cdot \sin(\psi + 26^0)] \qquad \textbf{(12A)}$$

The Fig. 54 green curve shows the Eqn. 12A relationship. The square data point in Fig. 54 indicates Pimenov et al.[89] $AmIII_3$ frequency of an anhydrous α-helix AP sample (Table 8) as discussed in detail in the Appendix A (Fig. 85).

In the case of a PB where only the C=O group is involved in PB-PB HB, we estimate that the $AmIII_3$ frequency is 12 cm^{-1} upshifted with respect to non-HB PB (Appendix A, Fig. 86). This would be the case for the three N-terminal PB of anhydrous α-helices and for half of the PB of the exterior strands of anhydrous β-sheets (Appendix A, Fig. 84 and 86). Thus, we can write:

$$\nu_{III3}^{e\alpha1,\,e\beta1}(\psi, T_0, HB) = [1204\ cm^{-1} - 54\ cm^{-1} \cdot \sin(\psi + 26^0)] \qquad \textbf{(12B)}$$

The Fig. 54 magenta curve shows the Eqn. 12B relationship.

In case of PB, where only the NH group is PB-PB HB, we estimate the $AmIII_3$ frequency to be 35 cm^{-1} upshifted with respect to non-HB PB (Appendix A, Fig. 87). This would be the case for the three C-terminal PB of anhydrous α-helix and half of the PB of the exterior strands of anhydrous β-sheet (Figs. 84 and 87 of Appendix A). Thus, we can write:

$$\nu_{III3}^{e\alpha1,\,e\beta1}(\psi, T_0, HB) = [1227\ cm^{-1} - 54\ cm^{-1} \cdot \sin(\psi + 26^0)] \qquad \textbf{(12C)}$$

The black curve in Fig. 54 shows the Eqn. 12C relationship.

The impact of different HB patterns, reflected by Eqns. 12A-C, produce much greater differences in $AmIII_3$ frequencies under anhydrous conditions compared to those in aqueous solutions (Compare Figs. 53 and 54), since PB-*water* HB-induced $AmIII_3$ frequency upshifts do not compensate for the differences in PB-PB HB-induced upshifts. It should be also noted that the Eqns. 12A-C behavior will only dominate the behavior of relatively long, anhydrous, lyophilized peptides.

Thus, the families of equations 11A-D and 12A-C predict the correlation between the $AmIII_3$ frequency and the Ψ angle for the common conformations of peptides and proteins. If the HB is known for a particular PB the appropriate equation can be used to determine its Ψ angle from the observed $AmIII_3$ frequency. In case the HB state of a PB in aqueous solution is unknown, one can use the Eqn. 11E. These relationships will become less accurate if the PB has an unusual Φ angle or unusual HB pattern (see below).

5.3.12 Prediction of UVRR $AmIII_3$ Frequencies of Other Secondary Structures

Based on the known Ψ Ramachandran angle and HB patterns we can predict the $AmIII_3$ frequencies of other secondary structures such as the π-helix, 3_{10}-helix (Fig. 55), parallel β-sheet and various turns (Fig. 56). Using Eqn. 11B we predict ~1281 cm^{-1}, ~1244 cm^{-1}, and ~1209 cm^{-1} $AmIII_3$ frequencies for two end-on PB-PB HB π-helix (Ψ=–70°), 3_{10}-helix (Ψ=–26°), and parallel β-sheet (Ψ=+113°) in water, respectively.

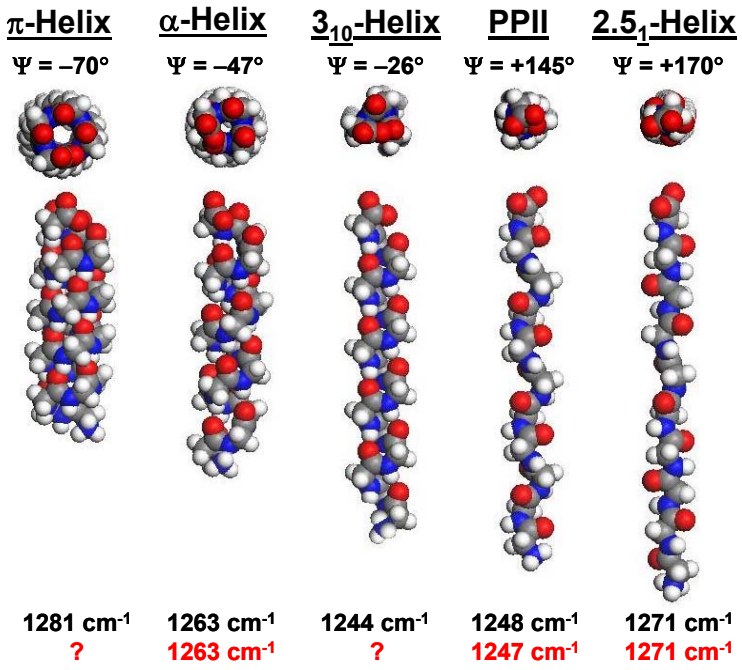

Figure 55. Predicted $AmIII_3$ frequencies (black numbers) from the Ψ Ramachandran angles and HB patterns for different types of helices in water. Red numbers: measured $AmIII_3$ frequencies at 0 °C. Eqn. 11A was used for PPII and 2.5_1 helices. Eqn. 11B was used for π-, α-, and 3_{10}-helices.

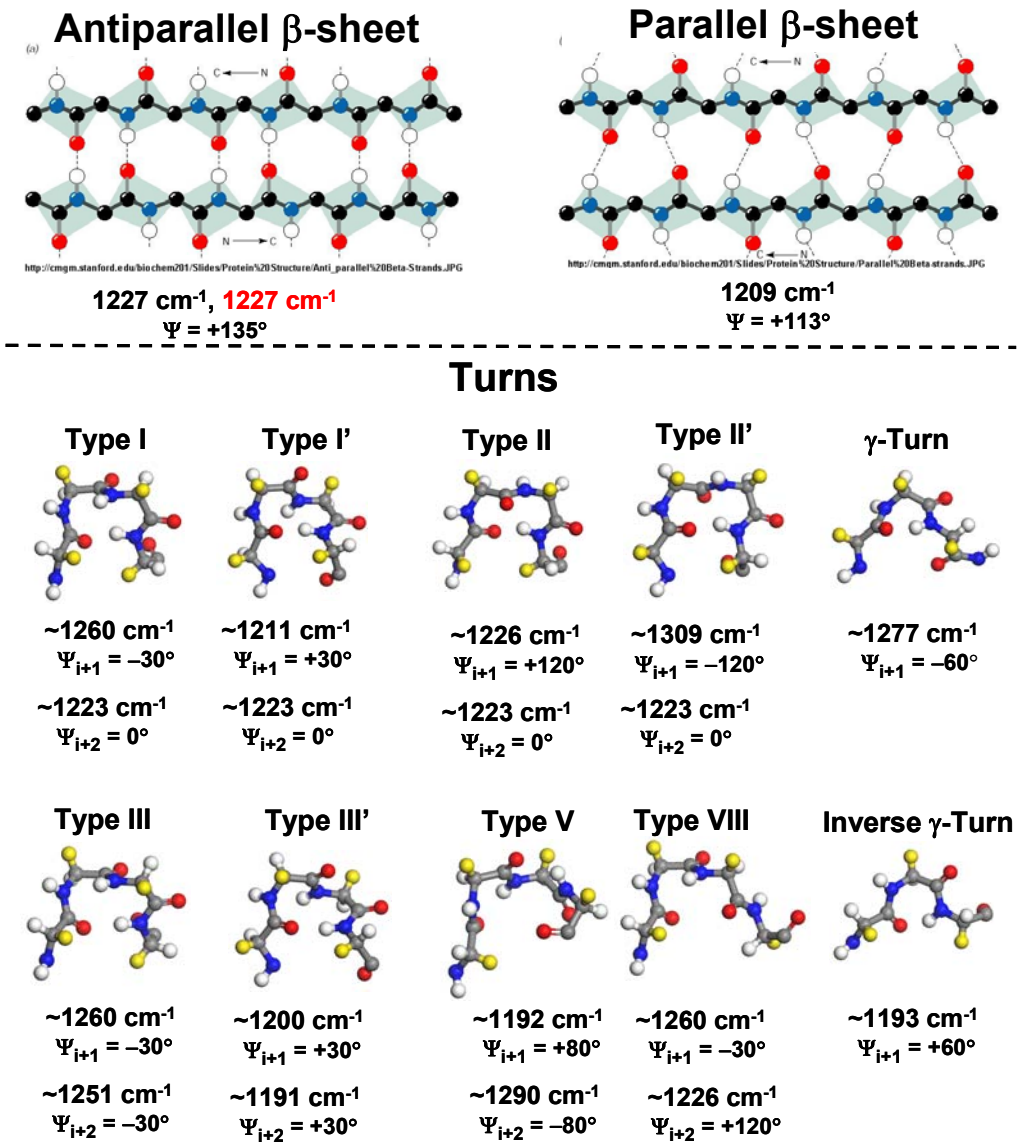

Figure 56. Predicted $AmIII_3$ frequencies from Ψ Ramachandran angle and HB pattern for interior strands of antiparallel and parallel β-sheets in water as well as that of different types of turns (Black numbers). Measured $AmIII_3$ frequencies of PLL-PGA antiparallel β-sheet, dominated by interior strands (red number). Pictures of β-sheets were taken from http:// cmgm.stanford.edu/biochem201/Slides/

Fig. 56 displays our estimates for interior strands of β-sheets and different turns in water. For the γ-turn we predict an $AmIII_3$ band at 1277 cm^{-1} (Eqn. 11D), for an inverse γ-turn at 1193 cm^{-1} (Eqn. 11D). Assuming that the different PB in the chain contribute to UVRR spectra independently from their neighbors,[61,62] for a type I turn we predict $AmIII_3$ bands at 1260 (Eqn. 11A) and 1223 cm^{-1} (Eqn. 11D) for the (i+1) and (i+2) PB in the turn, respectively; for a

type I' turn we predict 1211 (Eqn. 11A) and 1223 cm^{-1} (Eqn. 11D) for the two PB in the turn, respectively; for a type II turn we predict 1226 (Eqn. 11A) and 1223 cm^{-1} (Eqn. 11D) for the two PB in the turn; for a type II' turn we predict 1309 (Eqn. 11A) and 1223 cm^{-1} (Eqn. 11D) for the two PB in the turn. For a type III turn we predict 1260 (Eqn. 11A) and 1251 cm^{-1} (Eqn. 11D) for the two PB in the turn; for a type III' turn we predict 1200 (Eqn. 11A) and 1191 cm^{-1} (Eqn. 11D) for the two PB in the turn, for a type V turn we predict 1192 (Eqn. 11B) and 1290 cm^{-1} (Eqn. 11D) for the two PB in the turn, and for a type VIII turn we predict 1260 (Eqn. 11A) and 1226 cm^{-1} (Eqn. 11A) for the two PB in the turn.

UVRR spectra of HEWL amyloid fibrils,[100] which are dominated by β-sheet conformations contain three spectroscopic features in the $AmIII_3$ region: ~1210, ~1230, and ~1255 cm^{-1}. The dominating ~1230 cm^{-1} feature certainly derives from anti-parallel β-sheet, though a minor contribution of several turn conformations is also possible (Fig. 56). The ~1255 cm^{-1} feature probably derives from turn conformations. Our results above suggest that a type I turn, or a rare types III and VIII turns, could contribute to the ~1255 cm^{-1} feature of HEWL (Fig. 56). The ~1210 cm^{-1} feature most likely derives from aromatic amino acid sidechains, whose vibrations are enhanced with 197 nm excitation. However, there could be some contribution from either type I' turn or type III' turns (Fig. 56).

5.3.13 Ψ Ramachandran Angle Determination Error Estimates

To estimate the likely error and bias in the determination of the Ψ angle from the Raman measurements we have to analyze the likely errors in determination of the $AmIII_3$ frequency of the peptide bond of interest, as well as the error associated with the theoretical relationships that neglect the Φ dependence of the $AmIII_3$ frequency. In the simplest case, where we have only one amide bond our error is determined by the error in resolving the $AmIII_3$ band from the $AmIII_2$ band and other adjacent interfering bands. In the case of homopeptides we often attempt to determine the band frequency from a particular conformation, which presents the increased complexity of resolving between the $AmIII_3$ bands of multiple conformations. Finally, we expect to be challenged by the case where we specifically examine the $AmIII_3$ band of a particular peptide bond in a polypeptide or protein. In this case, for example, we isotopically substitute the C_α-H of that peptide bond and compare the spectra of the natural abundance and the isotopic

derivative to model the difference spectrum to selectively determine the peptide bond $AmIII_3$ frequency.

Thus, the likely error is very sample dependent and derives from the spectral S/N and the reliability of our modeling. In fitting, the resulting standard deviation of the fit depends upon peak overlap and spectral S/N. Typically our spectral fitting, assuming Voigt profiles, calculates standard deviations of ~2-3 cm^{-1} in the majority of cases; it is never more than ~7 cm^{-1}, even in the most unfavorable cases. The derivative of the Ψ angle with respect to the $AmIII_3$ frequency: $\partial\Psi/\partial\nu \cong 1 \text{ deg}/\ cm^{-1}$ over essentially all of the allowed values of Ψ (Figs. 52-54). Thus, we obtain measurement error standard deviations in the determined Ψ angles of ~2-3° for most cases, and extreme standard deviations of ~7° for rare unfavorable cases.

The error associated with neglecting the Φ angle also gives rise to the uncertainty in the Ψ angle determination. Ianoul et al.[59] theoretically and experimentally showed that different Φ angles could cause a maximum 9 cm^{-1} shift of the $AmIII_3$ frequency, while Mirkin and Krimm[73] indicates a potential span of AmIII frequency as much as 16 cm^{-1} in the allowed regions of Ramachandran plot (Fig. 50). However, in the β-strand region of the Ramachandran plot we find that a Φ span is less than ~6 cm^{-1}, while that in the α-helix region is less than ~8 cm^{-1} (Fig. 50). Thus, the extreme maximum spans of Ψ angle which could occur by neglecting the Φ angle is ~16°. Thus, the extreme standard error of Ψ angle associated with the neglecting the Φ angle is ±8° (for an average Φ angle). Further, for the most abundant secondary structure motifs from the α-helical and β-strand regions of Ramachandran plot, the Φ angle associated errors are only ±4° and ±3°, respectively.

Additional bias can occur if we do not know the HB state of a PB in water. This could give rise to a bias of the $AmIII_3$ frequency of ±6 cm^{-1}, which would lead to a Ψ angle bias of ±6° in equation 11E. **Thus, a typical UV Raman measurement of a typical sample would find a random error of ≤±8° in the Ψ angle, assuming a known HB state.** However, extreme alterations in the unknown HB state of a PB in water could additionally bias the Ψ angle by ±6°.

5.4 CONCLUSIONS

We used UV resonance Raman spectroscopy to investigate the dependence of the $AmIII_3$ frequency on the Ψ Ramachandran angle and on the nature of PB HB. These results allow us to formulate relationships that allow us to estimate the Ψ Ramachandran angles from observed $AmIII_3$ frequencies for both aqueous solutions of peptides and proteins as well as for the anhydrous states of peptides and proteins. **A typical Raman measurement of a typical sample would find a random error of ≤±8° in the Ψ angle, assuming a known HB state.** However, if HB state of a PB in water is unknown, extreme alterations in such a state could additionally bias the Ψ angle by ±6°.

We are optimistic that these relationships will be very useful for protein conformational studies, especially in the field of protein folding. This is because any attempt to understand reaction mechanisms, such as protein folding, requires elucidation of the relevant reaction coordinate(s). The Ψ angle is precisely the reaction coordinate that determines secondary structure changes. As shown elsewhere,[60] the correlation we propose can be used to determine features of the energy landscape along this Ψ reaction coordinate.

5.5 REFERENCES

(1) Kuszewski, J.; Schwieters, C. D.; Garrett, D. S.; Byrd, R. A.; Tjandra, N.; Clore, G. M. *J. Am. Chem. Soc.* **2004**, *126*, 6258.

(2) Tugarinov, V.; Hwang, P. M.; Kay, L. E. *Annu. Rev. Biochem.* **2004**, *73*, 107.

(3) Dyson, H. J.; Wright, P. E. *Chem. Rev.* **2004**, *104*, 3607.

(4) Sattler, M.; Schleucher, J.; Griesinger, C. *Progress in Nuclear Magnetic Resonance Spectroscopy* **1999**, *34*, 93.

(5) Wider, G.; Wuthrich, K. *Curr. Opin. Struc. Biol.* **1999**, *9*, 594.

(6) Clore, G. M.; Gronenborn, A. M. *Proc. Natl. Acad. Sci. USA* **1998**, *95*, 5891.

(7) Campbell-Burk, S.; Zhong, S. *Curr. Opin. Biotech.* **1994**, *5*, 346.

(8) Bax, A.; Grzesiek, S. *Accounts Chem. Res.* **1993**, *26*, 131.

(9) Billeter, M. *Q. Rev. Biophys.* **1992**, *25*, 325.

(10) Bonmatin, J. M.; Genest, M.; Petit, M. C.; Gincel, E.; Simorre, J. P.; Cornet, B.; Gallet, X.; Caille, A.; Labbe, H.; Vovelle, F.; Ptak, M. *Biochimie* **1992**, *74*, 825.

(11) Wagner, G.; Hyberts, S. G.; Havel, T. F. *Annu. Rev. Bioph. Biom.* **1992**, *21*, 167.

(12) MacKenzie, N. E.; Gooley, P. R.; Hardaway, L. A. *Annu. Rev. Physiology* **1992**, *54*, 749.

(13) James, T. L.; Basus, V. J. *Annu. Rev. Phys. Chem.* **1991**, *42*, 501.

(14) Hass, M. A. S.; Thuesen, M. H.; Christensen, H. E. M.; Led, J. J. *J. Am. Chem. Soc.* **2004**, *126*, 753.

(15) Palmer, A. G., III; Grey, M. J.; Wang, C. *Methods Enzymol.* **2005**, *394*, 430.

(16) Asher, S. A. *Handbook of Vibrational Spectroscopy, John Whiley & Sons, Ltd.* **2001**, *1*, 557.

(17) Schweitzer-Stenner, R. *J. Raman Spectrosc.* **2001**, *32*, 711.

(18) Thomas, G. J., Jr. *Annu. Rev. Biophys. Biomol. Struct.* **1999**, *28*, 1.

(19) Spiro, T. G.; Czernuszewicz, R. S. *Methods Enzymol.* **1995**, *246*, 416.

(20) Austin, J. C.; Jordan, T.; Spiro, T. G. *Advances in Spectroscopy (Chichester, United Kingdom)* **1993**, *20*, 55.

(21) Tuma, R.; Russell, M.; Rosendahl, M.; Thomas, G. J., Jr. *Biochemistry* **1995**, *34*, 15150.

(22) Lednev, I. K.; Karnoup, A. S.; Sparrow, M. C.; Asher, S. A. *J. Am. Chem. Soc.* **1999**, *121*, 8074.

(23) Huang, C.-Y.; Balakrishnan, G.; Spiro, T. G. *Abstracts of Papers, 229th ACS National Meeting, San Diego, CA, United States, March 13-17, 2005* **2005**, INOR.

(24) Gulotta, M.; Rogatsky, E.; Callender, R. H.; Dyer, R. B. *Biophys. J.* **2003**, *84*, 1909.

(25) Rubtsov, I. V.; Wang, J.; Hochstrasser, R. M. *J. Phys. Chem. A* **2003**, *107*, 3384.

(26) Callender, R.; Dyer, R. B. *Curr. Opin. Struc. Biol.* **2002**, *12*, 628.

(27) Haruta, N.; Kitagawa, T. *Biochemistry* **2002**, *41*, 6595.

(28) Pan, D.; Ganim, Z.; Kim, J. E.; Verhoeven, M. A.; Lugtenburg, J.; Mathies, R. A. *J. Am. Chem. Soc.* **2002**, *124*, 4857.

(29) Lednev, I. K.; Karnoup, A. S.; Sparrow, M. C.; Asher, S. A. *J. Am. Chem. Soc.* **2001**, *123*, 2388.

(30) Wang, J.; El-Sayed, M. A. *Biophys. J.* **2001**, *80*, 961.

(31) Yamamoto, K.; Mizutani, Y.; Kitagawa, T. *Biophys. J.* **2000**, *79*, 485.

(32) Hamm, P.; Lim, M.; Hochstrasser, R. M. *J. Phys. Chem. B* **1998**, *102*, 6123.

(33) Hochstrasser, R. M. *Ultrafast Processes in Chemistry and Photobiology* **1995**, 163.

(34) Spiro, T. G.; Smulevich, G.; Su, C. *Biochemistry* **1990**, *29*, 4497.

(35) Tuma, R. *J. Raman Spectrosc.* **2005**, *36*, 307.

(36) Jarzecki, A. A.; Spiro, T. G. *J. Phys. Chem. A* **2005**, *109*, 421.

(37) Venkateshrao, S.; Yin, J.; Jarzecki, A. A.; Schultz, P. G.; Spiro, T. G. *J. Am. Chem. Soc.* **2004**, *126*, 16361.

(38) Chi, Z.; Chen, X. G.; Holtz, J. S. W.; Asher, S. A. *Biochemistry* **1998**, *37*, 2854.

(39) Copeland, R. A.; Spiro, T. G. *Biochemistry* **1987**, *26*, 2134.

(40) Lord, R. C. *Appl. Spectrosc.* **1977**, *31*, 187.

(41) Overman, S. A.; Bondre, P.; Maiti, N. C.; Thomas, G. J., Jr. *Biochemistry* **2005**, *44*, 3091.

(42) Mikhonin, A. V.; Ahmed, Z.; Ianoul, A.; Asher., S. A. *J. Phys. Chem. B* **2004**, *108*, 19020.

(43) Asher, S. A.; Mikhonin, A. V.; Bykov, S. B. *J. Am. Chem. Soc.* **2004**, *126*, 8433.

(44) Cai, S.; Singh, B. R. *Biochemistry* **2004**, *43*, 2541.

(45) Ozaki, Y.; Murayama, K.; Wu, Y.; Czarnik-Matusewicz, B. *Spectroscopy (Amsterdam, Netherlands)* **2003**, *17*, 79.

(46) Blanch, E. W.; Hecht, L.; Barron, L. D. *Methods (San Diego, CA, United States)* **2003**, *29*, 196.

(47) Asher, S. A.; Ianoul, A.; Mix, G.; Boyden, M. N.; Karnoup, A.; Diem, M.; Schweitzer-Stenner, R. *J. Am. Chem. Soc.* **2001**, *123*, 11775.

(48) Jung, Y. M.; Czarnik-Matusewicz, B.; Ozaki, Y. *J. Phys. Chem. B* **2000**, *104*, 7812.

(49) Vedantham, G.; Sparks, H. G.; Sane, S. U.; Tzannis, S.; Przybycien, T. M. *Analytical Biochemistry* **2000**, *285*, 33.

(50) Vecchio, G.; Zambianchi, F.; Zacchetti, P.; Secundo, F.; Carrea, G. *Biotechnology and Bioengineering* **1999**, *64*, 545.

(51) Baello, B. I.; Pancoska, P.; Keiderling, T. A. *Anal. Biochem.* **1997**, *250*, 212.

(52) Bramanti, E.; Benedetti, E.; Sagripanti, A.; Papineschi, F.; Benedetti, E. *Biopolymers* **1997**, *41*, 545.

(53) Colaianni, S. E. M.; Aubard, J.; Hansen, S. H.; Nielsen, O. F. *Vibrational Spectroscopy* **1995**, *9*, 111.

(54) Griebenow, K.; Klibanov, A. M. *Proc. Natl. Acad. Sci. USA* **1995**, *92*, 10969.

(55) Jordan, T.; Spiro, T. G. *J. Raman Spectrosc.* **1994**, *25*, 537.

(56) Fu, F.-N.; DeOliveira, D. B.; Trumble, W. R.; Sarkar, H. K.; Singh, B. R. *Applied Spectroscopy* **1994**, *48*, 1432.

(57) DeGrazia, H.; Harman, J. G.; Tan, G. S.; Wartell, R. M. *Biochemistry* **1990**, *29*, 3557.

(58) Roberts, G. M.; Lee, O.; Calienni, J.; Diem, M. *J. Am. Chem. Soc.* **1988**, *110*, 1749.

(59) Ianoul, A.; Boyden, M. N.; Asher, S. A. *J. Am. Chem. Soc.* **2001**, *123*, 7433.

(60) Mikhonin, A. V.; Myshakina, N. S.; Bykov, S. V.; Asher, S. A. *J. Am. Chem. Soc.* **2005**, *127*, 7712.

(61) Mikhonin, A. V.; Asher, S. A. *J. Phys. Chem. B* **2005**, *109*, 3047.

(62) Mix, G.; Schweitzer-Stenner, R.; Asher, S. A. *J. Am. Chem. Soc.* **2000**, *122*, 9028.

(63) Fang, C.; Wang, J.; Charnley, A. K.; Barber-Armstrong, W.; Smith, A. B.; Decatur, S. M.; Hochstrasser, R. M. *Chem. Phys. Letters* **2003**, *382*, 586.

(64) Dudik, J. M.; Johnson, C. R.; Asher, S. A. *J. Phys. Chem.* **1985**, *89*, 3805.

(65) Robin, M. B. *"Higher Excited States of Polyatomic Molecules"; Academic Press: New York* **1975**, *Vol. II*.

(66) Chen, X. G.; Asher, S. A.; Schweitzer-Stenner, R.; Mirkin, N. G.; Krimm, S. *J. Am. Chem. Soc.* **1995**, *117*, 2884.

(67) Ianoul, A.; Mikhonin, A.; Lednev, I. K.; Asher, S. A. *J. Phys. Chem. A* **2002**, *106*, 3621.

(68) Chen, X. G.; Schweitzer-Stenner, R.; Asher, S. A.; Mirkin, N. G.; Krimm, S. *J. Phys. Chem.* **1995**, *99*, 3074.

(69) Garcia, A. E.; Onuchic, J. N. *Structure (Cambridge, MA, United States)* **2005**, *13*, 497.

(70) Snow, C. D.; Sorin, E. J.; Rhee, Y. M.; Pande, V. S. *Annual Review of Biophysics and Biomolecular Structure* **2005**, *34*, 43.

(71) Rhee, Y. M.; Sorin, E. J.; Jayachandran, G.; Lindahl, E.; Pande, V. S. *Proc. Natl. Acad. Sci. USA* **2004**, *101*, 6456.

(72) Bykov, S. V.; Lednev, I. K.; Ianoul, A.; Mikhonin, A. V.; Asher, S. A. *Appl. Spectrosc.* **2005**, *In Press*.

(73) Mirkin, N. G.; Krimm, S. *J. Phys. Chem. A* **2002**, *106*, 3391.

(74) Kubelka, J.; Keiderling, T. A. *J. Phys. Chem. A* **2001**, *105*, 10922.

(75) Besley, N. A. *J. Phys. Chem. A* **2004**, *108*, 10794.

(76) Torii, H.; Tatsumi, T.; Tasumi, M. *J. Raman Spectrosc.* **1998**, *29*, 537.

(77) Schmidt, P.; Dybal, J.; Rodriguez-Cabello, J. C.; Reboto, V. *Biomacromolecules* **2005**, *6*, 697.

(78) Torii, H.; Tatsumi, T.; Kanazawa, T.; Tasumi, M. *J. Phys. Chem. B* **1998**, *102*, 309.

(79) Torii, H.; Tatsumi, T.; Tasumi, M. *Mikrochimica Acta, Supplement* **1997**, *14*, 531.

(80) Gnanakaran, S.; Hochstrasser, R. M.; Garcia, A. E. *Proc. Natl. Acad. Sci. U.S.A.* **2004**, *101*, 9229.

(81) Ham, S.; Hahn, S.; Lee, C.; Kim, T.-K.; Kwak, K.; Cho, M. *J. Phys. Chem. B* **2004**, *108*, 9333.

(82) Del Bene, J. E.; Jordan, M. J. T. *Intl. Rev. Phys. Chem.* **1999**, *18*, 119.

(83) Bakker, H. J.; Nienhuys, H. K. *Science* **2002**, *297*, 587.

(84) Chaban, G. M.; Gerber, R. B. *J. Chem. Phys.* **2001**, *115*, 1340.

(85) Henri-Rousseau, O.; Blaise, P. *Chemical Physics* **1999**, *250*, 249.

(86) Torii, H. *J. Phys. Chem. A* **2004**, *108*, 7272.

(87) Cheatum, C. M.; Tokmakoff, A.; Knoester, J. *J. Chem. Phys.* **2004**, *120*, 8201.

(88) Schweitzer-Stenner, R.; Eker, F.; Huang, Q.; Griebenow, K.; Mroz, P. A.; Kozlowski, P. M. *J. Phys. Chem. B* **2002**, *106*, 4294.

(89) Pimenov, K. V.; Bykov, S. V.; Mikhonin, A. V.; Asher, S. A. *J. Am. Chem. Soc.* **2005**, *127*, 2840.

(90) Lovell, S. C.; Davis, I. W.; Arendall, W. B., III; de Bakker, P. I. W.; Word, J. M.; Prisant, M. G.; Richardson, J. S.; Richardson, D. C. *Proteins* **2003**, *50*, 437.

(91) Ho, B. K.; Thomas, A.; Brasseur, R. *Protein Science* **2003**, *12*, 2508.

(92) Kleywegt, G. J.; Jones, T. A. *Structure (London)* **1996**, *4*, 1395.

(93) Yennawar, H. P.; Natarajan, S.; Viswamitra, M. A. *International Journal of Peptide and Protein Research* **1991**, *38*, 569.

(94) Fletterick, R. J.; Tsai, C. C.; Hughes, R. E. *J. Phys. Chem.* **1971**, *75*, 918.

(95) Eggleston, D. S.; Hodgson, D. J. *International Journal of Peptide & Protein Research* **1983**, *21*, 288.

(96) Gorbitz, C. H. *Acta Crystallographica* **2000**, *C56*, 500.

(97) Eggleston, D. S. *Acta Crystallographica* **1984**, *C40*, 1250.

(98) Jones, P. G.; Falvello, L.; Kennard, O. *Acta Crystallographica* **1978**, *B34*, 1939.

(99) Chaturvedi, S.; Go, K.; Parthasarathy, R. *Biopolymers* **1991**, *31*, 397.

(100) Lednev, I. K.; Ermolenkov, V. V.; He, W.; Xu, M. *Analytical and Bioanalytical Chemistry* **2005**, *381*, 431.

(101) Dixon, D. A.; Dobbs, K. D.; Valentini, J. J. *J. Phys. Chem.* **1994**, *98*, 13435.

(102) Guo, H.; Karplus, M. *J. Phys. Chem.* **1992**, *96*, 7273.

(103) Jorgensen, W. L.; Swenson, C. J. *J. Am. Chem. Soc.* **1985**, *107*, 1489.

(104) Huang, H.; Malkov, S.; Coleman, M.; Painter, P. *J. Phys. Chem. A* **2003**, *107*, 7697.

(105) Avbelj, F.; Luo, P.; Baldwin, R. L. *Proc. Natl. Acad. Sci. USA* **2000**, *97*, 10786.

(106) Herrebout, W. A.; Clou, K.; Desseyn, H. O. *J. Phys. Chem. A* **2001**, *105*, 4865.

(107) Noda, I.; Liu, Y.; Ozaki, Y. *J. Phys. Chem.* **1996**, *100*, 8665.

(108) Fleming, P. J.; Fitzkee, N. C.; Mezei, M.; Srinivasan, R.; Rose, G. D. *Protein Science* **2005**, *14*, 111.

(109) Bochicchio, B.; Tamburro, A. M. *Chirality* **2002**, *14*, 782.

(110) Shi, Z.; Woody, R. W.; Kallenbach, N. R. *Adv. Prot. Chem.* **2002**, *62*, 163.

(111) Mayne, L. C.; Hudson, B. *J. Phys. Chem.* **1991**, *95*, 2962.

(112) Walsh, S. T. R.; Cheng, R. P.; Wright, W. W.; Alonso, D. O. V.; Daggett, V.; Vanderkooi, J. M.; DeGrado, W. F. *Prot. Sci.* **2003**, *12*, 520.

(113) Manas, E. S.; Getahun, Z.; Wright, W. W.; DeGrado, W. F.; Vanderkooi, J. M. *J. Am. Chem. Soc.* **2000**, *122*, 9883.

(114) McColl, I. H.; Blanch, E. W.; Hecht, L.; Barron, L. D. *J. Am. Chem. Soc.* **2004**, *126*, 8181.

(115) Sheu, S.-y.; Yang, D.-y.; Selzle, H. L.; Schlag, E. W. *Proc. Natl. Acad. Sci. USA* **2003**, *100*, 12683.

6.0 CHAPTER 6. UV RESONANCE RAMAN DETERMINATION OF POLYPROLINE II, EXTENDED 2.5_1-HELIX, AND β-SHEET Ψ ANGLE ENERGY LANDSCAPE FEATURES IN POLY-L-LYSINE AND POLY-L-GLUTAMIC ACID

Work, described in this chapter, is published in *J. Am. Chem. Soc.*, **2005**, *127(21)*, 7712-7720 (Authors: Mikhonin, A. V.; Myshakina, N. S; Bykov, S. V.; and Asher, S. A.). UV Resonance Raman (UVRR) spectroscopy was used to examine the solution conformation of poly-L-Lysine (PLL) and poly-L-Glutamic acid (PGA) in their non-α-helical states. UVRR measurements indicate that at pH=2 PLL and pH=9 PGA exist mainly in a mixture of PPII and a novel left-handed 2.5_1-helical conformation, which is an extended β-strand-like conformation with Ψ ~ +170° and Φ ~ −130°. Both of these conformations are highly exposed to water. The energies of these conformations are very similar. We see no evidence of any disordered "random coil" states. In addition, we find that a PLL and PGA mixture at neutral pH is ~60% β-sheet, and contains PPII and extended 2.5_1-helix conformations. The β-sheet conformation shows little evidence of amide backbone hydrogen bonding to water. We also developed a method to estimate the distribution of Ψ Ramachandran angles for these conformations, which we used to estimate an energy curve along the Ψ Ramachandran angle coordinate. We believe that these are the first experimental studies to give direct information on protein and peptide energy landscape features.

6.1 INTRODUCTION

The primary sequence of a protein encodes both the native structure as well its folding mechanism[1-8] (in the absence of chaperones or posttranslational modifications). The arguably most important problem in enzymology is to translate the primary sequence into the encoded protein folding mechanism(s), and to use this information to predict the ultimate native structure

from the primary sequence information. In general, the native conformation(s) are thought to be located at distinct minima in the potential energy landscape.[9-15] The native conformation occurs when the protein environment favors folding.[16-20]

Until recently, protein unfolded states were assumed to consist of random coil conformations, where the polypeptide chains would adopt energetically allowed, but randomly distributed Φ and Ψ dihedral angles. Ideally, these structures were considered to be completely disordered with no correlations between adjacent peptide bonds Φ and Ψ Ramachandran dihedral angles.[21] However, this assumption has recently been seriously challenged.[22-28]

Numerous theoretical and experimental groups have been working on elucidating protein folding mechanisms over the last fifty years.[1-21,23-28] A major challenge in this work is the required development of an energetic understanding of protein folding motifs, and the sequence specific phenomena which determine the folding energy landscape. In this regard new theoretical paradigms such as the energy landscape theories have significantly aided thinking about protein folding. In addition, new theoretical studies have examined the conformational subspace of small and large peptides and have examined conformational energies. Molecular dynamic studies are becoming available which examine the temporal evolution of protein structure in timescales which are relevant for folding into equilibrium structures.[29-33]

This work has been aided by new experimental studies which characterize peptide conformations.[34-49] What is most needed to make rapid continuing progress is additional experimental insight into protein folding motifs and the energy landscapes that surround these structures.

We[50-52] as well as others[53-58] have been developing UV resonance Raman (UVRR) spectroscopy to probe protein structure and dynamics. We recently examined the first stages in unfolding of α-helices and discovered that a mainly ala 21-residue peptide melts from an α-helix conformation into a polyproline II conformation (PPII).[34]

In the work here we now examine peptide conformations of charged peptides such as poly-L-glutamic acid (PGA) and poly-L-Lysine under conditions where their sidechains are charged. We find that they occur in a mixture of PPII and a novel conformation, which is a subset of extended β-strand conformations, but which is best described as a 2.5_1 helix. If the sidechain charges are neutralized these peptides form α-helices, while if peptides with oppositely charged sidechains are mixed, they form β-sheet conformations.[59]

We have developed insights into peptide secondary structures through examinations of their ~200 nm UVRR spectra. We obtain the most information from the amide III_3 ($AmIII_3$) vibration whose frequency we earlier found was correlated to the peptide conformational Ramachandran Ψ angle.[34,60,61] We have recently developed quantitative relationships between peptide bond $AmIII_3$ frequencies the peptide bond Ψ angle and its hydrogen bonding pattern.[61] In the work here these relationships are used to estimate the conformational energy differences between the PPII and 2.5_1 helix conformations, as well as the Ψ angle energy landscape for the PPII and 2.5_1 helix conformations as well as for the β-sheet structure. To our knowledge these are the first experimental studies to directly give information on the energy landscape of peptide conformations along coordinates involved in conformational evolution.

The work here shows clearly that the UVRR spectra of β-sheet conformations significantly differ from those of PPII and 2.5_1-helix ("single" β-strand) conformations. This ability to discriminate between conformations may prove useful for early detection of amyloidal fibril formation in solutions of proteins.[62]

6.2 EXPERIMENTAL SECTION

6.2.1 Sample preparation

Poly-L-Lysine HCl (PLL, MW_{vis} = 28,500, MW_{LALLS} = 20,200) and the sodium salt of poly-L-Glutamic acid (PGA, MW_{vis} – 17,000, MW_{mALLS} = 8853) were purchased from Sigma Chemical, and used as received. Solution spectra of PLL and PGA were measured at pH=2 and pH=9, respectively, to ensure the absence of α-helix contributions. The mixed PLL and PGA neutral pH sample solutions contained identical concentrations of lysine and glutamic acid residues. These samples were freshly prepared before the Raman measurements. The total peptide concentrations were kept below 0.3 mg/ml to avoid gel formation.

The 21-residue alanine-based peptide $AAAAA(AAARA)_3A$ (AP) was prepared (HPLC pure) at the Pittsburgh Peptide Facility by using the solid-state peptide synthesis method. The AP solutions in water contained 1 mg/ml concentrations of AP, and 0.2 M concentrations of sodium

perchlorate, which was used as an internal intensity and frequency standard. All Raman spectra were normalized to the intensity of the ClO_4^- Raman band (932 cm^{-1}).

A_5 and A_3 peptides were purchased from Bachem Bioscience Inc. (King of Prussia, PA), and used as received. The $A_5 - A_3$ Raman difference spectral measurements utilized identical molar concentrations of A_5 and A_3 (0.34 mg/ml and 0.2 mg/ml, respectively) in solutions containing identical sodium perchlorate concentrations (0.2 M). We normalized the Raman spectra to the intensity of the 932 cm^{-1} perchlorate internal standard band. The $A_5 - A_3$ difference spectra were calculated by subtracting the normalized A_3 spectrum from the normalized A_5 spectrum at each temperature.

The undecapeptide XAO (MW=985) was prepared (HPLC pure) at the Pittsburgh Peptide Facility by using the solid-state peptide synthesis method. The sequence of this peptide is Ac-XXAAAAAAAOO-amide, where all amino acids are in their L form, A is ala, X is diaminobutyric acid (side chain $CH_2CH_2NH_3^+$), and O is ornithine (side chain $(CH_2)_3NH_3^+$). We used 1 mg/ml solutions of XAO-peptide containing 0.15 M of sodium perchlorate. The UVRR spectra of XAO were also normalized to the ClO_4^- Raman band intensity.

6.2.2 UV Resonance Raman Instrumentation

The Raman instrumentation has been described in detail elsewhere.[51,63] A Coherent Infinity Nd:YAG laser produced 355 nm (3^{rd} harmonic) 3 nsec pulses at 100 Hz. This beam was Raman shifted to 204 nm (5^{th} anti-Stokes) by using a 1 m tube filled with hydrogen (60 psi). A Pellin Broca prism was used to select the 204 nm excitation beam. The Raman scattered light was imaged into a subtractive double spectrometer[64] and the UV light was detected by a Princeton Instruments solar blind ICCD camera. All samples were measured in a thermostatted free surface flow stream.

6.3 RESULTS AND DISCUSSION

6.3.1 Unfolded States of PLL and PGA

Fig. 57 shows the 204 nm UV resonance Raman (UVRR) spectra of the unfolded conformations of PLL (pH=2) and PGA (pH=9) at high (+70 °C) and low (0 °C) temperatures. At these pH values PLL and PGA have charged sidechains, whose repulsions prevent formation of α-helical conformations. The UVRR spectra of the PLL and PGA samples are essentially identical. Further, the insignificant spectral shifts occurring between the low and high temperature spectra indicate a lack of conformational transitions over this temperature range.

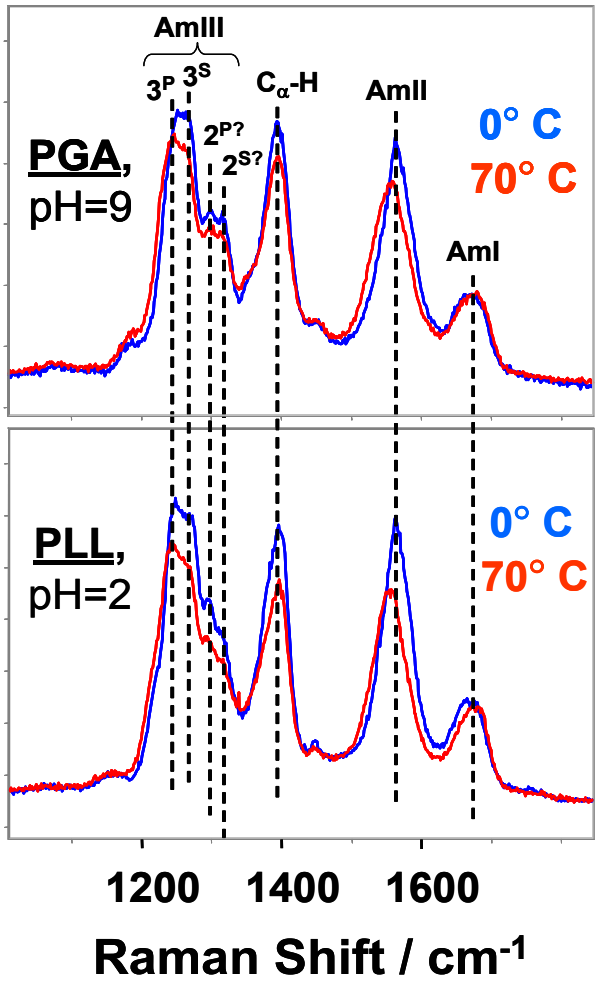

Figure 57. 204 nm UVRR spectra of unfolded states of PGA (pH=9) and PLL (pH=2) in water at 0 °C and at +70 °C

The 0 °C spectra show the AmI bands at ~1670 cm^{-1} (mainly CO s), the AmII bands at ~1564 cm^{-1} (mainly out of phase combination of CN s and NH b), the (C)C_α-H bending bands at ~1396 cm^{-1} and a complex series of bands in the AmIII region between 1210 and 1350 cm^{-1}. The AmIII region contains at least 4 resolved bands, which as discussed below derive from two conformations in equilibrium. We assign these two conformations to a polyproline II conformation (PPII, P superscript) and an extended β-strand-like conformation (S superscript). As discussed below, the latter conformation can be described as an extended 2.5_1-helix. As evident from previous UVRR studies[36,37,52,60] the AmIII bands are significantly more sensitive to conformation than are the AmI and AmII, bands that are more typically used by IR absorption and normal non resonance Raman secondary structure studies. Moreover, the UVRR $AmIII_3$ band is independently contributed by the individual peptide bonds in the polypeptides with no evidence of inter-amide coupling,[37,65] in contrast to commonly utilized AmI band.[37,40] This important observations dramatically simplify the spectral analysis in AmIII region.

Thus, we enumerate these bands as $AmIII_3^S$ (~1271 cm^{-1} (PLL) and ~1272 cm^{-1} (PGA)), and $AmIII_3^P$ (~1245 cm^{-1} (PLL) and ~1249 cm^{-1} (PGA), and $AmIII_2^{S?}$ (~1316 cm^{-1} (PLL) and ~1319 cm^{-1} (PGA)), $AmIII_2^{P?}$ (~1296 cm^{-1} (PLL) and ~1298 cm^{-1} (PGA)), where the subscripts label different amide III spectral region bands as we recently discussed in detail,[36] and the superscript question mark labels assignments which remain uncertain.

The temperature dependence of the spectra involves small downshifts for the AmIII and AmII bands and small upshifts for the AmI band (Table 11). This temperature dependence is characteristic of peptide backbone conformations where the amide carbonyl and N-H groups are hydrogen bonded to water.[34,36,66] The shifts occur because the water-amide hydrogen bond strengths decrease as the temperature increases.[34] This favors a peptide bond resonance form with stronger bonding for the carbonyl and weaker bonding for the C(O)-N linkage, which result in the observed amide band shifts.

Table 11. Temperature dependence of amide UV Raman bands of non-α-helical poly-peptides: pH=2 PLL, pH=9 PGA, and PPII peptides: XAO, Ala_5-Ala_3, AP

	XAO-peptide >80% PPII, neutral pH		**Ala_5 – Ala_3** essentially PPII, neutral pH		**AP** essentially PPII, neutral pH		**PLL** unfolded (PPII + extended), pH=2		**PGA** unfolded (PPII + extended), pH=9	
	dν/dT	$\nu_{60℃}$, cm^{-1}	dν/dT	$\nu_{50℃}$, cm^{-1}	dν/dT	$\nu_{60℃}$, cm^{-1}	dν/dT	$\nu_{70℃}$, cm^{-1}	dν/dT	$\nu_{70℃}$, cm^{-1}
AI	0.02 ± ±0.01	1659	0.052± ±0.02	1667	0.052± ±0.02	1659	0.06	1673	0.03	1673
AII	-0.14± ± 0.01	1545	-0.14 ± ± 0.01	1558	-0.14 ± ± 0.01	1548	-0.15	1553	-0.13	1555
$C_\alpha H_{(1)}$	0.008± ±0.016	1388	-0.015± ± 0.02	1397	-0.015± ± 0.02	1399	-0.01	1399	0.02	1396
$C_\alpha H_{(2)}$	0.018± ±0.017	1365	-0.01 ± ± 0.02	1373	-0.01 ± ± 0.03	1377 broad	-0.04	1377	0.036	1359
$AIII_2$	-0.03 ± ± 0.02	1300	-0.03 ± ± 0.01	1305	-0.03 ± ± 0.01	1311	-0.033 -0.036	1313 1293	-0.003 -0.006	1319 1298
$AIII_3^S$ (2.5_1-helix)	N/A	N/A	N/A	N/A	N/A	N/A		1270		1269
$AIII_3^P$ (PPII)	-0.10 ± ± 0.02	1241	-0.094± ± 0.018	1250	-0.094± ± 0.018	1247	-0.1	1242	-0.12	1240

6.3.2 $AmIII_3^P$ band (~1245 cm^{-1}) signals PPII conformations

Fig. 58 compares the 204 nm UVRR spectra of the unfolded PGA and PLL samples to spectra of the three ala-based peptides: XAO, AP, and A_5-A_3 under conditions where they are predominantly in PPII conformations. The observed $AmIII_3^P$ band frequency closely coincides with the $AmIII_3$ frequency of the PPII conformations of XAO, AP, A_5-A_3. Since we know that the $AmIII_3$ frequency strongly depends on the Ψ angle,[34,60] (and to much lesser degree on *allowed* Φ angles[34,60,67-69]) we conclude that both PLL and PGA have solution conformations with Ψ angles similar to that of the PPII conformation.

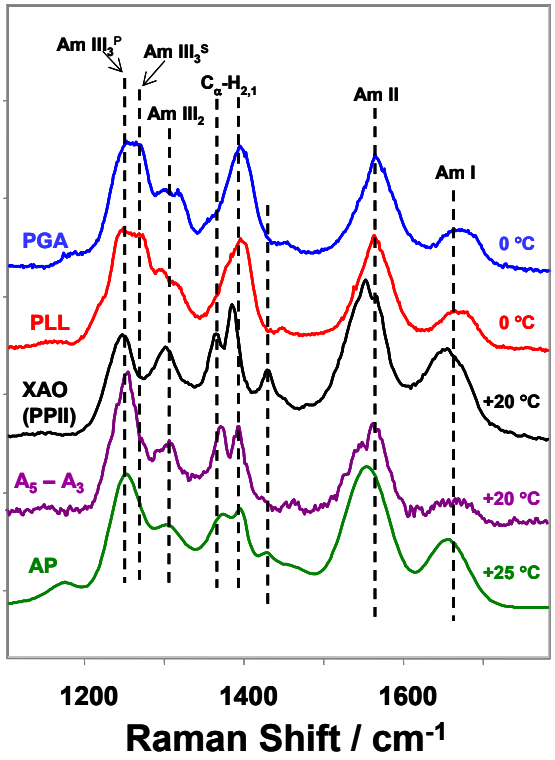

Figure 58. Comparison of 204 nm UVRR spectra of unfolded states of PGA (pH=9) and PLL (pH=2) in water at 0 °C to the spectra of the PPII states of alanine-rich peptides XAO, AP, A_5-A_3 at 0 °C.

The coincidence in frequency and the similar temperature dependencies (Table 11) of the $AmIII_3^P$ bands to those of PPII conformations militates for the assignment of this band to PPII conformations of PGA and PLL. This conclusion is consistent with previous studies which also concluded that the unfolded state(s) of PLL and PGA have significant PPII content.[22,70-81]

The PPII structure is a commonly observed non-α-helix low energy conformation because of its stabilization by peptide-water interactions.[72,82,83] This open conformation permits the simultaneous hydrogen bonding of water to amide bonds, as well as important bridging hydrogen bonds between water molecules. In addition, Hinderacker and Raines[84] recently proposed an additional PPII stabilization mechanism. They proposed that the PPII conformation is stabilized because of especially favorable n-π* interactions between the carbonyl oxygen of peptide bonds and the carbonyl carbons of adjacent peptide bonds. Whatever the case, investigators now find that the unfolded states of many proteins[71,82,85-89] as well as the unfolded states of moderate and long peptides[35,70-73], and even small peptides[90-92] contain significant fractions of PPII.

6.3.3 $AmIII_3^S$ band (~1271 cm^{-1}) signals the presence of a 2.5_1-helix conformation

The electrostatic repulsions between the PLL and PGA charged sidechains prevent formation of α-helical conformations, and should force more extended conformations, such as PPII and/or extended β-strand(s). The PPII conformation clearly does not require sidechain repulsion since it occurs for polyalanine derivatives such as AP and XAO.[34,35,93] Further, the K7 peptide shows significant PPII content at pH=12 in the absence of salt as well as in 4 M NaCl.[70]

The pH=2 PLL and pH=9 PGA spectra also show a second $AmIII_3$ region band at ~1271 cm^{-1} denoted as $AmIII_3^S$ (Fig. 57 and 58). This band is absent in mainly PPII ala-based peptides with neutral side chains. Thus, it must result from the additional PLL and PGA electrostatic repulsions between ionized side chains. We expect that these repulsions will induce a more extended conformation with a Ramachandran angle greater than the $\Psi = 145°$ of the PPII conformation. Given the dependence of the $AmIII_3$ frequency on the Ψ angle that we previously demonstrated,[34,36,60] we expect a new $AmIII_3$ band to occur at a higher frequency, as observed.

Because of the severe overlap with the $AmIII_3^P$ bands it is not possible to accurately determine the $AmIII^S$ temperature dependence. However, the temperature dependence is qualitatively similar to that of fully exposed conformations like PPII. Thus, we assign the conformation to an extended β-strand like conformation (2.5_1-helix, see below), and conclude

that these PGA and PLA samples contain a mixture of PPII and extended β-strand-like conformations.

Assuming similar Raman cross sections for these conformations, we roughly estimate that "unfolded" PLL and PGA both consist of ~60% PPII and ~40% β-strand. In contrast, we only detect very small contributions from β-strand-like conformations in AP at high temperature.[36] The lack of a temperature dependence of the relative intensity ratios suggests that these conformations have similar energies (as we prove later by Table 14).

It should be noted that Raman Optical Activity studies of "unfolded" peptides and proteins show positive features between ~1314 to ~1325 cm^{-1}, which are thought to signal the PPII conformation.[93-96] The large frequency spread for these positive bands may indicate the existence of a variety of PPII-like left-handed helical conformations with significantly differing Ψ and Φ angles.

Whatever the case, we detect only PPII and *extended* β-strand-like conformations which significantly differ spectrally from those of β-sheet conformations (Compare Figs. 58, 63 and 64).

As discussed in Chapter 5 (Eqn. 11A), the ~1271 cm^{-1} $AmIII_3^S$ band frequency results in a calculated β-strand-like Ψ angle of ~170°, if we neglect any Φ angle frequency dependence. This neglect of the Φ angle dependence is justified in view of the known small Φ angle amide III frequency dependence[60,67] and the fact that only modest changes in the Φ angle are likely to occur between the relevant conformations with different Ψ angles. Further, we and others recently estimated that the Ψ angle dependence can result in up to ~110 cm^{-1} shift,[61] while Φ angle only in no more than 20 cm^{-1} $AmIII_3$ frequency shift.[67,68]

6.3.4 The β-strand-like conformation is a 2.5_1-helix

We developed insight into this new conformation by examining the dependence of the electrostatic repulsion energies on the Φ angle, for a fixed Ψ = +170° (Fig. 59). We utilized the HyperChem© amino acid data base to construct approximate structures to estimate the distances between charges located on PLL and PGA side chains. Fig. 59 shows that the total electrostatic

repulsion energy has a minimum near Φ ~ −130° for PGA. The situation for PLL has the same trend (Table 12).

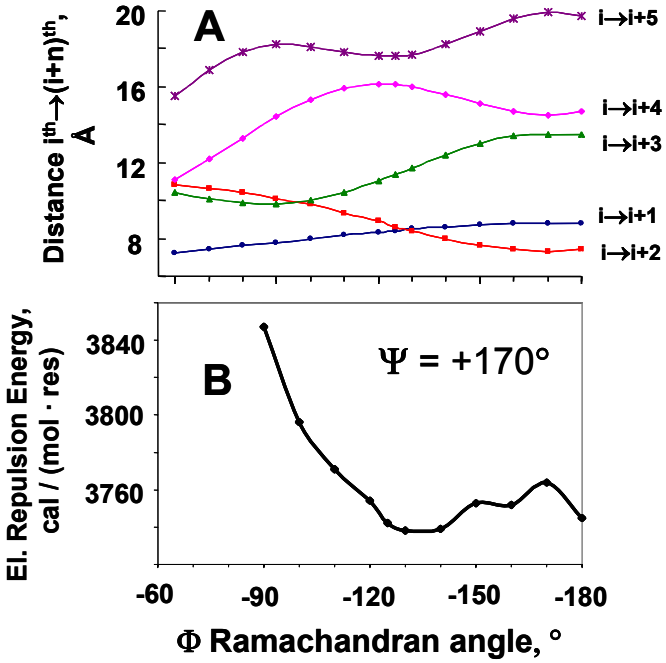

Figure 59. A) Distances between the i-th and (i+k)-th sidechain charges of PGA as a function of Φ Ramachandran angle as calculated using Hyperchem. B) Electrostatic repulsion energy between the sidechains as a function of Φ Ramachandran angle. NOTE: The Ψ angle is fixed at the value of 170° estimated from the UV Raman data.

Figure 60 indicates a rough structure for our PGA minimum repulsion energy conformation which utilizes the determined Ψ and Φ angles of +170° and −130°, respectively. The resulting extended β-strand occurs as a 2.5_1-helix conformation.

Krimm and Mark's[97] previous theoretical study of conformations of polypeptides with ionized sidechains, also proposed that the charged sidechains of PLL and PGA stabilize a helical conformation with approximately 2.5 residues per helical turn. They also showed that the number of residues per turn was essentially independent of sidechain length for side chains equal to or longer than that of glutamic acid. However, for a 64-residue PGA they proposed a minimum energy conformation with Ψ = −170° and Φ = −155° (in their original paper they used an older definition for the Ψ and Φ angles).[98] Future work will be required to discrimate between these very similar structures in order to determine the actual Φ angles for these structures.

Table 12. Distances between ionized sidechain charges in PLL and PGA for Ψ and Φ angles of PPII and 2.5_1 helix conformations.

	Distance between sidechain charges	**PPII** $\Psi = +145°, \ \Phi = -75°$	**Extended 2.5_1-helix** $\Psi = +170°, \ \Phi = -130°$
PLL	i→i+1	11.245	11.67
	i→i+2	12.389	10.146
	i→i+3	9.232	12.266
	i→i+4	16.427	18.130
PGA	i→i+1	8.328	8.421
	i→i+2	9.852	8.639
	i→i+3	9.232	11.381
	i→i+4	14.563	16.101

Our study here is the first, to our knowledge, to experimentally detect a stable 2.5_1-helix conformation in peptides and proteins. We also compared the distances between charges in our putative 2.5_1-helix to those in a PPII helix. Table 12 shows that the larger separation distances occur in the 2.5_1-helix compared to the PPII helix. This lowers the 2.5_1-helix total energy such that it is very close to that of the PPII conformation (Table 14).

Our spectral data and the lack of a significant temperature dependence of the relative Raman intensities clearly demonstrate that these conformations are close in energy. Given our present inability to accurately curve resolve the PPII peak from the 2.5_1 $AmIII_3$ peaks, our incomplete understanding of the degeneracies of these two conformation, the unknown dependence of the Raman cross sections on conformation, and the measured modest temperature dependence, on the basis of the relative intensity ratios, we can only visually roughly estimate from the relative Raman intensities that the 2.5_1 conformations of PLL and PGA are <300 cal/mol higher in energy than the PPII conformation at room temperature (however, see below).

We are in the process of modeling this 2.5_1 helix conformation to better determine its detailed geometry.

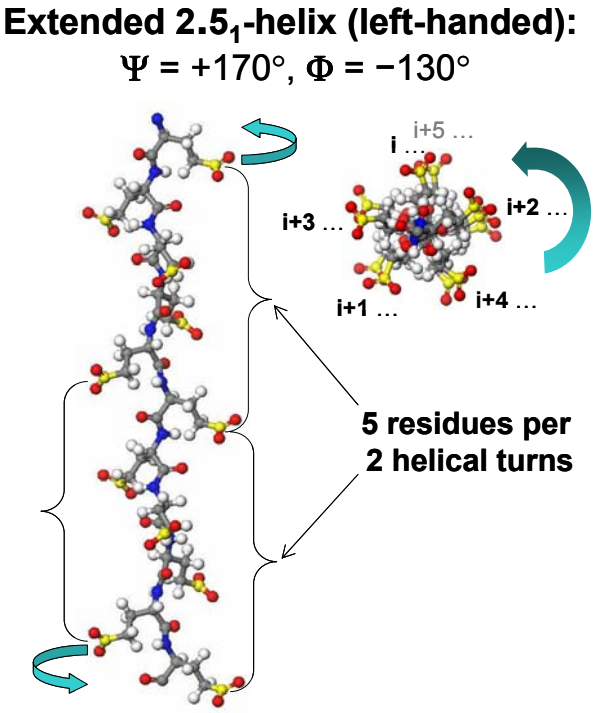

Figure 60. Visualization of 2.5_1-helix in PGA (Ψ=+170°, Φ=−130°). This structure occurs in both ionized PLL and PGA due to electrostatic repulsion between bulky and charged sidechains. Carboxyl carbons of glu side-chains are shown in yellow.

Our observations of the 2.5_1 helix was, in fact, partially presupposed by Tiffany and Krimm[22] who originally proposed that aqueous solution denatured states of PLL and PGA would contain some local order and would not be in a completely "disordered" form. The structure was suggested to involve an extended 3_1-helix or a PPII helix, which is also left-handed helix, with three amino acid residues per turn, with Φ and Ψ Ramachandran angles of -75° and 145°, respectively. In addition, more recent studies report evidence for PPII content in "unfolded" PLL and PGA.[70-78,94-96]

6.3.5 PLL-PGA Mixture β-Sheet Conformation

Equimolar mixtures of PLL and PGA at neutral pH are known to form antiparallel β-sheets.[59] This is clearly demonstrated in the Fig. 61 comparison of the CD spectrum of a PLL-PGA mixture to the CD spectra of α-helical, β-sheet and "unordered" peptides. The PLL-PGA mixture spectrum, especially the ~217 nm negative feature, clearly demonstrates a significant fraction of β-sheet. In addition, the CD spectra of the PLL-PGA mixture shows an increasing 217 nm trough as the temperature increases, which indicates that the β-sheet content slightly increases with temperature (see inset to Fig. 61).

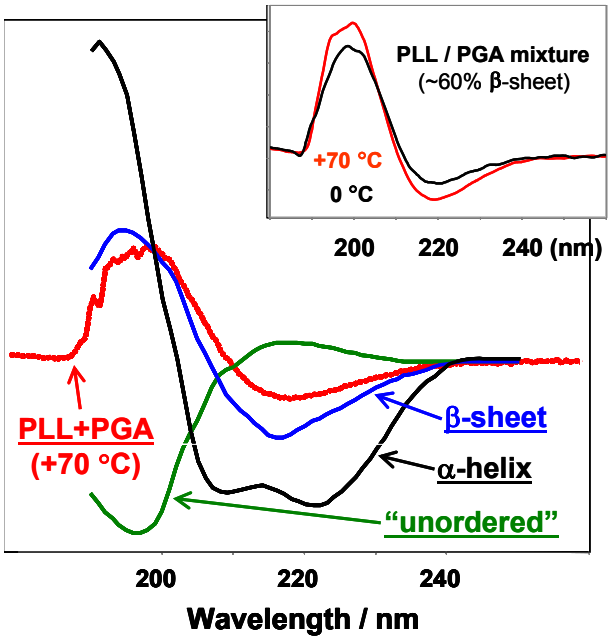

Figure 61. Comparison of CD spectra of different peptide and protein conformations to that of a neutral pH mixture of PLL and PGA at +70 °C. This sample obviously contains a significant fraction of β-sheet, due to the similarity of the PLL and PG mixture CD spectrum to that of the β-sheet. The pure secondary structure CD spectra were obtained from the Lawrence Livermore National Laboratory website (http://www-structure.llnl.gov/cd/cdtutorial.htm).

Fig. 62 shows that the UVRR spectra of the PLL-PGA mixture at 0 and +70 °C. The entire $AmIII_3$ band profile of the PLL-PGA mixture is red-shifted compared to unfolded PLL and PGA (Figs. 57, 58 and 63; Tables 11 and 13) due to formation of the antiparallel β-sheet structure. Fig. 62 shows that overall spectra of the PLL-PGA mixture are almost independent of temperature, indicating that the β-sheet conformation does not melt significantly over this

temperature range. Further, the temperature dependence of the AmI, II and III band frequencies in the PLL-PGA mixture (~60% β-sheet) is significantly decreased (~2-fold) compared to those in the PPII and β-strand (2.5_1-helix) conformations due to the decreased peptide-water hydrogen bonding of the β-sheet structure.

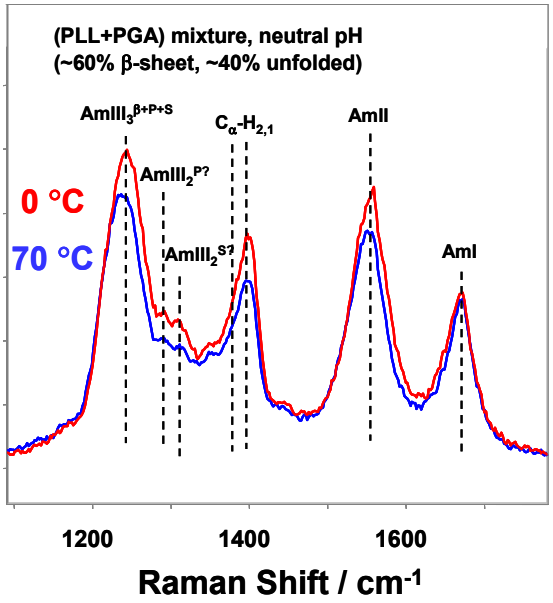

Figure 62. 204 nm UVRR spectra of neutral pH PLL-PGA mixture at 0 and +70 °C.

Table 13. Temperature dependencies of amide UV Raman bands of PLL-PGA mixture.

	PLL-PGA mixture, ~60% β-sheet, ~40% unfolded, [a] neutral pH		**PLL-PGA mixture, pure PPII, 2.5_1 conformations[b]** neutral pH		**PLL-PGA mixture, pure β-sheet spectrum[c]** neutral pH	
	dν/dT	$\nu_{70°C}$, cm^{-1}	dν/dT	$\nu_{70°C}$, cm^{-1}	dν/dT	$\nu_{70°C}$, cm^{-1}
AI	0.022	1668	0.045		0.018	1672
AII	-0.071	1548	-0.14		-0.005	1550
$C_\alpha H_{(1)}$	-0.007	1402	0.005		-0.031	1403
$C_\alpha H_{(2)}$	0	1381	-0.005		0	1379 weak
$AIII_2$	0	1290 1310	-0.03			
$AIII_3$	-0.062	1239	-0.11		-0.003	1228

[a] experimental spectra, neutral pH (~60% β-sheet, ~40% unfolded); [b, c] see text for details

6.3.6 Calculation of pure β-sheet spectrum from PLL-PGA mixture UV Raman spectra

The Figs. 62 and 63 PLL-PGA mixture UVRR spectra are broad and show high frequency shoulders. This contrasts with the AmIII symmetric bandshape found by Chi et al.[52] for the β-sheet conformation of a library of proteins (Fig. 63). Thus, the PLL-PGA mixture sample appears to contain additional peptide conformations. Since the PLL and PGA sidechains are highly ionized at this neutral pH, it is likely that these other conformations are the extended 2.5_1-helix and the PPII conformations discussed above.

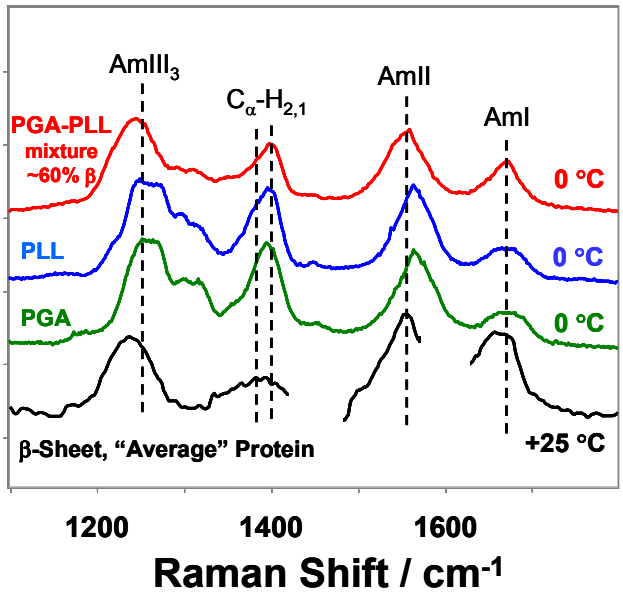

Figure 63. 204 nm UVRR spectra of PLL-PGA mixture at 0 °C, and those of the PPII and β-strand (2.5_1-helix) conformations of PLL and PGA. Also shown is the β-sheet basis spectrum determined by Chi et al.[52] from a library of proteins.

We can calculate the pure β-sheet PGA-PLL Raman spectrum by subtracting off the spectra of these other conformations. We assume that the spectra of these other conformations are the sum of the individual PLL and PGA PPII and β-strand (2.5_1-helix) spectra. The criteria for the amounts subtracted are that the resultant spectra (Fig. 63) best fit the β-sheet spectrum of Chi et al.[52] (except that we do not include the amide I region in the fit due to the potential residual contribution of the water bending band). We find non β-sheet conformation fractions of 42% at 0 °C, and 35% at 70 °C. Thus, the β-sheet content slightly increases with temperature.

Fig. 64 shows these calculated pure β-sheet spectra at 0 and 70 ºC. The β-sheet AmIII peak is symmetric without any shoulders and is similar to that found by Chi et al.[52] (Compare Figs. 63 and 64). As also shown in Fig. 64 the pure PLL-PGA mixture β-sheet spectrum shows a ~10-fold decreased temperature frequency dependence for the AmII and III bands and a ~3 fold decreased AmI band frequency dependence than occurs for the PPII and 2.5_1-helix conformations. This is expected due to the decreased water-amide bond hydrogen bonding of the β-sheet; since the β-sheet satisfies its hydrogen bonding mainly through inter-peptide hydrogen bonds.

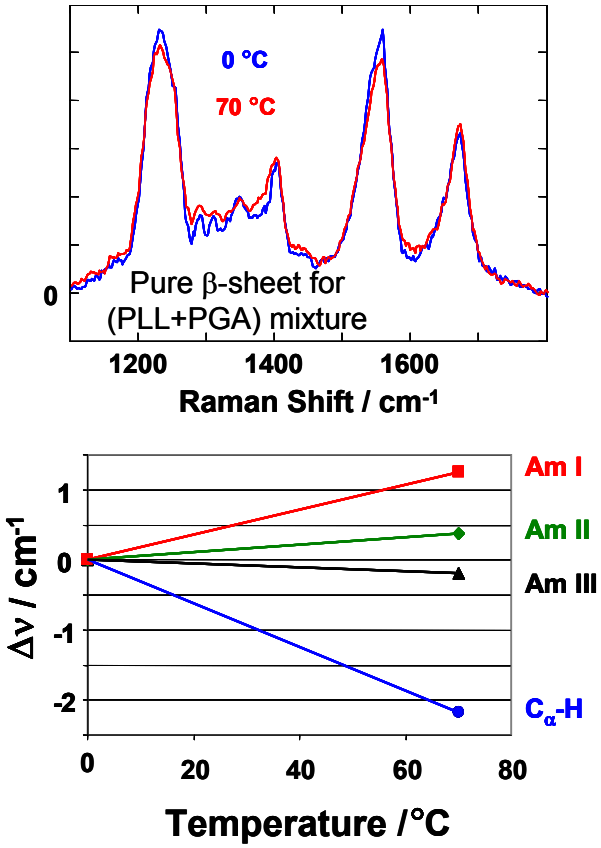

Figure 64. Calculated 204 nm UVRR spectra of PLL-PGA mixture β-sheet at 0 and +70 °C. The contributions from the PLL and PGA PPII and β-strand (2.5_1-helix) conformations were numerically removed (See text for details). UVRR bands of β-sheet show a very small temperature dependence compared to PPII (Compare Tables 11 and 13).

The large UVRR spectral differences between the PLL-PGA mixture pure β-sheet conformation and that of PLL and PGA in their unfolded states (compare Figs. 63-65) offers

opportunities for characterizing subtle issues of β-sheet conformation. This could be valuable in kinetic and steady state investigations of systems such as amyloid fibrils.[62]

6.3.7 Ψ Ramachandran Angular Distribution for PLL and PGA β-sheet, PPII and 2.5_1-helix

The β-sheet, PPII and 2.5_1-helix amide bands are significantly broadened from their estimated 7.5 cm^{-1} homogeneous linewidth determined in crystals.[34] This broadening probably results from the distribution of Ψ angles that occurs for these conformations in solution. We developed a deconvolution method for the $AmIII_3$ band frequencies which determines the inhomogeneous distribution of $AmIII_3$ band frequencies.[34] We then developed a method to use this frequency distribution to calculate the Ψ angle distribution from the measured $AmIII_3$ bandshapes.[34,61] Originally[34] we utilized the Eqn. 4 of Chapter 2 below:

$$\upsilon_{III3}(\Psi) = 1265\ cm^{-1} - 46.8\ cm^{-1} \sin(\Psi + 5.2°)$$

which allows to roughly estimate the relationship between the $AmIII_3$ frequency and Ψ Ramachandran angle for peptides and proteins in water solutions. The sinusoidal nature of the Eqn. 4 was theoretically predicted by Asher et al.,[60] and explained in terms of different degree of coupling between the N-H and C_α-H bending motions at different Ψ angles.

In our most recent study[61] (see also Chapter 5 of the thesis), we examined the dependence of the $AmIII_3$ frequencies of peptide bonds upon the peptide bond hydrogen bonding. This study also elucidated the temperature dependence of the $AmIII_3$ frequencies which result from the temperature dependence of its hydrogen bonding. We quantified this hydrogen bonding-induced frequency dependencies for all major peptide/protein secondary structure conformations;[61] and were able to propose a family of equations to relate the $AmIII_3$ frequency directly to the Ψ Ramachandran angle given its particular state of hydrogen bonding.

Thus, for extended and highly exposed to water conformations, such as PPII and 2.5_1-helix, we would use the Eqn. 11A below, which is developed in Chapter 5:

$$\nu_{III3}^{EXT}(\psi, T, HB) = [1256\ cm^{-1} - 54\ cm^{-1} \cdot \sin(\psi + 26^0)] - 0.11 \cdot \frac{cm^{-1}}{^oC} \cdot (T - T_0)\}$$

where T_0=0 °C.

In contrast, for PLL-PGA mixture antiparallel β-sheet, which is dominated by two end-on peptide bond-peptide bond hydrogen bonding,[61] we would use Eqn. 11B from Chapter 5:

$$\nu_{III3}^{i\alpha,\,i\beta}(\psi, T_0, HB) = [1244\ cm^{-1} - 54\ cm^{-1} \cdot \sin(\psi + 26^0)]$$

Fig. 65 shows the Ψ angle distribution calculated for PLL (pH=2) and PGA (pH=9) and for the PLL-PGA mixture β-sheet. Fig. 65 displays the existence of the two different conformations of unfolded PLL and PGA, with two distinct maxima near Ψ~145° (PPII) and Ψ~170° (2.5_1-helix).

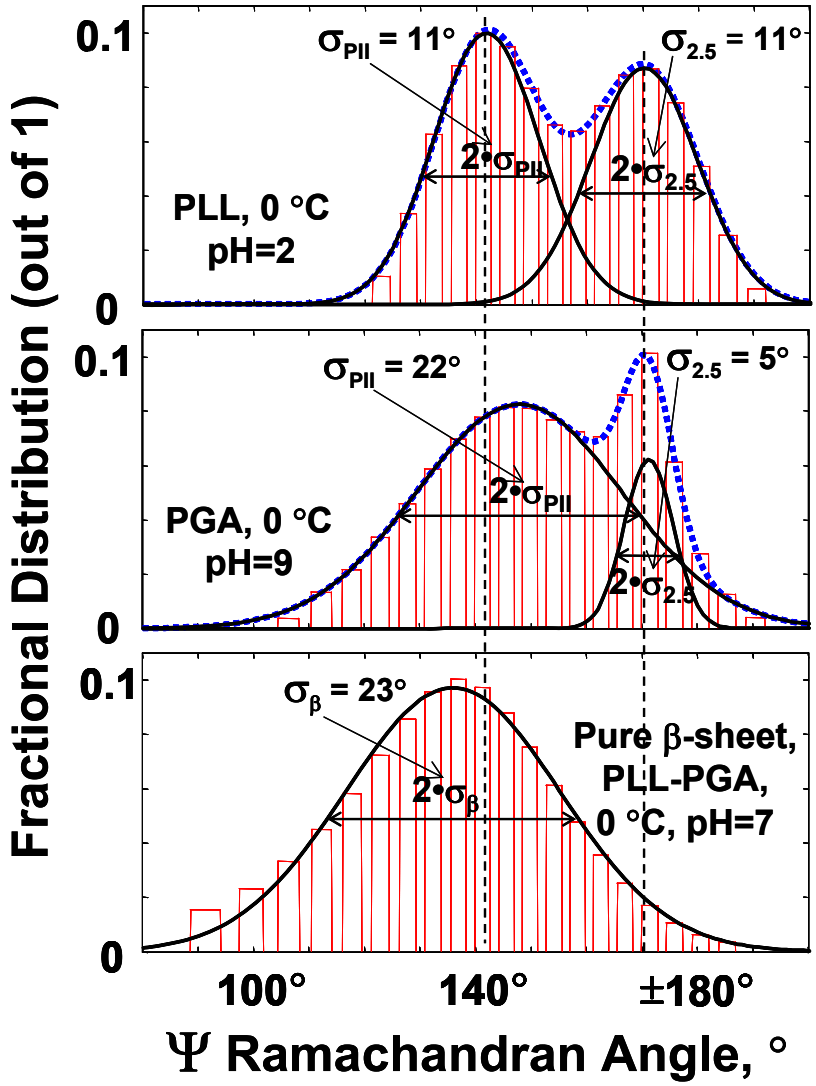

Figure 65. Estimated Ψ-Ramachandran angular distribution for pH=2 PLL and pH=9 PGA samples and for the pure β-sheet conformation of the PLL-PGA mixture. The pure β-sheet spectrum was calculated by numerically removing the unfolded state contribution as discussed in the text.

As shown in Fig. 65 these calculated distributions are well fit by Gaussian lineshapes. The estimated standard deviation for PLL at pH=2 is σ~11º for both the PPII and the 2.5_1-helix conformations, while PGA at pH=9 shows a broader distribution for PPII with σ~22º and a sharper distribution for the 2.5_1-helix with σ~5º (Table 14). Both of these distributions are consistent with an electrostatic repulsive interaction which destabilizes the PPII conformation relative to the 2.5_1-helix. The electrostatic interactions are larger for the shorter sidechain PGA relative to PLL, which should lead to a sharper distribution of angles for the 2.5_1 helix. In fact, the PGA PPII conformation minimum Ψ angle is shifted towards that of the 2.5_1 helix conformation.

The calculated β-sheet spectrum of the PLL-PGA mixture shows the broadest distribution of Ψ angles with σ~23º. This indicates that the β-sheet conformations shows the smallest energy penalty for changes in their Ψ angles. This is expected since a significant flexibility should exist for interpeptide bond hydrogen bond linkages; the angular dependence of hydrogen bond energies should be small around the equilibrium configuration.

Table 14. Ψ angle distribution of PPII-helix, 2.5_1-helix and β-sheet conformations of PLL and PGA. The table lists the standard deviation of the Ψ angle, σ, the ratio R of amplitudes of the 2.5_1-helix relative to that of the PPII conformation, the Gibbs free energy difference between the 2.5_1-helix and the PPII conformations, and the torsional constant K for Ψ angle deformations.

Conformation	σ, deg	R = 2.5_1-helix/ PPII-helix	ΔG=G(PPII)–G(2.5_1), cal/mole	K, cal/(deg)^2
PLL PPII-	11°	0.87	–74	2.7
PLL 2.5_1	11°			2.6
PGA PPII	22°	0.76	–152	1.0
PGA 2.5_1	5°			4.9
PLL-PGA β-sheet	23°	N/A	N/A	0.73

6.3.8 Determination of Gibbs Free Energy Curves for PPII↔2.5_1-Helix along the Ψ Angle Reaction Coordinate

We can estimate the Gibbs free energy landscape of the PPII and 2.5_1-helix conformations along the Ψ angle reaction coordinate from the calculated Ψ angle distributions. We assume that the distributions have identical degeneracies and that the probability of each conformation to occur at a particular Ψ angle is given by a simple Boltzmann distribution:

$$\frac{n(\Psi_i)}{n(\Psi_o)} = e^{-(G(\Psi_i) - G(\Psi_o)) / N_A k_B T} \quad \textbf{(13)}$$

where $n(\Psi_i)/n(\Psi_o)$ is the ratio of populations with Ramachandran angles Ψ_i and Ψ_o, $G(\Psi_i)$ is the Gibbs free energy of the conformation with angle Ψ_i, N_A is Avogadro's number, k_B is the Boltzmann constant, T is temperature.

Thus, Gibbs free energy difference between the PPII and 2.5_1-helix conformations can be estimated as:

$$\mathbf{\Delta G = G_{PPII} - G_{2.51} = -N_A\, k_B\, T\, \ln(n_{PPII}/n_{2.51}) = -N_A\, k_B\, T\, \ln R} \quad \textbf{(14)}$$

where R is the amplitude ratio at the energy minimum of the two conformations in Fig. 65.

Using the Eqn. 14, we obtain ΔG of -152 and -74 cal/mol for PGA and PLL, respectively, for Ψ angles at the minimum of these energy distributions (see Table 14). The fact that these Ψ angle distributions are well modeled by Gaussians (Fig. 65) results from the fact that the potential energy of a conformation about its equilibrium is given by $E = E_o + K\,\Delta\Psi^2$, where E_o is the energy at the minimum Ψ of a conformation and K is the torsional force constant. Table 14 shows that the torsional constant is the smallest for the β-sheet conformation while it is the largest for the PGA 2.5_1 conformation. The 2.5_1-helix → PPII crossing barriers for PLL and PGA have similar values of ~170 and ~200 cal/mol, respectively. In contrast, PPII → 2.5_1-helix crossing barriers for PLL and PGA have values of ~250 and ~100 cal/mol, respectively. These observations are expected, since the stronger electrostatic repulsion between charges located on shorter side chains of PGA (with respect to that of PLL) should stabilize the 2.5_1-helix and destabilize the PPII conformations.

We can use this information to calculate the Gibbs free energy landscape of these peptides along the Ramachandran Ψ angle coordinate (Fig. 66). We find similar energy landscapes for PGA and PLL when their side chains are ionized. The side chain electrostatic repulsions lower the 2.5_1-helix conformation energy relative to that of the PPII conformation. This effect is more significant for the shorter side chain PGA peptides, where the electrostatic repulsions exert a larger energetic penalty for deviations from the minimum energy Ψ angle conformation geometry of the 2.5_1 helix. The barriers between these two conformations are slightly less than $N_A k_B T$ (~540 cal/mol at 0 °C). Thus, it is likely in solution that these conformations rapidly interconvert. The major changes in geometry would involve mainly the Ψ and Φ coordinates. These changes would merely change the number of residues per turn.

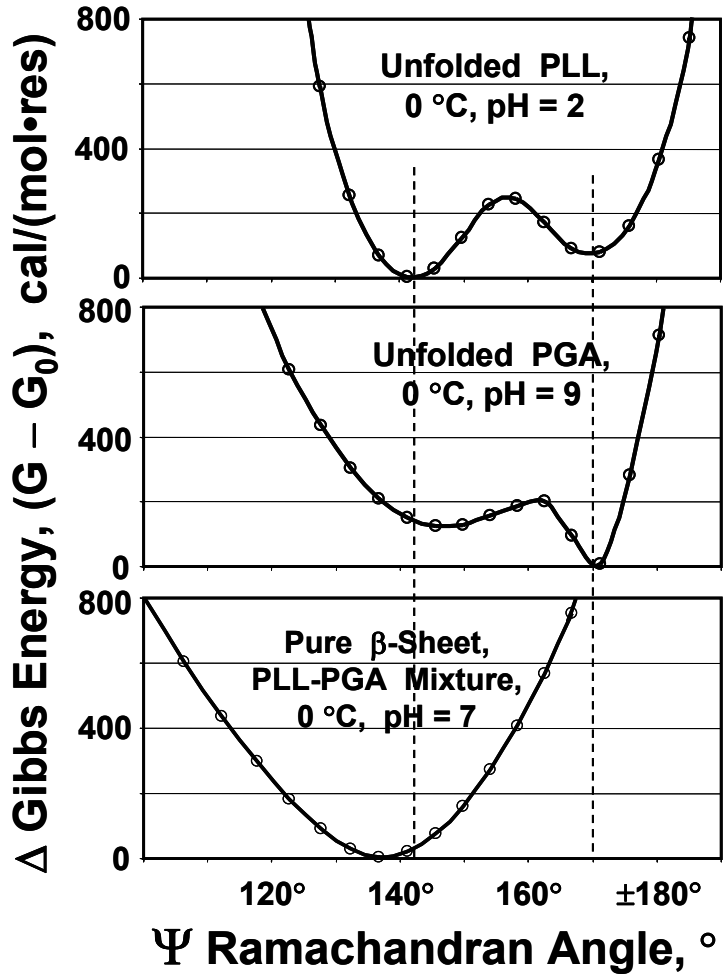

Figure 66. Estimated Gibbs free energy landscapes $G-G_0$ for pH=2 PLL, pH=9 PGA, and PLL-PGA pure β-sheet along the Ψ angle coordinate. We define $G_0=G(\Psi_0)=0$ (see text for detail).

The α-helix conformation is the most stable PGA and PLL conformation at 0 ºC if the side chains are neutralized by changing pH.[60,99] In this case the α-helix conformations melt mainly to the PPII conformations upon temperature increases to room temperature.

The molecular mechanism of this conformational change is difficult to envision since not only do the interpeptide hydrogen bonds have to rupture, but the helix must unwind and then rewind to reverse its handedness. Previous considerations of α-helix melting imagined that it was induced by a the step-wise α-helix hydration which stabilized intermediates such as β-turns and reverse turns.[100-102] However, the set of steps that would lead to a reverse helix are harder to visualize.

6.4 CONCLUSIONS

Our study of unfolded states of PLL and PGA indicates that they exist as a mixture of PPII and the extended 2.5_1-helix (β-strand-like) conformations. The charged side chains of pH=2 PLL and pH=9 PGA force the PLL and PGA chains in water to adopt a more extended conformations that minimize interchain repulsions. The β-sheet structure of the PLL-PGA mixture showed little evidence for hydrogen bonding between the polypeptide backbone and water. We also utilized a new algorithm which allows us to estimate the Ψ Ramachandran angle from the $AmIII_3$ frequency. This analysis demonstrates that each conformation has a distribution of Ψ-angles about the minimum Ψ conformational energy. The sharper Ψ angle distribution of the PGA 2.5_1-helix than that of PLL 2.5_1-helix, as well as, the absence of the 2.5_1-helix conformation in alanine-based peptides are consistent with the hypothesized electrostatic mechanism of stabilization of the 2.5_1-helix. We were able to calculate the Ψ-angle energy landscape features of these observed conformations. This is an important advance since the Ψ-angle coordinate is the most important coordinate for protein and peptide secondary structure changes.

6.5 REFERENCES

(1) Creighton, T. E. *Protein Folding;* W. H. Freeman: Ney York, **1992**.

(2) Baldwin, R. L. *Nature* **1990**, *346*, 409-410.

(3) Kim, P. S.; Baldwin, R. L. *Annu. Rev. Biochem.* **1990**, *59*, 631-660.

(4) Matthews, C. R. *Annu. Rev. Biochem.* **1993**, *62*, 653-683.

(5) Fernandez-Carneado, J.; Grell, D.; Durieux, P.; Hauert, J.; Kovacsovics, T.; Tuchscherer, G. *Bioploymers (Peptide Sci.)* **2000**, 55, 451-458.

(6) Bryngelson, J. D.; Onuchic, J. N.; Socci, N. D.; Wolynes, P. G. *Proteins* **1995**, *21*, 167-195.

(7) Thirumalai, D.; Woodson, S. A. *Acc. Chem. Res.* **1996**, *29*, 433-439.

(8) Pennisi, E. *Science* **1996**, *273*, 426-428.

(9) Chan, H. S.; Dill, K. A. *Proteins* **1998**, *30*, 2-33.

(10) Dill, K. A. *Biochemistry* **1990**, *29*, 7133-7155.

(11) Pokarowski, P.; Kolinski, A.; Skolnick, J. *Biophys. J.* **2003**, *84*, 1518-1526.

(12) Jewett, A. I.; Pande, V. S.; Plaxco, K. W. *J. Mol. Biol.* **2003**, *326*, 247-253.

(13) Hardin, C.; Eastwood, M. P.; Prentiss, M.; Luthey-Schulten, Z.; Wolynes, P. G. *J. Comp. Chem.* **2002**, *23*, 138-146.

(14) Alm, E.; Baker, D. *Proc. Natl. Acad. Sci. U.S.A.* **1999**, *96*, 11305-11310.

(15) Socci, N. D.; Onucic, J. N.; Wolynes, P. G. *Proteins* **1998**, *32*, 136-158.

(16) Anfinsen, C. B. *Science* **1973**, *181*, 223-230.

(17) Mayor, U.; Guydosh, N. R.; Johnson, C. M.; Grossmann, J. G.; Sato, S.; Jas, G. S.; Freund, S. M. V.; Alonso, D. O. V.; Daggett, V.; Fersht, A. R. *Nature* **2003**, *421*, 863-867.

(18) Myers, J. K.; Oas, T. G. *Annu. Rev. Biochem.* **2002**, *71*, 783-815.

(19) Mirny, L.; Shakhnovich, E. *Annu. Rev. Biophys. Biomol. Struct.* **2001**, *30*, 361-396.

(20) Englander, S. W. *Annu. Rev. Biophys. Biomol. Struct.* **2000**, *29*, 213-238.

(21) Flory, P. J. *Statistical Mechanics of Chain Molecules* **1969**.

(22) Tiffany, M. L.; Krimm, S. *Biopolymers* **1968**, *6*, 1379-1382.

(23) Pappu, R. V.; Srinivasan, R.; Rose, G. D. *Proc. Natl. Acad. Sci. U.S.A.* **2000**, *97*, 12565-12570.

(24) Srinivasan, R.; Rose, G. D. *Proc. Natl. Acad. Sci. U.S.A.* **1999**, *96*, 14258-14263.

(25) Marqusee, S.; Robbins, V. H.; Baldwin, R. L. *Proc. Natl. Acad. Sci. U.S.A.* **1989**, *86*, 5286-5290.

(26) Pal, D.; Suhnel, J.; Weiss, M. S. *Angew. Chem., Intl. Edition* **2002**, *41*, 4663-4665.

(27) Watson, J. D.; Milner-White, E. J. *J. Mol. Biol.* **2002**, *315*, 183-191.

(28) Watson, J. D.; Milner-White, E. J. *J. Mol. Biol.* **2002**, *315*, 171-182.

(29) Sreerama, N.; Woody, R. W. *Proteins* **1999**, *36*, 400-406.

(30) Park, C.; Carlson, M. J.; Goddard, W. A. I. *J. Phys. Chem. A* **2000**, *104*, 2498-2503.

(31) Wu, X.; Wang, S. *J. Phys. Chem. B* **2001**, *105*, 2227-2235.

(32) Wieczorek, R.; Dannenberg, J. J. *J. Am. Chem. Soc.* **2003**, *125*, 8124-8129.

(33) Avbelj, F.; Fele, L. *J. Mol. Biol.* **1998**, *279*, 665-684.

(34) Asher, S. A.; Mikhonin, A. V.; Bykov, S. B. *J. Am. Chem. Soc.* **2004**, *126*, 8433-8440.

(35) Shi, Z.; Olson, C. A.; Rose, G. D.; Baldwin, R. L.; Kallenbach, N. R. *Proc. Natl. Acad. Sci. U.S.A.* **2002**, *99*, 9190-9195.

(36) Mikhonin, A. V.; Ahmed, Z.; Ianoul, A.; Asher., S. A. *J. Phys. Chem. B* **2004**, *108*, 19020-19028.

(37) Mikhonin, A. V.; Asher, S. A. *J. Phys. Chem. B* **2005**, *109*, 3047-3052.

(38) Woutersen, S.; Hamm, P. *J. Chem. Phys.* **2001**, *114*, 2727-2737.

(39) Eker, F.; Cao, X.; Nafie, L.; Schweitzer-Stenner, R. *J. Am. Chem. Soc.* **2002**, *124*, 14330-14341.

(40) Fang, C.; Wang, J.; Charnley, A. K.; Barber-Armstrong, W.; Smith, A. B.; Decatur, S. M.; Hochstrasser, R. M. *Chem. Phys. Lett.* **2003**, *382*, 586-592.

(41) Fang, C.; Wang, J.; Kim, Y. S.; Charnley, A. K.; Barber-Armstrong, W.; Smith, A. B., III; Decatur, S. M.; Hochstrasser, R. M. *J. Phys. Chem. B* **2004**, *108*, 10415-10427.

(42) Eker, F.; Griebenow, K.; Cao, X.; Nafie, L. A.; Schweitzer-Stenner, R. *Biochemistry* **2004**, *43*, 613-621.

(43) Demirdoeven, N.; Cheatum, C. M.; Chung, H. S.; Khalil, M.; Knoester, J.; Tokmakoff, A. *J. Am. Chem. Soc.* **2004**, *126*, 7981-7990.

(44) Hamm, P.; Lim, M.; DeGrado, W. F.; Hochstrasser, R. M. *Proc. Natl. Acad. Sci. U.S.A.* **1999**, *96*, 2036-2041.

(45) Kocak, A.; Luque, R.; Diem, M. *Biopolymers* **1998**, *46*, 455-463.

(46) Woutersen, S.; Hamm, P. J. *Physics.: Condensed Matter* **2002**, *14*, R1035-R1062.

(47) Woutersen, S.; Hamm, P. *J. Chem. Phys.* **2001**, *115*, 7737-7743.

(48) Eker, F.; Griebenow, K.; Cao, X.; Nafie, L. A.; Schweitzer-Stenner, R. *Proc. Natl. Acad. Sci. U.S.A.* **2004**, *101*, 10054-10059.

(49) Pimenov, K. V.; Bykov, S. V.; Mikhonin, A. V.; Asher, S. A. *J. Am. Chem. Soc.* **2005**, *127*, 2840-2841.

(50) Asher, S. A. *Handbook of Vibrational Spectroscopy, John Whiley & Sons, Ltd.* **2001**, *1*, 557-571.

(51) Lednev, I. K.; Karnoup, A. S.; Sparrow, M. C.; Asher, S. A. *J. Am. Chem. Soc.* **1999**, *121*, 8074-8086.

(52) Chi, Z.; Chen, X. G.; Holtz, J. S. W.; Asher, S. A. *Biochemistry* **1998**, *37*, 2854-2864.

(53) Wen, Z. Q.; Thomas, G. J., Jr. *Biochemistry* **2000**, *39*, 146-152.

(54) Wang, D.; Zhao, X.; Shen, T.-J.; Ho, C.; Spiro, T. G. *J. Am. Chem. Soc.* **1999**, *121*, 11197-11203.

(55) Kim, J. E.; Pan, D.; Mathies, R. A. *Biochemistry* **2003**, *42*, 5169-5175.

(56) Serban, D.; Arcineigas, S. F.; Vorgias, C. E.; Thomas, G. J., Jr. *Prot. Sci.* **2003**, *12*, 861-870.

(57) Haruta, N.; Kitagawa, T. *Biochemistry* **2002**, *41*, 6595-6604.

(58) Thomas, G. J., Jr. *Annu. Rev. Biophys. Biomol. Struct.* **1999**, *28*, 1-27.

(59) Ismail, A. A.; Mantsch, H. H. *Biopolymers* **1992**, *32*, 1181-1186.

(60) Asher, S. A.; Ianoul, A.; Mix, G.; Boyden, M. N.; Karnoup, A.; Diem, M.; Schweitzer-Stenner, R. *J. Am. Chem. Soc.* **2001**, *123*, 11775-11781.

(61) Mikhonin, A. V.; Bykov, S. V.; Myshakina, N. S.; Asher, S. A. *J. Phys. Chem. B*. **2005**, *In Press*.

(62) Lednev, I. K.; Carlsen, A.; Ermolenkov, V. V.; He, W.; Higashiya, S.; Topilina, N.; Wells, C. C.; Welch, J. T.; Xu, M. *Book of Abstracts. 31st Annual Meeting of FACSS, Portland, OR, October 3-7;* **2004**, p. 142.

(63) Lednev, I. K.; Karnoup, A. S.; Sparrow, M. C.; Asher, S. A. *J. Am. Chem. Soc.* **2001**, *123*, 2388-2392.

(64) Bykov, S. B.; Lednev, I. K.; Ianoul, A.; Asher, S. A. *Appl. Spectrosc.,* **2005,** *In Press*

(65) Mix, G.; Schweitzer-Stenner, R.; Asher, S. A. *J. Am. Chem. Soc.* **2000**, *122*, 9028-9029.

(66) Torii, H.; Tatsumi, T.; Tasumi, M. *J. Raman Spectrosc.* **1998**, *29*, 537-546.

(67) Ianoul, A.; Boyden, M. N.; Asher, S. A. *J. Am. Chem. Soc.* **2001**, *123*, 7433-7434.

(68) Mirkin, N. G.; Krimm, S. *J. Phys. Chem. A* **2002**, *106*, 3391-3394.

(69) Abbruzzetti, S.; Viappiani, C.; Small, J. R.; Libertini, L. J.; Small, E. W. *J. Am. Chem. Soc.* **2001**, *123*, 6649-6653.

(70) Rucker, A. L.; Creamer, T. P. *Prot. Sci.* **2002**, *11*, 980-985.

(71) Smyth, E.; Syme, C. D.; Blanch, E. W.; Hecht, L.; Vasak, M.; Barron, L. D. *Biopolymers* **2001**, *58*, 138-151.

(72) Woody, R. W. *Adv. Biophys. Chem.* **1992**, *2*, 37-79.

(73) Keiderling, T. A.; Silva, R. A.; Yoder, G.; Dukor, R. K. *Bioorg. & Med. Chem.* **1999**, *7*, 133-141.

(74) Drake, A. F.; Siligardi, G.; Gibbons, W. A. *Biophys. Chem.* **1988**, *31*, 143-146.

(75) Wilson, G.; Hecht, L.; Barron, L. D. *J. Chem. Soc., Faraday Trans.*, **1996**, *92*, 1503-1509.

(76) Yasui, S. C.; Keiderling, T. A. *J. Am. Chem. Soc.* **1986**, *108*, 5576-5581.

(77) Birke, S. S.; Agbaje, I.; Diem, M. *Biochemistry* **1992**, *31*, 450-455.

(78) Paterlini, M. G.; Freedman, T. B.; Nafie, L. A. *Biopolymers* **1986**, *25*, 1751-1765.

(79) Dukor, R. K.; Keiderling, T. A. *Biopolymers* **1991**, *31*, 1747-1761.

(80) Dukor, R. K.; Keiderling, T. A. *Pept., Proc. Eur. Pept. Symp., 20th* **1989**, 519-521.

(81) Dukor, R. K.; Keiderling, T. A.; Gut, V. *Intl. J. Peptide & Protein Research* **1991**, *38*, 198-203.

(82) Bochicchio, B.; Tamburro, A. M. *Chirality* **2002**, *14*, 782-792.

(83) Mezei, M.; Fleming, P. J.; Srinivasan, R.; Rose, G. D. *Proteins* **2004**, *55*, 502-507.

(84) Hinderaker, M. P.; Raines, R. T. *Prot. Sci.* **2003**, *12*, 1188-1194.

(85) Shi, Z.; Woody, R. W.; Kallenbach, N. R. *Adv. Prot. Chem.* **2002**, *62*, 163-240.

(86) Adzhubei, A. A.; Sternberg, M. J. E. *J. Mol. Biol.* **1993**, *229*, 472-493.

(87) Syme, C. D.; Blanch, E. W.; Holt, C.; Jakes, R.; Goedert, M.; Hecht, L.; Barron, L. D. *Eur. J. Biochem.* **2002**, *269*, 148-156.

(88) Sreerama, N.; Woody, R. W. *Biochemistry* **1994**, *33*, 10022-10025.

(89) Cao, W.; Bracken, C.; Kallenbach, N. R.; Lu, M. *Prot. Sci.* **2004**, *13*, 177-189.

(90) Gnanakaran, S.; Hochstrasser, R. M. *J. Am. Chem. Soc.* **2001**, *123*, 12886-12898.

(91) Woutersen, S.; Hamm, P. *J. Phys. Chem. B* **2000**, *104*, 11316-11320.

(92) Schweitzer-Stenner, R.; Eker, F.; Huang, Q.; Griebenow, K.; Mroz, P. A.; Kozlowski, P. M. *J. Phys. Chem. B* **2002**, *106*, 4294-4304.

(93) McColl, I. H.; Blanch, E. W.; Hecht, L.; Kallenbach, N. R.; Barron, L. D. *J. Am. Chem. Soc.* **2004**, *126*, 5076-5077.

(94) Barron, L. D.; Blanch, E. W.; Hecht, L. *Adv. Prot. Chem.* **2002**, *62*, 51-90, 51 plate.

(95) Blanch, E. W.; McColl, I. H.; Hecht, L.; Nielsen, K.; Barron, L. D. *Vibrational Spectrosc.* **2004**, *35*, 87-92.

(96) McColl, I. H.; Blanch, E. W.; Gill, A. C.; Rhie, A. G. O.; Ritchie, M. A.; Hecht, L.; Nielsen, K.; Barron, L. D. *J. Am. Chem. Soc.* **2003**, *125*, 10019-10026.

(97) Krimm, S.; Mark, J. E. *Proc. Natl. Acad. Sci. U.S.A.* **1968**, *60*, 1122-1129.

(98) Note, that Krimm and Mark in their paper (Ref 97) used old Psi- and Fi- angle convention, since the modern one was not yet in effect. Thus, their Psi= 10° and Fi=+25° correspond to -170° and -155° of the modern convention, respectively.

(99) Song, S.; Asher, S. A. *J. Am. Chem. Soc.* **1989**, *111*, 4295-4305.

(100) Sundaralingam, M.; Sekharudu, Y. C. *Science* **1989**, *244*, 1333-1337.

(101) Blanch, E. W.; Morozova-Roche, L. A.; Cochran, D. A. E.; Doig, A. J.; Hecht, L.; Barron, L. D. *J. Mol. Biol.* **2000**, *301*, 553-563.

(102) McColl, I. H.; Blanch, E. W.; Hecht, L.; Barron, L. D. *J. Am. Chem. Soc.* **2004**, *126*, 8181-8188.

7.0 CHAPTER 7. UV RESONANCE RAMAN STUDY OF THE SPATIAL DEPENDENCE OF α-HELIX UNFOLDING

Work described in this chapter is published in *J. Phys. Chem. A,* **2002**, *106*, 3621-3624 (Authors: Ianoul, A.; Mikhonin, A. V.; Lednev, I. K.; and Asher, S. A.). We used ultraviolet resonance Raman (UVRR) spectra to examine the spatial dependence and the thermodynamics of α-helix melting of an isotopically labeled α-helical, 21-residue, mainly alanine peptide. The peptide was synthesized with six natural abundance amino acids at the center and mainly perdeuterated residues elsewhere. C_α deuteration of a peptide bond decouples C_α-H bending from N-H bending, which significantly shifts the PPII conformation amide III band; this shift clearly resolves it from the amide III band of the nondeuterated peptide bonds. Analysis of the isotopically spectrally resolved amide III bands from the external and central peptide amide bonds show that the six central amide bonds have a higher α-helix melting temperature (~ 32 °C) than that of the exterior amide bonds (~5 °C).

7.1 INTRODUCTION

An elucidation of the mechanism of protein folding requires the understanding of the structural and dynamical aspects of α-helix unfolding.[1-4] Previous theoretical examinations of α-helix unfolding predicted that at equilibrium all but the longest α-helices would contain only a single helix sequence and that this helix would unfold from its ends.[5] Recent transient fluorescence probe,[6,7] IR absorption[4] and UV resonance Raman (UVRR) studies[1,8] have found that the unfolding dynamics occurs on a 200 ns time scale and that the kinetics have the appearance of a two state unfolding mechanism. However, detailed kinetic temperature dependent measurements

indicate that the unfolding does not show a simple two state Arrhenius behavior.[1] This clearly signals that the true mechanism follows an intrinsically complicated energy landscape.

Our recent kinetic UVRR investigations[1,8] have allowed us to examine the dynamics of peptide unfolding by examining the evolution of the UVRR spectra caused by a ns T-jump. The Raman spectra are highly resolved and can be used to quantitatively determine the secondary structure composition. The obvious next step in the study of the helix unfolding process is to understand the spatial dependence of unfolding.

We show here that it is possible to determine the spatial dependence of peptide unfolding through isotopic labeling. Isotopic labeling shifts the vibrational bands such that the conformational evolution of an isotopically labeled region can be resolved from the conformational evolution of an unlabeled region. We, thus, measure the temperature induced melting of different parts of the α-helix, and find different melting temperatures for the exterior versus the central peptide amide bonds.

7.2 EXPERIMENTAL

7.2.1 Materials.

The alanine based polypeptide (AP) of composition $A_5(A_3RA)_3A$ and the deuterium labeled peptide **AAAAAAAA**-RAAAAR-**AAAA**-R-**AA** (AdP), where **A** is L-Ala(2,3,3,3-D_4) were synthesized (>95% purity) at the Pittsburgh Cancer Institute by the solid-phase peptide synthesis method.

7.2.2 Instrumentation

The UV-Raman instrumentation is described in detail elsewhere.[1,8] UVRR spectra were measured using 204 nm excitation obtained by antiStokes Raman shifting the third harmonic of an Infinity YAG laser (Coherent Inc.) in H_2. The Raman scattered light was collected in a ~135° back-scattering geometry and dispersed by a Spex double monochromator. An intensified CCD

detector (Princeton Instrument Co.) was used for detection. The samples were measured in a temperature controlled free-surface flow stream.

All spectra were normalized to the ClO_4^- internal standard band at 932 cm^{-1}. The broad 1640 cm^{-1} H_2O Raman bending band was subtracted using a measured solvent reference spectrum.

The CD spectra were measured by using a Jasco 710 spectropolarimeter.

7.3 RESULTS AND DISCUSSION

In order to spectrally spatially resolve the central from the exterior peptide bonds we compared the UVRR spectra of natural abundance AP to the deuterium labeled peptide **AAAAAAAA**-RAAAAR-**AAAA**-R-**AA** (AdP), where **A** is L-Ala(2,3,3,3-D_4). Both peptide termini are fully deuterated, except for the residue nineteen arg group, while the central two arg and the four ala are natural abundance.

7.3.1 UVRR spectra of AP and AdP.

Figure 67 shows 204 nm excited UVRR spectra of AdP and the natural abundance alanine peptide (AP) at low (-0.2 °C) and high (+70 °C) temperatures as well as their temperature difference spectra. Originally, Lednev et al.[1] incorrectly assumed that unfolded AP at 70 °C is essentially random coil and shows bands at ~1660 cm^{-1}, ~1550 cm^{-1}, ~1380 cm^{-1} and ~1249 cm^{-1} which are assigned to the amide I, amide II, C_α-H bending and amide III vibrations, respectively.[1] However, later we showed that unfolded AP is essentially in a PPII conformation (see Chapter 2 for detail). We measure an amide III Raman cross section of ~60 mBarn/(peptide bond·sr).

As shown previously, the temperature-induced spectral differences result from the α-helix→PPII transition combined with a modest monotonic temperature dependence for the PPII Raman bands.[1] The AP difference spectrum (Fig. 67c) shows a peak at 1234 cm^{-1} due to the loss of the PPII amide III intensity. The broad peak at ~1377 cm^{-1} derives from the loss of the PPII

C_α-H bending band. Other difference features also occur, such as the derivative shaped amide I feature, due to the fact that the PPII amide I band occurs at higher frequency than does the α-helix form.

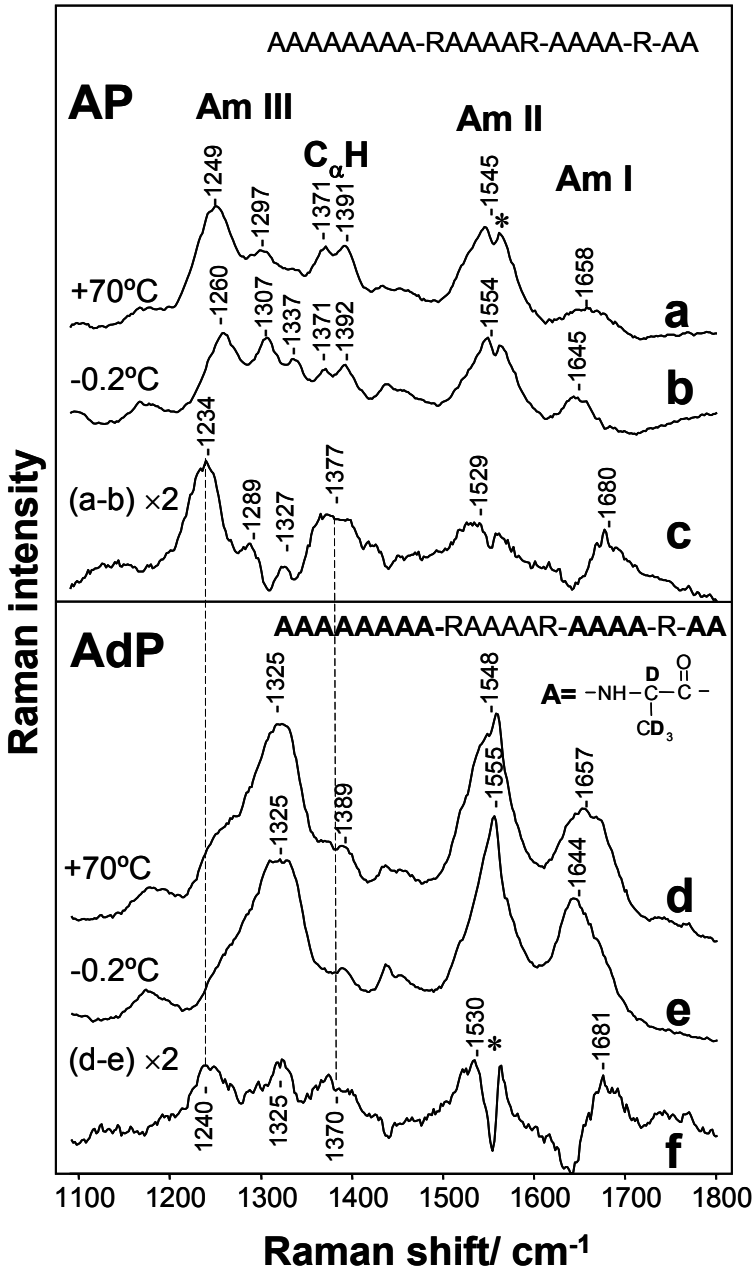

Figure 67. 204 nm excited UV RR spectra of the 21 unit peptide AP (AAAAAAAA-RAAAAR-AAAA-R-AA) (a, b, c) and the deuterated peptide AdP (**AAAAAAAA**-RAAAAR-**AAAA**-R-**AA**, where **A** is L-Ala(2,3,3,3-D_4)). alanine peptide AP (d, e, f) at –0.2°C (b, e), +70°C (a, d) and their difference spectra (c, f). The experimental setup is described in ref.[1] The 932 cm^{-1} band of 0.15 M sodium perchlorate was used as an internal standard, and the

peptide concentrations were 0.5 mg/ml. We utilize a spectral accumulation time of 20 min, with a spectral resolution of ~10 cm^{-1}. The star marks a peak assigned to molecular oxygen. Spectra (c) and (f) were multiplied by 2.

The UVRR spectra of AdP differ from those of AP mainly in an upshift of the C_α deuterated amide III band to ~1325 cm^{-1}.[9-13] The deuterated amide III band displays a dramatically increased Raman cross section of ~217 mBarn/(peptide bond·sr). In addition, the C_α-H bending band intensity decreases due to deuteration of some of the C_α carbon amide bonds.

Thus, the ~1325 cm^{-1} band intensity derives mainly from the amide III band from the deuterated amide bonds. The non-deuterated part of AdP shows a spectrum similar to that of AP (Fig. 67); the shoulders observed at ~1240 and 1380 cm^{-1} in the spectrum of AdP derives from the amide III bands of the non-deuterated amide bonds. The remainder of the AdP spectrum is very similar to that of AP.

The AdP difference spectrum shows peaks at 1240, 1325, and 1370 cm^{-1}, in addition to the derivative shaped amide I difference band (Fig. 67f). The 1240 and 1370 cm^{-1} peaks are similar to those in the AP difference spectrum (Fig. 67c). They derive from the amide III and C_α-H bending of the increased concentration of the PPII conformation in the non-deuterated, center of AdP. In contrast, the 1325 cm^{-1} band, absent in the difference spectrum of AP (Fig. 67c), derives mostly from the deuterated part of AdP and is dominated by the conversion of deuterated amide bonds from the α-helix to the PPII conformation.

The intensity of the 1325 cm^{-1} deuterated amide III difference spectral peak is determined mainly by the difference in the amide III Raman cross section between the α-helix and the PPII deuterated amide bonds, since there is little change in the amide III frequency between the α-helix and PPII conformations. The temperature dependence of the frequencies appears to be negligible, as evident from the lack of a derivative feature in the difference spectrum.

The intensities of the 1240 and 1370 cm^{-1} difference spectral peaks are determined mainly by the increase in the number of PPII amide bonds, since only PPII amide bonds give rise to the peaks at 1235 and 1370 cm^{-1}. Thus, the magnitude of the deuterated and non-deuterated peptide bond temperature difference spectral peaks is proportional to the total number of amide bonds undergoing the conformational transition from α-helix to PPII.

7.3.2 Melting of AP and AdP.

Fig. 68A shows the calculated α-helical fractions of AP and AdP determined from their measured CD spectra, according to the method described in reference 1. Figs. 68B and 68C show the calculated α-helical fraction of AP, and the spatially resolved calculated α-helical fractions of the central six and exterior fourteen amide bonds of AdP determined by analyzing the UVRR spectra as described in the **Appendix B** below.

The Fig. 68A CD data show the expected identical α-helix melting curves for AdP and AP, which yield T_m=5° C for the average peptide bond melting temperatures. As previously[1] discussed in detail, we calculate a significantly higher average peptide bond T_m = 17 °C from the Fig. 68B UV Raman data because the Raman spectra more heavily weight shorter α-helical segments than do the CD spectra.[1,14] This modeling assumes that a total of six penultimate residues will not form an α-helix, since they cannot have both stabilizing α-helix hydrogen bonds. Thus, we expect that a maximum of eight of the thirteen deuterated external peptide bonds can be involved in an α-helix (62% maximum α-helix fraction).

The Fig. 68B peptide melting curves are scaled to the total number of amide bonds (twenty), while the Fig. 68C melting curves are scaled to show the relative α-helical fraction of the central six residues, and the relative α-helical fraction of the exterior eight dueterated residues that can potentially form an α-helix.

Fig. 68B and 68C show significantly different melting curves for the central and exterior AdP peptide bonds. The six central peptide bonds show a complete melting curve with an apparent T_m = 32 °C (Fig. 68C). The central six peptide bonds are essentially 100 % α-helical at 0 °C and have negligible α-helix content at 60 °C.

In contrast, the exterior peptide bonds are ~60 % α-helical at 0 °C and are negligibly α-helical by 40 °C. We calculate a T_m = 5° C. Thus, at the average AdP and AP peptide bond melting temperature of T_m= 17 °C, where the α-helix conformation involves half (seven) of all of the amide bonds capable of forming an α-helix (fourteen), ~80% of the six central amide bonds (~five) occur in an α-helix. In contrast, only ~20 % of the exterior peptide amide bonds (eight) are α-helical (~two) as shown in Fig. 68C. These results, which demonstrate a decreased T_m for

exterior amide bonds, are predicted by theory,[5] and are similar to the results of ^{13}C NMR studies of the α-helical peptide acetyl-W(EAAAR)$_3$A.[15]

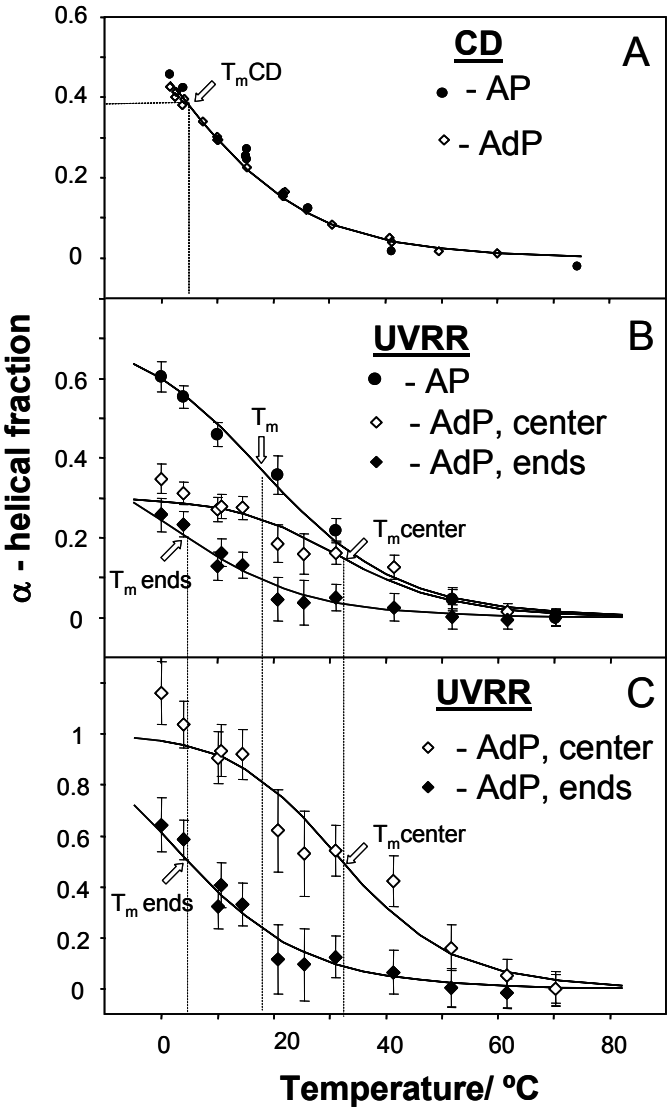

Figure 68. A) Temperature dependence of the AP and AdP α-helicity as calculated from CD measurements using the method described in reference 1. The CD data were fitted to expressions for the molar ellipticity analogous to equations 15 and 16 assuming the maximum α-helical fraction 0.78.[1] B) α-helical fraction temperature dependence calculated from the UVRR spectra of AP (●), non- deuterated central amide bonds (◊) and deuterated external amide bonds (♦) of AdP. The α-helix composition was ratiod to the total number of AdP peptide bonds (twenty). Solid lines are the best fits obtained using Eqs. 15 and 16 with the parameters listed in Table 15, assuming the maximum α-helical fractions 0.7 for AP, 0.3 for the central peptide bonds of AdP and 0.4 for the external peptide bonds of AdP.[1] C) α-helical fraction temperature dependence from Fig. 68B normalized to the number of peptide bonds of the central and of the external segments that can form an α-helix. Solid lines are the best fits obtained using Eqs. 15 and 16 with the parameters listed in the Table 15.

Table 15. Thermodynamic Parameters for AdP and AP Coil↔Helix Transition.

	T_m, °C	ΔH, kcal/mol $_{peptide}$	ΔS, kcal/(mol $_{peptide}$·K)
AP	17+/-5	-14.8+/-2	-51+/-6
AdP, ends	5+/-5	-14.4+/-4.1	-51.9+/-14
AdP, center	32+/-5	-18.7+/-5.5	-61.2+/-18

We calculated the thermodynamic parameters for the central, and exterior peptide bonds (Table 15) from the UVRR melting curves by assuming the simplest two- state model for both internal as well as penultimate amide bonds of AdP:

$$f_{\alpha}(T) = \frac{f_{max}}{1 + exp(-\frac{\Delta H}{RT} + \frac{\Delta S}{R})} \qquad (15)$$

$$fd_{\alpha}(T) = \frac{fd_{max}}{1 + \exp(-\frac{\Delta H_d}{RT} + \frac{\Delta S_d}{R})} \qquad (16)$$

Here $f_{\alpha}(T)$ and $fd_{\alpha}(T)$ are the temperature dependent fractional α-helix content of the central and exterior peptide bonds, while f_{max} is maximum α-helix fraction of the six central nondeuterated peptide bonds. fd_{max} is the α-helix fraction of eight exterior peptide bonds which can occur in an α-helix. f_{max} = 6/20=0.3 and fd_{max} = 8/20 = 0.4.

Although we see clear differences in T_m, the differences in ΔH and ΔS for the central residues compared to the external residues, are within the error bars of the modeling, due to the limited spectral signal to noise ratios. We will revisit this issue in the future when we obtain higher signal to noise ratio data from higher concentration peptide samples; we presently have only small amounts of the AdP peptide.

7.4 CONCLUSIONS

The work here demonstrates that UVRR measurements of a selectively deuterium labeled α-helical peptide allows us to spatially resolve the conformation of individual peptide bonds. We observe significantly higher T_m values for peptide bonds in the center of the peptide compared to the external peptide bonds. We are beginning nsec UV resonance Raman T-jump studies of this peptide to spatially resolve the dynamics of α-helix unfolding (See Chapter 9 for detail).

7.5 REFERENCES

(1) Lednev, I.K.; Karnoup, A.S.; Sparrow, M.C.; Asher, S. A. *J. Am. Chem. Soc.* **1999**, *121*, 8074-8086.

(2) Karplus, M.; Weaver, D. L. *Prot. Sci.* **1994**, *3*, 650-668.

(3) Kim, P. S.; Baldwin, R. L. *Annu. Rev. Biochem.* **1990**, *59*, 631-660.

(4) Williams, K.; Causegrove, T.P.; Gilmanshin, R.; Fang, K.S.; Callender, R.H.; Woodruff, W.H.; Dyer, R.B. *Biochemistry* **1996**, *35*, 691-697.

(5) Poland, D.; Sheraga, H.A. *Theory of Helix-Coil Transition in Biopolymers; Academic press: New York and London,* **1970**.

(6) Thompson, P. A.; Eaton, W. A.; Hofrichter, J. *Biochemistry* **1997**, *36*, 9200- 9210.

(7) Thompson, P. A.; Munoz, V.; Jas, G.S.; Henry, E.R.; Eaton, W. A.; Hofrichter, J *J. Phys. Chem. B* **2000**, *104*, 378- 389.

(8) Lednev, I.K.; Karnoup, A.S.; Sparrow, M.C.; Asher, S. A. *J. Am. Chem. Soc.* **2001**, *123*, 2388-2393.

(9) Asher, S.A.; Ianoul, A.; Mix, G.; Boyden, M.; Karnoup, A.; Diem, M.; Schweitzer-Stenner, R. *J. Am. Chem. Soc.* **2001**, *123*, 11775-11781.

(10) Overman, S.A.; Thomas, G.J.Jr. *Biochemistry* **1998**, *37*, 5654-5665.

(11) Oboodi, M.R.; Alva, C.; Diem, M. *J.Phys.Chem.* **1984**, *88*, 501-505.

(12) The PPII (originally incorrectly called "random coil") amide band Raman band frequencies and intensities show a significant temperature dependence,[1] presumably due

to population of higher energy landscape Ψ and Φ Ramachandran angles. Much of the dependence of the PPII amide III band on the Ψ angle results from a Ψ dependent coupling with amide C_α-H bending motion.[9] This coupling cannot occur for the C_α-deuterated derivative. Thus, the amide III band shows a negligible Ψ angle conformational dependence and a much smaller temperature dependence.

(13) Chen, X.G.; Asher, S.A.; Schweitzer-Stenner, R.; Mirkin, N.G.; Krimm, S. *J. Am. Chem. Soc.* **1995**, *117*, 2884-2895.

(14) Ozdemir, A.; Lednev, I. K.; Asher, S. A. *Biochemistry* **2002**; *41,* 1893-1896

(15) Shalongo, W.; Dugad, L.; Stellwagen, E. *J. Am. Chem. Soc.* **1994**, *116*, 2500-2507.

8.0 CHAPTER 8. DIRECT UV RAMAN MONITORING OF 3_{10}- AND π-HELIX PREMELTING DURING α-HELIX UNFOLDING

Work, described in this chapter, is published in *J. Am. Chem. Soc.*, **2006**, *128(42)*, 13789-13795 (Authors: Mikhonin, A. V.; and Asher, S. A.). We used UV resonance Raman (UVRR) spectroscopy exciting at ~200 nm within the peptide bond π→π* transitions to selectively study the amide vibrations of peptide bonds during α-helix melting. The dependence of the amide frequencies on their Ψ Ramachandran angles and hydrogen bonding enables us, for the first time, to experimentally determine the temperature dependence of the peptide bond Ψ Ramachandran angle population distribution of a 21-residue mainly alanine peptide. These Ψ distributions allows us to easily discriminate between α-helix, 3_{10}-helix and π-helix/bulge conformations, obtain their individual melting curves, and estimate the corresponding Zimm and Bragg parameters. A striking finding is that α-helix melting is more cooperative and shows a higher melting temperature than previously erroneously observed. These Ψ distributions also enable the experimental determination of the Gibbs free energy landscape along the Ψ reaction coordinate, which further allows us to estimate the free energy barriers along the AP melting pathway. These results will serve as a benchmark for the numerous untested theoretical studies of protein and peptide folding.

8.1 INTRODUCTION

The formation and melting of α-helices is the most fundamental secondary structure dynamic of peptides and proteins in their conformational search between their folded and unfolded structures. This conformational search has been studied for well over 50 years. The basic theory, which modeled this transition was proposed by Zimm and Bragg[1] and Poland and Sheraga[2]

approximately forty five years ago, envisioned a transition between an ordered α-helix structure and a disordered random coil structure. Cooperativity in the transition was modeled through the assumption that the nucleation step for α-helix formation occurs at a higher free energy because of the entropic expense associated with restricting four amino acid residues to occur in α-helical conformation prior to compensation by the intrahelix hydrogen bonding.

This theory, which appeared to adequately model α-helix stability is parameterized in terms of three parameters, б, the small nucleation parameter, s the propagation parameter and N the length of the peptide. Experimental studies of typical synthetic peptides which form α-helices (such as peptides rich in ala) indicate that the α-helix melting and formation is only weakly cooperative, with melting temperatures of between 10 and 30 °C.[3-7] Recent kinetic α-helix melting studies, which have utilized pump-probe spectroscopic techniques such as temperature-jump fluorescence, IR and UV Raman investigations often demonstrate single exponential melting.[3-6,8] More complex multiexponential and/or nonexponential behavior is also sometimes observed,[7,9,10] as are different kinetics for T-jumps between different initial and final temperatures. IR studies of peptides isotopically labeled at specific positions, also indicate that the different parts of polypeptide chains have different melting rates.[11,12] The time scale for melting appears to be ~200 nsec, a long time compared to the sub-nsec expected propagation times required to add or remove individual α-helical residues at the α-helix ends.

Recent molecular dynamics (MD) simulations of α-helix conformational dynamics have demonstrated that α-helix melting and formation is likely to be complex,[13-19] since the other states such as turns, 3_{10}- and π-helices are involved as the α-helix conformation nucleates, grows and melts.[20-32] These MD studies suggest that these 3_{10} and π helical conformations, as well as different turn motifs, are intermediates in α-helix formation and melting, and can also be present as defects in long α-helices.

A number of recent experimental α-helix melting studies have begun to challenge the standard view of the α-helix conformational dynamics discussed above. A major challenge is the clear recent demonstrations that α-helices do not melt to random coil conformations.[33-37] Rather, the unfolded peptides and proteins exist in PPII conformations,[33-50] which consist of left handed helices with 3 residues per helical turn, where the peptide bonds hydrogen bond to water.[51-53]

In the work here, we utilize UV resonance Raman (UVRR) spectroscopy with excitation within the peptide bond $\pi \rightarrow \pi^*$ transitions[54] to selectively probe the vibrational spectra of the peptide bonds.[55-58] Our recent examination of the UVRR spectra of peptides and proteins has uncovered a quantitative correlation between the frequency of a particular vibrational band called the amide III_3 ($AmIII_3$) band and the peptide bond Ramachandran Ψ angle.[59] This quantitative correlation enables the revolutionary determination of motion along the major reaction coordinate for secondary structure evolution. Here, we utilize this correlation for the first time to quantitatively monitor the different secondary structures involved in α-helix melting and how they evolve with temperature. This enables us for the first time to monitor both the change in average α-helical length and the presence of non α-helical defects.

8.2 EXPERIMENTAL SECTION

8.2.1 Materials

The 21-residue alanine-based peptide $AAAAA(AAARA)_3A$ (AP) was prepared (HPLC pure) at the Pittsburgh Peptide Facility by using the solid-state peptide synthesis method. The AP solutions in water contained 3 mg/ml concentrations of AP, and 0.2 M concentrations of sodium perchlorate, which was used as internal intensity and frequency standards. All UVRR spectra were normalized to the intensity of the ClO_4^- Raman band (932 cm^{-1}).

8.2.2 UV resonance Raman Instrumentation

The UVRR apparatus is described in detail by Bykov et al.[60] and Lednev et al.[5] Briefly, the third harmonic of a Coherent Infinity Nd:YAG laser operating at 100 Hz with a 3 nsec pulse width was Raman shifted by five anti-Stokes harmonics in 40 psi hydrogen gas to 204 nm to excite the amide band UVRR spectra. The Raman scattered light was collected at an angle close to backscattering and was dispersed with a partially subtractive double monochromator. The Raman scattered light was detected by using a Princeton Instruments Spec-10:400B CCD camera

purchased from Roper Scientific. The spectral accumulation times were ~5 min with a spectral resolution of ~10 cm^{-1}.

8.3 RESULTS AND DISCUSSION

8.3.1 UVRR α-Helix-Like $AmIII_3$ Band Dramatically Narrows at Elevated Temperatures

Fig. 69 shows the temperature dependence of the 204 nm-excited UVRR spectra of a 21 amino acid residue mainly ala peptide, AP, containing three arg for solubility. This peptide is >55 % α-helical at 0°C and less than 10 % α-helical by 50°C.[5,6] At 50°C, the peptide is predominantly in the PPII conformation.[34]

The measured UVRR spectra at different temperatures are shown in Fig. 69A, while Fig. 69B shows spectra of the pure PPII conformation at different temperatures. The 49 and 65 °C Fig. 69A spectra are essentially pure PPII spectra, while the lower temperature spectra are a mixture of PPII and α-helix-like spectra.

We previously[5] calculated the underlying pure PPII spectra at different temperatures, as shown in Fig. 69B. Originally, we incorrectly denoted these spectra as "random coil"[5], but later showed that these are essentially pure PPII spectra, although minor contributions from various turns and β-strand conformations could also exist.[34] The major temperature induced spectral differences in the PPII spectra derive from small frequency shifts due to the decreased peptide bond-water hydrogen bond strength as the temperature increases.[34,38,61] The Figs 69C-F difference spectra at different temperatures, which were calculated by subtracting off the PPII spectral contributions, look α-helix-like,[5] but contain additional features.

The high temperature Fig. 69A spectra and the Fig. 69B PPII spectra show a strong $AmIII_3$ band at ~1245, a minor $AmIII_2$ band at ~1303, and a ~1370 and 1394 cm^{-1} doublet from the C_α-H b of the PPII conformation. The Fig. 69C-F spectra are α-helix-like. The α-helical spectrum shows an $AmIII_3$ band (which we denote $AmIII_{3H}$) at ~1261 cm^{-1}, a ~1306 cm^{-1} $AmIII_2$ band, and a ~1337 cm^{-1} $AmIII_1$ band. Small bands at ~1365 and 1387 cm^{-1} may originate either from the CH_3 umbrella mode of ala side chains,[61,62] or derive from C_α-H b of minor turn or β-

strand conformations (see below). The band at ~1165 cm^{-1} originates from the arg side chain,[63] and is useful as an additional internal standard band since its intensity should be independent of temperature.

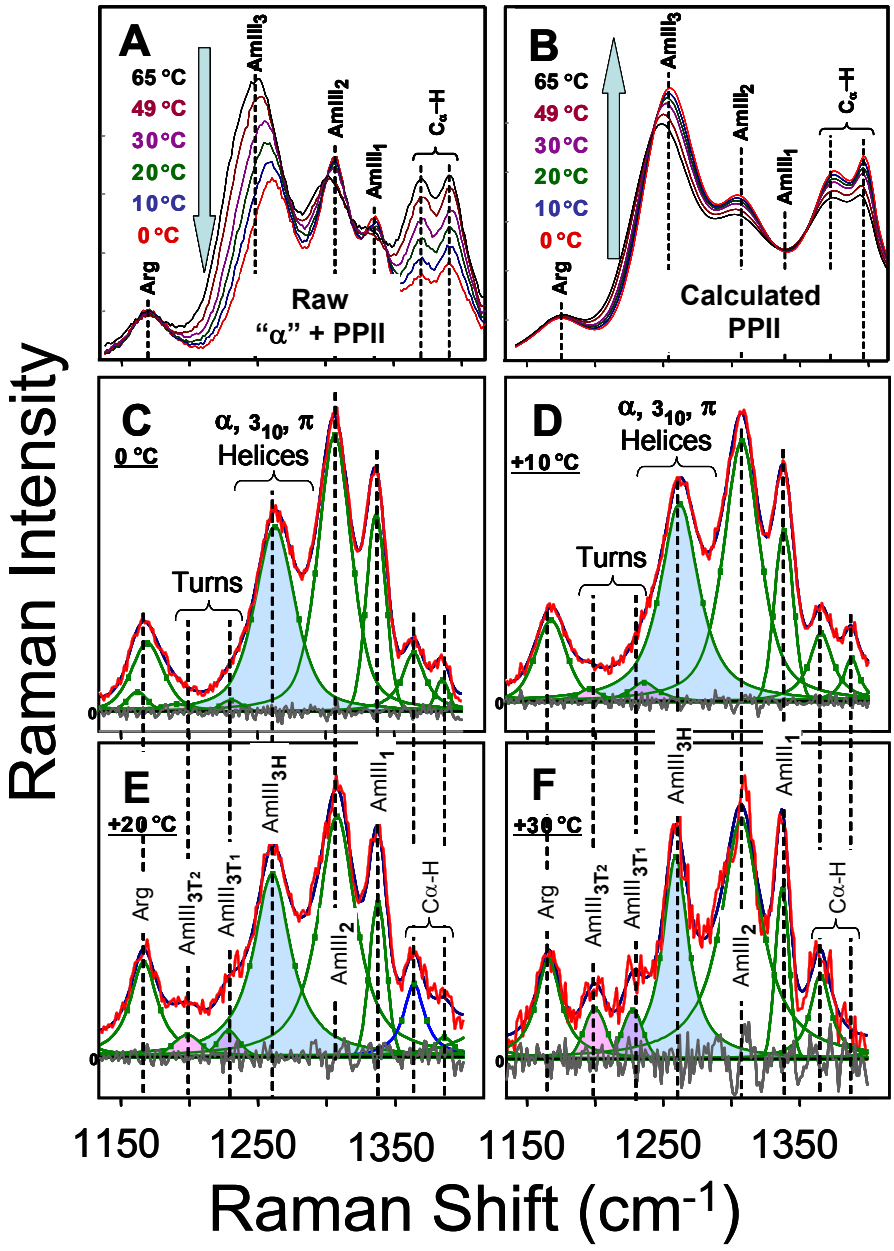

Figure 69. Temperature dependence of the Amide III region of the 204 nm excited UV resonance Raman (UVRR) spectra of AP. (A) Experimental spectra. (B) Calculated temperature dependent PPII spectra. Temperature dependence of the residual α-helical spectra at after removal of the PPII contributions: (C) 0 °C, (D) 10 °C, (E) 20 °C, and (F) 30 °C. The $AmIII_3$ bands of α-helix-like conformations are shown in blue.

As shown in detail below, the ~1228 and ~1200 cm^{-1} bands (30 °C), which increase in relative intensity with temperature in Fig. 69C-F, derive from turn (or β-strand) conformations.[59] Thus, we designate them as $AmIII_{3T1}$ and $AmIII_{3T2}$ bands.

The most striking spectral change with increasing temperature is an about two-fold decrease in the $AmIII_{3H}$ peak width with little accompanying change in the relative peak heights. In addition, the relative intensities of the $AmIII_{3T1}$ and $AmIII_{3T2}$ bands increase with temperature. The decreased signal-to noise ratio (S/N) of the higher temperature α-helix spectra (Fig. 69E, F) results from the decreased α-helical fractions of AP at 20 and 30 °C, compared to that at lower temperatures.[5,6]

8.3.2 Temperature Dependence of Ψ Ramachandran Angle Distributions of AP

We recently developed a method to determine the peptide bond Ψ Ramachandran angular distributions from the UVRR $AmIII_3$ profiles.[34,38,59,64] Fig. 70 shows the temperature dependence of the Ψ angular distributions calculated from the $AmIII_3$ bands of the Fig. 69 UVRR spectra of AP.

The Fig. 70 Ψ distributions shown in "blue-green" were obtained from the Fig. 69C-F $AmIII_{3H}$ band profiles using the Eq. 11B from Chapter 5 below developed for the interior α-helix peptide bonds.[59]

$$\nu_{III3}^{i\alpha,i\beta}(\psi) = [1244\ cm^{-1} - 54\ cm^{-1} \cdot \sin(\psi + 26^0)]$$

where $\nu_{III3}^{i\alpha,i\beta}(\psi)$ is the "α-helical" $AmIII_3$ frequency, which sinusoidally depends on Ψ angle.

The "blue-green" distributions for "α-helical" peptide bonds remain essentially identical between 0 and 20 °C (Fig. 70A-C), but begin to narrow and upshift as the temperature increases to 30 °C (Fig. 70D). If these distributions are modeled as Gaussians; their average Ψ angle shifts from 48° to 42°, while their bandwidth parameter, σ_α (half width at half height), narrows from 14.7°±3.3° to 5.2°±1.4° (Fig. 70).

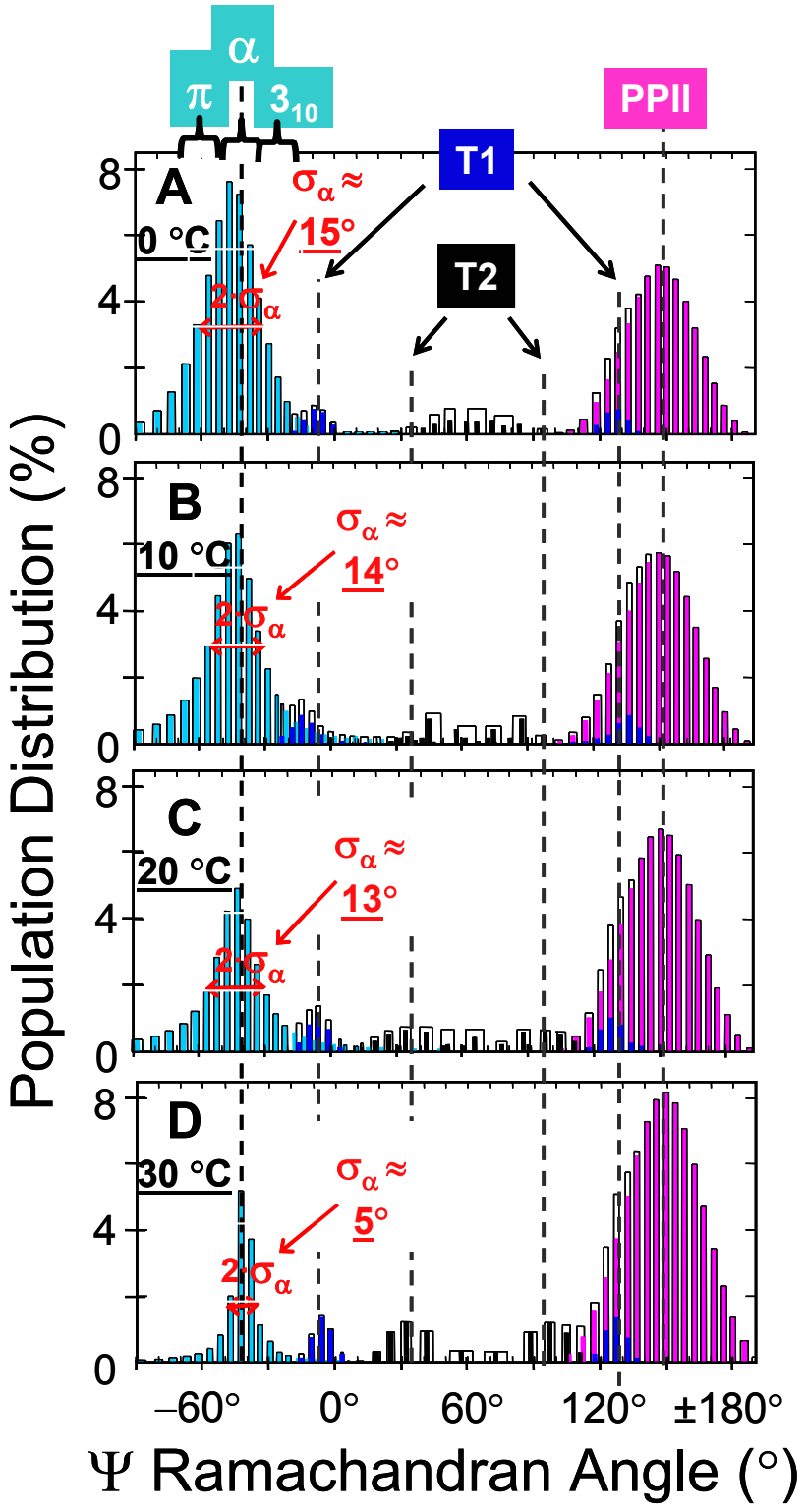

Figure 70. Temperature dependence of the calculated α-helix Ψ Ramachandran angular distributions from the Fig.69C-F AP α-helix UVRR spectra: (A) 0 °C; (B) 10 °C; (C) 20 °C; (D) 30 °C.

The Fig. 70 magenta distributions were calculated from the $AmIII_3$ bands of PPII conformations shown in Fig. 69B, using the Eqn. 11A from Chapter 5 developed for peptide bonds fully exposed to water[59]:

$$\nu_{III3}^{PPII}(\psi,T) = [1256\ cm^{-1} - 54\ cm^{-1} \cdot \sin(\psi + 26^0)] - 0.11 \cdot \frac{cm^{-1}}{^oC} \cdot (T - T_0)\}$$

where $\nu_{III3}^{PPII}(\psi,T)$ is the PPII $AmIII_3$ frequency, T is the experimental temperature, $T_0 = 0$ °C.

The Fig. 70 Ψ angle distributions shown in blue and black, were calculated from the $AmIII_{T1}$ and $AmIII_{T2}$ bands shown in Fig. 69C-F using the Eq. 11E from Chapter 5 developped for peptide bonds with unknown hydrogen bonding pattern in water solutions[59]:

$$\nu_{III3}^{TURNS}(\psi,T) = [1250\ cm^{-1} - 54\ cm^{-1} \cdot \sin(\psi + 26^0)] - 0.06 \cdot \frac{cm^{-1}}{^oC} \cdot (T - T_0)\}$$

where all the parameters have the same physical meanings as in the Eqs. 11A and 11B.

Each of the $AmIII_{T1}$ and $AmIII_{T2}$ bands gives two physically possible Ψ angle solutions as shown in Fig. 70. The $AmIII_{T1}$ band at ~1228 cm^{-1} (30 °C) gives a "blue" Ψ distribution which is either centered at Ψ ≈ –5° (which would derive from the i+2 residue of either type I, I', II, II' turns[59]), or Ψ ≈ +133° (which would derive from the i+1 residues of type II turns, the i+2 residues of type VIII turns or β-strands[59]). The $AmIII_{T2}$ band at 1200 cm^{-1} (30 °C) has solutions Ψ ≈ +34° (which would derive from the i+1 residue of type I' or III' turns, or the i+2 residue of type III' turns, or from an inverse γ-turn[59]), or Ψ ≈ +94° (which would derive from the i+1 residues of type V turns, and β-strand conformations[59]). We are working on developing a method to determine the Φ angle to discriminate between these conformations.

The relative contribution of these turn (or β-strand) conformations increases as the temperature increases, while the integrated intensity of the broad "α-helix-like" $AmIII_{3H}$ band decreases and its Ψ angle distribution narrows. The intensities of the turn (or β-strand) bands are small, indicating concentrations of less than 7 % presuming UVRR cross sections similar to that of the α-helix, or less then 3.5% presuming UVRR cross sections similar to that of PPII.[61]

8.3.3 Simultaneous Existence of α-Helix, 3_{10}-Helix, and π-Helix/Bulge Conformations

The very broad $AmIII_{3H}$ Ψ angle distribution at low temperatures (Fig. 70A-C) spans the Ψ angles of the 3_{10}-helix and π-helix/bulge conformations. In contrast at 30 °C the bandwidth is only ~50% larger than the homogeneous bandwidth of 7.5 cm^{-1}, which we measured for a small peptide in a single well defined crystal conformation.[34]

The AP α-helical ensemble at 30 °C is centered at $\Psi_{MAX} = -42°$ with a standard deviation of ±5.2° (Fig. 70D). This ±5.2° standard deviation is less than that found in the protein data bank for α-helices in single-crystal proteins.[65] Thus, we conclude that the "α-helix-like" conformation of AP at 30 °C is a pure homogeneous α-helical conformation, while at lower temperatures additional conformations occur. The low Ψ angle standard deviation for the AP pure α-helix conformation presumably results from the high homogeneity of the AP primary sequence.

The 3-fold broader "α-helix-like" Ψ angular distributions (Fig. 70A-C, "blue-green" distributions) compared to that at 30 °C (Fig. 70D) indicates the presence of additional conformations. We investigated the lower temperature Ψ angular distributions by subtracting the 30 °C pure α-helix distribution from the lower temperature "α-helix-like" distributions. This subtraction is appropriate, because the individual peptide bonds Raman scatter UV light in the AmIII region independently,[63] thus, the resulting UVRR spectra are the linear sums of individual peptide bond contributions. Fig. 71, which shows the resulting Ψ angle distributions at 0, 10 and 20 °C, demonstrates two relatively symmetric maxima at approximately –28° and –58°.

The –28° maximum can be directly assigned to 3_{10}-helices (type III turns) which have Ψ and Φ Ramachandran angles of –26° and –60°, respectively. Hydrogen bonding in the 3_{10}-helix occurs between the ith and i+3th peptide bonds, making the 3_{10}-helix more tightly coiled than the α-helix. Our observation of 3_{10}-helices agrees with the recent evidence for 3_{10}-helices in ala-rich peptides.[20,23-26,66-81]

The Ψ≈–58° distribution most likely originates from π-bulges, which are known to be a common deformation in α-helices.[65] These π-bulges are short intrahelical deformations involving "π-helix-like" hydrogen bonding between the ith and i+5th residues. Though ideal π-helices show Ψ and Φ Ramachandran angles of –69° and –57°, respectively, π-bulges show Ψ

angles close to Ψ≈–58°. Our observation of π-bulges agrees with recent reports on π-helix/π-bulge conformations in ala rich peptides.[21,25-27,30,80,82]

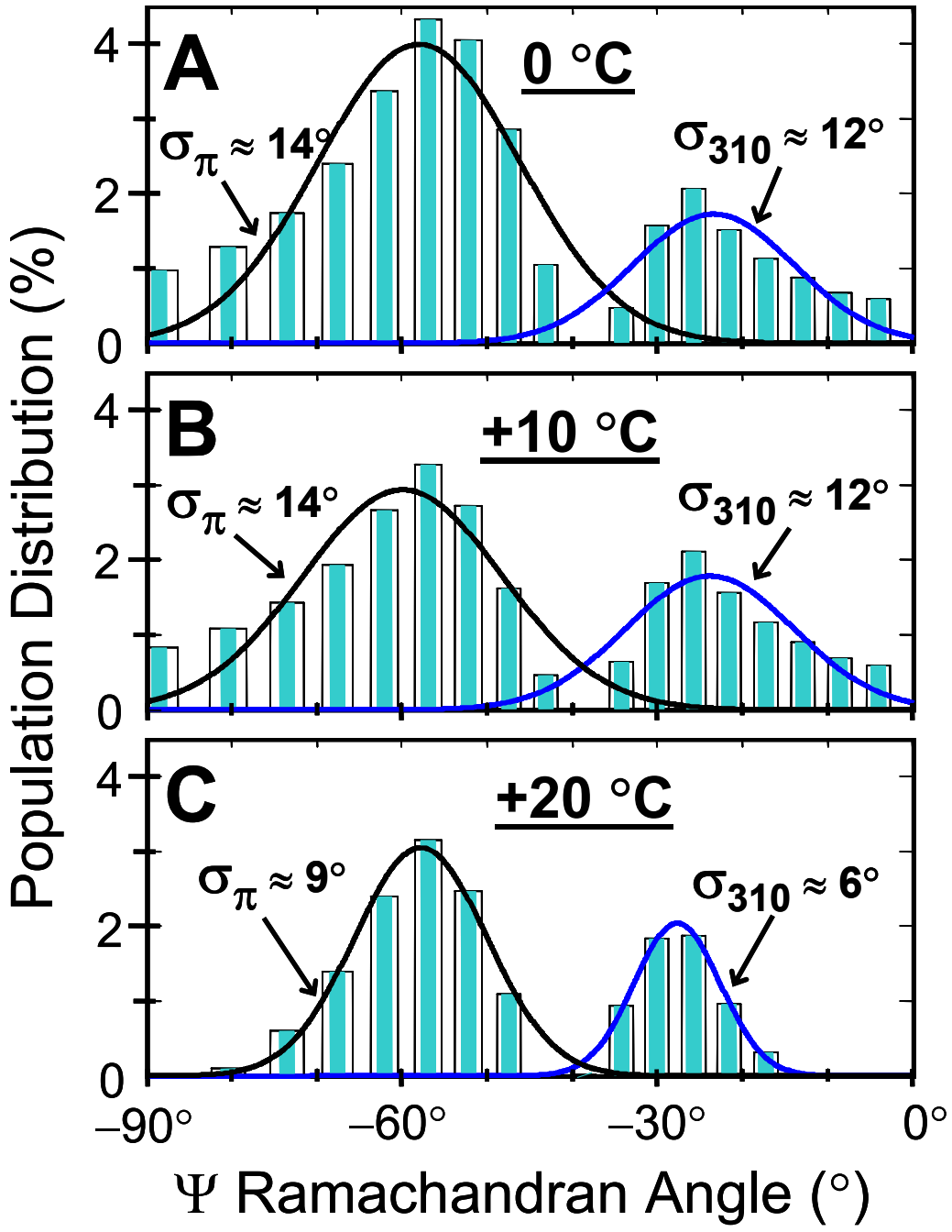

Figure 71. Temperature dependence of Ψ angular distributions for α-helical "defects", calculated by subtracting pure α-helix (Fig. 70D) from total (Fig. 70A-C) distributions: **(A)** 0 °C; **(B)** +10 °C; **(C)** +20 °C.

We considered the possibility that the Ψ angle distribution assigned to π-bulges instead resulted from the three N-terminal and three C-terminal residues of α-helices which cannot fully intrahelix hydrogen bond. These peptide bonds, which are hydrogen bonded to water, would be frequency upshifted by 9 and 3 cm^{-1}, respectively, compared to those which intrahelix hydrogen bond.[59] However, the high temperature Fig. 70D α-helix distribution indicates that the terminal pure α-helix Ψ angle conformations overlap those of the central α-helix peptide bonds. Thus, we conclude that the terminal residues of the α-helices do not contribute to the Ψ = –58° distribution.

8.3.4 Different Melting Temperatures (T_m) For α-Helix, 3_{10}-Helix, and π-Helix/Bulge

If we assume identical Raman cross sections for the internal and terminal α-helix residues, as well as for the 3_{10}- and π-helices, we can calculate the melting curves for these conformations (Fig. 72), as well as the temperature dependence of their Gibbs free energy landscapes (Fig. 73). The most striking feature of the Fig. 72 melting curves is that α-helix melting now looks highly cooperative, with a T_m~45 °C, a substantially larger T_m than previously determined by CD[4] and Raman[5]. Melting of the 3_{10}-helices and π-bulges is also cooperative with T_m~20 and 10 °C, respectively. Previous studies,[6] unable to distinguish between these conformations, determined a much less cooperative average melting curve which could be well fit by a Zimm and Bragg nucleation parameter, б, of ~$8 \cdot 10^{-4}$ and a lower T_m = ~27 °C for the so called "α-helix". As discussed later, we find that the Fig. 72 resolved α-helix melting curve results in quite different Zimm and Bragg nucleation and thermodynamic parameters.

Recently, Ianoul et al.[83] deuterium substituted the penultimate AP residues and demonstrated that the α-helix-like penultimate segments melt at lower temperatures than do the ~6 central α-helical peptide bonds. This allows us to conclude that the 3_{10}-helices and π-bulge conformations preferentially occur in regions outside the six central AP peptide bonds, towards the ends of the α-helical segments. We can now reconsider the kinetic Raman melting studies of Lednev et al.[6] who measured melting using a T-jump from 4 to 26 °C. Fig. 72 shows that the π-bulges are the dominant melting species between these temperatures. Thus, we now can conclude that melting of π-bulges occurs with a relaxation time of 180±60 ns. If these π-bulges melted to

PPII conformations directly in a two-state transition, we would estimate π-bulge folding and unfolding rate constants of as 4.0 x 10^5 and 5.2·x 10^6 s^{-1}, respectively.

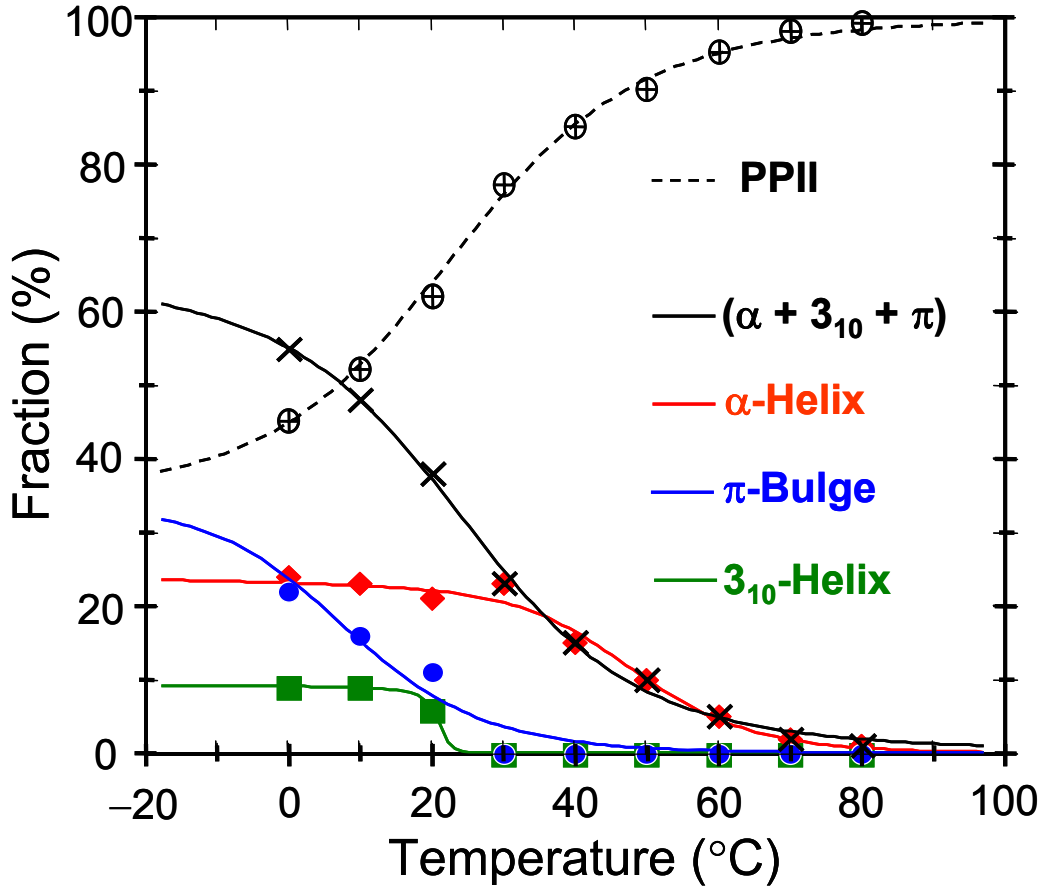

Figure 72. Melting/formation curves for AP major pure secondary structure conformations. (×) – Original "α-helix" melting curve as reported by Lednev et al.[5,6], which is a sum of individual α- π- and 3_{10}-helical melting curves; (♦) – Perfect α-helix melting; (■) – 3_{10}-helix (type III turn) melting; (●)– π-bulge (π-helix) melting; (⊕) – PPII formation. The lines through the points for the "α-helix-like" conformations derive from the Zimm-Bragg model as described in the text.

However, molecular dynamical studies indicate that the 3_{10}-helix and π-bulge conformations are transient α-helix defect structures,[23-27] which are less stable than the pure α-helix conformations and, therefore, melt at lower temperatures. Thus, our estimation of rate constants using a 2-state model is questionable. The stability of 3_{10}-helix and π-bulge conformations derives from the increased peptide bond-water hydrogen bonding stabilization[34,38] that occurs at lower temperatures for the more solvent exposed 3_{10}-helices (type III turns)[84] and π-bulges[65].

8.3.5 Experimental Gibbs Free Energy Landscapes

We can utilize our calculated conformation population distributions (Fig. 70) to calculate portions of the Gibbs free energy landscape (GFEL) along the Ψ Ramachandran angle folding reaction coordinate, applying the simple Boltzmann argument.[38] Fig. 73 shows the resulted AP GFEL at 0, 10, 20 and 30 °C. The black lines through circles show the well-determined portions of the GFEL in the α-helix and the PPII regions of the Ramachandran plot. The red line shows the fit of α-helical part of the GFEL using a harmonic oscillator model $G_\alpha=G_{0\alpha}+k_\alpha\cdot(\Psi-\Psi_0)^2/2$. This fit allows us to estimate the torsional restoring force constant (k_α) for a perfect α-helix conformation at 30 °C, $k_\alpha\approx92$ J/deg^2.

The dotted blue line in Fig. 73 shows a very roughly estimated GFEL in the "turn" regions of the Ramachandran plot, assuming that the assigned turns T1 and T2 exist at Ψ≈–5° and +34°, respectively. In this case, it is not possible to determine the portion of GFEL between Ψ values of ~60° and 100°, nor to reliably determine the free energy barrier between the α-helix and the PPII conformations (60° to 100°, Fig. 73). However, we can estimate that the barriers at other angles are <12.5 kJ/mol·peptide bond (kJ/mol·PB).

The dashed green line in Fig. 73 shows another option for the GFEL in the "turn" region of the Ramachandran plot, which assumes that the turns T1 and T2 (or β-strands) exist at Ψ≈+133° and +94°, respectively. Under this assumption, we estimate that the free energy barriers between the α-helix and PPII conformations lie between 9 and 14 kJ/mol·PB.

The experimental Fig. 73 AP GFELs are qualitatively similar to those theoretically estimated by Young and Brooks[20] for Ace-$(Ala)_n$-NMe (n=4, 5, 10, 15) in water. However, the Fig. 73 GFELs, in addition to pure α-helix and 3_{10}-helix conformations, also include contributions from a π-bulge conformation. It is striking that the Fig. 73 activation free energy barriers of ~10-12 kJ/mol·PB are essentially identical to that of Young and Brooks[20] (~2-3 kcal/mol·PB). However, we find that the apparent Gibbs free energy difference between the α-helix and 3_{10}-helix conformations is ~2 kJ/mol·PB, which is smaller than the ~0.6-1.6 kcal/mol·PB values calculated by Young and Brooks,[20] as well as the ~1 kcal/mol·PB calculated value of Tirado-Rives et al.[31]

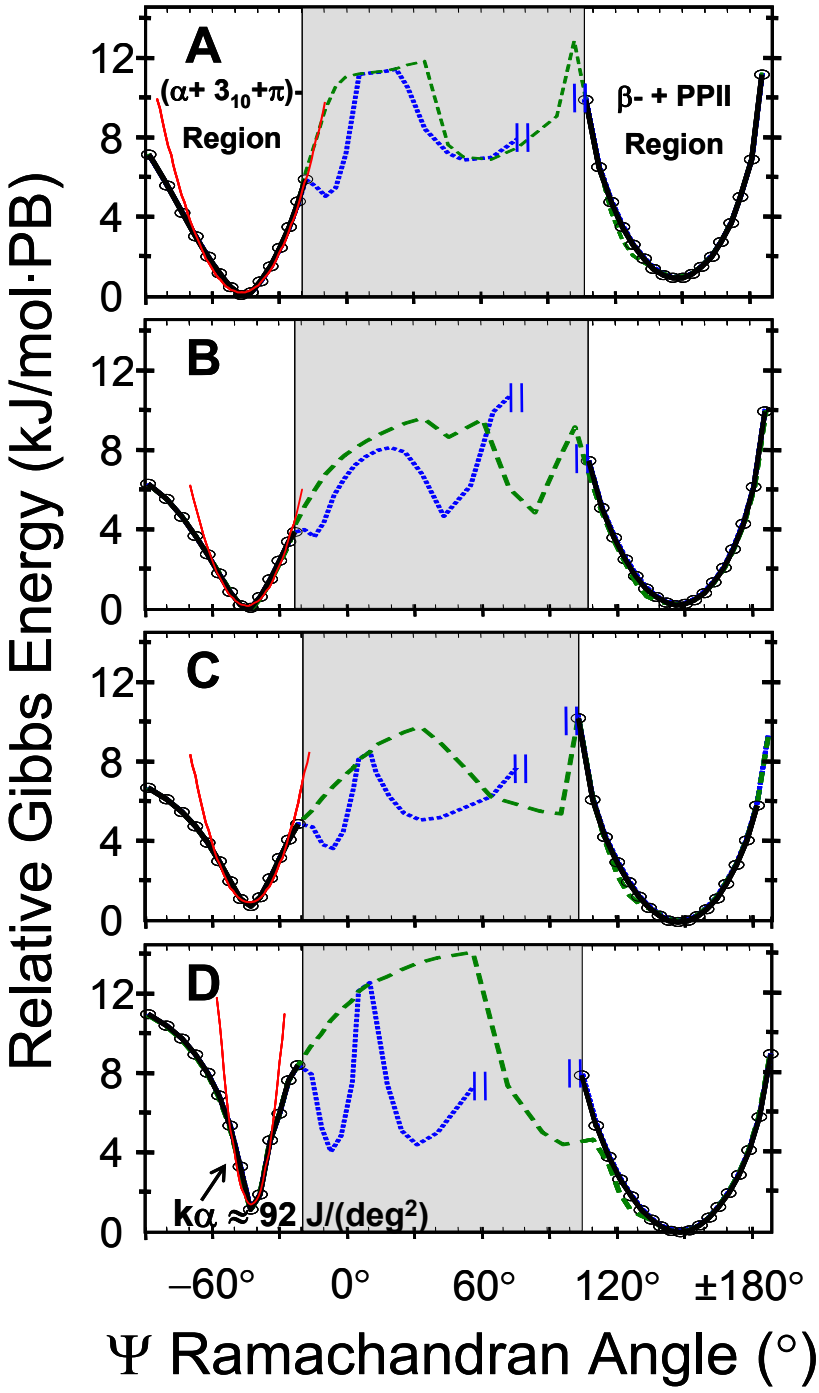

Figure 73. Relative Gibbs energy landscapes (GFEL) for AP at different temperatures: (A) 0 °C, (B) +10 °C, (C) +20 °C, (D) +30 °C. Black lines with circles represent well-determined portions of the GFEL in the α-helix and PPII regions of the Ramachandran plot. The dotted blue line in the uncertain "turn" regions of the Ramachandran plot, assumes that the turns T1 and T2 exist at Ψ≈–10° and +30°, respectively. The dashed green line assumes that turns T1 and T2 exist at Ψ≈+130° and +90°, respectively. The red line shows the fit of α-helical part of GFEL using the harmonic oscillator approximation. "PB" means "peptide bond".

Applying the similar Boltzmann distribution argument,[38] we can use, for example, the Fig. 71C 3_{10}-helix and π-bulge peptide bond distribution to estimate their relative Gibbs free energies, which allows us to determine the torsional constants for the 3_{10}-helix and the π-bulge/helix conformations (Fig. 74). We find torsional constants $k_{310}\approx146$ and $k_{\pi}\approx33$ J/deg^2 for the 3_{10}-helix and the π-bulge at 20 °C, respectively. Thus, the more tightly coiled the "helical" structure, the larger is its torsional force constant ($k_{\pi}<k_{\alpha}<k_{310}$), as expected.

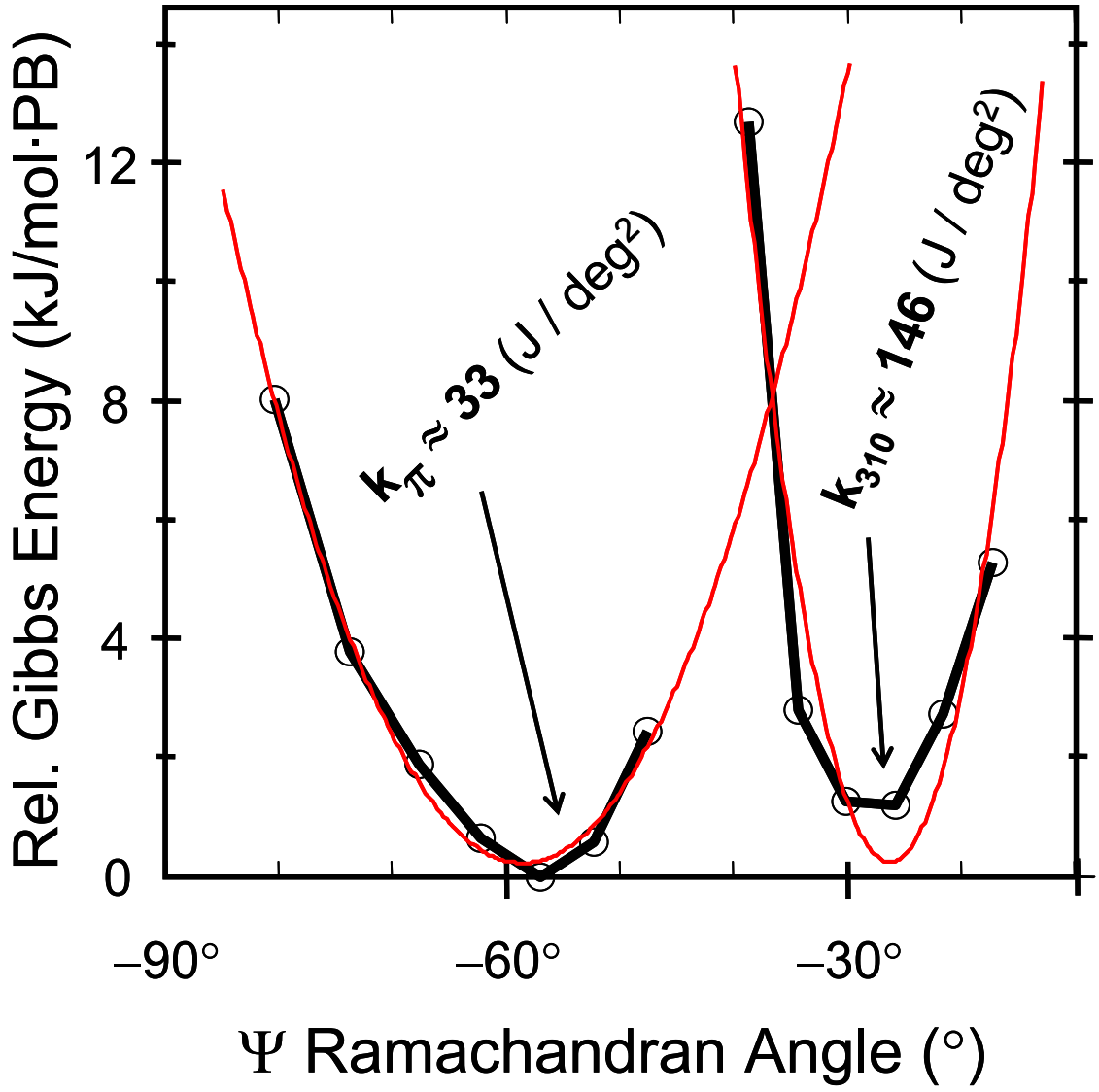

Figure 74. Relative Gibbs free energies of 3_{10}-helix and π-bulge at +20 °C as a function of Ψ angle. Black line through circles shows the calculated GFEL obtained from the Fig. 71C distributions. The red line shows the fit of these data points to a harmonic oscillator model. "PB" means "peptide bond".

8.3.6 Insights into Complex Melting Kinetics of AP-like Peptides

Our results provide new insights into the melting phenomena of α-helices. The obvious population heterogeneity of the low temperature α-helix-like ensembles should contribute to complicated multi-exponential and/or non-exponential kinetics for α-helix melting, which is, in fact, observed for similar peptides.[7,9] This population heterogeneity clarifies why the observed α-helix kinetic melting in these peptides depends on the initial and final temperatures; complicated kinetic behaviors occur for low initial T-jump temperatures,[7,9] whereas at higher initial temperatures sample the pure α-helix shows essentially monoexponential kinetic melting.[7,9]

In addition, the recent kinetic studies of Decatur and coworkers[11,12] suggest that the ala-rich peptides show different mono-exponential relaxation times for different isotopically labeled segments of the ala-rich chains, which clearly suggests that the melting of these peptides is not a simple two-state process.

Our melting studies here simply explain the anti-Arrhenius melting kinetics observed by Lednev et al.[5] Folding kinetics are fast at low temperatures where relaxation involves 3_{10}-helices and π-bulges melting to PPII conformations. In contrast, the higher temperature melting T-jumps sampled only pure α-helix melting which was slower. The kinetic measurements were unable at that time to differentiate these different conformations.

8.3.7 Zimm-Bragg Parameters for α-Helix, 3_{10}-Helix, and π-Helix/Bulge Conformations

We can compare the Zimm and Bragg apparent nucleation parameters for these structures and estimate the melting enthalpies and entropies. The system is underdetermined so that these parameters are not independent. Since the perfect α-helix melting is more cooperative than that of the "so-called α-helix" (Fig. 72), we will assume that the perfect α-helix $б_{\alpha} = \sim 10^{-5}$, somewhat less than the $б_{\alpha} = \sim 8 \cdot 10^{-4}$ reported by Lednev et al.[6] The entropic cost for forming the first hydrogen bond in 3_{10}- and α-helices is counted in the nucleation parameter, б. Sheinerman and Brooks[85] argued that two additional dihedral angles must be restricted to initially form a 3_{10}-helical turn, while four additional dihedral angles must be restricted to initially form an α-helical turn. This led them to estimate that the nucleation parameter for the 3_{10}-helix is $б_{310} \sim (б_{\alpha})^{0.5}$.

Applying this argument to a π-bulge we estimate that $б_\pi \sim (б_\alpha)^{1.5}$, since six additional dihedral angles must be restricted to form first π-helical turn. Thus, taking $б_\alpha \sim 10^{-5}$, we estimate $б_{310} \sim 3 \cdot 10^{-3}$ and $б_\pi \sim 3 \cdot 10^{-8}$. This approach allows for an adequate fit to the observed melting curves for perfect α-helices and π-helices/bulges (Fig. 72). We find hydrogen bonding enthalpies of ΔH = –7.2 and –4.4 kJ/(mol·res) for the perfect α-helix and the π-helix/bulge, respectively. We also estimate entropies ΔS = –17.4 and –7.8 J/(mol·K·res) for the perfect α-helix and π-helix/bulge, respectively. In contrast, the Zimm and Bragg model fails to adequately describe the melting of 3_{10}-helices with physically reasonable nucleation and propagation parameters б and s, although it is possible to get an adequate fit (Fig. 72).

Alternatively we can constrain the enthalpy for all these structures to be –6.3 kJ/(mol·res) and then estimate the nucleation parameters and the entropies. This approach provides the nucleation parameters of $\sim 1 \cdot 10^{-7}$, $1 \cdot 10^{-8}$, and $1 \cdot 10^{-5}$, for α-helix, 3_{10}-helix and π-helix/bulge respectively. We also estimate entropies of ~ –7.9, –7.8 and –14.6 J/(mol·K·res), respectively. Assuming the same enthalpies we find that the nucleation parameters follows a trend, exactly opposite of that expected by Sheinerman and Brooks.[85] Whatever the case, the melting of α-helix-like AP is definitely far from a two state transition. Thus, the physical meaning of these Zimm and Bragg parameters is no longer straightforward.

8.4 CONCUSIONS

Our ability to directly monitor the Ψ Ramachandran angles of peptide bonds allows us for the first time to separately study the melting of the α-, 3_{10}- and π-helix/bulge conformations. It is somewhat surprising to find that the 3_{10}- and π-helix/bulge conformations melt prior to melting of pure α-helices, since these conformations are proposed to be intermediates in the unfolding pathway. Apparently they are much more transient at the higher α-helix melting temperature.

We estimated Zimm and Bragg nucleation (б) and propagation (s) parameters for perfect α-helix, and π-helix/bulge conformations. A striking finding is that the AP pure α-helix melts with much higher cooperativity and shows much higher $T_m \sim 45$ °C then it was originally reported by CD[4] and Raman[5]. We were able for the first time to experimentally monitor the

Gibbs free energy landscapes and the free energy barriers on the AP melting reaction pathway. These experimental measurements should serve as a benchmark for theoretical studies of protein folding. Future equilibrium and kinetic studies of isotopically edited peptides will allow us to more deeply examine "α-helix" to PPII melting, as well as other peptide backbone conformational transitions.

8.5 REFERENCES

(1) Zimm, B. H.; Bragg, J. K. *J. Chem. Phys.* **1959**, *31*, 526-535.

(2) Poland, D.; Scheraga, H. A. *J. Chem. Phys.* **1966**, *45*, 2071-2090.

(3) Williams, S.; Causgrove, T. P.; Gilmanshin, R.; Fang, K. S.; Callender, R. H.; Woodruff, W. H.; Dyer, R. B. *Biochemistry* **1996**, *35*, 691-697.

(4) Thompson, P. A.; Munoz, V.; Jas, G. S.; Henry, E. R.; Eaton, W. A.; Hofrichter, J. *J. Phys. Chem. B* **2000**, *104*, 378-389.

(5) Lednev, I. K.; Karnoup, A. S.; Sparrow, M. C.; Asher, S. A. *J. Am. Chem. Soc.* **1999**, *121*, 8074-8086.

(6) Lednev, I. K.; Karnoup, A. S.; Sparrow, M. C.; Asher, S. A. *J. Am. Chem. Soc.* **2001**, *123*, 2388-2392.

(7) Huang, C.-Y.; Klemke, J. W.; Getahun, Z.; DeGrado, W. F.; Gai, F. *J. Am. Chem. Soc.* **2001**, *123*, 9235-9238.

(8) Werner, J. H.; Dyer, R. B.; Fesinmeyer, R. M.; Andersen, N. H. *J. Phys. Chem. B* **2002**, *106*, 487-494.

(9) Bredenbeck, J.; Helbing, J.; Kumita, J. R.; Woolley, G. A.; Hamm, P. *Proc. Natl. Acad. Sci. U.S.A.* **2005**, *102*, 2379-2384.

(10) Huang, C.-Y.; Getahun, Z.; Zhu, Y.; Klemke, J. W.; DeGrado, W. F.; Gai, F. *Proc. Natl. Acad. Sci. U.S.A.* **2002**, *99*, 2788-2793.

(11) Ramajo, A. P.; Petty, S. A.; Starzyk, A.; Decatur, S. M.; Volk, M. *J. Am. Chem. Soc.* **2005**, *127*, 13784-13785.

(12) Decatur, S. M. *Acc. Chem. Res.* **2006**, *39*, 169-175.

(13) Hummer, G.; Garcia, A. E.; Garde, S. *Phys. Rev. Lett.* **2000**, *85*, 2637-2640.

(14) Ferrara, P.; Apostolakis, J.; Caflisch, A. *J. Phys. Chem. B* **2000**, *104*, 5000-5010.

(15) Sorin, E. J.; Pande, V. S. *Biophys. J.* **2005**, *88*, 2472-2493.

(16) Bertsch, R. A.; Vaidehi, N.; Chan, S. I.; Goddard, W. A., III *Proteins* **1998**, *33*, 343-357.

(17) Levy, Y.; Jortner, J.; Becker, O. M. *Proc. Natl. Acad. Sci. U.S.A.* **2001**, *98*, 2188-2193.

(18) Irbaeck, A.; Mohanty, S. *Biophys. J.* **2005**, *88*, 1560-1569.

(19) DiCapua, F. M.; Swaminathan, S.; Beveridge, D. L. *J. Am. Chem. Soc.* **1990**, *112*, 6768-6771.

(20) Young, W. S.; Brooks, C. L., III *J. Mol. Biol.* **1996**, *259*, 560-572.

(21) Shirley, W. A.; Brooks, C. L., III *Proteins* **1997**, *28*, 59-71.

(22) Doruker, P.; Bahar, I. *Biophys. J.* **1997**, *72*, 2445-2456.

(23) Takano, M.; Yamato, T.; Higo, J.; Suyama, A.; Nagayama, K. *J. Am. Chem. Soc.* **1999**, *121*, 605-612.

(24) Sorin, E. J.; Rhee, Y. M.; Shirts, M. R.; Pande, V. S. *J. Mol. Biol.* **2006**, *356*, 248-256.

(25) Armen, R.; Alonso, D. O. V.; Daggett, V. *Prot. Sci.* **2003**, *12*, 1145-1157.

(26) Freedberg, D. I.; Venable, R. M.; Rossi, A.; Bull, T. E.; Pastor, R. W. *J. Am. Chem. Soc.* **2004**, *126*, 10478-10484.

(27) Lee, K.-H.; Benson, D. R.; Kuczera, K. *Biochemistry* **2000**, *39*, 13737-13747.

(28) Zhang, W.; Lei, H.; Chowdhury, S.; Duan, Y. *J. Phys. Chem. B* **2004**, *108*, 7479-7489.

(29) Huo, S.; Straub, J. E. *Proteins* **1999**, *36*, 249-261.

(30) Mahadevan, J.; Lee, K.-H.; Kuczera, K. *J. Phys. Chem. B* **2001**, *105*, 1863-1876.

(31) Tirado-Rives, J.; Maxwell, D. S.; Jorgensen, W. L. *J. Am. Chem. Soc.* **1993**, *115*, 11590-11593.

(32) Wang, Y.; Kuczera, K. *J. Phys. Chem. B* **1997**, *101*, 5205-5213.

(33) Mezei, M.; Fleming, P. J.; Srinivasan, R.; Rose, G. D. *Proteins* **2004**, *55*, 502-507.

(34) Asher, S. A.; Mikhonin, A. V.; Bykov, S. B. *J. Am. Chem. Soc.* **2004**, *126*, 8433-8440.

(35) Garcia, A. E. *Polymer* **2004**, *45*, 669-676.

(36) Shi, Z.; Woody, R. W.; Kallenbach, N. R. *Adv. Prot. Chem.* **2002**, *62*, 163-240.

(37) Blanch, E. W.; Morozova-Roche, L. A.; Cochran, D. A. E.; Doig, A. J.; Hecht, L.; Barron, L. D. *J. Mol. Biol.* **2000**, *301*, 553-563.

(38) Mikhonin, A. V.; Myshakina, N. S.; Bykov, S. V.; Asher, S. A. *J. Am. Chem. Soc.* **2005**, *127*, 7712-7720.

(39) McColl, I. H.; Blanch, E. W.; Hecht, L.; Kallenbach, N. R.; Barron, L. D. *J. Am. Chem. Soc.* **2004**, *126*, 5076-5077.

(40) Syme, C. D.; Blanch, E. W.; Holt, C.; Jakes, R.; Goedert, M.; Hecht, L.; Barron, L. D. *Eur. J. Biochem.* **2002**, *269*, 148-156.

(41) Smyth, E.; Syme, C. D.; Blanch, E. W.; Hecht, L.; Vasak, M.; Barron, L. D. *Biopolymers* **2001**, *58*, 138-151.

(42) Blanch, E. W.; Gill, A. C.; Rhie, A. G. O.; Hope, J.; Hecht, L.; Nielsen, K.; Barron, L. D. *J. Mol. Biol.* **2004**, *343*, 467-476.

(43) Shi, Z.; Olson, C. A.; Rose, G. D.; Baldwin, R. L.; Kallenbach, N. R. *Proc. Natl. Acad. Sci. U.S.A.* **2002**, *99*, 9190-9195.

(44) Creamer, T. P.; Campbell, M. N. *Adv. Prot. Chem.* **2002**, *62*, 263-282.

(45) Rucker, A. L.; Creamer, T. P. *Prot. Sci.* **2002**, *11*, 980-985.

(46) Chellgren, B. W.; Creamer, T. P. *Biochemistry* **2004**, *43*, 5864-5869.

(47) Liu, Z.; Chen, K.; Ng, A.; Shi, Z.; Woody, R. W.; Kallenbach, N. R. *J. Am. Chem. Soc.* **2004**, *126*, 15141-15150.

(48) Adzhubei, A. A.; Sternberg, M. J. E. *J. Mol. Biol.* **1993**, *229*, 472-493.

(49) Pappu, R. V.; Rose, G. D. *Prot. Sci.* **2002**, *11*, 2437-2455.

(50) Rath, A.; Davidson, A. R.; Deber, C. M. *Biopolymers* **2005**, *80*, 179-185.

(51) Fleming, P. J.; Fitzkee, N. C.; Mezei, M.; Srinivasan, R.; Rose, G. D. *Prot. Sci.* **2005**, *14*, 111-118.

(52) Bochicchio, B.; Tamburro, A. M. *Chirality* **2002**, *14*, 782-792.

(53) Eisenhaber, F.; Adzhubei, A. A.; Eisenmenger, F.; Esipova, N. G. *Biofizika* **1992**, *37*, 62-67.

(54) Robin, M. B. *"Higher Excited States of Polyatomic Molecules"; Academic Press: New York* **1975**, *Vol. II*.

(55) Song, S.; Asher, S. A. *J. Am. Chem. Soc.* **1989**, *111*, 4295-4305.

(56) Dudik, J. M.; Johnson, C. R.; Asher, S. A. *J. Phys. Chem.* **1985**, *89*, 3805-3814.

(57) Copeland, R. A.; Spiro, T. G. *Biochemistry* **1987**, *26*, 2134-2139.

(58) Mayne, L. C.; Ziegler, L. D.; Hudson, B. *J. Phys. Chem.* **1985**, *89*, 3395-3398.

(59) Mikhonin, A. V.; Bykov, S. V.; Myshakina, N. S.; Asher, S. A. *J. Phys. Chem. B* **2006**, *110*, 1928-1943.

(60) Bykov, S. V.; Lednev, I. K.; Ianoul, A.; Mikhonin, A. V.; Munro, C. H.; Asher, S. A. *Appl. Spectrosc.* **2005**, *59*, 1541-1552.

(61) Mikhonin, A. V.; Ahmed, Z.; Ianoul, A.; Asher., S. A. *J. Phys. Chem. B* **2004**, *108*, 19020-19028.

(62) Lee, S.-H.; Krimm, S. *Biopolymers* **1998**, *46*, 283-317.

(63) Mikhonin, A. V.; Asher, S. A. *J. Phys. Chem. B* **2005**, *109*, 3047-3052.

(64) Asher, S. A.; Ianoul, A.; Mix, G.; Boyden, M. N.; Karnoup, A.; Diem, M.; Schweitzer-Stenner, R. *J. Am. Chem. Soc.* **2001**, *123*, 11775-11781.

(65) Cartailler, J.-P.; Luecke, H. *Structure* **2004**, *12*, 133-144.

(66) Miick, S. M.; Martinez, G. V.; Fiori, W. R.; Todd, A. P.; Millhauser, G. L. *Nature* **1992**, *359*, 653-655.

(67) Fiori, W. R.; Miick, S. M.; Millhauser, G. L. *Biochemistry* **1993**, *32*, 11957-11962.

(68) Millhauser, G. L. *Biochemistry* **1995**, *34*, 3873-3877.

(69) Millhauser, G. L.; Stenland, C. J.; Hanson, P.; Bolin, K. A.; van de Ven, F. J. M. *J. Mol. Biol.* **1997**, *267*, 963-974.

(70) Bolin, K. A.; Millhauser, G. L. *Acc. Chem. Res.* **1999**, *32*, 1027-1033.

(71) Moran, A. M.; Park, S.-M.; Dreyer, J.; Mukamel, S. *J. Chem. Phys.* **2003**, *118*, 3651-3659.

(72) Long, H. W.; Tycko, R. *J. Am. Chem. Soc.* **1998**, *120*, 7039-7048.

(73) Wieczorek, R.; Dannenberg, J. J. *J. Am. Chem. Soc.* **2004**, *126*, 14198-14205.

(74) Hanson, P.; Martinez, G.; Millhauser, G.; Formaggio, F.; Crisma, M.; Toniolo, C.; Vita, C. *J. Am. Chem. Soc.* **1996**, *118*, 271-272.

(75) Hanson, P.; Millhauser, G.; Formaggio, F.; Crisma, M.; Toniolo, C. *J. Am. Chem. Soc.* **1996**, *118*, 7618-7625.

(76) Martinez, G.; Millhauser, G. *J. Struc. Biol.* **1995**, *114*, 23-27.

(77) Silva, R. A.; Gangani, D.; Yasui, S. C.; Kubelka, J.; Formaggio, F.; Crisma, M.; Toniolo, C.; Keiderling, T. A. *Biopolymers* **2002**, *65*, 229-243.

(78) Topol, I. A.; Burt, S. K.; Deretey, E.; Tang, T.-H.; Perczel, A.; Rashin, A.; Csizmadia, I. G. *J. Am. Chem. Soc.* **2001**, *123*, 6054-6060.

(79) Bour, P.; Kubelka, J.; Keiderling, T. A. *Biopolymers* **2002**, *65*, 45-59.

(80) Podtelezhnikov, A. A.; Wild, D. L. *Proteins* **2005**, *61*, 94-104.

(81) Han, W.-G.; Elstner, M.; Jalkanen, K. J.; Frauenheim, T.; Suhai, S. *Intl. J. Quant. Chem.* **2000**, *78*, 459-479.

(82) Feig, M.; MacKerell, A. D., Jr.; Brooks, C. L., III *J. Phys. Chem. B* **2003**, *107*, 2831-2836.

(83) Ianoul, A.; Mikhonin, A.; Lednev, I. K.; Asher, S. A. *J. Phys. Chem. A* **2002**, *106*, 3621-3624.

(84) Sundaralingam, M.; Sekharudu, Y. C. *Science* **1989**, *244*, 1333-1337.

(85) Sheinerman, F. B.; Brooks, C. L., III *J. Am. Chem. Soc.* **1995**, *117*, 10098-10103.

9.0 CHAPTER 9. UV RAMAN SPATIALLY RESOLVED MELTING DYNAMICS OF ISOTOPICALLY LABELED POLYALANYL PEPTIDE: SLOW α-HELIX MELTING FOLLOWS 3_{10}-HELICES AND π-BULGES PREMELTING

Work, described in this Chapter, is submitted to the *J. Phys. Chem. B,* **2006**. (Authors: Mikhonin, A. V.; Asher, S. A.; Bykov, S. V.; and Murza, A.). We used UV resonance Raman (UVRR) to examine the spatial dependence of the T-jump secondary structure relaxation of an isotopically labeled 21-residue mainly ala peptide, AdP. The AdP penultimate ala residues were perdeuterated, leaving the central residues hydrogenated, to allow separate monitoring of melting of the middle versus the end peptide bonds. For 5 to 30 °C T-jumps, the central peptide bonds show a ~2-fold slower relaxation time (189±31 ns) than do the exterior peptide bonds (97±15 ns). In contrast, for a 20 to 40 ºC T-jump, the central peptide bond relaxation appears to be faster (56±6 ns) than that of the penultimate peptide bonds (131±46 ns). We show that if the data are modeled as a 2-state transition, we find that only exterior peptide bonds show anti-Arrhenius folding behavior; while the middle peptide bonds show both normal Arrhenius-like folding and unfolding. This anti-Arrhenius behavior results from the involvement of π-bulges/helices and 3_{10}-helix states in the melting. The unusual temperature dependence of the (un)folding rates of the interior and exterior peptide bonds is due to the different relative (un)folding rates of 3_{10}-helices, α-helices and π-bulges/helices. Pure α-helix unfolding rates are ~12-fold slower (~1 μsec) than that of π-bulges and 3_{10}-helices. In addition, we also find that the α-helix is most stable at the AdP N-terminus where eight consecuitive ala occur; whereas the three hydrophilic arg located in the middle and at the C-terminus destabilize the α-helix in these regions and induce defects such as π-bulges and 3_{10}-helices.

9.1 INTRODUCTION

The classical picture of α-helix melting envisions an elementary process whereby individual peptide bonds at the ends of the α-helix rotate from conformations with α-helical Ramachandran Ψ and Φ dihedral angles to random coil conformations with uncorrelated, but allowed Ramachandran Ψ and Φ dihedral angles.[1-3] This melting also involves breaking the intra-α-helical hydrogen bonds. This highly simplistic view is the basis for the standard theories which are used to model the cooperativity in melting from the α-helix to its melted conformational state(s). This helix↔coil transition for short helix-forming peptides has recently been the subject of numerous experimental[4-52] and theoretical[53-116] investigations.

This simple view of α-helix melting is now being challenged, because it appears that simple α-helical peptides often melt to a PPII conformation.[117-124] In fact, there is no evidence in favor of melting to, or even for the existence of random coil peptides in solution. Thus, the standard theories for α-helix formation and melting must be modified to include the fact that the transition is not between an ordered α-helix and a disordered random coil conformation, but rather the transition is between two ordered conformations. Further, this transition must be more complex, since at least one additional interfacial state must occur to connect the α-helix segment to the PPII segment, due to the steric features that prevent any simple connection.[68]

Given these complications, it is somewhat surprising that existing theory predicts the α-helix melting behavior pretty well. In most cases, the melting relaxation kinetics appears to follow a single exponential decay.[4-6,10,13-15,17,18,21,26] It should, however, be noted that clear departures from simple theory to date have been observed such as an α-helix peptide position dependence for the melting kinetics by Werner et al.'s[10], Huang et al.'s[32] and Ramajo et al.'s[25] time-resolved IR isotopically (C=O) labeled spectral study of the unfolding kinetics of ~20-residue α-helical peptides. In addition, Huang et al.[32-34] and Bredenbeck et al.[22] found evidence for nonexponential relaxation. Theoretical models have been proposed to explain the observed nonexponential kinetics.[33,63]

We recently used UV resonance Raman (UVRR) spectroscopy[7] to examine the spatial dependence of melting of an isotopically labeled mainly ala α-helical peptide, AdP. UVRR spectroscopy is a powerful method to quantitatively determine peptide secondary

structures.[4,7,125-130] UV excitation within the peptide bond $\pi' \rightarrow \pi^*$ transition selectively enhances a number of amide vibrations, whose frequencies and intensities report on the polypeptide backbone conformation.[4,125-128,131] The UVRR spectra are highly resolved. Laser induced temperature-jump (T-jump) kinetic UVRR measurements allow detailed studies of peptide unfolding.[4-6] In these studies the temperature of the peptide aqueous solution is increased within nsec by an IR laser pulse whose wavelength is completely absorbed by a water combination band. The temperature increase initiates peptide unfolding. A subsequent 204 nm UV excitation pulse at the appropriate delay time after the T-jump excites the UVRR spectra.

These UVRR spectra can be used to monitor the relaxation of the peptide conformation. For natural abundance AP we previously observed[4-6] a simple moderately cooperative melting curve with apparently simple single exponential relaxation kinetics (~200 nsec). The only indication of complexity in the kinetics came from a 2-state analysis of the temperature dependence which demonstrated an anti-Arrhenius temperature dependence for α-helix folding rate constant. The relaxation kinetics observed were similar to the melting behaviors observed for similar α-helical polypeptides.[4-6,10,13-15,17,18,21]

In a previous study we isotopically labeled AP in order to separately monitor the end peptide bonds melting versus that of the interior peptide bonds.[7] We found that the central peptide bonds have a higher equilibrium melting temperature than do the end peptide bonds. In the work here we directly examine the spatial dependence of unfolding kinetics for this partially deuterated peptide, AdP. As discussed below we find faster relaxation kinetics for the end peptide bonds compared to the middle for a 5 to 30 °C T-jump. In contrast, we find slower relaxation kinetics for the end peptide bonds compared to the middle for the 20 to 40 °C T-jump. We find that this behavior results from different relative contributions in the different regions of slower melting pure α-helices and faster melting π-bulges and 3_{10}-helices to the observed melting kinetics.

The AdP kinetic data can be adequately fit by single exponentials, within the S/N of our data. However, if we apply a two-state model similar to that of Lednev et al.[4] we calculate strong anti-Arrhenius behavior for folding of the end peptide bonds, whereas, the middle peptide bond (un)folding shows a normal Arrhenius behavior. This apparent anti-Arrhenius behavior results from involvement of additional states. These results are consistent with recent evidence that the ends of AdP-like peptides are frayed.[7,12,23,25,28,29,31,37,43,75,80] We successfully model the observed

anti-Arrhenius behavior by taking into account π-bulge and 3_{10}-helical conformation melting, in addition to that of pure α-helix. This model is supported by recent studies by us and others, which report evidence for 3_{10}-helix[56,72,74,86,132-145] and π-helix/bulge[57,98,140,145-148] conformations in ala-rich peptides. Further, our model also explains the complicated nonexponential behavior observed earlier by Huang et al.[34] and Bredenbeck et al.[22] for similar peptides.

9.2 MATERIALS AND METHODS

9.2.1 Materials

The partially deuterated 21-residue alanine-based peptide (AdP) as well as its natural abundance analog AP, were synthesized by AnaSpec. Inc. The eight terminal ala at the amino end and the six terminal ala at the carboxyl end of the AdP peptide were perdeuterated while maintaining a non-deuterated center (**$A_dA_dA_dA_dA_dA_dA_dA_d$**-RAAAA-R**$A_dA_dA_dA_d$**-R**A_dA_d**, where the bold letters label the 2,3,3,3-deuterated residues).

The AdP purity as well as the position of deuterated amino-acid residues was independently verified by MALDI MS analysis kindly performed by Anton Karnoup (The Dow Chemical Company, Midland, MI). Analysis was carried out using a Voyager DE-STR MALDI-TOF mass spectrometer (Applied biosystems) operated in reflection and post-source decay (PSD) modes.

9.2.2 T-jump Raman Spectral Measurements.

The UV Raman spectrometer is described in detail elsewhere.[4,149] Briefly, the third harmonic of a Coherent Infinity Nd:YAG laser operating at 90 Hz with a 3 nsec pulse width was Raman shifted five anti-Stokes harmonics in 40 psi hydrogen gas to 204 nm to excite the amide band UVRR spectra. The Raman scattered light was collected at an angle close to backscattering and dispersed with a partially subtractive double monochromator. The Raman scattered light was

detected by using a Princeton Instruments Spec-10:400B CCD camera (Roper Scientific). We used spectral accumulation times of ~5 min with spectral resolutions of ~10 cm^{-1}.

To selectively heat the water solvent, we Raman-shifted the 1.06-μm Nd YAG fundamental to 1.9 μm (1st H_2 Stokes shift) by using a 1-m Raman shifter (Light Age Inc.; 1000 psi H_2) to obtain 1.5 mJ pulse energies at our 90 Hz repetition rate. This 1.9 μm excitation is absorbed by a water combination band and the energy is thermalized in psec by vibrational relaxation.

We studied T-jumps from 5 to 30 °C and from 20 to 40 °C. These T-jumps were obtained by focusing the 1.5 mJ 1.9 μm laser pulses to a ~300 μm diameter spot in the flowing sample stream. To ensure that the Raman signal was obtained from the sample volume maximally heated by the IR pulse[4] we adjusted the sample absorbance at 204 nm to 40 cm^{-1} by utilizing a 15 mg/ml concentration of AdP.

We independently verified the magnitude of the *T*-jump by measuring the pump beam energy dependence of the 204 nm excited ~3000 cm^{-1} water Raman band. This band shows a large, well-known frequency and band shape temperature dependence.[4,150,151] We constructed a *T*-jump calibration curve as described by Lednev et al.[4], by using the UVRR water difference spectrum in the presence versus absence of the IR pump beam to determine the actual *T*-jump in the probed volume.

There exist low temporal frequency variations of the measured Raman spectral intensities that can interfere with the T-jump spectral measurements. These variations may derive from variations in the UV laser pulse energy at the sample. Alternatively this variation may derive from low frequency motion of the sample stream, which may correlate with changes in the sample stream surface. We found that we could remove this fluctuation in the spectra by measuring for each time delay two duplicate T-jump spectra which were bracketed by identically measured cold spectra where the T-jump pump pulses were blocked. We only accepted as valid, T-jump spectra which were bracketed by essentially identical cold UVRR spectra. This allowed us to ignore the set of fluctuations which did not span the time scale of repeated T-jump measurements.

9.2.3 Uncertainties in the Nonlinear Parameter Estimation

We determined the secondary structure composition from the steady state and transient spectra for the AdP C_α-H peptide bonds in the center, and for the C_α-D penultimate amide bonds by fitting the experimentally measured spectra to a linear combination of the four basis spectra of the α-helix and PPII conformations of the C_α-H and C_α-D peptide bonds, as deteremined earlier.[127] The fits were obtained by using least-squares criteria. In this modeling, we assume that each of the amide groups scatter independently,[152] and the spectra derived from the previously determined basis spectra of the α-helix and PPII conformations,[4,120,127] taking into account that the PPII basis spectra were previously[4] incorrectly denoted as deriving from the "random coil" conformation.

We deconvoluted the 82 ºC PPII spectrum of AdP into a minimum number of bands as in Lednev et al.[4] We then determined the temperature dependence of the band intensities, bandwidths and frequencies in spectra measured of AdP at 52, 62, 70 and 82 ºC, temperatures at which AP and, thus, AdP is predominantly PPII.[4,6,120] We assumed that this observed linear temperature dependence extrapolates down to 0 ºC, and calculated the pure temperature dependent PPII spectra of AdP. Since the individual PPII peptide bonds independently contribute to the UVRR spectra,[152] the AdP PPII spectra have a 35 % contribution from the C_α-H PPII peptide bonds (7 out of 20 bonds) and a 65% contribution from the C_α-D PPII peptide bonds (13 out of 20 bonds). We subtracted the necessary amount of the temperature dependent C_α-H AP PPII spectra from the AdP PPII spectra to uniquely calculate the temperature dependent C_α-D AdP PPII spectra.

We know that AdP is ~53% α-helix-like at 5 °C.[4,6,7,145] Since AdP contains 35% C_α-H peptide bonds and 65% C_α-D peptide bonds, and the C_α-H b Raman band derives only from the C_α-H peptide bond PPII Raman spectrum,[4,126,127,131] we can determine the C_α-H PPII fraction at 5 °C directly from the C_α-H b band intensity. This C_α-H PPII fraction knowledge allows us to directly estimate the C_α-D PPII and C_α-H α-helix-like fractional compositions. We can also calculate the pure C_α-D peptide bond α-helix-like basis spectrum by subtracting the calculated 5 °C C_α-D peptide bond PPII spectrum, as well as the calculated 5 °C C_α-H peptide bond PPII and α-helix spectra from the measured 5 °C AdP spectrum. We assume that this α-helix-like basis spectrum is independent of temperature.[4,153]

We estimated the errors in our secondary structure determinations by calculating the Jacobian matrix as we iterate to the best fit solutions.[154-156] To relate the parameter standard error to the experimental error and to the Jacobian matrix we make the following assumptions: The measured spectral data are assumed to have the form

$$y_{i,j} = f(x_i; p_1, p_2, \ldots) + \varepsilon_i \qquad \textbf{[17]}$$

where the errors ε_i are assumed to be normally distributed random values with standard deviation, σ_i. The second assumption is that the true noiseless spectrum can be $f(x_i; p_1, p_2, \ldots)$ exactly modeled as for the specific set of **j** parameters $(p_1, p_2, \ldots, p_j)$. Under these assumptions we express an uncertainty bound for each individual parameter using information obtained from the variance-covariance matrix *c*, which is approximated by the Jacobian matrix[155-157] evaluated at the sum of squares minimum values p^*, which give rise to the best spectral **fit** $f(x_i; p_1^*, p_2^*, \ldots)$. Thus,

$$c(p^*) = C^{-1}(p^*) = [J^T(p^*) \cdot J(p^*)]^{-1} \qquad \textbf{[18]}$$

where J is the Jacobian $\qquad J_{i,j} = \partial f(x_i; p_1, p_2, \ldots) / \partial p_j \qquad \textbf{[19]}$.

Equation **[18]** implies the additional assumptions: *(1)* that the optimal function $f(x_i; p_1^*, p_2^*, \ldots)$ is well approximated by a multidimensional Taylor expansion around the minimum, which includes the curvature matrix $C(p^*)$ in its second-order term, and *(2)* that $C(p^*)$ is, in turn, well approximated by the product $J^T(p^*) \cdot J(p^*)$.[156,157]

The estimated standard error of the parameter p_j is

$$\sigma_j = (c_{jj} \cdot \chi^2)^{1/2} \qquad \textbf{[20]}$$

where c_{jj} refers to the diagonal element of the variance-covariance matrix and χ^2 is the reduced chi-squared statistical parameter.[154-157] χ^2 is calculated as:

$$\chi^2 = \frac{\sum_{i=0}^{n} [y_i - f(x_i; p_1, p_2, \ldots)]^2}{DOF} \qquad \textbf{[21]}$$

where DOF is the degrees of freedom, $DOF = n-j$, as previously described[158].

9.2.4 Weighting the Least-Squares Fit

We performed weighted least-squares fitting of the resulting calculated time-dependent AdP C_α-H peptide bond and C_α-D peptide bond PPII concentrations to single exponential functions to

determine relaxation rates for the center and penultimate peptide bonds. The weighted sum of squares to be minimized was evaluated as[159]:

$$\chi^2 = \frac{\sum_{i=0}^{n} w_i \cdot [t_i - f(x_i; p_1, p_2, \ \ldots\ )]^2}{\sum_{i=0}^{n} w_i} \qquad \textbf{[22]}$$

where the weights w_i are calculated from the estimated variances σ_i^2 in the fractions of AdP C_α-H peptide bond and C_α-D peptide bond PPII concentrations:

$$w_i = (1 / \sigma_i)^2 \qquad \textbf{[23]}$$

and t is the kinetic delay time after the T-jump. Equation **[20]** estimates the standard error of the calculated parameter. The reduced χ^2 was obtained as:

$$\chi^2 = \frac{\sum_{i=0}^{n} w_i \cdot [y_i - f(t_i; p_1, p_2, \ \ldots\ )]^2}{DOF \cdot \sum_{i=0}^{n} w_i} \qquad \textbf{[24]}$$

9.3 RESULTS

9.3.1 AdP UV Resonance Raman Spectra

Fig. 75 shows the 5 °C 204 nm excited UVRR spectra of aqueous solutions of the 21 amino acid residue peptides AdP and AP, where AP is the natural abundance analog of AdP. At 5 °C, AdP and AP are ~53 % α-helix-like and ~47 % PPII.[4,6,7,120,145] We previously calculated the UVRR spectra of the individual α-helix-like and PPII conformations.[7,127] Most recently we showed that the 5 °C α-helix-like conformations actually consist of ~24% pure α-helix, ~20% π-bulges/helices, and ~9% 3_{10}-helices whose spectra overlap (see below).[145]

As discussed in detail elsewhere,[127,145] α-helix-like AP conformations display a triplet of bands in the amide III region. The 1261 cm^{-1} $AmIII_{3H}$ band was originally[127] assigned to the "classical α-helix AmIII band" and involves mainly N-H b, C-N s and possibly C_α-C s. However, we recently showed that this $AmIII_{3H}$ band has contributions not only from pure α-helix conformations but also from overlapping bands due π-bulges and 3_{10}-helices at T<30 °C,

that broaden the $AmIII_{3H}$ band.[145] The 1306 cm^{-1} band was assigned to the $AmIII_2$ vibration, which mainly involves C_α-C s, N-C s, with possibly a small amount of C-N s and N-H b,[127] while the 1337 cm^{-1} band was assigned to the $AmIII_1$ band which derives from a vibration mainly involving C_α-C s and N-C s with possibly a small amount of C-N s.[127] The α-helix-like AmII band, which occurs at 1542 cm^{-1} is mainly associated with C-N s and N-H ib, while the 1647 cm^{-1} α-helix-like Am I band involves mainly C=O s.[127,160]

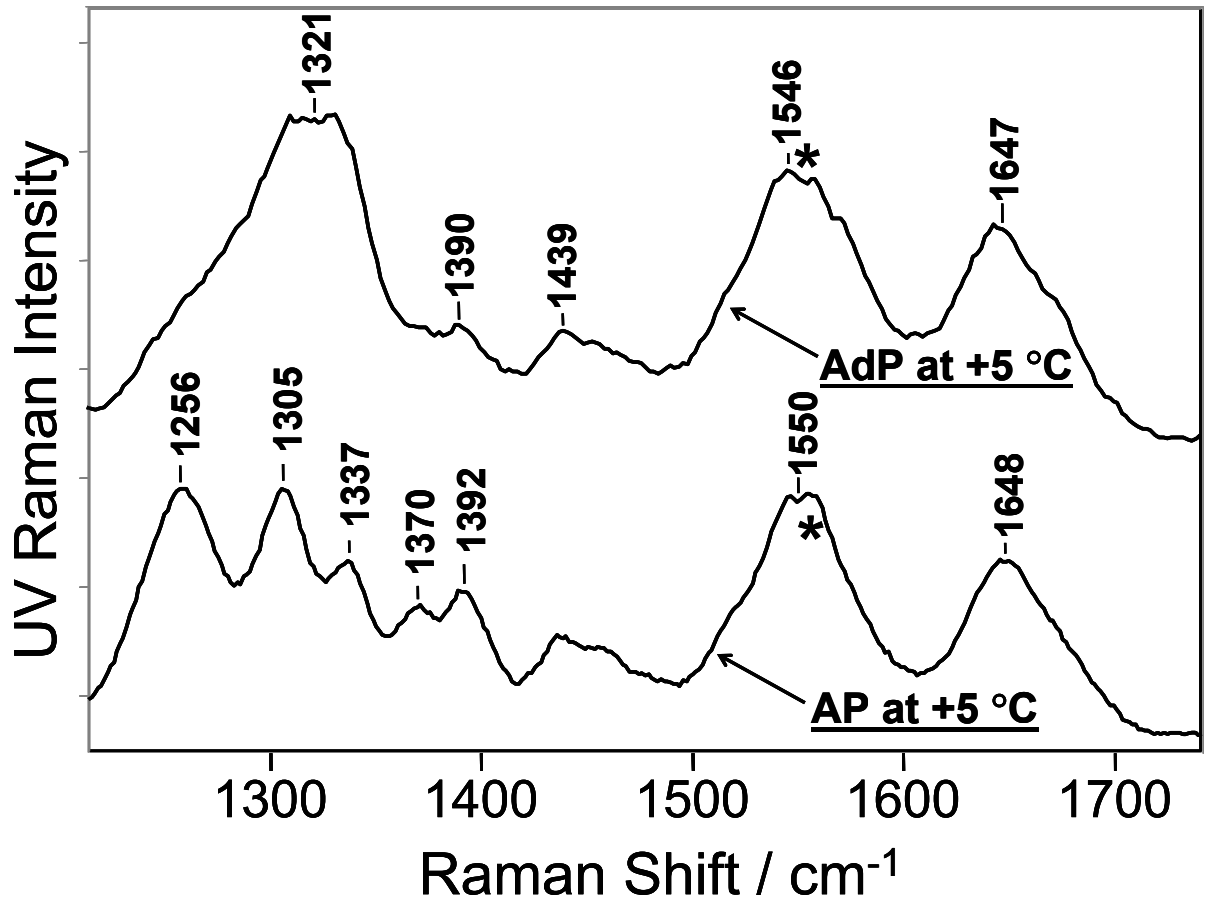

Figure 75. 204 nm UV Resonance Raman spectra of AdP (15 mg/mL) and its natural abundance analog AP (3 mg/mL) at 5 ºC. The AP solution contained 0.2 M $NaClO_4$. The star marks an overlapping molecular oxygen stretching band.

We demonstrated earlier[127] that the AmIII band triplet of the AP *PPII* conformation occurs at 1245 ($AmIII_3$), 1303 ($AmIII_2$) and 1337 cm^{-1} ($AmIII_1$), with the 1245-cm^{-1} band labeled as the "classical AmIII band". The PPII conformation of AP also shows a doublet at 1370 and

1394 cm^{-1} which mainly derives from C_α-H b with maybe some contribution from CH_3 umbrella modes. These C_α-H bands are absent in the α-helix conformation.[4,126,127,131,161]

The AP PPII conformation AmII and AmI bands are upshifted and broadened compared to those of the α-helix-like conformations.[4,127] AmII appears at 1558 cm^{-1}, while AmI appears at 1655 cm^{-1} in the PPII conformation. There are also relatively broad arg side chain bands, one of which occurs at ~1646 cm^{-1} in water and overlaps the AP AmI band.[152] In contrast, this arg band in D_2O is much sharper, and occurs at ~1614 cm^{-1}, well separated from the AmI' band.[152]

The AdP UVRR spectra are much more complex because of contributions from both C_α-H and C_α-D peptide bonds which occur in both α-helix-like and PPII conformations. Mikhonin and Asher[152] recently demonstrated that the peptide amide III – C_α-H bands region UVRR spectra result from the independent UVRR contributions of the different peptide bonds. Thus, the spectra of AdP can be considered to result from independent scattering from C_α-H and C_α-D peptide bonds in α-helix-like and PPII conformations.

The C_α-D peptide bonds show UVRR spectra[126,127] that differ from those of natural abundance AP mainly in an upshift of the C_α-D peptide bond amide III band envelope to ~1321 cm^{-1}. In AdP, the 1321 cm^{-1} band dominates the amide III spectral region (Fig. 75). Deuteration of the ala residue C_α-H decouples the NH bend from the C_α-H bending motion.[126] The resulting C_α-D amide III band no longer shows a triplet, but displays a complex bandshape with an increased Raman cross section.[7,126,127] The loss of C_α-H bending coupling leaves this band's frequency insensitive to the peptide bond conformational difference between the α-helix and PPII conformations.[7,126,127] However, the Raman cross section of this band is much larger for the PPII conformation,[127] due to the hypochromism present in the α-helix conformation.[162-171]

Although the C_α-H ala CH_3 sidechain umbrella bending vibration contributes to the 1370-1400 cm^{-1} spectral region,[160] the intensity in this region is dominated by the resonantly enhanced C_α-H b doublet of the C_α-H ala PPII conformation.[120,127] Thus, changes in PPII concentration dominate the intensity changes within this spectral region. Furthermore, the CH_3 umbrella UVRR bands are expected to be insensitive to conformational changes in the peptide backbone, as shown recently.[127]

9.3.2 Transient AdP UVRR Difference Spectra

Fig. 76 shows a series of calculated UVRR difference spectra measured at different delay times subsequent to a T-jump. The raw spectra were obtained by measuring UVRR spectra at specified delay times after the T-jump. The time delay difference spectra shown in Fig. 76 were calculated by subtracting a spectrum measured 10 nsec after the T-jump from the individual time delayed spectra. We utilized T-jumps which increased the sample temperature from 5 to 30 °C, and from 20 to 40 °C.

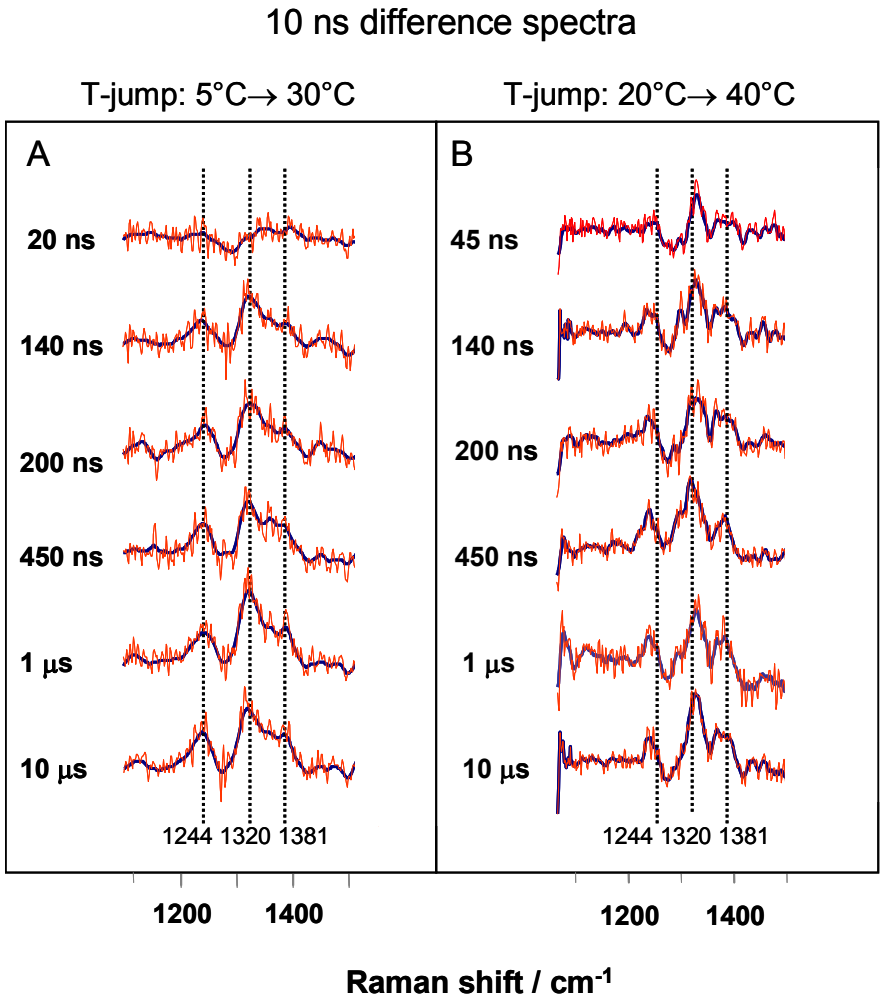

Figure 76. T-jump difference UVRR spectra of AdP at different delay times between the pump and probe laser pulses. These difference spectra were obtained by subtracting the 10 nsec delay time spectra from each of the longer delay time spectra. A. Difference spectra for a T-jump from 5 to 30 °C. B. Difference spectra for a T-jump from 20 to 40 °C.

We subtracted the 10 nsec delay spectra from the original T-jump difference spectra to selectively remove spectral changes which derive from sample non-conformational temperature changes.[4-6,120] We earlier showed that these non-conformational changes derive from a decreased hydrogen bond strength to water at elevated temperatures.[4,6,120,127,128] This allows us to concentrate on spectral alterations induced by conformational changes, which occur at later times. Our previous AP studies[4-6,120] clearly showed that no conformational changes occur until longer (>50 nsec) delay times.

The main Fig. 76 UVRR difference features occur as bands at 1320 and 1381 cm^{-1} whose intensities increase with the time delay after the T-jump. The 1320 cm^{-1} feature derives from an AmIII band intensity increase from the C_α-D peptide bonds of AdP due to the increasing PPII concentration. Melting to the PPII conformation results in hyperchromism[162-171] of the resonant absorption band and a consequent hyperchromism of the Raman cross sections.[127] The 1381 cm^{-1} intensity increase results from the appearance of the C_α-H b band of the AdP melted C_α-H PPII conformation.[120]

9.3.3 Modeling the Transient Temperature Dependence of AdP Secondary Structure

We used the calculated AP and AdP pure secondary structure-Raman spectra (PSSRS) to determine the time delay dependent secondary structure composition for each observed transient AdP UVRR spectrum at each T-jump. Fig. 77A shows the calculated temperature-dependent *PPII* C_α-H peptide bond and C_α-D peptide bond basis spectra, and the temperature-independent *α-helix* C_α-H peptide bond and C_α-D peptide bond basis spectra.[4,127]

We did not attempt to resolve the underlying pure α-helix, π-helix/bulge and 3_{10}-helix conformations recently discovered by Mikonin and Asher[145] in these transient spectra given our limited S/N. The affect of their contribution is to broaden the C_α-H peptide bond "α-helix-like" $AmIII_3$ band.[145]

We can precisely determine AdP PPII fractions for the C_α-H peptide bonds using the basis spectra, since the C_α-H b band(s) between 1380-1400 cm^{-1} (Fig. 77A)serves as an isolated, extremely sensitive non-α-helical marker.[4,126,127,131] For the C_α-D peptide bonds, C_α-D deuteration breaks the coupling between the C_α-D b and N-H b motions, which makes the C_α-D

AmIII band frequency insensitive to the Ψ Ramachandran angle.[126,127] However, it is still possible to reliably find the C_α-D PPII fraction by using the normalized basis spectra, because the intensity of the C_α-D PPII AmIII band is more than 2-fold greater than that of C_α-D "α-helix-like" AmIII band (Fig. 77A)[127] due to hypochromic excitonic interactions in the α-helix.[162-171] Using this approach we can reliably estimate the PPII fractional compositions in AdP C_α-H center peptide bonds as well as in the C_α-D end peptide bonds from the different transient spectra shown in Fig. 76 at different delay times, ***t***, subsequent to T-jumps from 5 to 30 °C, and 20 to 40 °C.

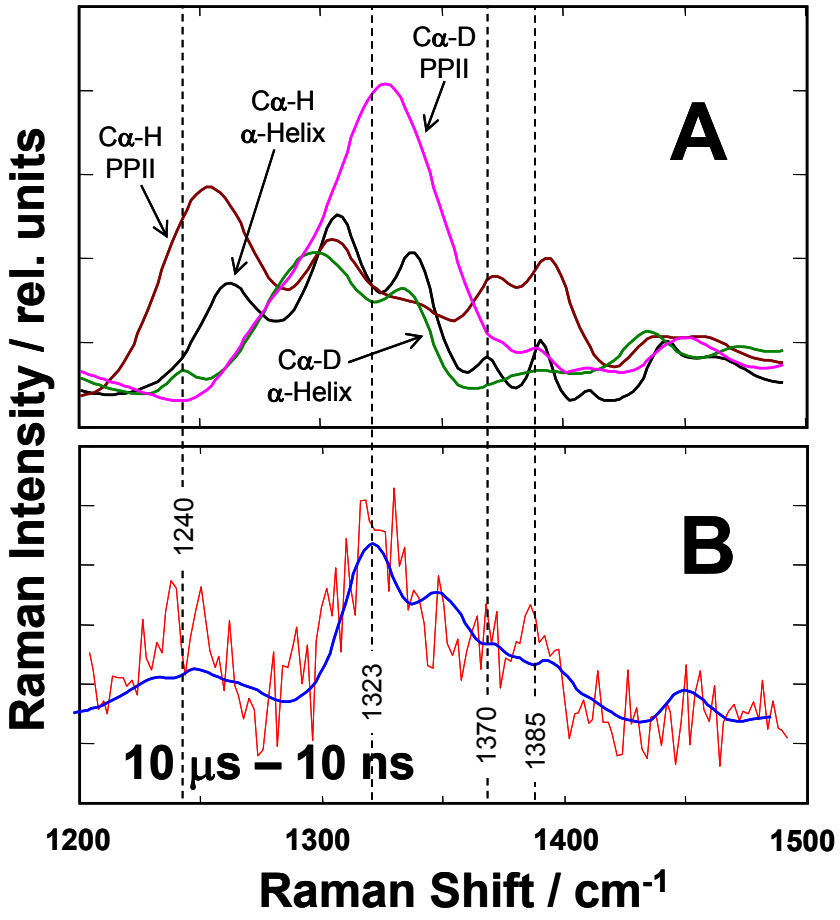

Figure 77. **A.** Calculated 30 °C pure secondary structure spectra of AdP: C_α-H peptide α-helix-like conformation (black); C_α-H peptide bond PPII conformation (brown); C_α-D peptide α-helix-like conformation (green); and C_α-D peptide PPII conformation (magenta). **B.** measured transient difference spectrum obtained after a time delay of 10 μs during a T-jump from 5 to 30 °C (red); Best fit of AmIII – C_α-H region (1200-1480 cm^{-1}) to a linear combination of the AdP basis spectra shown in Fig. 77A (blue).

9.3.4 AdP Mono-Exponential Relaxation Rates

Figs. 78A and B show the time dependence of the calculated total PPII concentration of AdP, as well as the individual end C_α-D PPII and the center C_α-H PPII concentrations for the T-jumps from 5 to 30 ºC and 20 to 40 ºC, respectively. Using mono-exponential fitting for total PPII concentration (C_α-D plus C_α-H peptide bonds), we find the relaxation time ($\tau_R=k_R^{-1}$) of 116±17 ns (Fig. 78A, Table 16) for the T-jump from 5 to 30 ºC, whereas for the T-jump from 20 to 40 ºC we find a 109±27 ns relaxation time (Fig. 78B, Table 16). These relaxation times are identical (within the experimental error) to that found earlier by Lednev and coworkers[4] for AP peptide, the natural abundance analog of AdP. Specifically Lednev et al.[4] found 180±60 ns, 120±50 ns and 70±30 ns relaxation times for T-jumps from 4 to 37 ºC, from 4 to 48 ºC and from 4 to 64 ºC, respectively.

As pointed out by Lednev et al.[4] if the α-helix melting in AdP were truly a two-state transition, the α-helix folding, k_F and unfolding rate constants, k_U could be simply calculated from the "two-state" relaxation rate constant relationship $k_R = k_U + k_F$, and from the two-state equilibrium constant $K_{EQ}= k_U/k_F$ independently obtained from the measured equilibrium UVRR spectra.[4,7] If we use the two-state model, then the C_α-H center (un)folding rate constant shows a "normal" Arrhenius behavior. In contrast, the C_α-D ends folding rate constant decreases with increasing temperature. This is an apparent anti-Arrhenius behavior (with negative folding activation barrier).

As expected, the end peptide bonds melt at lower temperatures than do the middle peptide bonds.[7] However, our kinetic results are quite unusual. For the 5 to 30 ºC we calculate a 2-fold faster relaxation time for the end peptide bonds (97±15 ns, Fig. 78C) than that of the middle (189±31 ns, Fig. 78E). In contrast, for the 20 to 40 ºC T-jump we calculate a somewhat slower relaxation time for the end peptide bonds (131±46 ns, Fig. 78D) than the middle (56±6 ns, Fig. 78F).

If this data are modeled as if they result from a two-state transition, we find that the folding rate constants for the AdP end peptide bonds show the strong anti-Arrhenius behavior with negative activation energy barrier (Table 16). In contrast, we find that all the (un)folding

rate constants for the AdP center peptide bonds show the normal Arrhenius-like behavior with positive activation energy barriers (Table 16).

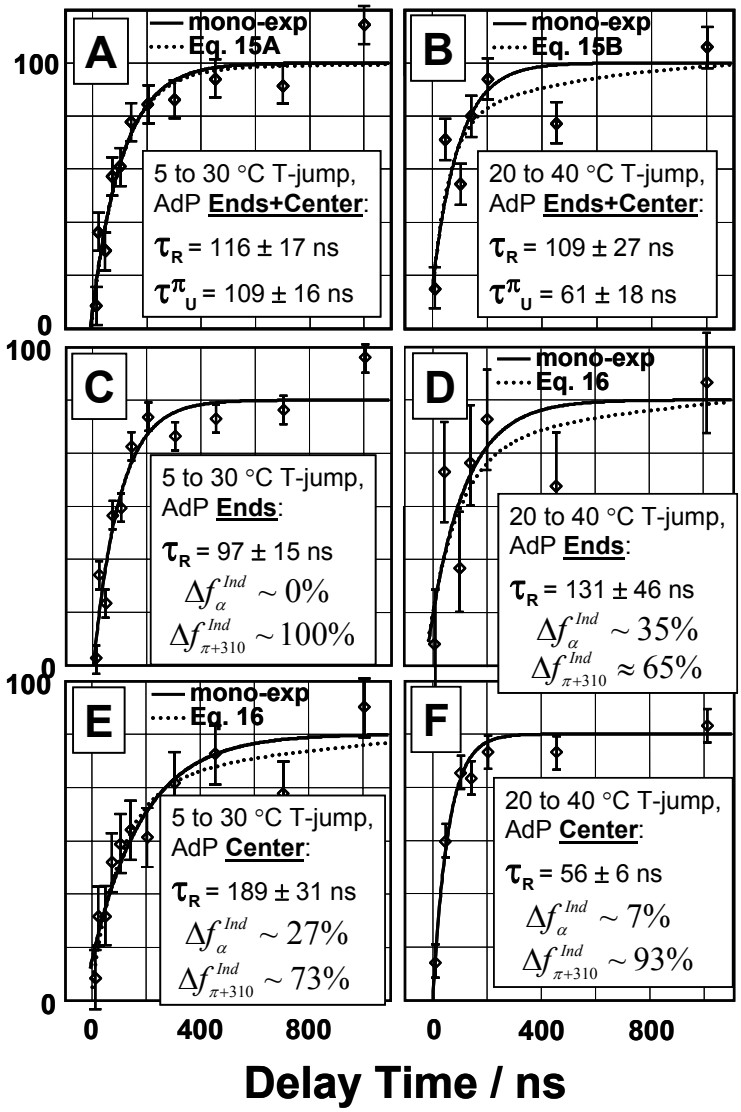

Figure 78. T-jump relaxation of the total PPII concentration (A and B) as well as the PPII concentrations of the end C_α-D (C and D) and center peptide bonds (E and F) due to T-jumps from 5 to 30 °C and 20 to 40 °C. Unfolding is monitored by changes in the relative compositions of the basis spectra shown in Fig. 77. The mono-exponential relaxation times are τ_{total} = 114 ± 46 ns, τ_{end} = 89 ±17 ns and τ_{cen} = 188 ± 46 ns for the T-jump from 5 to 30 ºC; and τ_{total} = 96 ± 39 ns, τ_{end} = 122±51 ns and τ_{cen} = 54 ± 11 ns for the T-jump from 20 to 40 °C. The dotted lines in Figs. 78A and 78B are fits to the Eq. 31 kinetics for the total PPII concentrations. These fits find the unfolding times, τ^{π}_{U}, for π-bulges (or 3_{10}-helices) of 109±24 ns for the 5 to 30 ºCT-jump and 61±23 ns for the 20 to 40 ºC T-jump. The dotted lines in Figs. 78C-F are fits to the Eq. 32 kinetics for the individual C_α-H and C_α-D PPII concentrations. These fits find the relative fractional contributions of slow melting α-helices (Δf_{α}^{Ind}) and fast melting π-bulges and 3_{10}-helices ($\Delta f_{\pi+310}^{Ind}$) to the individual melting kinetics of AdP C_α-H center and C_α-D ends peptide bonds.

Table 16. Two-State Kinetic Parameters and Equilibrium Constants for α-Helix↔PPII Conformational Transition Calculated for AdP, AdP, and the C_α-H Center and AdP C_α-D End Peptide Bonds

	Final T-jump Temperature,° C		Activation Energy,
	+30 °C	+40 °C	ΔG, kcal/mol·PB
Relaxation time, $\tau_R=(k_R)^{-1}$ / ns			
C_α-H + C_α-D	116 ± 17 ns	109 ± 27 ns	1.0 ± 5.5
C_α-H Center	189 ± 31 ns	56 ± 6 ns	22.8 ± 3.6
C_α-D Ends	97 ± 15 ns	131 ± 46 ns	–5.6 ± 7.3
Equilibrium constant,[a] $K_{EQ}=f_{PPII}/f_\alpha$			
C_α-H + C_α-D	3.35	5.25	
C_α-H Center	0.75	2.03	
C_α-D Ends	9.0	19.0	
Unfolding time constant, $\tau_U=(k_U)^{-1}$, ns			
C_α-H + C_α-D	150 ± 28 ns	130 ± 39 ns	2.7 ± 6.5
C_α-H Center	440 ± 100 ns	84 ± 11 ns	31.2 ± 4.9
C_α-D Ends	108 ± 19 ns	138 ± 51 ns	–4.6 ± 7.7
Folding time constant, $\tau_F=(k_F)^{-1}$, ns			
C_α-H + C_α-D	502 ± 91 ns	684 ± 202 ns	–5.8 ± 6.5
C_α-H Center	332 ± 75 ns	164 ± 21 ns	13.3 ± 4.9
C_α-D Ends	971 ± 167 ns	2620 ± 970 ns	–18.7 ± 7.7

[a] Equilibrium constant between α-helix-like and PPII conformations (see text for detail).

The anti-Arrhenius behavior of AdP ends folding rate constants indicates that the AdP ends melting is clearly not a two-state state process, and that the additional states must be involved in the α-helix melting. This is consistent with the recent reports that indicate that the ends of AP and AdP-like peptides are frayed.[7,12,23,25,28,29,31,37,43,75,80]

In contrast, the normal Arrhenius-like behavior of AdP center (un)folding rate constants, at the first glance, could indicate that the AdP center melting occurs in "two-state-like" mechanism. However, the Table 16 calculated "two-state" activation energy barriers of ~10-35 kcal/mol·peptide bond (kcal/mol·PB) are much higher than those of ~2–4 kcal/mol·PB estimated earlier for ala-rich peptides both theoretically[56,89,93] and experimentally.[145] Below, we explain this unusual kinetic behaviors of both AdP ends and AdP center in terms of competition between the slower melting pure α-helices, and faster melting π-bulges and 3_{10}-helices.

9.4 DISCUSSION

We show below that this apparent anti-Arrhenius behavior (Table 16) is the result of the failure of the two-state model to describe both the conformational equilibrium and the dynamics of AP or AdP melting. As shown below, we can model the observed melting behavior by including the melting of 3_{10}-helical and π-bulge conformational states,[145] in addition to that of pure α-helix (Fig. 79 and Table 17). This modeling explains the observed apparent anti-Arrhenius behavior (Table 16). The individual (un)folding rate constants for pure α-helices, π-bulges and 3_{10}-helices show normal Arrhenius behavior (Table 18).

9.4.1 Resolved AdP Equilibrium Melting Curves show melting of α-Helix, π-Helix/Bulge and 3_{10}-Helix Conformations

Recently we showed that the "α-helix-like" UVRR spectra of AP, which is the natural abundance analog of AdP contains contributions from π-bulges/helices and 3_{10}-helices.[145] Fig. 79 shows the melting curves for AP (and, thus, AdP) and demonstrates that the pure α-helix, π-helix/bulge and 3_{10}-helix conformations have different melting curves. The π-bulges/helices and 3_{10}-helices melt at lower temperatures than the pure α-helices, and are fully melted by 30 °C. The decreased T_m values for the π-bulge and 3_{10}-helix conformations results from their less optimized intra-peptide hydrogen bonding compared to that of the α-helix. The more solvent

exposed π-bulges[172] and 3_{10}-helices (type III turns)[173] populate due to the increased *peptide bond-water* hydrogen bond strengths at lower temperatures.[4,120,127,128]

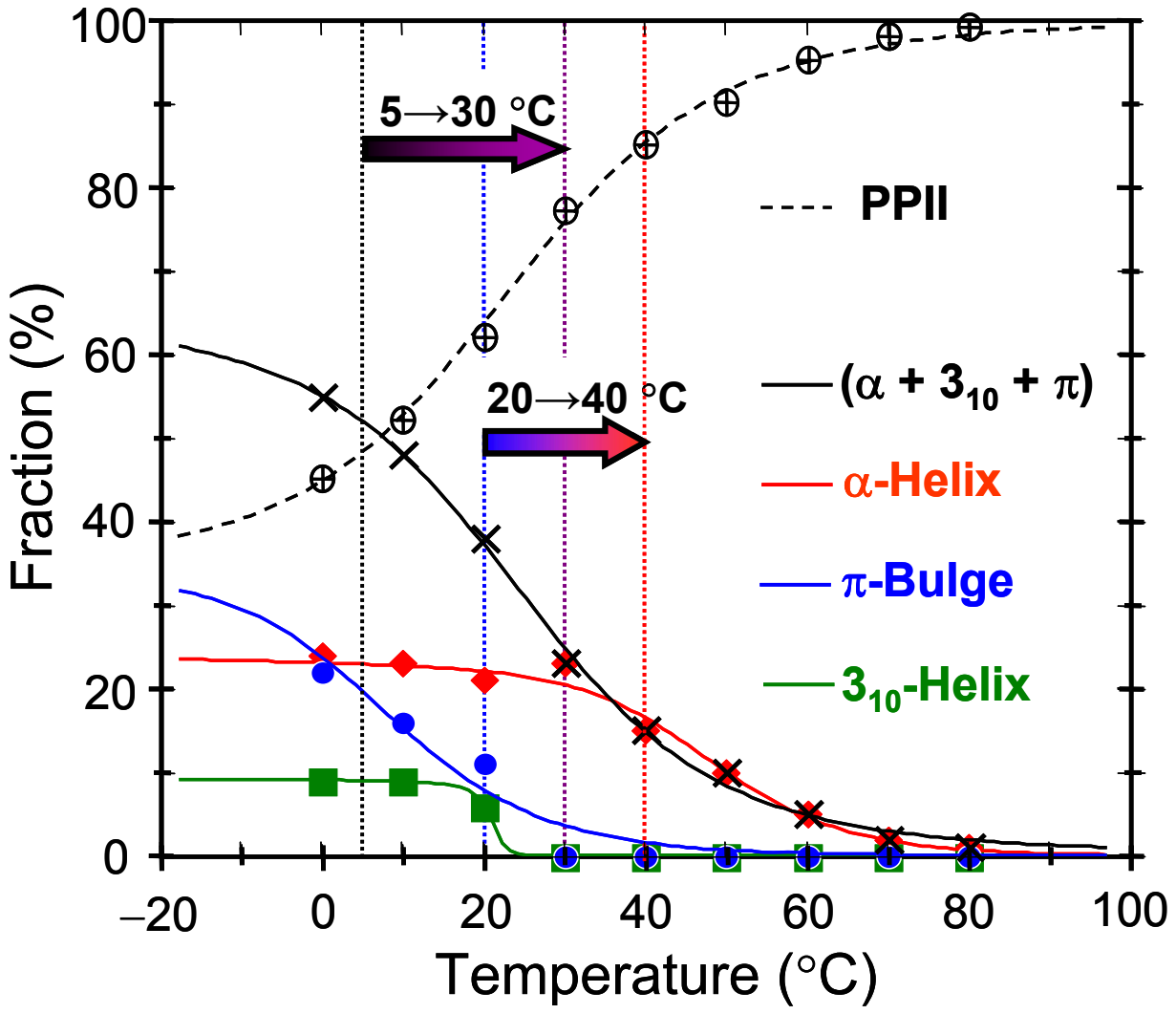

Figure 79. Melting/formation curves for AdP "α-helix-like" conformations. (×) – Original "α-helix" melting curve as reported for the natural abundance analog of AdP, AP, by Lednev et al.[4,6], which is actually the sum of the individual α- π- and 3_{10}-helical melting curves; (♦) – Pure α-helix melting; (■) – 3_{10}-helix (type III turn) melting; (●)– π-bulge (π-helix) melting; (⊕) – PPII formation. Arrows show the conformational differences spanned by the 5 to 30 °C and 20 to 40 °C T-jumps. Adapted from Ref[145].

The arrows in Fig. 79 show the temperature intervals for the 5→30 °C and 20→40 °C T-jumps, while Table 17 summarizes the α-helical, 3_{10}-helical and π-bulge/helical fractions of AdP at initial and final T-jump temperatures. Clearly, different conformations are melting to the PPII

conformation at the different intial and final T-jump temperatures. These different conformations have different (un)folding rates and different relative contributions to the net AP melting kinetics at the different temperatures (Fig. 79).

Table 17. Total equilibrium concentrations of AdP α-helix like conformations (including both C_α-H and C_α-D peptide bonds) at initial and final T-jump temperatures

Temperature, °C	α-helix fraction[a], %	π-helix/bulge fraction[a], %	3_{10}-helix fraction[a], %	Total α-helix-like fraction[b], %
+5 °C	24%	20%	9%	53%
+30 °C	23%	0%	0%	23%
	$\Delta f_\alpha = 1\%$	$\Delta f_\pi = 20\%$	$\Delta f_{310} = 9\%$	$\Delta f_{\alpha+\pi+310} = 30\%$
+20 °C	22%	11%	6%	39%
+40 °C	15%	0%	0%	15%
	$\Delta f_\alpha = 7\%$	$\Delta f_\pi = 11\%$	$\Delta f_{310} = 6\%$	$\Delta f_{\alpha+\pi+310} = 24\%$

[a] We assume that AdP contains the same fractions of α-helix-like conformations as its natural abundance analog, AP[145].

[b] As was originally reported by Lednev et al.[4,6], since it was not possible at that time to discriminate between the different α-helix-like conformations.

Below we show that the AdP π-bulge and 3_{10}-helix conformations have ~12-fold faster unfolding rates than that of pure α-helix conformation (Table 18). Thus, the lower temperature T-jumps predominantly samples the faster melting π-bulge and 3_{10}-helix conformations (Fig. 79). In contrast, the higher temperature T-jump (Fig. 79) samples a larger fraction of pure α-helix melting with slower (un)folding rates.

9.4.2 Model for the Summed C_α-H and C_α-D Peptide Bonds AdP Kinetics

We expect that the relaxations of the π, 3_{10}, and α-helical conformations occur in parallel. This results in mono-exponential relaxations for these conformations with relaxation times, which are determined by their activation free energy barriers, which separate each "α-helix-like"

conformations from the PPII basin conformation. We expect identical attempt frequencies since the motions will involve similar Ψ torsional motions.

The relative contribution of each relaxation to the overall kinetics is determined by the differences in equilibrium fractions of each conformation between the final and initial T-jump temperatures (Table 17).

Thus, the time dependence of the fractional PPII conformation (summing both the C_α-H and C_α-D peptide bonds) subsequent to the T-jump is:

$$f_{PPII}^{Ti\rightarrow Tf}(t) \cong f_{PPII}^{Tf}(\infty) - \Delta f_{\pi} \cdot \exp[-(k_U^{\pi} + k_F^{\pi}) \cdot t] - \\ - \Delta f_{310} \cdot \exp[-(k_U^{310} + k_F^{310}) \cdot t] - \Delta f_{\alpha} \cdot \exp[-(k_U^{\alpha} + k_F^{\alpha}) \cdot t] \qquad \textbf{[25]}$$

where $f_{PPII}^{Ti\rightarrow Tf}(t)$ is the PPII fraction monitored at delay time ***t*** for the T-jump between the initial, *Ti* and final temperatures, *Tf*; $f_{PPII}^{Tf}(\infty)$ is the known equilibrium PPII fraction at *Tf* (Table 17); while $\Delta f_{\pi,310,\alpha} = f_{\pi,310,\alpha}(Ti) - f_{\pi,310,\alpha}(Tf)$ are the known differences in the equilibrium fractions of the π, 3_{10}, and α-helical conformations at *Ti* and *Tf* (Table 17). $k_U^{\pi,310,\alpha}$ and $k_F^{\pi,310,\alpha}$ are the ***unknown*** unfolding and folding rate constants of the π-bulges, 3_{10}-helices and α-helices, respectively, at *Tf*.

Inserting the corresponding α-helix, π-bulge, 3_{10}-helix and PPII fractions from Table 17 we can describe the time dependence of the PPII fractions for the 5→30 °C and 20→40 °C T-jumps:

$$f_{PPII}^{5\rightarrow 30^{o}C}(t) = 0.77 - 0.2 \cdot \exp[-(k_U^{\pi} + k_F^{\pi}) \cdot t] - \\ - 0.09 \cdot \exp[-(k_U^{310} + k_F^{310}) \cdot t] - 0.01 \cdot \exp[-(k_U^{\alpha} + k_F^{\alpha}) \cdot t] \qquad \textbf{[26A]}$$

$$f_{PPII}^{20\rightarrow 40^{o}C}(t) = 0.84 - 0.11 \cdot \exp[-(k_U^{\pi} + k_F^{\pi}) \cdot t] - \\ - 0.06 \cdot \exp[-(k_U^{310} + k_F^{310}) \cdot t] - 0.07 \cdot \exp[-(k_U^{\alpha} + k_F^{\alpha}) \cdot t] \qquad \textbf{[26B]}$$

At the final T-jump temperatures of 30 and 40 °C, there are essentially no π-bulges and 3_{10}-helices left (Table 17 and Fig. 79). Thus, $k_U^{\pi} >> k_F^{\pi}$ and $k_U^{310} >> k_F^{310}$. Indicating that:

$$f_{PPII}^{5\to 30^{o}C}(t) \cong 0.77 - 0.2\cdot\exp[-k_U^{\pi}\cdot t] - 0.09\cdot\exp[-k_U^{310}\cdot t] - \quad \textbf{[27A]}$$
$$- 0.01\cdot\exp[-(k_U^{\alpha}+k_F^{\alpha})\cdot t]$$

$$f_{PPII}^{20\to 40^{o}C}(t) \cong 0.84 - 0.11\cdot\exp[-k_U^{\pi}\cdot t] - 0.06\cdot\exp[-k_U^{310}\cdot t] - \quad \textbf{[27B]}$$
$$- 0.07\cdot\exp[-(k_U^{\alpha}+k_F^{\alpha})\cdot t]$$

As discussed in the Appendix (Fig. 88), the Gibbs free energy activation barriers for unfolding of the π-bulge and 3_{10}-helix conformations are essentially identical. Thus, their unfolding rate constants will be equal and:

$$f_{PPII}^{5\to 30^{o}C}(t) \cong 0.77 - 0.29\cdot\exp[-k_U^{\pi}\cdot t] - 0.01\cdot\exp[-(k_U^{\alpha}+k_F^{\alpha})\cdot t] \quad \textbf{[28A]}$$

$$f_{PPII}^{20\to 40^{o}C}(t) \cong 0.84 - 0.17\cdot\exp[-k_U^{\pi}\cdot t] - 0.07\cdot\exp[-(k_U^{\alpha}+k_F^{\alpha})\cdot t] \quad \textbf{[28B]}$$

Also as shown in the Appendix (Fig. 88), the AdP pure α-helix conformation is stabilized by ~1.5 kcal/mol·PB with respect to both π-bulge and 3_{10}-helix conformations (at T≥+30 °C). Thus, we can estimate the ratio between the α-helix and π-bulge (3_{10}-helix) unfolding rate constants as:

$$k_U^{\pi} \approx k_U^{310} \cong k_U^{\alpha}\cdot\exp(+\frac{1.5\ kcal/mol}{R\cdot T}) \quad \textbf{[29]}$$

Thus, we estimate that at 30 °C: $k_U^{\pi} \approx k_U^{310} \cong 12.1\cdot k_U^{\alpha}$, whereas at 40 °C $k_U^{\pi} \approx k_U^{310} \cong 11.1\cdot k_U^{\alpha}$.

Since only pure α-helix remains at the *Tf* values of 30 °C and 40 °C. Thus:

$$k_F^{\alpha} = K_{EQ}^{-1}\cdot k_U^{\alpha} = \frac{f_{\alpha}(Tf)}{f_{PPII}(Tf)}\cdot k_U^{\alpha} \quad \textbf{[30]}$$

where $K_{EQ} = f_{PPII}(Tf)/f_{\alpha}(Tf) = k_U^{\alpha}/k_F^{\alpha}$ is the known equilibrium constant for the pure α-helix↔PPII melting (Tables 16 and 18); $f_{\alpha,PPII}(Tf)$ are the known equilibrium pure α-helix and PPII fractions at *Tf* (Table 17).

Thus, we estimate that the "apparent two-state relaxation constant"

at +30°C to be: $k_U^{\alpha} + k_F^{\alpha} \cong 1.3\cdot k_U^{\alpha} \cong 0.11\cdot k_U^{\pi}$

and at +40 °C to be: $k_U^{\alpha} + k_F^{\alpha} \cong 1.2\cdot k_U^{\alpha} \cong 0.11\cdot k_U^{\pi}$

Thus, we can further simplify Eqs 28A and 28B:

$$f_{PPII}^{5\rightarrow 30^{\circ}C}(t) \cong 0.77 - 0.29 \cdot \exp[-k_U^{\pi} \cdot t] - 0.01 \cdot \exp[-(0.11 \cdot k_U^{\pi}) \cdot t] \quad \textbf{[31A]}$$

$$f_{PPII}^{20\rightarrow 40^{\circ}C}(t) \cong 0.84 - 0.17 \cdot \exp[-k_U^{\pi} \cdot t] - 0.07 \cdot \exp[-(0.11 \cdot k_U^{\pi}) \cdot t] \quad \textbf{[31B]}$$

The Eq. 31A fit to the summed C_α-H and C_α-D peptide bond kinetics (Fig. 78A dotted line) is slightly improved compared to the original mono-exponential fit (Fig. 78A solid line); while the Eq. 31B fit (Fig 78B dotted line) is significantly improved compared to the monoexponential fit (Fig. 78B solid line).

Specifically, the pure α-helix relaxation time (τ_R) at +30 °C is 1017±148 nsec, while the relaxation times for the π-bulge and 3_{10}-helix conformations at +30 °C are much faster, 109±16 ns (Table 18). At 40 °C the relaxation times decrease; the pure α-helix relaxation time at +40 °C is 568±165 nsec, while the π-bulge and 3_{10}-helix conformation relaxation times decrease to 61±18 nsec. These results are striking, since they indicate that the pure α-helix melting is much slower than the 100–200 ns times, which are typically reported for ~20 residues-long alanine-rich peptides.[4-6,10,13,17,18,22,25,32-35] This discreapancy derives from the previous inability to discriminate between the different α-helix like conformations (Fig. 79 and Table 18).

In addition, our results here explain the complicated non-exponential and/or multi-exponential behavior of melting kinetics of alanine-rich peptides previously observed.[22,34] Specifically, the heterogeneity of the low temperature α-helical ensembles (Fig. 79) explains the observed complicated kinetic behavior for low initial T-jump temperatures.[22,34] In contrast, the homogeneity of the above room temperature α-helical ensembles (Fig. 79) explains the essentially mono-exponential melting behavior of these peptides for higher initial temperature T-jumps.[22,34]

Table 18. Eqns 31 Kinetic parameters for AdP pure α-Helix, π-Bulge and 3_{10}-Helix (un)folding, calculated from the overall (C_α-H and C_α-D peptide bond) kinetic and equilibrium data, as well as that of Eq. 32 calculated from the individual C_α-H center peptide bonds and and C_α-D end peptide bond kinetic and equilibrium data

	Final T-jump Temperature,° C		Activation Energy,
	+30 °C	+40 °C	ΔG / kcal/mol·PB
Equilibrium constant [a], $\mathbf{K_{EQ}=f_{PPII}/f_\alpha}$			
C_α-H + C_α-D	3.35	5.25	
C_α-H Center	0.75	2.03	
C_α-D Ends	9.0	19.0	
Mono-exp relaxation time, $\tau_R=(k_R)^{-1}$ / ns			
C_α-H + C_α-D	116 ± 17 ns	109 ± 27 ns	1.0 ± 5.5
C_α-H Center	189 ± 31 ns	56 ± 6 ns	22.8 ± 3.6
C_α-D Ends	97 ± 15 ns	131 ± 46 ns	–5.6 ± 7.3
Pure conformation **folding** time, $\tau_F = (k_F)^{-1}$ / ns			
Pure α-Helix [b]	4421 ± 802 ns	3553 ± 1207 ns	4.1 ± 7.2
π-Bulge and/or 3_{10}-Helix [b]	τ_F >> 109 ns	τ_F >> 61 ns	4.1 ± 7.2 [c]
Pure conformation **unfolding** time, $\tau_U = (k_U)^{-1}$ / ns			
Pure α-Helix [b]	1321 ± 239 ns	677 ± 230 ns	12.6 ± 7.2
π-Bulge and/or 3_{10}-Helix [b]	109 ± 16 ns	61 ± 18 ns	11.0 ± 6.2
Pure conformation relaxation time, $(1/\tau_U + 1/\tau_F)^{-1}$ / ns			
Pure α-Helix [b]	1017 ± 148 ns	568 ± 165 ns	11.0 ± 6.2
π-Bulge and/or 3_{10}-Helix [b]	109 ± 16 ns	61 ± 18 ns	11.0 ± 6.2
Relative contributions of ***slower*** pure α-helix relaxation to the observed relaxation kinetics, Δf_α / %			

C_α-H + C_α-D [b]	5 ± 8 %	29 ± 14 %	
C_α-H Center [d]	27 ± 9 %	7 ± 12 %	
C_α-D Ends [d]	−3 ± 9 %	35 ± 22 %	
Relative contributions of ***faster*** π-bulges and 3_{10}-helix relaxations to the observed relaxation kinetics, $\Delta f_{\pi+310}$ / %			
C_α-H + C_α-D [b]	95 ± 8 %	69 ± 14 %	
C_α-H Center [d]	73 ± 9 %	93 ± 12 %	
C_α-D Ends [d]	103 ± 9 %	65 ± 22 %	

[a] These data are identical to those in Table 16. However here we recognize that for T≥+30 °C that the equilibrium includes only the pure α-helix and the PPII conformations[145] (see text for detail). Data from Ianoul et al[7].

[b] We calculated these parameters from the overall (C_α-H and C_α-D peptide bond) kinetic data using Eqs. 31A and 31B and the equilibrium data summarized in Table 17 (see text for detail).

[c] We assume that the activation energy barriers for both the π-bulge and 3_{10}-helix formation (folding) are equal to that of the pure α-helix, because formation of α-helix, π-bulge and 3_{10}-helix conformations should start from the same (presumably PPII) basin, and pass through the same intermediate "turn" region of the Ramachandran plot.

[d] We calculated these parameters from the individual C_α-H center and C_α-D end peptide bond kinetic data using Eq. 32 (see text for detail).

9.4.3 Model for Individual C_α-H Center and C_α-D End Peptide Bonds Melting Kinetics

Table 18 summarizes our pure α-helix, π-bulge and 3_{10}-helix folding and unfolding rate constants that we determined by fitting the overall (C_α-D plus C_α-H peptide bond) kinetic data to Eqns 31A and 31B. If we assume that the (un)folding rates of the π, 3_{10}, and α-helical conformations are independent of location along the AdP chain, we can estimate the relative contributions of both the slow α-helix melting, and fast 3_{10}-helix and π-bulge melting to the observed individual relaxation kinetics of C_α-D *end* and C_α-H *center* peptide bonds using the following equation:

$$f_{PPII}^{Ti\rightarrow Tf}(t) \cong f_{PPII}^{Tf}(\infty) - \Delta f_{\pi+310}^{Ind} \cdot \exp[-t/\tau_{\pi+310}] - \Delta f_{\alpha}^{Ind} \cdot \exp[-t/\tau_{\alpha}] \quad \textbf{[32]}$$

where $f_{PPII}^{Ti\rightarrow Tf}(t)$ is the time dependent PPII concentration for the C_α-D or the C_α-H peptide bonds; $f_{PPII}^{Tf}(\infty)$ is the known equilibrium C_α-D or C_α-H peptide bond PPII fraction at *Tf* (Tables 16 and 18); $\Delta f_{\pi+310}^{Ind}$ is the ***unknown*** weighted contribution of π-bulges and 3_{10}-helices melting to the observed individual C_α-D (or C_α-H) peptide bond kinetics; Δf_{α}^{Ind} is the ***unknown*** weighted contribution of pure α-helix melting to the observed individual C_α-D (or C_α-H) peptide bond kinetics, τ_α and $\tau_{\pi+310}$ are the known relaxation times for the pure α-helix, π-bulge and 3_{10}-helix conformations (Table 18).

Thus, we find the relative contributions of the slow α-helix melting (Δf_{α}^{Ind}) and fast 3_{10}-helix and π-bulge melting ($\Delta f_{\pi+310}^{Ind}$) to the observed individual relaxation kinetics of C_α-D *end* and C_α-H *center* peptide bonds (after the 5→30 °C and 20→40 °C T-jumps) by fitting the experimental data (Figs. 78C-F) to Eq. 32 above. The calculated fractions are summarized in Table 18.

9.4.4 Dynamics of End C_α-D Peptide Bond Unfolding

Figs. 78C and 78D show the time-dependence of the calculated PPII concentration of the C_α-D ends peptide bonds as a result of the T-jumps from 5 to 30 ºC and 20 to 40 ºC, respectively. If the time dependent changes in the C_α-D peptide bond PPII concentration were modeled assuming mono-exponential decays, we find that the C_α-D end peptide bonds show a relaxation time ($k_{R\text{-}Ends}^{-1}$) of 97±15 ns (Fig. 80C) for the 5 to 30 °C *T*-jump, whereas for the 20 to 40 °C *T*-jump we obtain a relaxation time of 131±46 ns (Fig. 78D).

The fast mono-exponential relaxation time of 97 ± 15 ns found for the 5 to 30 °C *T*-jump (Fig. 78C and Table 18), indicates that the melting kinetics of C_α-D end peptide bonds is contributed mainly by the melting of π-bulges and 3_{10}-helices (109±16 ns at +30 °C). Using Eq. 32, we estimate that the C_α-D end kinetics is essentially completely due to melting of π-bulges and 3_{10}-helices, without contributions from pure α-helix melting for the 5 to 30 °C *T*-jump (Fig. 78C and Table 18).

In contrast, the relaxation time of 131±46 ns found for the 20 to 40 °C *T*-jump (Fig. 78D and Table 18) indicates that in addition to fast π-bulge and 3_{10}-helix melting (61±18 ns at +40

°C), there is also a contribution of slow α-helix melting (568±165 ns at +40 °C). Using Eq. 32, we roughly estimate that in this case the C_α-D end peptide bonds kinetics is still dominated by the melting of π-bulges and 3_{10}-helices (~65%) but there is also a ~35% contribution from the pure α-helix melting of (Fig. 78D and Table 18).

Summarizing, we observe that the melting kinetics of C_α-D end peptide bonds is dominated by the faster melting of π-bulges and 3_{10}-helices over the slower melting of pure α-helices for both 5→30 °C and 20→40 °C *T*-jumps. These results are consistent with the with the number of recent studies, which propose that the α-helical ends are frayed.[7,25,28,29,31,32,37,43,75,80] They are also consistent with the recent NMR and ESR results of Millhauser and coworkers[133,138] as well as with that of Sorin and Pande's MD simulation studies[72], which report that 3_{10}-helices tend to occur at the ends of α-helical segments in ala rich peptides.

9.4.5 Dynamics of Center C_α-H Peptide Bond Unfolding

Figs. 78E and 78F show the time-dependent changes in the PPII concentration of the central AdP C_α-H peptide bonds due to the T-jumps from 5 to 30 ºC and from 20 to 40 ºC. The unfolding kinetics of C_α-H peptide bonds shown in Figs. 78E and 78F, depend upon the T-jump initial and final temperatures. We find that for the 5 to 30 °C *T*-jump the C_α-H peptide bonds show a 189±31 ns mono-exponential unfolding relaxation time (Fig. 78E), while for the 20 to 40 °C T-jump we obtained 56±6 ns relaxation time (Fig. 78F).

The 189±31 ns mono-exponential relaxation time calculated for the 5 to 30 °C T-jump (Fig. 78C and Table 18) indicates that the slow α-helix melting (1017±148 ns at 30 °C) contributes to the observed kinetics. However, the observed kinetics is dominated by the fast π-bulge and 3_{10}-helix melting (109±16 ns at 30 °C). Using Eq. 32 (Fig. 78D dotted line), we roughly estimate a ~73% contribution from the π-bulges and 3_{10}-helices to the C_α-H center peptide bonds kinetics; and a ~27% contribution from pure α-helix melting (Fig. 78D and Table 18).

In contrast, the 56±6 ns mono-exponential relaxation time found for the 20 to 40 °C T-jump (Fig. 78D, Table 18), surprisingly indicates that the C_α-H center peptide bond kinetics are dominated by π-bulge and 3_{10}-helix melting (61±18 ns at 40 °C), with little contribution of slow

α-helix melting (568±165 ns at 40 °C). This is a surprising result, since at 20 °C "α-helix-like" segments[6] are assumed to preferrentially occur in the middle of the peptide, and thus α-helix melting should dominate the observed C_α-H center peptide bond kinetics. This suggests that the α-helix stability/propensity in AdP is position-dependent (see below). Specifically, we suggest below that the AdP N-terminus has the higher α-helical propensity than does the AdP middle and C-terminal regions.

9.4.6 Dynamics of Center C_α-H versus End C_α-D Peptide Bond Unfolding

The Figs. 78C and 78E show that for the 5 to 30 °C T-jump, the AdP center unfolds slower (189±31 ns) than do the ends (97±15 ns). We also estimated that at 30 °C the relaxation time of pure α-helices is 1017±148 ns, whereas that of π-bulges and 3_{10}-helices is 109±16 ns (Table 18). If the relaxation rates of these "α-helix-like" species are independent of location in the AdP chain, we can conclude that the melting of π-bulges and 3_{10}-helices dominate both the AdP C_α-D ends (~100%) and C_α-H center (~73%) melting kinetics (Table 18). However, pure α-helix melting also have a small contribution (~27%) to the C_α-H center melting kinetics for the 5 to 30 °C T-jump (Table 18). These kinetic results are consistent with the Fig. 79 equilibrium melting curves obtained for pure α-helix, π-bulge and 3_{10}-helix conformations,[145] as well as with the earlier studies of us[7] and others[12,23,25,28,29,31,37,43,75,80], which indicate that the ends of AdP-like peptides are frayed.

In contrast, for the 20 to 40 °C T-jump, the center of AdP unfolds faster (56±6 ns, Fig. 78F) than do the ends (131±46 ns, Fig. 78D). The faster center melting for the 20 to 40 °C T-jump, especially given the higher T_m of the center peptide bonds[7] appears initially surprising. We suggest that the faster melting of π-bulges and 3_{10}-helices still dominate both the C_α-H center (~93%) and C_α-D ends (~65%) melting kinetics. However, we surprisingly find that the pure α-helix melting contributes ~35% to the C_α-D ends melting kinetics, and contributes very little to the C_α-H center kinetics (Table 18). These results can only be understood if one of the AdP termini has a significantly higher pure α-helix propensity than the AdP center and the other terminus.

We propose that the AdP N-terminus has a higher α-helix propensity, than the middle and C-terminus. Such a preference would derive from the AdP primary sequence. Specifically, the N-terminus of AdP contains a sequence of eight ala, which stabilize the α-helix conformation.[52] In contrast, three hydrophilic arg are distributed within the AdP center and C-terminus. These three arg partially destabilize the α-helices and favor formation of the water-mediated α-helical defects such as π-bulges[172] and 3_{10}-helices[173].

The higher α-helix stability at the AdP N-terminus agrees well with the MD simulation studies of Sorin and Pande,[72] which suggested that the N-terminus of 21-residue α-helical Fs-peptide (which is a natural abundance analog of AdP) has a higher α-helical content than occurs in the middle and at the C-terminus. These MD studies also suggest that the arginines destabilize α-helices in Fs (and, thus, in AdP). We suggest that these hydrophilic arg are likely not only to partially destabilize α-helices but also induce the formation of water-mediated α-helical defects such as π-bulges[172] and 3_{10}-helices (type III turns)[173] at low temperatures, at which the peptide bond-water hydrogen bonding strength increases.[120,127,128]

Whatever the case, our calculated ~4.4 and ~1.3 μsec (+30 °C) and ~3.6 and ~0.7 μsec (+40 °C) pure α-helix folding and unfolding times (Table 18), respectively, are much slower than the (un)folding times previously reported for similar peptides. It is now obvious that the ~100–200 ns relaxation times typically reported for ala-rich peptides,[4-6,10,13,17,18,22,25,32-35,120] signal the dominating contribution of π-bulge and/or 3_{10}-helix melting to the observed overall relaxation kinetics. In addition, it is also clear that at least some of the observed deviations from the mono-exponential behavior[22,33,34] for ala-rich peptide melting results from the temperature dependence of the relative contributions of pure α-helices, π-bulges and 3_{10}-helices melting to the overall relaxation kinetics. Our results here are the first to resolve the kinetic behavior of the different α-helix like conformations.

9.5 CONCLUSIONS

We examined the relaxation kinetics of a 21 amino acid residues mainly ala peptide AdP, which contains three arg to give solubility. This peptide is ≥55% α-helix-like at 0 ºC and melts to a

PPII conformation at higher temperature. Previous isotopic substitution studies demonstrated a significantly higher T_M=32 ºC for the 6 center residues compared to a T_M=5 ºC for the end residues.[7] We used T-jump measurements to examine the melting kinetics. We find that the middle AdP peptide bonds show a relaxation time ~2-fold slower than the end residues for 5 to 30 °C T-jump. In contrast, for a 20 to 40 °C T-jump the middle AdP peptide bonds appear to show faster kinetics than the end AdP peptide bonds.

We explain the observed kinetics in terms of different relative contributions of different α-helix-like motifs such as pure α-helices, π-bulges and 3_{10}-helices to the observed melting kinetics. We estimated that the melting rate constant of pure α-helices is ~12-fold slower than those of π-bulges and 3_{10}-helices (Table 18). This strikingly suggests that the pure α-helix (un)folding occurs at ~μsec time scale at room temperature.

For 5 to 30 °C T-jump, the faster melting of π-bulges and 3_{10}-helices dominate both the AdP ends and center kinetics, with also a minor contribution of slower pure α-helix melting to the AdP center kinetics. In contrast, for 20 to 40 °C T-jump the faster melting of π-bulges and 3_{10}-helices dominates both the AdP ends and center kinetics, whereas there is also a minor contribution of slower pure α-helix melting to the AdP ends kinetics. These surprising results can be explained in terms of a higher pure α-helical propensity at the AdP N-terminus compared to the middle and C-terminus.

The higher stability of pure α-helix at the AdP N-terminus can be understood in terms of AdP primary sequence. Specifically, three hydrophilic arg located in the AdP middle and at the AdP C-terminus destabilize the pure α-helices and induce formation of water-mediated α-helical defects (such as π-bulges and 3_{10}-helices), which melt faster.

In addition, we developed a kinetic model to calculate the (un)folding rate constants for pure α-helices, π-bulges and 3_{10}-helices. We successfully explain the apparent anti-Arrhenius behavior observed earlier by Lednev et al.[4] as resulting from the parallel melting of these different conformations. Further, our model also explains the complicated nonexponential behavior observed earlier by Huang et al.[34] and Bredenbeck et al.[22] for similar peptides.

Summarizing, we believe that our results here are the first experimental ones to quantitatively show that the folding mechanism of end residues of ala-rich peptides significantly differs from that of middle residues in terms of different relative contributions of different "α-

helix-like" species to the melting kinetics. In addition, we for the first time measured the kinetic (un)folding rate constants for pure α-helices, 3_{10}-helices and π-bulges in ala-rich peptides of ~20 residues long. Thus, our results not only directly demonstrate that α-helix melting and formation in peptides are not a simple two-state processes but also provide an important quantitative basis for testing theoretical studies in the field of peptide and protein folding.

9.6 ACKNOWLEDGMENT

We gratefully acknowledge Ahmed Zeeshan, Bhavya Sharma, Konstantin Pimenov and Dr. Natalyia Myshakina for useful discussions. We thank Dr. Leon J. Gleser, Dr. Sunil Saxena and Dr. Carlos Gomes for their assistance in the statistical evaluation. We also thank Mr. Anton Karnoup who performed the MALDI MS analysis to verify the AdP sequence. This work was supported by NIH grant GM8RO1EB002053021.

9.7 REFERENCES

(1) Creighton, T. E. *Protein Structure, Second Edition*, 1997.

(2) Zimm, B. H.; Bragg, J. K. *J. Chem. Phys.* **1959**, *31*, 526-535.

(3) Poland, D.; Scheraga, H. A. *J. Phys. Chem.* **1966**, *45*, 2071-2091.

(4) Lednev, I. K.; Karnoup, A. S.; Sparrow, M. C.; Asher, S. A. *J. Am. Chem. Soc.* **1999**, *121*, 8074-8086.

(5) Lednev, I. K.; Karnoup, A. S.; Sparrow, M. C.; Asher, S. A. *J. Am. Chem. Soc.* **1999**, *121*, 4076-4077.

(6) Lednev, I. K.; Karnoup, A. S.; Sparrow, M. C.; Asher, S. A. *J. Am. Chem. Soc.* **2001**, *123*, 2388-2392.

(7) Ianoul, A.; Mikhonin, A.; Lednev, I. K.; Asher, S. A. *J. Phys. Chem. A* **2002**, *106*, 3621-3624.

(8) Lockhart, D. J.; Kim, P. S. *Science* **1992**, *257*, 947-951.

(9) Lockhart, D. J.; Kim, P. S. *Science* **1993**, *260*, 198-202.

(10) Werner, J. H.; Dyer, R. B.; Fesinmeyer, R. M.; Andersen, N. H. *J. Phys. Chem. B* **2002**, *106*, 487-494.

(11) Gruebele, M. *Annu. Rev. Phys. Chem.* **1999**, *50*, 485-516.

(12) Fesinmeyer, R. M.; Peterson, E. S.; Dyer, R. B.; Andersen, N. H. *Protein Sci.* **2005**, *14*, 2324-2332.

(13) Williams, S.; Causgrove, T. P.; Gilmanshin, R.; Fang, K. S.; Callender, R. H.; Woodruff, W. H.; Dyer, R. B. *Biochemistry* **1996**, *35*, 691-697.

(14) Dyer, R. B.; Gai, F.; Woodruff, W. H.; Gilmanshin, R.; Callender, R. H. *Acc. Chem. Res.* **1998**, *31*, 709-716.

(15) Callender, R.; Dyer, R. B.; Gilmanshin, R.; Woodruff, W. H. *Annu. Rev. Phys. Chem.* **1998**, *49*, 173-202.

(16) Causgrove, T. P.; Dyer, R. B. *Chemical Physics* **2006**, *323*, 2-10.

(17) Thompson, P. A.; Eaton, W. A.; Hofrichter, J. *Biochemistry* **1997**, *36*, 9200-9210.

(18) Thompson, P. A.; Munoz, V.; Jas, G. S.; Henry, E. R.; Eaton, W. A.; Hofrichter, J. *J. Phys. Chem. B* **2000**, *104*, 378-389.

(19) Kubelka, J.; Hofrichter, J.; Eaton, W. A. *Curr. Opin. Struc. Biol.* **2004**, *14*, 76-88.

(20) Lapidus, L. J.; Eaton, W. A.; Hofrichter, J. *Proc. Natl. Acad. Sci. U.S.A.* **2000**, *97*, 7220-7225.

(21) Lapidus, L. J.; Eaton, W. A.; Hofrichter, J. *J. Mol. Biol.* **2002**, *319*, 19-25.

(22) Bredenbeck, J.; Helbing, J.; Kumita, J. R.; Woolley, G. A.; Hamm, P. *Proc. Natl. Acad. Sci. U.S.A.* **2005**, *102*, 2379-2384.

(23) Decatur, S. M.; Antonic, J. *J. Am. Chem. Soc.* **1999**, *121*, 11914-11915.

(24) Decatur, S. M. *Biopolymers* **2000**, *54*, 180-185.

(25) Ramajo, A. P.; Petty, S. A.; Starzyk, A.; Decatur, S. M.; Volk, M. *J. Am. Chem. Soc.* **2005**, *127*, 13784-13785.

(26) Pozo Ramajo, A.; Petty, S. A.; Volk, M. *Chem. Phys.* **2006**, *323*, 11-20.

(27) Gooding, E. A.; Ramajo, A. P.; Wang, J.; Palmer, C.; Fouts, E.; Volk, M. *Chem. Commun.* **2005**, 5985-5987.

(28) Silva, R. A.; Kubelka, J.; Bour, P.; Decatur, S. M.; Keiderling, T. A. *Proc. Natl. Acad. Sci. U.S.A.* **2000**, *97*, 8318-8323.

(29) Yoder, G.; Pancoska, P.; Keiderling, T. A. *Biochemistry* **1997**, *36*, 15123-15133.

(30) Keiderling, T. A.; Silva, R. A.; Yoder, G.; Dukor, R. K. *Bioorgan. Med. Chem.* **1999**, *7*, 133-141.

(31) Decatur, S. M. *Accounts Chem. Res.* **2006**, *39*, 169-175.

(32) Huang, C.-Y.; Getahun, Z.; Wang, T.; DeGrado, W. F.; Gai, F. *J. Am. Chem. Soc.* **2001**, *123*, 12111-12112.

(33) Huang, C.-Y.; Getahun, Z.; Zhu, Y.; Klemke, J. W.; DeGrado, W. F.; Gai, F. *Proc. Natl. Acad. Sci. U.S.A.* **2002**, *99*, 2788-2793.

(34) Huang, C.-Y.; Klemke, J. W.; Getahun, Z.; DeGrado, W. F.; Gai, F. *J. Am. Chem. Soc.* **2001**, *123*, 9235-9238.

(35) Wang, T.; Zhu, Y.; Getahun, Z.; Du, D.; Huang, C.-Y.; DeGrado, W. F.; Gai, F. *J. Phys. Chem. B* **2004**, *108*, 15301-15310.

(36) Wang, T.; Du, D.; Gai, F. *Chem. Phys. Lett.* **2003**, *370*, 842-848.

(37) Rohl, C. A.; Baldwin, R. L. *Biochemistry* **1994**, *33*, 7760-7767.

(38) Chakrabartty, A.; Kortemme, T.; Baldwin, R. L. *Protein Sci.* **1994**, *3*, 843-852.

(39) Scholtz, J. M.; Marqusee, S.; Baldwin, R. L.; York, E. J.; Stewart, J. M.; Santoro, M.; Bolen, D. W. *Proc. Natl. Acad. Sci. U.S.A.* **1991**, *88*, 2854-2858.

(40) Marqusee, S.; Baldwin, R. L. *Proc. Natl. Acad. Sci. U.S.A.* **1987**, *84*, 8898-8902.

(41) Marqusee, S.; Robbins, V. H.; Baldwin, R. L. *Proc. Natl. Acad. Sci. U.S.A.* **1989**, *86*, 5286-5290.

(42) Padmanabhan, S.; Marqusee, S.; Ridgeway, T.; Laue, T. M.; Baldwin, R. L. *Nature* **1990**, *344*, 268-270.

(43) Venyaminov, S. Y.; Hedstrom, J. F.; Prendergast, F. G. *Proteins* **2001**, *45*, 81-89.

(44) Cochran, D. A. E.; Doig, A. J. *Protein Sci.* **2001**, *10*, 1305-1311.

(45) Cochran, D. A. E.; Penel, S.; Doig, A. J. *Protein Sci.* **2001**, *10*, 463-470.

(46) Miller, J. S.; Kennedy, R. J.; Kemp, D. S. *Biochemistry* **2001**, *40*, 305-309.

(47) Kennedy, R. J.; Walker, S. M.; Kemp, D. S. *J. Am. Chem. Soc.* **2005**, *127*, 16961-16968.

(48) Heitmann, B.; Job, G. E.; Kennedy, R. J.; Walker, S. M.; Kemp, D. S. *J. Am. Chem. Soc.* **2005**, *127*, 1690-1704.

(49) Goch, G.; Maciejczyk, M.; Oleszczuk, M.; Stachowiak, D.; Malicka, J.; Bierzynski, A. *Biochemistry* **2003**, *42*, 6840-6847.

(50) Gans, P. J.; Lyu, P. C.; Manning, M. C.; Woody, R. W.; Kallenbach, N. R. *Biopolymers* **1991**, *31*, 1605-1614.

(51) Kallenbach, N. R.; Lyu, P.; Zhou, H. *Circular Dichroism and the Conformational Analysis of Biomolecules* **1996**, 201-259.

(52) Spek, E. J.; Olson, C. A.; Shi, Z.; Kallenbach, N. R. *J. Am. Chem. Soc.* **1999**, *121*, 5571-5572.

(53) Doruker, P.; Bahar, I. *Biophys. J.* **1997**, *72*, 2445-2456.

(54) Scholtz, J. M.; Qian, H.; York, E. J.; Stewart, J. M.; Baldwin, R. L. *Biopolymers* **1991**, *31*, 1463-1470.

(55) Scholtz, J. M.; Baldwin, R. L. *Annu. Rev. Biophys. Biomol. Struct.* **1992**, *21*, 95-118.

(56) Young, W. S.; Brooks, C. L., III *J. Mol. Biol.* **1996**, *259*, 560-572.

(57) Shirley, W. A.; Brooks, C. L., III *Proteins* **1997**, *28*, 59-71.

(58) Tobias, D. J.; Brooks, C. L., III *Biochemistry* **1991**, *30*, 6059-6070.

(59) Brooks, C. L., III *J. Phys. Chem.* **1996**, *100*, 2546-2549.

(60) Ohkubo, Y. Z.; Brooks, C. L., III *Proc. Natl. Acad. Sci. U.S.A.* **2003**, *100*, 13916-13921.

(61) Garcia, A. E.; Sanbonmatsu, K. Y. *Proc. Natl. Acad. Sci. U.S.A.* **2002**, *99*, 2782-2787.

(62) Gnanakaran, S.; Garcia, A. E. *Proteins* **2005**, *59*, 773-782.

(63) Hummer, G.; Garcia, A. E.; Garde, S. *Phys. Rev. Lett.* **2000**, *85*, 2637-2640.

(64) Hummer, G.; Garcia, A. E.; Garde, S. *Proteins* **2001**, *42*, 77-84.

(65) Nymeyer, H.; Garcia, A. E. *Proc. Natl. Acad. Sci. U.S.A.* **2003**, *100*, 13934-13939.

(66) Paschek, D.; Gnanakaran, S.; Garcia, A. E. *Proc. Natl. Acad. Sci. U.S.A.* **2005**, *102*, 6765-6770.

(67) Daggett, V.; Levitt, M. *J. Mol. Biol.* **1992**, *223*, 1121-1138.

(68) Fitzkee, N. C.; Rose, G. D. *Prot. Sci.* **2004**, *13*, 633-639.

(69) Doshi, U.; Munoz, V. *Chem. Phys.* **2004**, *307*, 129-136.

(70) Doshi, U. R.; Munoz, V. *J. Phys. Chem. B* **2004**, *108*, 8497-8506.

(71) Munoz, V.; Serrano, L. *J. Mol. Biol.* **1995**, *245*, 297-308.

(72) Sorin, E. J.; Pande, V. S. *Biophys. J.* **2005**, *88*, 2472-2493.

(73) Sorin, E. J.; Pande, V. S. *J. Comp. Chem.* **2005**, *26*, 682-690.

(74) Sorin, E. J.; Rhee, Y. M.; Shirts, M. R.; Pande, V. S. *J. Mol. Biol.* **2006**, *356*, 248-256.

(75) Zagrovic, B.; Jayachandran, G.; Millett, I. S.; Doniach, S.; Pande, V. S. *J. Mol. Biol.* **2005**, *353*, 232-241.

(76) Bertsch, R. A. In *California Institute of Technology,Pasadena,CA,USA.*, 1998, pp 190 pp.

(77) Bertsch, R. A.; Vaidehi, N.; Chan, S. I.; Goddard, W. A., III *Proteins* **1998**, *33*, 343-357.

(78) Ferrara, P.; Apostolakis, J.; Caflisch, A. *J. Phys. Chem. B* **2000**, *104*, 5000-5010.

(79) Irbaeck, A.; Mohanty, S. *Biophys. J.* **2005**, *88*, 1560-1569.

(80) Doig, A. J. *Biophys. Chem.* **2002**, *101-102*, 281-293.

(81) Doig, A. J.; Errington, N.; Iqbalsyah, T. M. *Protein Folding Handbook* **2005**, *1*, 247-313.

(82) Kim, J. G.; Fukunishi, Y.; Nakamura, H. *Chem. Phys. Lett.* **2004**, *392*, 34-39.

(83) Levy, Y.; Jortner, J.; Becker, O. M. *Proc. Natl. Acad. Sci. U.S.A.* **2001**, *98*, 2188-2193.

(84) Nguyen, H. D.; Marchut, A. J.; Hall, C. K. *Protein Sci.* **2004**, *13*, 2909-2924.

(85) Peng, Y.; Hansmann, U. H. E.; Alves, N. A. *J. Chem. Phys.* **2003**, *118*, 2374-2380.

(86) Takano, M.; Yamato, T.; Higo, J.; Suyama, A.; Nagayama, K. *J. Am. Chem. Soc.* **1999**, *121*, 605-612.

(87) Takano, M.; Nagayama, K.; Suyama, A. *J. Chem. Phys.* **2002**, *116*, 2219-2228.

(88) Takano, M.; Nakamura, H. K.; Nagayama, K.; Suyama, A. *J. Chem. Phys.* **2003**, *118*, 10312-10322.

(89) Mortenson, P. N.; Evans, D. A.; Wales, D. J. *J. Chem. Phys.* **2002**, *117*, 1363-1376.

(90) Ulmschneider, J. P.; Jorgensen, W. L. *J. Chem. Phys.* **2003**, *118*, 4261-4271.

(91) Ulmschneider, J. P.; Jorgensen, W. L. *J. Am. Chem. Soc.* **2004**, *126*, 1849-1857.

(92) Tirado-Rives, J.; Jorgensen, W. L. *Biochemistry* **1991**, *30*, 3864-3871.

(93) Tirado-Rives, J.; Maxwell, D. S.; Jorgensen, W. L. *J. Am. Chem. Soc.* **1993**, *115*, 11590-11593.

(94) Mitsutake, A.; Okamoto, Y. *J. Chem. Phys.* **2000**, *112*, 10638-10647.

(95) Samuelson, S.; Martyna, G. J. *J. Phys. Chem. B* **1999**, *103*, 1752-1766.

(96) Hansmann, U. H. E.; Okamoto, Y. *J. Chem. Phys.* **1999**, *110*, 1267-1276.

(97) Wu, X.; Wang, S. *J. Phys. Chem. B* **2001**, *105*, 2227-2235.

(98) Wang, Y.; Kuczera, K. *J. Phys. Chem. B* **1997**, *101*, 5205-5213.

(99) Van Giessen, A. E.; Straub, J. E. *J. Chem. Theory Comput.* **2006**, *2*, 674-684.

(100) Chakrabartty, A.; Baldwin, R. L. *Adv. Prot. Chem.* **1995**, *46*, 141-176.

(101) Chakrabartty, A.; Schellman, J. A.; Baldwin, R. L. *Nature* **1991**, *351*, 586-588.

(102) Arashiro, E.; Drugowich de Felicio, J. R.; Hansmann, U. H. E. *Phys. Rev. E* **2006**, *73*, 040902/040901-040902/040904.

(103) Soto, P.; Mark, A. E. *J. Phys. Chem. B* **2002**, *106*, 12830-12833.

(104) Peng, Y.; Hansmann, U. H. E. *Biophys. J.* **2002**, *82*, 3269-3276.

(105) Smith, A. V.; Hall, C. K. *Proteins* **2001**, *44*, 344-360.

(106) Alves, N. A.; Hansmann, U. H. E. *Physica A* **2001**, *292*, 509-518.

(107) Pellegrini, M.; Gronbech-Jensen, N.; Doniach, S. *Physica A* **1997**, *239*, 244-254.

(108) Klein, C. T.; Mayer, B.; Koehler, G.; Wolschann, P. *Theochem* **1996**, *370*, 33-43.

(109) Hoffmann, D.; Knapp, E.-W. *Eur. Biophys. J.* **1996**, *24*, 387-403.

(110) Scheraga, H. A.; Vila, J. A.; Ripoll, D. R. *Biophys. Chem.* **2002**, *101-102*, 255-265.

(111) Zhang, W.; Lei, H.; Chowdhury, S.; Duan, Y. *J. Phys. Chem. B* **2004**, *108*, 7479-7489.

(112) Rathore, N.; Yan, Q.; de Pablo, J. J. *J. Chem. Phys.* **2004**, *120*, 5781-5788.

(113) Agostini, F. P.; Soares-Pinto, D. D. O.; Moret, M. A.; Osthoff, C.; Pascutti, P. G. *J. Comput. Chem.* **2006**, *27*, 1142-1155.

(114) Baumketner, A.; Shea, J. E. *Phys. Rev. E* **2003**, *68*, 051901/051901-051901/051910.

(115) Baumketner, A.; Shea, J. E. *Condens. Matter Phys.* **2004**, *38*, 421-434.

(116) Ho, B. K.; Dill, K. A. *PLoS Comput. Biol.* **2006**, *2*, 228-237.

(117) Mezei, M.; Fleming, P. J.; Srinivasan, R.; Rose, G. D. *Proteins* **2004**, *55*, 502-507.

(118) Kentsis, A.; Mezei, M.; Gindin, T.; Osman, R. *Proteins* **2004**, *55*, 493-501.

(119) Blanch, E. W.; Morozova-Roche, L. A.; Cochran, D. A. E.; Doig, A. J.; Hecht, L.; Barron, L. D. *J. Mol. Biol.* **2000**, *301*, 553-563.

(120) Asher, S. A.; Mikhonin, A. V.; Bykov, S. B. *J. Am. Chem. Soc.* **2004**, *126*, 8433-8440.

(121) Adzhubei, A. A.; Sternberg, M. J. E. *J. Mol. Biol.* **1993**, *229*, 472-493.

(122) Chen, K.; Liu, Z.; Kallenbach, N. R. *Proc. Natl. Acad. Sci. U.S.A.* **2004**, *101*, 15352-15357.

(123) Garcia, A. E. *Polymer* **2004**, *45*, 669-676.

(124) Pappu, R. V.; Rose, G. D. *Protein Sci.* **2002**, *11*, 2437-2455.

(125) Chi, Z.; Chen, X. G.; Holtz, J. S. W.; Asher, S. A. *Biochemistry* **1998**, *37*, 2854-2864.

(126) Asher, S. A.; Ianoul, A.; Mix, G.; Boyden, M. N.; Karnoup, A.; Diem, M.; Schweitzer-Stenner, R. *J. Am. Chem. Soc.* **2001**, *123*, 11775-11781.

(127) Mikhonin, A. V.; Ahmed, Z.; Ianoul, A.; Asher., S. A. *J. Phys. Chem. B* **2004**, *108*, 19020-19028.

(128) Mikhonin, A. V.; Myshakina, N. S.; Bykov, S. V.; Asher, S. A. *J. Am. Chem. Soc.* **2005**, *127*, 7712-7720.

(129) Chi, Z.; Asher, S. A. *Biochemistry* **1998**, *37*, 2865-2872.

(130) Chi, Z.; Asher, S. A. *Biochemistry* **1999**, *38*, 8196-8203.

(131) Wang, Y.; Purrello, R.; Jordan, T.; Spiro, T. G. *J. Am. Chem. Soc.* **1991**, *113*, 6359-6368.

(132) Miick, S. M.; Martinez, G. V.; Fiori, W. R.; Todd, A. P.; Millhauser, G. L. *Nature* **1992**, *359*, 653-655.

(133) Fiori, W. R.; Miick, S. M.; Millhauser, G. L. *Biochemistry* **1993**, *32*, 11957-11962.

(134) Millhauser, G. L. *Biochemistry* **1995**, *34*, 3873-3877.

(135) Martinez, G.; Millhauser, G. *J. Struct. Biol.* **1995**, *114*, 23-27.

(136) Millhauser, G. L.; Stenland, C. J.; Bolin, K. A.; van de Ven, F. J. M. *J. Biomol. NMR* **1996**, *7*, 331-334.

(137) Hanson, P.; Martinez, G.; Millhauser, G.; Formaggio, F.; Crisma, M.; Toniolo, C.; Vita, C. *J. Am. Chem. Soc.* **1996**, *118*, 271-272.

(138) Millhauser, G. L.; Stenland, C. J.; Hanson, P.; Bolin, K. A.; van de Ven, F. J. M. *J. Mol. Biol.* **1997**, *267*, 963-974.

(139) Hanson, P.; Anderson, D. J.; Martinez, G.; Millhauser, G.; Formaggio, F.; Crisma, M.; Toniolo, C.; Vita, C. *Mol. Phys.* **1998**, *95*, 957-966.

(140) Armen, R.; Alonso, D. O. V.; Daggett, V. *Protein Sci.* **2003**, *12*, 1145-1157.

(141) Long, H. W.; Tycko, R. *J. Am. Chem. Soc.* **1998**, *120*, 7039-7048.

(142) Topol, I. A.; Burt, S. K.; Deretey, E.; Tang, T.-H.; Perczel, A.; Rashin, A.; Csizmadia, I. G. *J. Am. Chem. Soc.* **2001**, *123*, 6054-6060.

(143) Podtelezhnikov, A. A.; Wild, D. L. *Proteins* **2005**, *61*, 94-104.

(144) Han, W.-G.; Elstner, M.; Jalkanen, K. J.; Frauenheim, T.; Suhai, S. *Int. J. Quantum Chem.* **2000**, *78*, 459-479.

(145) Mikhonin, A. V.; Asher, S. A. *Submitted to the J. Am. Chem. Soc.* **2006**.

(146) Lee, K.-H.; Benson, D. R.; Kuczera, K. *Biochemistry* **2000**, *39*, 13737-13747.

(147) Mahadevan, J.; Lee, K.-H.; Kuczera, K. *J. Phys. Chem. B* **2001**, *105*, 1863-1876.

(148) Feig, M.; MacKerell, A. D., Jr.; Brooks, C. L., III *J. Phys. Chem. B* **2003**, *107*, 2831-2836.

(149) Bykov, S. V.; Lednev, I. K.; Ianoul, A.; Mikhonin, A. V.; Munro, C. H.; Asher, S. A. *Appl. Spectrosc.* **2005**, *59*, 1541-1552.

(150) Walrafen, G. E.; Fisher, M. R.; Hokmabadi, M. S.; Yang, W. H. *J. Chem. Phys.* **1986**, *85*, 6970-6982.

(151) Risovic, D.; Furic, K. *J. Raman Spectrosc.* **2005**, *36*, 771-776.

(152) Mikhonin, A. V.; Asher, S. A. *J. Phys. Chem. B* **2005**, *109*, 3047-3052.

(153) Mikhonin, A. V.; Bykov, S. V.; Myshakina, N. S.; Asher, S. A. *J. Phys. Chem. B* **2006**, *110*, 1928-1943.

(154) Nelles, O. *Nonlinear System Identefication,* **2001**, Springer-Verlag, Germany.

(155) Dennis, J. E.; Schnabel, R. B. *Numerical Methods for Unconstrained Optimization and Nonlinear Equation,* **1983**, Prentice-Hall, Inc. Englewood Cliffs, New Jersey: USA.

(156) Budil, D. E.; Lee, S.; Saxena, S.; Freed, J. H. *J. Magn. Reson., Ser. A* **1996**, *120*, 155-189.

(157) Gleser, L. J. *Statistical Science* **1998**, *13*, 277-290.

(158) *Grams/32AI User's Guide,* **2001**, Galactic Industries Corporation, Salem New Hampshire: USA.

(159) Wadsworth, H. M. *Handbook of Statistical Methods for Engineers and Scientists,* **1990**, McGraw-Hill: USA.

(160) Lee, S.-H.; Krimm, S. *Biopolymers* **1998**, *46*, 283-317.

(161) Pimenov, K. V.; Bykov, S. V.; Mikhonin, A. V.; Asher, S. A. *J. Am. Chem. Soc.* **2005**, *127*, 2840-2841.

(162) Copeland, R. A.; Spiro, T. G. *J. Am. Chem. Soc.* **1986**, *108*, 1281-1285.

(163) Tanaka, M.; Tanaka, J. *Molecular Physics* **1970**, *19*, 889-897.

(164) Rosenheck, K.; Doty, P. *Proc. Natl. Acad. Sci. USA* **1961**, *47*, 1775-1785.

(165) Moffit, W. *Proc. Natl. Acad. Sci. U.S.A.* **1956**, *42*, 736.

(166) Schellman, J. A.; Becktel, W. J. *Biopolymers* **1983**, *22*, 171-187.

(167) Momii, R. K.; Urry, D. W. *Macromolecules* **1968**, *1*, 372.

(168) Painter, P. C.; Koenig, J. L. *Biopolymers* **1976**, *15*, 241-255.

(169) Weissbluth, M. *Q. Rev. Biophys.* **1971**, *4*, 1-34.

(170) Rhodes, W.; Barnes, D. G. *J. Chim. Phys. PCB* **1968**, *65*, 78-90.

(171) McLachlan, A. D.; Ball, M. A. *Molecular Physics* **1964**, *8*, 581-595.

(172) Cartailler, J.-P.; Luecke, H. *Structure* **2004**, *12*, 133-144.

(173) Sundaralingam, M.; Sekharudu, Y. C. *Science* **1989**, *244*, 1333-1337.

10.0 CONCLUSION SUMMARY

The main conclusion of this thesis is that we developed an extremely powerful UV resonance Raman (UVRR) analytical tool to directly monitor the major peptide and protein folding reaction coordinate (the Ψ Ramachandran angle). We demonstrated the power of this methodology to directly obtain Ψ Ramachandran angular population distributions of peptide bonds from the UVRR amide III_3 band profile for water solutions of natural abundance peptides and proteins. Then, this Ψ angular distributions can be used to estimate the Ψ angular Gibbs free energy landscape features. Potentially, this methodology combined with isotopic labeling can be used even to determine Ψ angles of individual peptide bonds (see future work chapter for detail).

Numerous groups recently demonstrated the occurrence of PPII conformations in large and small peptides. We verified these conclusions in Chapters 2 of this thesis for small peptides as well as for a 21 residue, mainly Ala peptide, AP, which exists below room temperature as a mixture of α-helix and PPII helix, while it is mainly in a PPII conformation above room temperature. At least in this peptide, α-helix melting is a distinctly different transition than that envisioned by previous theoretical methods, which considered such a melting as a transition between an ordered α-helical state and a completely disordered "random coil" state.

In Chapter 3, we have reexamined in detail the assignment of the amide III region of the PPII and α-helix conformations of peptides and proteins using UV Raman spectra of a mainly polyala peptide, AP, utilizing isotopic substituions, conformational sensitivity and hydration sensitivity of UVRR amide bands. Many of our assignments agree with previous studies, while others challenge the conventional understanding. In addition, we succinctly show, that the conformational dependence of the UVRR spectra make this analytical technique a sensitive probe of protein and peptide secondary structure.

In Chapter 4, we show that α-helical and PPII conformations of AP in mixed H_2O and D_2O samples show that the UVRR AmIII (PPII and α-helix), AmII (PPII) and AmII' (PPII and α-helix) bands can be modeled as being independently Raman scattered by the individual peptide

bonds. Negligible coupling occurs for these vibrations between the adjacent peptide bonds. This dramatically simplifies the use of vibrational spectral modeling to elucidate peptide and protein structure. The AmI and AmI' vibrations of PPII also show no evidence of coupling between adjacent peptide bonds. In contrast, the AmI and AmI' bands of the α-helical conformation clearly indicate the occurrence of interamide coupling, which may complicate spectral modeling in AmI region for α-helix-like conformations. The interamide coupling in the α-helix is probably the result of the proximity of the amide C=O groups to one another, the fact that they are oriented parallel to one another, and because the C=O of different amides are linked through interamide hydrogen bonding.

In Chapter 5, we used UV resonance Raman spectroscopy to investigate the dependence of the $AmIII_3$ frequency on the Ψ Ramachandran angle and on the nature of peptide bond hydrogen bonding. These results allow us to formulate relationships that allow us to estimate the Ψ Ramachandran angles from the observed $AmIII_3$ frequencies for both aqueous solutions of peptides and proteins as well as for the anhydrous states of peptides and proteins. A typical Raman measurement of a typical sample would find a random error of $\leq \pm 8°$ in the Ψ angle, assuming a known HB state. However, if HB state of a PB in water is unknown, extreme alterations in such a state could additionally bias the Ψ angle by ±6°. We are optimistic that these relationships will be very useful for protein conformational studies, especially in the field of protein folding. This is because any attempt to understand reaction mechanisms, such as protein folding, requires elucidation of the relevant reaction coordinate(s). The Ψ angle is precisely the reaction coordinate that determines secondary structure changes. As shown in Chapters 6, 8 and 9 of this thesis, the correlation we propose can be used to determine features of the Gibbs free energy landscape along this Ψ reaction coordinate.

In Chapter 6, we use UVRR spectroscopy to study the unfolded conformations of individual pH=2 poly-L-lysine and pH=9 poly-L-glutamic acid, as well as to study the anti-parallel β-sheet conformation of pH=7 PLL-PGA equimolar mixture. Our study indicates that the unfolded states of individual PLL and PGA exist as a mixture of PPII and the extended 2.5_1-helix (β-strand-like) conformations. The charged side chains of pH=2 PLL and pH=9 PGA force the PLL and PGA chains in water to adopt more extended conformations (compared to classical PPII) to minimize electrostatic interchain repulsions. The β-sheet structure of the PLL-PGA mixture showed little evidence for hydrogen bonding between the polypeptide backbone and

water. We also utilized our new methodology (developed in Chapter 5), which allows us to estimate the Ψ Ramachandran angle from the $AmIII_3$ frequency. This analysis demonstrates that each conformation has a distribution of Ψ-angles about the minimum Ψ conformational energy. The sharper Ψ angle distribution of the PGA 2.5_1-helix than that of PLL 2.5_1-helix, as well as, the absence of the 2.5_1-helix conformation in alanine-based peptides are consistent with the hypothesized electrostatic mechanism of stabilization of the 2.5_1-helix. We were able to calculate the Ψ-angle energy landscape features of these observed conformations. This is an important advance since the Ψ-angle coordinate is the most important coordinate for protein and peptide secondary structure changes.

In Chapter 7, we use UVRR spectroscopy to study the equilibrium α-helix melting in isotopically labeled derivative of AP, AdP. The work here demonstrates that UVRR measurements of a selectively deuterium labeled α-helical peptide allows us to spatially resolve the conformation of individual peptide bonds. We observe significantly higher T_m values for peptide bonds in the center of the peptide compared to the external peptide bonds. We use the results of this equilibrium studies in Chapter 9 of this thesis, where we kinetically examine α-helix melting in AdP.

In Chapter 8, we show the power of Chapter 5 methodology to directly monitor the temperature-induced evolution of Ψ Ramachandran angle population distributions of peptide bonds in AP, which allows us for the first time to separately study the melting of the α-, 3_{10}- and π-helix/bulge conformations. It is somewhat surprising to find that the 3_{10}- and π-helix/bulge conformations melt prior to melting of pure α-helices, since these conformations are proposed to be intermediates in the unfolding pathway. Apparently they are much more transient at the higher α-helix melting temperature. We estimated Zimm and Bragg nucleation (σ) and propagation (s) parameters for perfect α-helix, and π-helix/bulge conformations. A striking finding is that the AP pure α-helix melts with much higher cooperativity and shows much higher $T_m \sim 45$ °C then it was originally reported by CD and Raman. We were able for the first time to experimentally monitor the Gibbs free energy landscape and the free energy barriers on the AP melting reaction pathway. These experimental measurements should serve as a benchmark for future theoretical and experimental studies of protein folding.

In Chapter 9, we examined the relaxation kinetics of a 21 amino acid residues mainly ala peptide AdP. This peptide is ≥55% α-helix-like at 0 ºC and melts to a PPII conformation at higher temperature. The isotopic labeling allowed us to separately monitor the T-jump induced secondary structure relaxation of middle versus end peptide bonds. Previous equilibrium isotopic substitution studies (see Chapter 7) demonstrated a significantly higher T_M=32 ºC for the 6 center residues compared to a T_M=5 ºC for the end residues. In addition, our T-jump kinetic data indicates that the end and the middle of the peptide show significantly different and non-classical relaxation behaviors. We find that the middle AdP peptide bonds show a relaxation time ~2-fold slower than the end residues for 5 to 30 °C T-jump. In contrast, for a 20 to 40 °C T-jump the middle AdP peptide bonds appear to show ~2-fold faster kinetics than the end AdP peptide bonds. We explain the observed kinetics in terms of different relative contributions of different α-helix-like motifs such as pure α-helices, π-bulges and 3_{10}-helices to the observed melting kinetics. We developed a kinetic model to calculate the (un)folding rate constants for pure α-helices, π-bulges and 3_{10}-helices. Strikingly, we estimate that the melting rate constant of pure α-helices is ~12-fold slower than those of π-bulges and 3_{10}-helices (Table 18). This suggests that the pure α-helix (un)folding occurs at ~μsec time scale at room temperature. In addition, our model successfully explains the apparent anti-Arrhenius behavior observed earlier by Lednev et al. (*J. Am. Chem. Soc.*, **1999**, *121*, 8074) as resulting from the parallel melting of these different conformations. Further, our model also explains the complicated nonexponential behavior observed earlier by Huang et al. (*J. Am. Chem. Soc.*, **2001**, *123*, 9235) and Bredenbeck et al. (*Proc. Natl. Acad. Sci. USA*, **2005**, *102*, 2379) for similar peptides. We also see the evidence of a higher pure α-helical propensity at the AdP N-terminus compared to the middle and C-terminus. These results are the first experimental ones to quantitatively show that the folding mechanism of end residues of ala-rich peptides significantly differs from that of middle residues in terms of different relative contributions of different "α-helix-like" species to the melting kinetics. Future equilibrium and kinetic studies of isotopically edited peptides will allow us to more deeply examine "α-helix" to PPII melting, as well as other peptide backbone conformational transitions.

It should be emphasized that most of novel quantitative experimental results, reported in this thesis, seriously challenge classical theories of α-helix melting, which envision such a melting as a transition between ordered α-helix and completely disordered "random coil"

conformations. First, we see no evidence for "true random coil" conformations in protein and peptide unfolded state ensembles. Rather, unfolded states of peptides and proteins exhibit a significant amount of extended polyproline II-like structures (Chapters 2, 6 and 8). In addition, we also show that low temperature "α-helix-like" ensembles of relatively simple "α-helical" peptide, AP, are not homogenious and contain the additional contributions from π-bulges and 3_{10}-helices (Chapter 8). Further, we developed a quantitative kinetic model (Chapter 9), which includes the melting of all these α-helix-like conformations, and for the first time estimates their (un)folding rates as well as their relative contributions to exterior and interior peptide bond melting in ala-rich peptides ~20 residues long. Summarizing, our results not only directly demonstrate that α-helix melting and formation in relatively simple peptides are not simple two-state processes but also provide an important quantitative basis for testing theoretical studies in the field of peptide and protein folding.

11.0 FUTURE WORK

11.1.1 Ultimate Goal of the Methodology Described in the Thesis

It was discussed in the introduction, that essentially all secondary structure conformational transitions in peptides and proteins can be accurately described in terms of change in two Ramachandran angles, Ψ and Φ (Fig. 2). Thus, to completely elucidate a protein and/or peptide secondary structure from the UVRR experiment, ***it is ultimately necessary to enable the direct experimental monitor of both Ψ and Φ Ramachandran angles for any peptide bond of interest, or any selected group of peptide bonds.***

11.1.2 Further Developments of the Described Methodology Required for Achieving the Ultimate Goal.

The methodology described in this thesis has been demonstrated to provide the Ψ Ramachandran angular population distributions of peptide bonds in water solutions of peptides and proteins. Thus, UVRR spectroscopy has been shown to directly monitor the Ψ angles, but not yet at individual peptide bond level (however, see sub-section 1.3.2.1 below). In addition, our methodology in its current form cannot yet provide the direct experimental monitor of the Φ Ramachandran angle. Thus, recalling the ultimate goal of this methodology (see sub-section 1.3.1 above), there are two obvious future directions to improve the described methodology:

a) Demonstrate the ability of this methodology to monitor the Ψ angles of individual peptide bonds of interest (or any selected group of peptide bonds). We show below, that such a monitoring is quite possible by combining the described methodology (even in its current form) with selective C_α-D labeling.

b) Elucidate the UVRR bands sensitive to the second Ramachandran angle, Φ; quantitatively relate the parameters of these bands to Φ Ramachandran angle; and then develop a quantitative practical method to directly monitor Φ angles of peptide bonds ideally at individual peptide bond level.

11.1.2.1 Combining the Developed Methodology with C_α-D Labeling Enables Monitor of Ψ Ramachandran Angles of Individual Peptide Bonds!

It was mentioned above, that the methodology described in this thesis has been shown to provide the Ψ angular population distributions of peptide bonds in natural isotope abundance peptides and proteins. The application of this methodology, even in its current form, has led us to many novel and important discoveries. However, there exists another extremely powerful ability of this methodology, which has not yet been demonstrated in this thesis.

Specifically, this methodology combined with a C_α-D labeling can monitor the Ψ angles of individual peptide bonds of interest (or any selected group of peptide bonds). As discussed in the thesis (Chapters 3, 5, 7 and 9), the C_α-D labeling dramatically upshifts the amide III_3 frequency of a peptide bond, resulting in an up to ~110 cm^{-1} frequency upshift. Thus, the UVRR difference spectrum between a natural abundance peptide or protein and its derivative with a C_α-D labeled peptide bond of interest, would reveal the amide III_3 frequency and, thus, the Ψ angle of the labeled peptide bond.

This powerful ability to monitor the Ψ Ramachandran angles of individual peptide bonds in equilibrium and dynamic (as well as those of any chosen group of peptide bonds) leads to a great variety of important future projects. Some of them are discussed in sub-section 1.3.3.

11.1.2.2 Elucidation of Φ Ramachandran Angle.

In case of α-helix melting to PPII or β-strand-like conformations, the Ψ Ramachandran angle is the major secondary structure reaction coordinate, as pointed out in this thesis. However, monitoring of the second Ramachandran angle, Φ, will provide the important additional information. Obviously, the additional ability to monitor Φ angle is especially attractive for studying those conformational transitions, which does not involve large Ψ angle changes, such as, for example, β-hairpin, β-sheet formation and amyloid fibril formations. In addition, the

simultaneous monitoring of Ψ and Φ angles should help to better characterize the intermediate states, which show up in protein folding pathway.

Summarizing, the elucidation of both Ψ and Φ angles of peptide bonds would simply provide the complete secondary structure information. It would enable the additional quantitative insight into the mechanisms of most (if not all) peptide and proteins conformational transitions.

Concerning this thesis, the additional elucidation of Φ angles of peptide bonds would allow us to further refine the Chapter 5 correlation between the Ψ angle and amide III_3 frequency. In addition, we would be able to distinguish between different intermediate turn conformations detected in Chapter 8 and ultimately obtain more accurate Gibbs free energy landscape features along the Ψ angle coordinate of AP (Fig. 73, Chapter 8).

We are currently working on the elucidation of UVRR bands, which are sensitive to the second Ramachandran angle, Φ. For example, UVRR spectra of peptide crystals with known Ψ and Φ Ramachandran angles (Chapters 3 and 5) combined with normal mode calculations using Gaussian, may help to resolve this issue.

11.1.3 Possible Applications of the Developed Methodology.

11.1.3.1 Quantitative Insight into the Mechanisms of Conformational Transitions in Model Peptides.

First, this methodology combined with isotopic labeling can be applied for studying of conformational transitions in different model peptides to reveal the Ψ angles of individual peptide bonds. Such experimental data are crucially needed to test the validity of many recent theoretical works in the field of protein folding, since the theoretical works are often limited to model peptide studies by current computer abilities.

For example, it is now possible to continue our UVRR studies of 21-residue mainly ala peptide, AP, and reveal the equilibrium and dynamic Ψ angular evolution of any chosen peptide bond or group of peptide bonds. As mentioned above, this could be done by subtracting the UVRR spectra of different C_α-D labeled derivatives of AP from those of natural abundance AP. Specific questions of interest could be the detailed information about the exact location of

recently resolved pure π-bulges, α-helices and 3_{10}-helices (Fig. 72, Chapter 8), as well as that about their formation and melting times.

We can also continue our studies of various conformational transitions, which occur in poly-L-lysine and poly-L-glutamic acid peptides. For example, in case of poly-L-lysine, our methodology can provide an important additional quantitative insight into the mechanisms of salt-induced, pH-induced and/or temperature-induced α-helix melting and/or formation. In case of poly-L-glutamic acid, we can also revisit the mechanism(s) of pH- and/or temperature-induced α-helix melting.

In addition, we can also continue the Ahmed and Asher studies of a 3_{10}-helix forming peptide, gp41659-671 (*Biochemistry*, **2006**, *45*, 9068). This peptide shows the evidence of 3_{10}-helix, π-helix/bulge-like conformations, but little α-helix conformations in its folded state. In contrast, this peptide exhibits the PPII and β-turn-like conformations in its unfolded states. The use of isotopic substitutions can reveal the Ψ angles of individual peptide bonds. This information should provide the explaination why this peptide shows a uniquely rough energy landscape with nearly degenerate folded and unfolded states over a wide temperature range.

11.1.3.2 Quantitative Insight into the Mechanisms of Conformational Transitions in Proteins.

In addition to model peptide studies, we can apply the described methodology to quantitative characterize the conformational transition in naturally occurred proteins. We demonstrated our ability to do so in Chapter 2 of this thesis, where we obtained the Ψ angular population distributions of acid denatured apo-myoglobin as well as that for non-α-helical and non-β-sheet conformations of a small library of native proteins.

We can continue these studies, for example, to quantitatively characterize the equilibrium and dynamic Ψ angular evolution during the temperature and/or acid-induced α-helix melting in apo-myoglobin. These studies will definitely provide the additional insight into the equilibrium conformations and dynamics of cold, heat and acid induced denaturation of proteins.

In addition, Ahmed et al.'s UVRR equilibrium studies of Trp-cage, showed that melting of this synthetic mini-protein is not a simple two-state process (*J. Am. Chem. Soc.*, **2005**, *127*, 10943). We can continue these studies by combining our novel methodology and the C_α-D

labeling to reveal the equilibrium and dynamic mechanism of Trp-cage melting at individual peptide bond level.

11.1.3.3 Developing a Methodology to Experimentally Monitor Ψ and Φ Ramachandran Angles of Peptide Bonds and Hydrogen Bond Strengths in Peptide Crystals.

In Chapter 5 of this thesis, we showed that the amide III_3 frequencies of peptide crystals with known structure qualitatively follow the sinusoidal trend predicted by equations 8 and 9. However, peptide crystal amide III_3 frequencies are systematically upshifted compared to those of relatively long peptides and proteins in water solutions (Fig. 53). We explained this observation in terms of increased hydrogen bond (HB) strengths in these peptide crystals, which results in the additional amide III_3 frequency upshift. The origin of the HB strengths increase is that peptide bond carbonyls in these crystals hydrogen bond to NH_3^+ groups (instead of NH groups in case of relatively long peptides and proteins in water solutions); whereas the peptide bond NH groups hydrogen bond to carboxyl groups (instead of carbonyl groups).

Thus, it is now possible to quantitate these HB-induced upshifts in these peptide crystals and ultimately develop a methodology to quantitatively monitor the Ψ Ramachandran angles of peptide bonds directly from UVRR experiment. In addition, these crystal data may also help to elucidate the UVRR bands sensitivity to the Φ Ramachandran angle, and to develop a quantitative methodology to monitor the Φ Ramachandran angle using UVRR spectroscopy.

11.1.4 Other Possible Future Projects

Finally, we want to mention possible future projects, which do not necessarely require the use or further developments of methodology described in this thesis, but logically follow some of the thesis findings.

11.1.4.1 Direct Measurements of Pure α-Helix and π-Bulge Relaxation Melting Rates in AP.

In Chapter 8 of this thesis (Fig. 72), we for the first time obtained the individual melting curves for pure α-helix, π-helix/bulge and 3_{10}-helix conformations in 21-residue mainly ala peptide, AP. In Chapter 9, we estimated the melting and formation rates of these "α-helix-like" conformations using a fit of the experimental data to equations 31A and 31B. These studies can be continued to directly measure (rather than estimate from the fit to equations 31A and 31B) the pure α-helix and pure π-bulge relaxation melting rates. Specifically, the T-jump measurements at both final (T_f) and initial (T_i) T-jump temperatures < +20 °C would report the pure π-bulge relaxation rates; whereas the T-jumps at T_f and $T_i \geq +30$ °C would reveal that for pure α-helix (Fig. 72).

11.1.4.2 Equilibrium and Dynamic Melting of N-terminus vs C-Terminus in AP Derivatives.

In Chapter 9 of this thesis we found an evidence that the AdP (and, thus, AP) N-terminus has higher pure α-helical content than that of C-terminus. These studies can be continued by equilibrium and dynamic melting studies of AP derivatives, which contain, for example, ten C_α-D labeled peptide bonds at either N- or C-terminus. If the pure α-helical content at the N-terminus is indeed higher than that at the C-terminus, then we should observe the following:

a) equilibrium melting temperature (T_m) of ten N-terminal peptide bonds is higher than that of ten C-terminal peptide bonds. This is because pure α-helices show higher T_m's than those of the 3_{10}-helices and π-bulges (Fig. 72);

b) dynamic relaxation melting time(s) for ten N-terminal peptide bonds is slower than that of ten C-terminal peptide bonds. This is because pure α-helices show ~10-fold slower relaxation times than those of π-bulges and 3_{10}-helices (Table 18, Chapter 9).

APPENDIX A

QUANTITATIVE CORRELATION BETWEEN THE PEPTIDE BOND AMIDE III_3 FREQUENCY, HYDROGEN BONDING AND Ψ RAMACHANDRAN ANGLE

In this Appendix, which is directly related to Chapter 5 of this thesis, we carefully investigate the dependence of $AmIII_3$ frequency on the Ψ Ramachandran angle, the peptide bond-water hydrogen bonding (PB-water HB) and the peptide bond-peptide bond hydrogen bonding (PB-PB HB) based on both experimental and theoretical studies. These considerations allow us to quantitatively characterize the HB-induced $AmIII_3$ frequency shifts (summarized in Table 9 of Chapter 5) in the cases of the common protein/peptide secondary structure conformations. Then, we subtract these HB-induced shifts from the experimentally measured UVRR $AmIII_3$ frequencies for pure secondary structure conformations (Table 8), in order to refine Asher et al's. theoretically predicted[47] sinusoidal correlation between the $AmIII_3$ frequency and Ψ Ramachandran angle (Eqn. 8, Chapter 5). The reason we neglect the Φ angular dependence of $AmIII_3$ frequency is explained in great detail in Chapter 5.

NOTE: All the references to this Appendix can be found after the Chapter 5.

A.1 DEPENDENCE OF AMIDE III_3 FREQUENCY ON PB HB

In N-methylacetamide (NMA), theoretical calculations[75,76] show that the formation of a single N-H PB-*water* HB upshifts the AmIII band by ~17–20 cm^{-1}, while formation of a C=O PB-*water* HB upshifts the AmIII frequency only 11–13 cm^{-1}. Qualitatively, similar shifts should occur for

PB-PB HB. However, N-H group PB-PB HB are somewhat stronger than PB-*water* N-H group HB.[101] In contrast, C=O group PB-PB HB have strengths similar to individual PB-*water* C=O HB.[101] To complicate things, the total AmIII frequency shift nonlinearly depends both on the number of PB HB formed, as well as on their individual strengths.[75,76] For example, three simultaneous waters HB to a PB result in a larger AmIII frequency upshift, than the sum of upshifts of the individual HB.

Recently[42] we identified the $AmIII_3$ band in peptides and proteins, the normal mode composition of which is essentially similar to that of "classical" AmIII band of NMA (Fig. 81), which shows the possible water HB geometries to a PB, indicates the estimated hydrogen bond $AmIII_3$ frequency shift for each possibility.

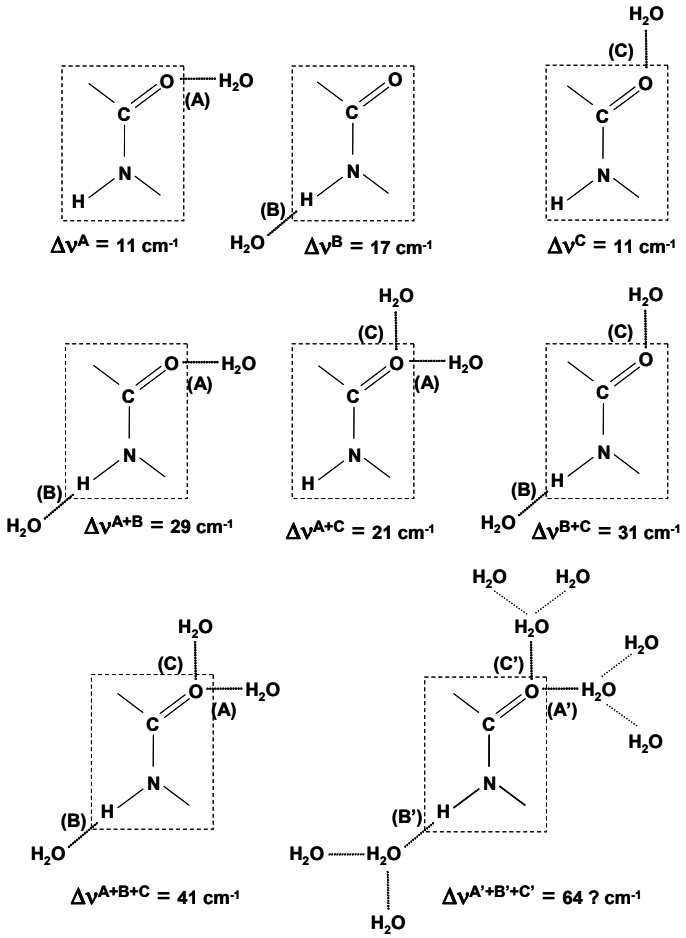

Figure 80. $AmIII_3$ upshifts due to PB-*water* HB in case of fully exposed PB, i.e. for PPII, 2.5_1-helix and extended β-strand conformations. Note that water can HB to the PB at sites A, B and C. The values of these upshifts derive from calculations of NMA by Torii et al.[76] and measurements by Kubelka and Keiderling.[74] The largest shift of 62 cm^{-1} at room temperature (or 64 cm^{-1} for NMA in water at 0 °C, Tables 9 and 19) is measured by Kubelka and

Keiderling. These upshifts are explained in terms of water cluster hydrogen bonding by the very recent important paper of Schmidt et al.[77]

PB-*water* HB gives rise to a large temperature dependence of the $AmIII_3$ frequency[22,29,42,43] due to anharmonicities.[25,82-87] A significantly smaller temperature dependence of the $AmIII_3$ frequency occurs for α-helix and β-sheet peptides because they are extensively PB-PB HB.[22,42,43,60,89] This difference occurs between NMA dissolved in water and pure NMA, where the pure NMA HB only to other NMA molecules (Table 19).

Table 19. Frequencies and temperature dependencies of 204 nm UVRR amide bands of neat NMA and 0.13 M (1 volume %) NMA in water.

Amide Band	**NMA, neat liquid**		**0.13 M NMA in water**	
	ν at 79 °C, cm^{-1}	**Δν/ ΔT, cm^{-1}/°C**	**ν at 70°C, cm^{-1}**	**Δν/ ΔT, cm^{-1}/°C**
AmIII	**1293**	**– 0.05 ± 0.01**	**1309**	**– 0.09 ± 0.01**
AmII	**1558**	**– 0.069 ± 0.015**	**1574**	**– 0.11 ± 0.01**
AmI	**1668**	**+ 0.04 ± 0.01**	**1649**	**+ 0.01 ± 0.03 ***

***** it is hard to accurately determine the temperature dependence of AmI band of 0.13 M NMA in water due to overlap between strong AmII and weak AmI bands (see Fig. 81).

Fig. 81 compares the 204 nm UVRR spectra of neat liquid NMA to a 0.13 M solution (1 volume %) of NMA in water at high and low temperatures. We find that the neat NMA AmII and AmIII frequency shifts/ºC are ~40% less than that those of NMA in water (Table 19), showing that the impact on the $AmIII_3$ frequency of the anharmonicity in the PB-PB HB is less than that of PB-*water* HB.[42,43] PBs fully exposed to water usually have three PB-*water* HBs (Fig. 82, I).[75-77,102] Two water molecules HB to the PB C=O group at sites A and C, while a third water molecule HB to the PB N-H group at site B.[75,76] Monte Carlo simulation studies of NMA hydration,[103] show that the NMA is dominantly HB to three waters at sites A, B and C as shown in Fig. 80.

PB-PB HB is dominated by two-end-on HB[77,104-107] between the N-H and C=O groups at sites E and F (Fig. 82, II). We recently showed that formation of an additional PB-*water* HB to

the PB C=O groups at sites D and D* (Fig. 82, II) gives rise to an additional ~5 cm^{-1} frequency upshift.[89] This smaller ~5 cm^{-1} upshift results from water HB simultaneously at sites D and D* because the D* water hydrogen bond weakens the C=O to H-N HB (Fig. 9 of Schmidt et al.[77]).

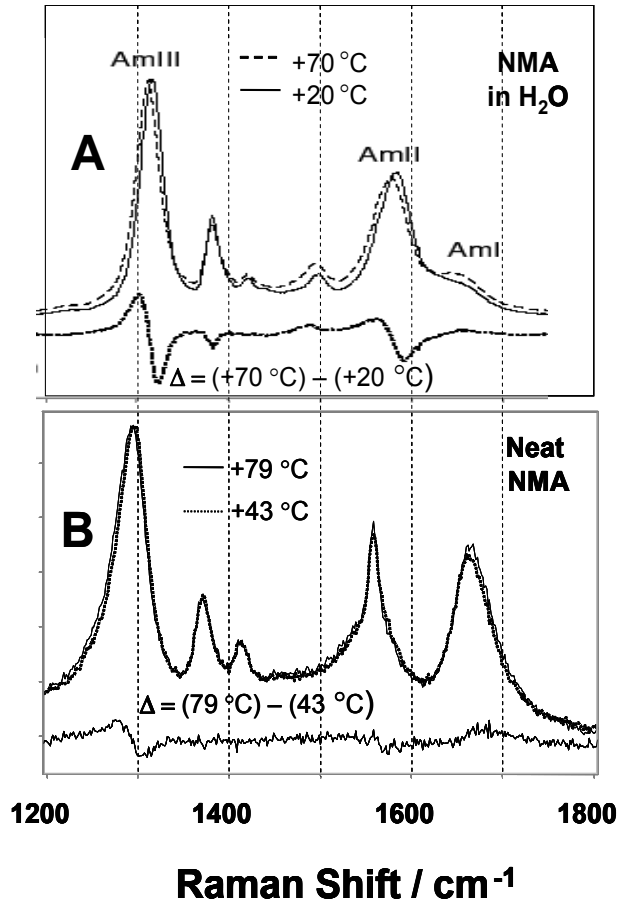

Figure 81. 204 nm UVRR spectra of NMA at high and low temperatures as well as their difference spectra (high – low T): A) 0.13 M NMA in water at +20 and +70 °C; B) NMA neat liquid at +43 and +79 °C. Sharp band at ~1555 cm^{-1} originates from atmospheric O_2.

Thus, the resulting $AmIII_3$ HB-induced frequency dependence in Eqn. 9 (Chapter 5) is:

$$\Delta\nu\ (HB_{P-W},\ HB_{P-P},T) \cong \{n^A \cdot \Delta\nu^A_{P-W}(T) + n^B \cdot \Delta\nu^B_{P-W}(T) + n^C \cdot \Delta\nu^C_{P-W}(T)\} + \{n^F \cdot \Delta\nu^F_{P-P}(T) + n^E \cdot \Delta\nu^E_{P-P}(T) + n^{D,D^*} \cdot \Delta\nu^{D,D^*}_{P-W}(T)\} \quad \textbf{[33]}$$

where $\Delta\nu^{A,B,C,D,D^*}_{P-W}(T)$ are the temperature dependent $AmIII_3$ frequency shifts due to HB of individual water molecules to specific sites ***A***, ***B***, ***C or D and D**** (Figs. 80 and 82); $\Delta\nu^{E,F}_{P-P}(T)$ are the temperature dependent $AmIII_3$ frequency shifts due to individual PB-PB HB at NH and/or

CO sites (Fig. 82); n^{A,B,C,D,D^*} and $n^{E,F}$ are the coordination numbers, which are equal to "1" if a particular site HB and "0" otherwise.

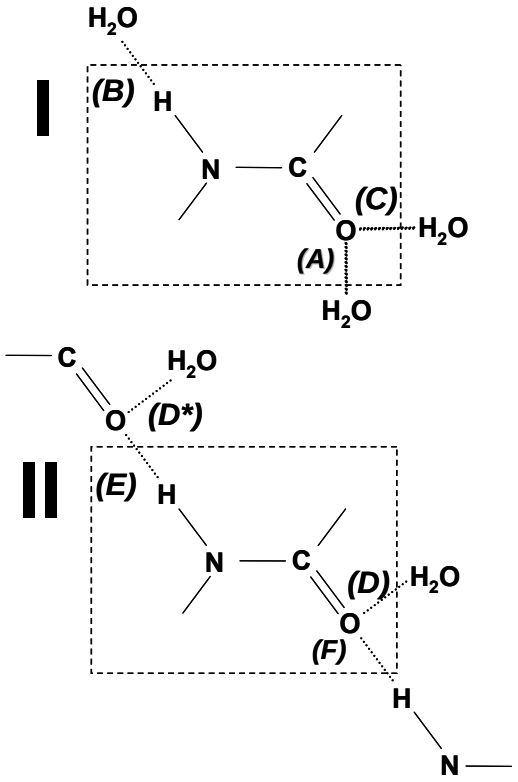

Figure 82. Definitions of all possible HB sites for: I) a PB, which is fully exposed to water (PPII, 2.5_1-helix and extended β-strand); II) a PB, with two PB-PB end-on HB (as in the interior PBs of an α-helix, and PBs of interior strands of β-sheet).

In this Appendix we will concentrate on exploring the two cases where the PB is either fully exposed to water (PPII, 2.5_1-helix and extended β-strand conformations), or is involved in two-end-on PB-PB HB, as in an infinite α-helix or multiple-stranded β-sheet conformation. We assume that the N-H HB is completely fulfilled by one HB of either type, while the C=O may have one or two HBs. If a PB is fully exposed to water, its N-H will always HB to one water/water cluster, while its C=O will always HB to two waters/water clusters (Figs. 82, I). Thus, in *Eqn. 33 if* $n^A = n'^B = n^C = 1$, *then we define* $n^D = n^{D^*} = n^E = n^F = 0$.

If the PB N-H is HB to another PB, it cannot additionally HB (Fig. 82, II). Thus, *in Eqn. 33 if* $n^E = 1$, *then* $n'^B = 0$ *and vice versa)*. If the C=O of a PB is HB to another PB, it cannot

HB to an additional PB, but it can additionally HB to water at site D, depending upon its water exposure (Fig. 82, II).

Thus, Eqn. 9 of Chapter 5 can be rewritten inserting Eqn. 33:

$$\begin{aligned} \nu_{III3}(\psi, HB_{P-P}, HB_{P-W}, T) \cong & [\nu_{VAC}(\psi = 0) - A_C \cdot \sin(\psi - \alpha_C)] \\ & + [n^A \cdot \Delta\nu^A_{P-W}(T) + n^B \cdot \Delta\nu^B_{P-W}(T) + n^C \cdot \Delta\nu^C_{P-W}(T)] \\ & + [n^E \cdot \Delta\nu^E_{P-P}(T) + n^F \cdot \Delta\nu^F_{P-P}(T) + n^{D,D^*} \cdot \Delta\nu^{D,D^*}_{P-W}(T)] \end{aligned} \quad \textbf{[34]}$$

where $\nu_{vac}(\psi=0)$ is the $AmIII_3$ frequency of a non-HB PB in vacuum with $\psi = 0°$. $\mathbf{A_c}$ measures the impact on the $AmIII_3$ frequency of the coupling between the N-H and C_α-H bending motions.

We found that maximum coupling occurs at a Ψ Ramachandran angle[43] of ~ +85 °, where the C_α-H and N-H bonds are approximately cis, while a minimum coupling occurs for an α-helix-like Ramachandran angles[43,47] of Ψ ~ –95° (in a sterically forbidden region of Ramachandran surface), where these bonds are essentially trans.

We now need to quantitatively characterize the remaining parameters of Eqn. 34.

A.2 DEPENDENCE OF AMIDE III_3 FREQUENCY ON PB-WATER HB (PPII, 2.5_1 HELIX, AND EXTENDED β-STRAND CONFORMATIONS)

Kubelka and Keiderling's[74] experimental studies of NMA hydration indicate that the AmIII frequency of fully hydrated NMA at room temperature is 62 cm^{-1} upshifted, compared to that of gas-phase NMA at ~100 °C. Taking into account the slope of temperature-induced coefficients (Table 19), we estimate the AmIII frequency upshift from the high-temperature gas-phase NMA to 0 °C NMA in water to be 64 cm^{-1} (Fig. 80). However, the theoretical studies of Besley[75] and Torii et al.[76] suggest somewhat lower upshifts of 54 and 41 cm^{-1} for NMA HB to the three individual water molecules at sites A, B, and C. We think that a larger experimental PB-*water* HB-induced shift of NMA occurs in real liquid water, since water clusters rather than the individual water molecules HB to NMA (especially at low temperatures), increasing the actual PB-*water* HB strength (Fig. 80).

Calculations of Schmidt et al.[77] also suggest that HB of a three-water cluster to site B results in a 20 cm^{-1} larger upshift of the AmII band of NMA, than occurs upon HB of one water to site B. Table 19 shows, that temperature slope of the AmIII frequency shifts/ºC of NMA (which are measures of the temperature dependence of the HB strength) are ~25 % less than that of AmII. Thus, we estimate an additional upshift for the AmIII band due to HB to the water cluster compared to that of one water at site B to be ~0.75•20 = 15 cm^{-1}. This is consistent with Kubelka and Keiderling's[74] FTIR measurements which suggest that the upshift of the NMA AmIII band (62 cm^{-1}) from the gas phase to water solution is ~75% of that of the NMA AmII band upshift (83 cm^{-1}). Thus, HB of NMA to water clusters, instead of to individual water molecules at sites A, B and C additionally increase the AmIII frequency upshift from 41 to 62 cm^{-1} at room temperature, or to ~64 cm^{-1} at 0 °C (Fig. 80).

The situation becomes more complex for PBs of long peptides and proteins, since different side chains and different secondary structural motifs will show different water exposures of C=O and N-H groups. Thus, we will need to carefully specify the HB pattern for each PB for these systems.

The PPII structure, which is an extended structure with all of its PBs fully exposed to water, appears to be mainly stabilized by PB-*water* interactions.[108-110] The PPII conformation has three waters/water clusters HB at each A, B, and C PB site, like that of NMA. Thus, we expect that the PPII conformation will show an $AmIII_3$ HB-induced frequency shift from vacuum to water similar to that of NMA. Fig. 80 shows our estimated $AmIII_3$ frequency upshifts for all possible HB to water situations; we estimate that the $AmIII_3$ frequency of fully hydrated PPII at T_0=0 °C will be ~64 cm^{-1} upshifted relative to the PPII chain in vacuum, similar to that of NMA.[74]

Thus, hydration of the PPII conformation gives rise to a shift of:

$$\Delta\nu_{P-W}^{PPII}(A,B,C,T_0) = \Delta\nu_{P-W}^{MAX}(T_0) \approx \Delta\nu_{P-W}^{A}(T_0) + \Delta\nu_{P-W}^{B}(T_0) + \Delta\nu_{P-W}^{C}(T_0) \cong 64\ cm^{-1}. \quad \textbf{[35]}$$

We recently discovered 2.5_1-helix conformations of PLL and PGA, which are stabilized by charged sidechain electrostatic repulsions.[60] These almost fully extended conformations have Ramachandran angles not far from those of the PPII conformation, and show a similar water exposure (based on monotonic frequency shifts[60]) with three water/water clusters HB to the PB.

Thus, we expect the 2.5_1-helix $AmIII_3$ frequency will also be 64 cm^{-1} upshifted from vacuum to water (Tables 8 and 9 of Chapter 5):

$$\Delta\nu_{P-W}^{2.5_1}(A,B,C,T_0) \approx \Delta\nu_{P-W}^{PPII}(T_0) \cong 64\ cm^{-1} \qquad \textbf{[36]}$$

We also expect a similar result for all water-exposed extended β-strand structures:

$$\Delta\nu_{P-W}^{EXTENDED}(A,B,C,T_0) \approx \Delta\nu_{P-W}^{PPII}(T_0) \cong 64\ cm^{-1} \qquad \textbf{[37]}$$

Assuming, that the PB of these extended β-strand-like structures HB to water clusters, rather than to single water molecules, we can quantitatively estimate the individual HB $AmIII_3$ upshifts at site A, B and C from the AmII upshifts of Schmidt et al.[77] The HB-induced upshifts of $AmIII_3$ band are ~75% of the AmII frequency upshifts (see discussion above).

However, the sum of the $AmIII_3$ upshifts, estimated from the Shmidt et al.'s[77] AmII upshifts, is slightly lower than the empirically obtained 64 cm^{-1} upshift (Eqn. 37). This is consistent with theoretical studies of Besley[75] and Torii et al.[76], which propose that the three simultaneous PB-*water* HBs at sites A, B, and C result in a slightly higher $AmIII_3$ frequency upshift, than the sum of upshifts due to the individual HB. For simplicity, we neglect this non-linearity and estimate the parameters in Eqn. 37 as $\Delta\nu_{P-W}^{A}$=15 cm^{-1}, $\Delta\nu_{P-W}^{B}$=33 cm^{-1}, and $\Delta\nu_{P-W}^{C}$=16 cm^{-1} to make their sum equal to 64 cm^{-1}. Thus, in the case of a fully exposed to water extended β-strand structures we write:

$$\Delta\nu_{III3}(T_0, HB) = n_{P-W}^{A} \cdot 15\ cm^{-1} + n_{P-W}^{B} \cdot 33\ cm^{-1} + n_{P-W}^{C} \cdot 16\ cm^{-1} \qquad \textbf{[38]}$$

where T_0=0 °C.

A.3 DEPENDENCE OF AMIDE III_3 FREQUENCY ON PEPTIDE BOND-PEPTIDE BOND HB IN NEAT NMA

We can estimate the influence of PB-PB HB on the $AmIII_3$ frequency directly from the experimentally measured AmIII frequencies of neat NMA and NMA in water (Fig. 81 and Table 19). NMA in water shows a 1315 cm^{-1} AmIII frequency at 0 °C, 64 cm^{-1} upshifted with

respect to that in vacuum[74] at 1251 cm^{-1}. There seems to be some systematic difference between the gas-phase NMA 1255 cm^{-1} value reported by Kubelka and Keiderling[74] and the 1259 cm^{-1} value reported by Mayne and Hudson.[111]

The NMA AmIII frequency upshifts from 1251 cm^{-1} in the gas phase to 1295 cm^{-1} in the neat liquid (at +40 °C) is caused by PB-PB HB. Neat NMA solutions are dominated by NMA clusters with only two PB-PB HB.[104,106,107] Thus, utilizing the temperature induced frequency shifts of Table 19, we estimate a 46 cm^{-1} $AmIII_3$ frequency upshift at 0 °C due to PB-PB HB:

$$\Delta\nu_{P-P}^{NMA}(T_1) \approx \Delta\nu_{P-P}^{E}(T_1) + \Delta\nu_{P-P}^{F}(T_1) \cong 46\ cm^{-1} \qquad \textbf{[39]}$$

since $n^E = n^F = 1$.

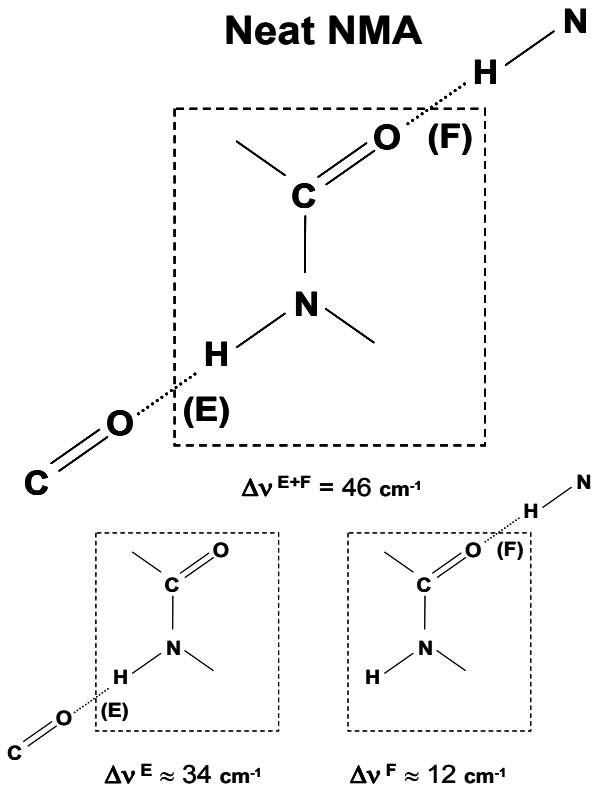

Figure 83. $AmIII_3$ frequency upshifts due to N-H (site E) and C=O (site F) PB-PB HB in neat NMA. Note: ~48 cm^{-1} AmIII upshift for two end-on PB-PB HB was measured, while the AmIII upshifts for PB-PB HB at individual sites E and F were estimated from their AmII band upshifts.[77]

Alternatively, Schmidt et al's.[77] calculations predict a 43 cm^{-1} NMA AmII upshift upon N-H PB-PB HB at site E, and 16 cm^{-1} AmII upshift upon C=O PB-PB HB at site F. Recalling[74] that $\Delta\nu_{III} \approx 0.75 \bullet \Delta\nu_{II}$, we can estimate the AmIII frequency upshifts due to NH (site E) and C=O

(site F) PB-PB HB as 35 + 12 cm^{-1}= 47 cm^{-1}, respectively. Our third independent estimate of the $AmIII_3$ upshift due to PB-PB HB in antiparallel β-sheet (see Eqn. 41) gives the value of 48 cm^{-1}. These values are very close to the 46 cm^{-1} value measured for NMA (Figs. 81 and 83). We will use the 47 cm^{-1} value for PB-PB HB-induced $AmIII_3$ frequency upshifts, since it is the average of these three estimates.

In spite of the theoretical studies,[75,76] which propose that two simultaneous HBs to NH and C=O groups of a PB may result in a slightly higher $AmIII_3$ frequency upshift than the sum of upshifts due to the individual HB, we for simplicity estimate the NMA parameters in Eqn. 39 as $\Delta\nu^{E}_{P-P}$=35 cm^{-1}, while $\Delta\nu^{F}_{P-P}$=12 cm^{-1}.

A.4 DEPENDENCE OF AMIDE III_3 FREQUENCY ON α-HELIX HB

The ideal α-helix conformation has the i-th residue N-H group intramolecularly HB to the i+4-th residue C=O group (Fig. 84). In addition, there is evidence of HB of the exposed PBs to the surrounding sheath of waters.[80,81,89,105,112-114] The three C-terminal α-helix residues have just their N-H groups intramolecularly HB (Fig. 84), while the three N-terminal α-helix residues have just their C=O groups intramolecularly HB (Fig. 84). Since each PB contributes to the AmIII Raman bands independently from their neighbors,[61] the UVRR spectra of an α-helix of seven or more residues long will have contributions from three differently HB PBs, which have the same α-helix Ramachandran angles (Fig. 85-87).

We expect the $AmIII_3$ frequency of the PB of interior residues, which have two-end-on PB-PB HB at their C=O and N-H sites (Fig. 85) to be 47 cm^{-1} upshifted due to PB-PB HB (sites E, F), with an additional 5 cm^{-1} upshift due to PB-*water* HB (sites D and D*).[89] Thus, the $AmIII_3$ frequency of a long α-helix in water is expected to show an $AmIII_3$ band 52 cm^{-1} upshifted when compared to the fictitious case of an identical 3D-structure where no HB occurred.

Ham et al.[81] α-helix hydration studies suggest that for a polyalanine α-helix, only one water molecule (on average) HB, and that this water HB to the carbonyl oxygen. The water HB results in only an additional ~5 cm^{-1} upshift, as observed by Pimenov et al.,[89] because the water

HB to the adjacent (i+4) PB carbonyl weakens the (i+4)C=O•••H-N(i) HB as explained by Schmidt et al.[77]

It should be noted, that α-helices consisting of amino-acid residues with larger side chains than ala will be less hydrated than are polyalanine α-helices,[112] and their $AmIII_3$ frequency should be less upshifted. Thus, α-helical segments of real proteins will be, in general, less upshifted because they will be involved in less PB-*water* HB.

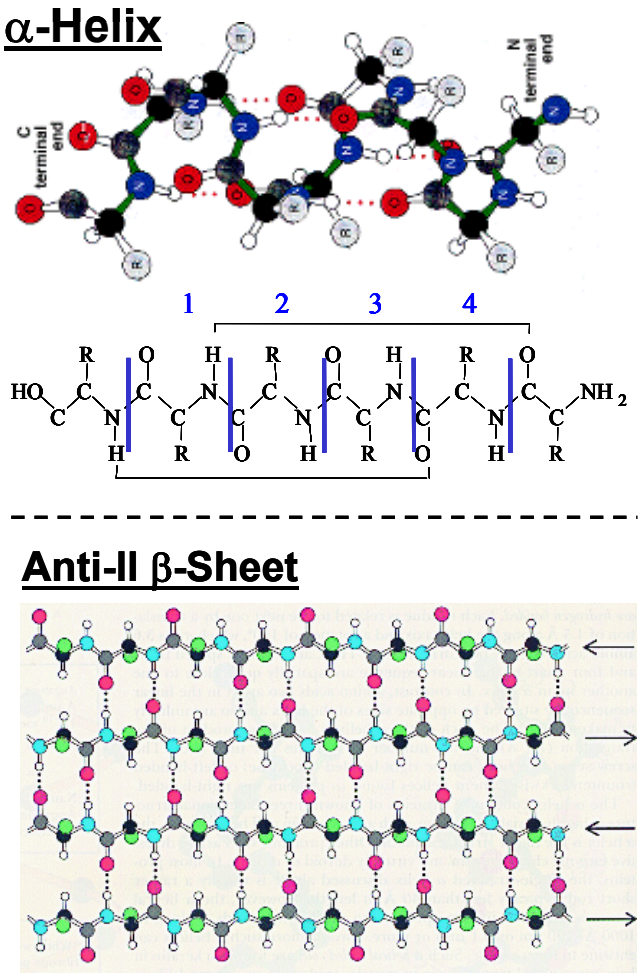

Figure 84. Diagram of α-helix and anti-parallel (anti-||) β-sheet PB-PB HB patterns. Note: Both α-helical segment of N≥7 residues long and β-sheet segment of n≥3 strands contain three types of PBs, which differ in PB-PB HB (see text and Figs. 85-87 for detail).

We can easily estimate the $AmIII_3$ frequency upshift for the three PB N-terminal residues that are PB-PB HB at their C=O sites from Schmidt et al.'s[77] AmII upshifts due to PB-PB HB

(Fig. 86). We expect the $AmIII_3$ frequency to be 12 cm^{-1} upshifted due to PB-PB HB (site F), with an additional 11 cm^{-1} upshift due to PB-*individual water* HB (site D)[77] or 16 cm^{-1} due to PB-*water sheath* HB (site D, Fig. 86). An additional 33 cm^{-1} upshift comes from HB of their N-H group to water clusters at sites B (Eqn. 38). Thus, we calculate a total $AmIII_3$ frequency upshift of 61 cm^{-1}.

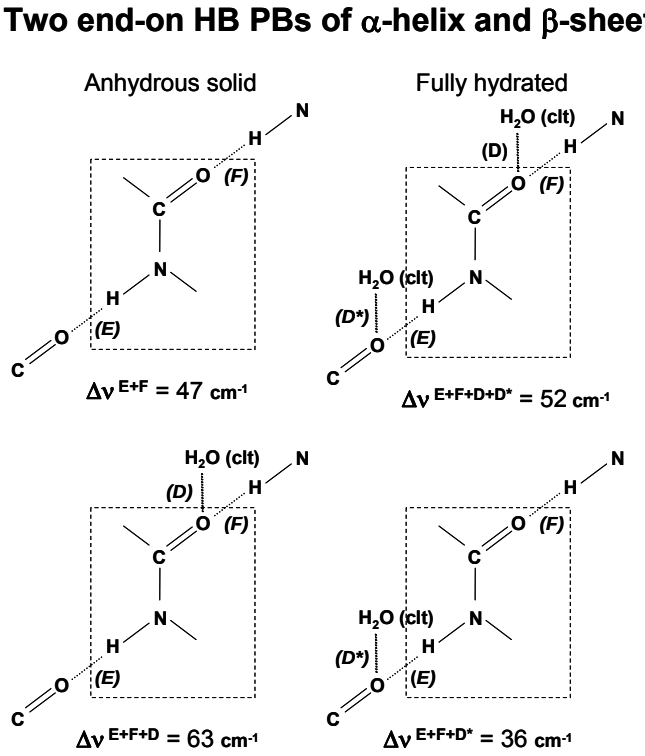

Figure 85. $AmIII_3$ frequency upshifts due to two-end-on HB; i.e. for interior PBs of α-helix and for PBs of interior strands of β-sheet. Note: 46 cm^{-1} $AmIII_3$ upshifts are estimated from the neat NMA (Fig. 83) and anhydrous α-helix data, while 51 cm^{-1} upshifts are measured from α-helix in water data of Pimenov et al.[89] The individual upshifts upon HB at sites D and D* are estimated from the calculated AmII frequencies of NMA.[77]

In contrast, the PBs of the three C-terminal residues (Figs. 84 and 87) will show a 35 cm^{-1} upshift due to PB-PB HB at the N-H site (E), with an additional 31 cm^{-1} upshift due to HB of the C=O to two waters at sites A and C, as can be estimated from Eqn. 38 (total 66 cm^{-1}). However, the additional PB-*water* HB at site D* of the neighboring PB (Figs. 82 and 87) will cause an 11 cm^{-1} $AmIII_3$ frequency downshift. Thus, the total $AmIII_3$ frequency upshift for the three C terminal PB of an α-helix will be 55 cm^{-1}.

These considerations indicate that there is no more than a 9 cm^{-1} $AmIII_3$ frequency difference (Figs. 53, 85-87) between any of the different α-helical HB states in water, given that the PB is constrained to be at the α-helix Ψ angle. In contrast, the terminal six α-helical residues of anhydrous α-helices which are not bound to water could show $AmIII_3$ frequencies 35 and/or 12 cm^{-1} below that of the interior of the α-helix (Figs. 54, 85-87).

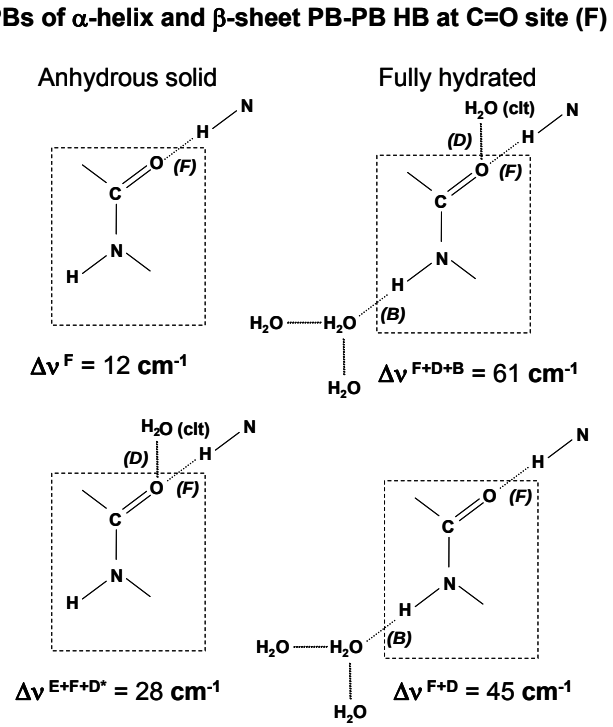

Figure 86. HB pattern and $AmIII_3$ frequency upshifts due to HB of PBs, which are PB-PB HB at their C=O sites; i.e. for the three N-terminal PBs of α-helices and half of PBs of exterior strands of β-sheet. Note: all these $AmIII_3$ upshifts were estimated from the calculated AmII frequencies of NMA.[77]

The impact of this $AmIII_3$ HB dependence on the measured UVRR spectra of our α-helical 21-residue AP peptide depends upon the detailed melting behavior. If melting conformations followed the all-or-none α-helix peptide model,[22] the UVRR spectra of α-helical AP would be dominated by the interior α-helix PBs whose $AmIII_3$ frequencies are upshifted by 52 cm^{-1} due to PB-PB and water HB. The three C-terminal residues would be shifted by 61 cm^{-1}, while the three N-terminal residues would by shifted by 55 cm^{-1}. Thus, the $AmIII_3$ would be slightly broadened by the contributions of the terminal residues.

In contrast, the relative contributions of the interior α-helix PBs will decrease if we assume the zipper model where a distribution of α-helical lengths occur.[29] In fact it appears that an examination of the $AmIII_3$ bandshape might allow us to distinguish the all-or-none versus the zipper model behaviors.

Thus, in case $AmIII_3$ upshift of AP α-helix (T_0=0 °C), which is dominated by two-end-on PB-PB HB, we write:

$$\Delta\nu^{\alpha-Helix}(HB,T_0) \cong [n^E \cdot \Delta\nu^E_{P-P} + n^F \cdot \Delta\nu^F_{P-P}] + n^{D,D^*} \cdot \Delta\nu^{D,D^*}_{P-W} \cong$$
$$= [n^E \cdot 35\ cm^{-1} + n^F \cdot 12\ cm^{-1}] + n^{D,D^*} \cdot 5\ cm^{-1} \qquad \textbf{[40]}$$

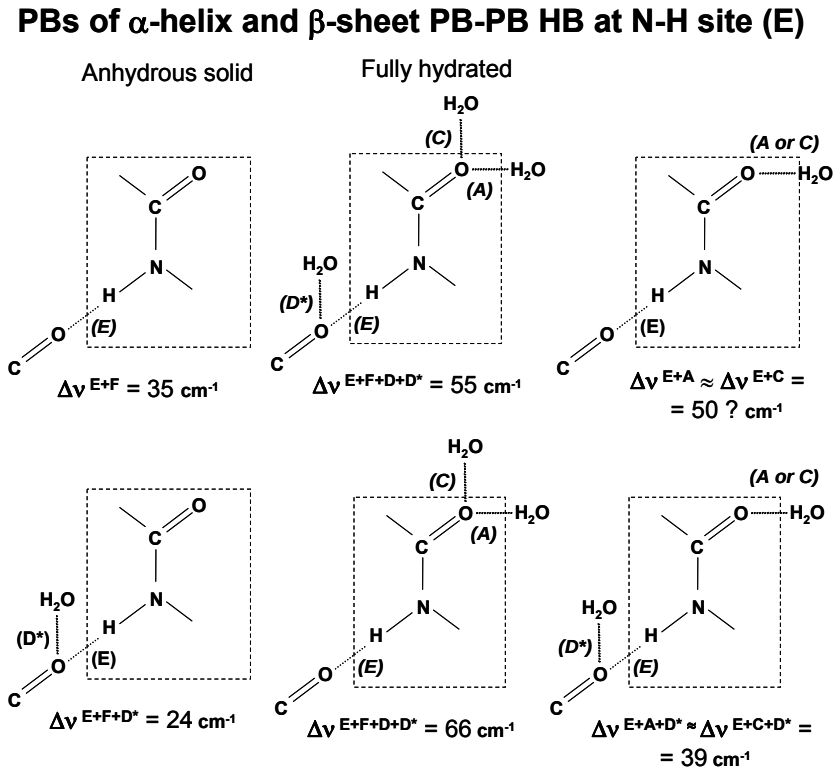

Figure 87. HB pattern and $AmIII_3$ frequency upshifts due to HB of PBs, which are PB-PB HB at their N-H site; these include the three C-terminal PBs of α-helix and half of PBs of exterior strands of β-sheet. Note: all these $AmIII_3$ upshifts were estimated from the calculated AmII upshifts of NMA.[77]

A.5 DEPENDENCE OF AMIDE III_3 FREQUENCY ON β-SHEET HB

Fig. 84 shows a schematic diagram of an anti-parallel β-sheet structure. The total number of PB-PB HBs formed in anti-parallel and parallel β-sheet depends on the number of participating single peptide strands. In a double-stranded β-sheet, half of the water exposed PBs are involved in both PB-PB C=O HB (site F) and C=O PB-*water* HB (sites D and D*, Figs. 86, 87), while their N-H groups HB to *water* (site B, Fig. 86); and the other half participate in N-H PB-PB HB (E site, Fig. 87) while their C=O groups HB to water (sites A and C, Fig. 87).

Interior strand PBs of multiple-strand β-sheets participate in two PB-PB HBs (sites E and F, Fig. 85), and additionally may have C=O PB-water HB (sites D and D*, Fig. 85). The PBs of their exterior strands will have the same HB pattern as those of double stranded β-sheets (Figs. 86 and 87).

Since each PB is expected to independently contribute to the AmIII region[61,62] we expect that the β-sheet spectrum will contain overlapping contributions of the three different HB species which have the same β-strand-like Ramachandran angles, but different HB patterns (Figs. 85-87; Table 8 of Chapter 5).

A.6 HB SHIFTS FOR B-SHEET ASSUMING A-HELIX-LIKE PB-PB HB STRENGTHS

If PB-PB HBs in anti-parallel β-sheet are equivalent to those in α-helices (Eqn. 40), we expect that half of the PBs (Figs. 84 and 86) of exterior strands of β-sheet will show $AmIII_3$ bands, which are 12 cm^{-1} upshifted due to the C=O PB-PB HB (site F), 16 cm^{-1} upshifted due to the additional PB-*water clusters* HB (sites D), and 33 cm^{-1} upshifted due to N-H PB-water clusters HB at site B, for a total upshift of 61 cm^{-1} (Fig. 86).

In contrast, the other half of PBs from exterior strands of a β-sheet (Fig. 87) will produce an $AmIII_3$ band, which is 35 cm^{-1} upshifted due to N-H PB-PB HB (site E) and 31 cm^{-1} upshifted due to two C=O PB-*water* HB at sites A and C. However, the additional PB-*water sheath* HB at

site D* of the neighboring PB reduces the $AmIII_3$ frequency by 11 cm^{-1}, giving a total $AmIII_3$ frequency upshift of 55 cm^{-1} (Fig. 87).

In contrast, the interior PBs in β-sheet strands will have the HB pattern shown in Fig. 85, and will show an $AmIII_3$ band which is 47 cm^{-1} upshifted due to both N-H and C=O PB-PB HBs (sites E and F) and 5 cm^{-1} upshifted due to an additional C=O PB-*water* HB at sites D and D*, for a total upshift of 52 cm^{-1} (Table 9 of Chapter 5). Thus, the maximum $AmIII_3$ frequency difference which can result due to different β-sheet hydration states, given identical β-sheet Ψ angles, is only 9 cm^{-1}.

The PLL-PGA antiparallel β-sheet structure is multistranded. Thus, its UVRR spectra are dominated by its interior strand PBs (Fig. 85). The antiparallel β-sheet chains have their PB more exposed to water than occurs in an α-helix. Although water could HB to the β-sheet carbonyls from both sides, it is unlikely that more than one water/water cluster will HB to each C=O (Fig. 85). Thus, we estimate that PB-*water* HB at sites D and D* for a β-sheet will also cause a 5 cm^{-1} upshift of the $AmIII_3$ frequency of the PBs in the interior β-sheet strands. Because HB at sites D and D* compensate,[77] differing PB-water HB strengths in β-sheets from those in α-helices would cause only small differences in the $AmIII_3$ frequency upshifts (Fig. 85).

We achieve a similar conclusion by using a second independent argument which allows the possibility that the β-sheet PB-PB HB strengths may be somewhat weaker than in α-helices.[115] We can calculate the $AmIII_3$ band frequencies of two non-HB β-strand-like conformations with similar Ψ angles. We measured a 1247 cm^{-1} (at 0 °C) $AmIII_3$ frequency for the PPII conformation of XAO,[42,43] and a 1227 cm^{-1} (at 0 °C) frequency for anti-parallel β-sheet of a PLL-PGA mixture.[60] PPII and anti-parallel β-sheet have similar Ψ angles of 145° and 135°, respectively.

We can calculate the downshifts which would occur if their HB were removed, while maintaining their conformations. The PPII $AmIII_3$ frequency in water at 0 °C is expected to be 64 cm^{-1} upshifted with "anhydrous PPII" (Fig. 80) which gives a 1183 cm^{-1} $AmIII_3$ frequency for this fictitious isolated PPII (Ψ~145º, Table 8 of Chapter 5). From the correlations in Eqn. 10 (Chapter 5) and Eqn. 4 (Chapter 2), which have similar $\partial\Psi/\partial\nu_{III3}$ derivatives of ~ 1 °/cm^{-1} in PPII/β-strand region of Ramachandran plot, we conclude that the $AmIII_3$ frequency of an isolated non-HB β-strand will be at 1174 cm^{-1}.

Anti-parallel PLL-PGA β-sheets (Ψ~135º) participate in both PB-PB and PB-water HBs. We estimate a 48 cm^{-1} of this upshift derives from the PB-PB HB.

$$\Delta\nu_{P-P}^{\beta-Sheet} \approx 1227 - 1174 + 5 \approx 48\ cm^{-1} \qquad \textbf{[41]}$$

Thus, the upshift value of 48 cm^{-1} due to PB-PB HB in PLL-PGA antiparallel β-sheet, estimated by Eqn. 41, is very close to the 46 cm^{-1} value for PB-PB HB in NMA (Eqn. 39). We will utilize a refined value of 47 cm^{-1}, and assign an $AmIII_3$ 1175 cm^{-1} frequency to an isolated non-HB β-strand (Ψ~135º). Thus, for PLL-PGA β-sheet in water at 0 °C we write:

$$\Delta\nu_{P-P}^{\beta-Sheet} \cong [n^{E} \cdot \Delta\nu_{P-P}^{E} + n^{F} \cdot \Delta\nu_{P-P}^{F} + n^{D} \cdot \Delta\nu_{P-W}^{D} n^{D} + n^{D^*} \cdot \Delta\nu_{P-W}^{D^*} n^{D^*} \approx \qquad \textbf{[42]}$$
$$\approx [n^{E} \cdot 35\ cm^{-1} + n_{P-P}^{F} \cdot 12\ cm^{-1} + n_{P-W}^{D,D^*} \cdot 5\ cm^{-1}]$$

where all the parameters have the same meaning as in Eqns. 40.

A.7 TEMPERATURE DEPENDENCE OF AMIDE III_3 FREQUENCY

The $AmIII_3$ UVRR bands as well as AmI and AmII bands of the pure secondary structure conformations, show monotonic frequency shifts with temperature that are independent of conformational changes.[22,29,42,43] These monotonic frequency shifts occur due to a decrease in the PB-to-water HB strength as the temperature increases.[42,43,80,81,105,112-114] For example, in case of XAO peptide, which is in a highly hydrated PPII conformation, the $AmIII_3$ band monotonically downshifts with an increase of temperature with a slope of –0.11 cm^{-1}/°C.[43]

Thus, we can write for PPII conformation:

$$\Delta\nu_{III}^{PPII}(T) \cong (T - T_0) \cdot \frac{\partial\nu^{A} + \partial\nu^{B} + \partial\nu^{C}}{\partial T}) = -0.11 \cdot (T - T_0)\ cm^{-1} \qquad \textbf{[43]}$$

where T_0=0 °C.

Assuming the similar HB pattern for 2.5_1-helix, we can write:

$$\Delta\nu_{III}^{2.5_1-Helix}(T) \cong \Delta\nu_{III}^{PPII}(T) = -0.11 \cdot (T - T_0)\ cm^{-1} \qquad \textbf{[44]}$$

We can generalize this result for any extended β-strand structure, i.e. any extended structure consisting of a single strand with Ψ and Φ Ramachandran angles in the β-strand region of the Ramachandran plot:

$$\Delta\nu_{III}^{EXTENDED}(T) \cong \Delta\nu_{III}^{PPII}(T) = -0.11\cdot(T - T_0)\ cm^{-1} \qquad \textbf{[45]}$$

We recently measured the temperature slope of the frequency shifts of the $AmIII_3$ and other amide bands for systems dominated by PB-PB HB, for the pure β-sheet[60] and pure α-helix[42,89] conformations and for neat NMA (Fig. 81, Table 19). The temperature slopes for neat NMA are ~40% less than that of fully hydrated NMA (Table 19). In contrast, in water we found much smaller $AmIII_3$ shifts for two-end-on HB (Fig. 85) α-helix[42,89] and β-sheet[60] conformations at the edge of measurability:

$$\Delta\nu_{III}^{\alpha-Helix}(T) \cong \Delta\nu_{III}^{\beta-Sheet}(T) \approx 0\ cm^{-1} \qquad \textbf{[46]}$$

The smaller dependence of the amide band frequencies on temperature in the α-helix and β-sheet intramolecularly hydrogen bonded structures results from collective nature of the extensive hydrogen bonding network, which requires more perturbation to significantly change the average hydrogen bond lengths.

Generalizing, we can write for monotonic frequency shifts of $AmIII_3$ band of any conformation:

$$\Delta\nu_{III}(T) \cong \delta\cdot\{-0.11\cdot(T - T_0)\}\ cm^{-1} \qquad \textbf{[47]}$$

where δ is a parameter, which mainly reflects the degree of hydration of a particular secondary structure element, and which we set at this time equal to "0" for long α-helix and multi-stranded β-sheet, and is equal to "1" in case of PPII, 2.5_1-helix, or any extended β-strand-like conformation consisting of a single strand.

We estimate δ to be 0.8 for both the three N-terminal PB in α-helices and the exterior PB in β-sheet strands (Figs. 84, 86). In contrast, we estimate δ to be ~ 0.5 for both the *three C-terminal PB of α-helices* and the exterior *PB of β-sheet strands* (Figs. 84, 87). These estimates derive from the assumption that the temperature dependence originates from PB-*water* HB

strength changes, and that the relative frequency dependence scales with the extent of water HB frequency upshift compared to that found in the PPII conformation.

A.8 QUANTITATIVE CORRELATION OF THE AMIDE III$_3$ FREQUENCY TO THE PB Ψ RAMACHANDRAN ANGLE, AND HB

Inserting Eqns. 10, 38, 40, 42, and 47 into the Eqn. 34 we obtain the following general expression, which relates the AmIII$_3$ frequency, Ψ Ramachandran angle and HB:

$$\begin{aligned} \nu_{III3}(\Psi,T,HB) = {} & [1192\ cm^{-1} - 54\ cm^{-1}\cdot\sin(\Psi + 26^0)] + \\ & + [n^{E}_{P-P}\cdot 35\ cm^{-1} + n^{F}_{P-P}\cdot 12\ cm^{-1} + n^{D,D^*}_{P-W}\cdot 5\ cm^{-1}] + \\ & + [n^{A}_{P-W}\cdot 15\ cm^{-1} + n^{B}_{P-W}\cdot 33\ cm^{-1} + n^{C}_{P-W}\cdot 16\ cm^{-1}] + \\ & + \delta\cdot\{-0.11\cdot\frac{cm^{-1}}{^{O}C}\cdot(T - T_0)\} \end{aligned} \qquad \textbf{[48]}$$

where all the parameters are described above (in the text of the Appendix A).

For ease of use we have decomposed Eqn. 48 into three different families of equations which are listed as Eqns. 10, 11A-D, and 12A-C. These are each specific to particular secondary structures with their particular HB patterns as described above in the Results and Discussion section of this manuscript. We also created an "average" Eqn. 11E for estimation of Ψ Ramachandran angle of a PB in aqueous solution, if the HB state of a PB is unknown.

APPENDIX B

SPECTRAL ANALYSIS OF ADP STEADY STATE UVRR SPECTRA

NOTE: All references in this Appendix can be found after the Chapter 7 of this thesis.

The AP α-helical fraction was calculated from the AP Raman spectra using the temperature dependent AP α-helix and PPII basis Raman spectra and the procedure of Lednev et al.[1] It should be noted though that AP PPII conformation was originally[1] incorrectly assumed to be a random coil.

We modeled the AdP UVRR spectra $I(T,\nu)$ by:

$$I(T,\nu) = fd_{\alpha}(T)\cdot Id_{\alpha}(T,\nu) + fd_{PII}(T)\cdot Id_{PII}(T,\nu) + f_{\alpha}(T)\cdot I_{\alpha}(T,\nu) + f_{PII}(T)\cdot I_{PII}(T,\nu) \quad \textbf{[49]}$$

where T is the temperature and v is the Raman frequency. The terms $fd_{\alpha}(T)$ and $f_{\alpha}(T)$ are the fractional α-helix content of the deuterated and nondeuterated segments of AdP. $fd_{PII}(T)$ and $f_{PII}(T)$ *are* the fractional PPII content of the deuterated and nondeuterated segments of AdP and are normalized by the total number of amide bonds in the peptide (deuterated plus non-deuterated). $Id_{\alpha}(T,v)$ and $Id_{PII}(T,v)$, are the spectra of the pure α-helix and the PPII (PII) conformations of the deuterated segments of AdP. $I_{\alpha}(T,v)$ and $I_{PII}(T,v)$, are the α-helix and PPII spectra of the nondeuterated peptide segments.

Thus, $fd_{\alpha}(T) + fd_{PII}(T) + f_{\alpha}(T) + f_{PII}(T) = 1$. **[50]**

The α-helical amide III frequency and bandshape is temperature independent, while the AP PPII amide III shows modest temperature dependence.[1] Therefore, $Id_\alpha(T,\nu) = Id\alpha(\nu)$ and $I_\alpha(T,\nu) = I_\alpha(\nu)$.

We find that the PPII deuterated amide III band is also essentially temperature independent. This probably results from the fact that C_α deuteration removes the variable contribution of C_α-H bending,[9-11] which is responsible for the large sensitivity of the amide III band to the peptide bond conformation.[9] Therefore, $Id_{PII}(T,\nu) = Id_{PII}(\nu)$ for the amide III spectral region (1200-1400 cm^{-1}).

Thus,

$$I(T,\nu) = fd_\alpha(T)\cdot Id_\alpha(\nu) + fd_{PII}(T)\cdot Id_{PII}(\nu) + f_\alpha(T)\cdot I_\alpha(\nu) + f_{PII}(T)\cdot I_{PII}(T,\nu) \qquad \textbf{[51]}$$

At high temperature (T≥60 °C) AP and AdP are essentially 100% PPII (Chapter 2 and ref. 1). Thus, n_d deuterated and n_n non-deuterated amide bonds ($n_d + n_n = n = 20$) occur in the PPII form. The high temperature, T_1 AdP spectrum $I(T_1,\nu)$ is thus:

$$I(T_1,\nu) = \frac{n_d}{n}\cdot Id_{PII}(\nu) + \frac{n_n}{n}\cdot I_{PII}(T_1,\nu) \qquad \textbf{[52]}$$

and the difference spectrum can be written:

$$\Delta I = I(T_2,\nu) - I(T_1,\nu) = \qquad \textbf{[53]}$$
$$= fd_\alpha(T_2)\cdot[Id_\alpha(\nu) - Id_{PII}(\nu)] + f_\alpha(T_2)\cdot[I_\alpha(\nu) - I_{PII}(T_2,\nu)] - \frac{n_n}{n}\cdot[I_{PII}(T_2,\nu) - I_{PII}(T_1,\nu)]$$

Since the 1240 cm^{-1} AdP difference spectral peak results from the α-helix→PPIIl transition of the non-deuterated part of AdP:

$$\Delta I(\nu_1) = f_\alpha(T_2)\cdot[I_\alpha(\nu_1) - I_{PII}(T_2,\nu_1)] - \frac{n_n}{n}\cdot[I_{PII}(T_2,\nu_1) - I_{PII}(T_1,\nu_1)] \qquad \textbf{[54]}$$

Here ν_1 is 1240 cm^{-1}, since there is no contribution of the deuterated segment to the 1240 cm^{-1} spectral change. Using the previously calculated[1] temperature dependent AP UVRR spectra for the α-helix $I_\alpha(\nu)$ and PPII conformations $I_{PII}(T,\nu)$, we determined the temperature dependence of the α-helical fraction of the non-deuterated (internal) α-helical segments $f_\alpha(T_2)$

from Eqn. 54. The temperature dependence of this calculated α-helical fraction is shown in Fig. 68B of Chapter 7, ◊.

We calculated the α-helical fraction of the deuterated part of AdP from the UVRR spectra using the dependence of the 1325 cm^{-1} band Raman cross sections on the α-helix and PPII composition. Using values of $f_\alpha(T_2)$, obtained from Eqn. 54 by using the 1240 cm^{-1} non-deuterated amide III band, we can calculate the product $fd_\alpha(T_2)\cdot[Id_\alpha(\nu)-Id_{PII}(\nu)]$ from Eqn. 53 since all other parameters are known:

$$fd_\alpha(T_2)\cdot[Id_\alpha(\nu_2)-Id_{PII}(\nu_2)]= \quad \textbf{[55]}$$
$$=\Delta I(\nu_2)-f_\alpha(T_2)\cdot[I_\alpha(\nu_2)-I_{PII}(T_2,\nu_2)]+\frac{n_n}{n}\cdot[I_{PII}(T_2,\nu_2)-I_{PII}(T_1,\nu_2)]$$

where ν_2 is 1325 cm^{-1}. We obtained the value of $[Id_\alpha(\nu_2)-Id_{PII}(\nu_2)]$, which we assume is temperature independent,[12] from the measured value of $fd_\alpha(T)$ at T=0 °C obtained by subtracting the α-helical fraction of the non-deuterated part of AdP from the calculated α-helical fraction of AP, since AP and AdP show identical α-helical fraction temperature dependencies, Fig. 68A (Chapter 7). These calculated values are shown by the ♦ in the Fig. 68B (Chapter 7). In the future we will directly determine more accurate values of $[Id_\alpha(\nu_2)-Id_{PII}(\nu_2)]$ and its actual temperature dependence from UVRR spectra of fully deuterated peptides.

APPENDIX C

PURE ADP α-HELICES AT +30 AND +40 °C ARE STABILIZED BY ~1.5 KCAL/(MOL·PB) WITH RESPECT TO π-BULGES AND 3_{10}-HELICES.

Note: Bibliography for the Appendix C is given after Chapter 9 of this thesis

Recently we developed a method to estimate the Ψ Ramachandran angular population distributions of peptides and proteins from their UVRR $AmIII_3$ band profiles.[120,126,128,145,153] These Ψ angular population distributions can then be used to estimate the Gibbs free energy landscapes (GFEL) along the Ψ angle folding coordinate.[128,145]

Figure 88 shows the estimated GFELs for AdP at +30 and +40 °C, which are important in understanding the AdP kinetics. The +30 °C AdP GFEL (Fig. 88A) was estimated exactly same way as for AP,[145] which is a natural abundance analog of AdP. To estimate the +40 °C AdP GFEL (Fig. 88B), we assumed that the Ψ angular distribution of pure α-helix at +40 °C has the maximum value of Ψ= –42° and the same halfwidth, σ, of ~5° as that at +30 °C.[145] This is a reasonable assumption, because we showed earlier that the ~11 cm^{-1} half width at half height (HWHH) of the +30 °C α-helical $AmIII_3$ UVRR band in water[145] is only slightly larger than the ~7.5 cm^{-1} homogenious linewidth (HWHH) measured in peptide crystals.[120]

The black lines in Fig. 88 show the well determined portions of GFELs in the α-helical and PPII Ψ angular regions. This allows us to reliably determine the energy differences between pure α-helix, π-bulge and 3_{10}-helix conformations of AdP, whose minima occur at Ψ angles of –42°, –58° and –28°, respectively.[145] Specifically, we find that at both +30 and +40 °C, the Gibbs free energies of π-bulges and 3_{10}-helices are approximately equal to each other. In

contrast, the pure α-helix conformation is stabilized by ~1.5 kcal/mol·PB with respect to π-bulges and 3_{10}-helices (Fig. 88), as expected.[56,93]

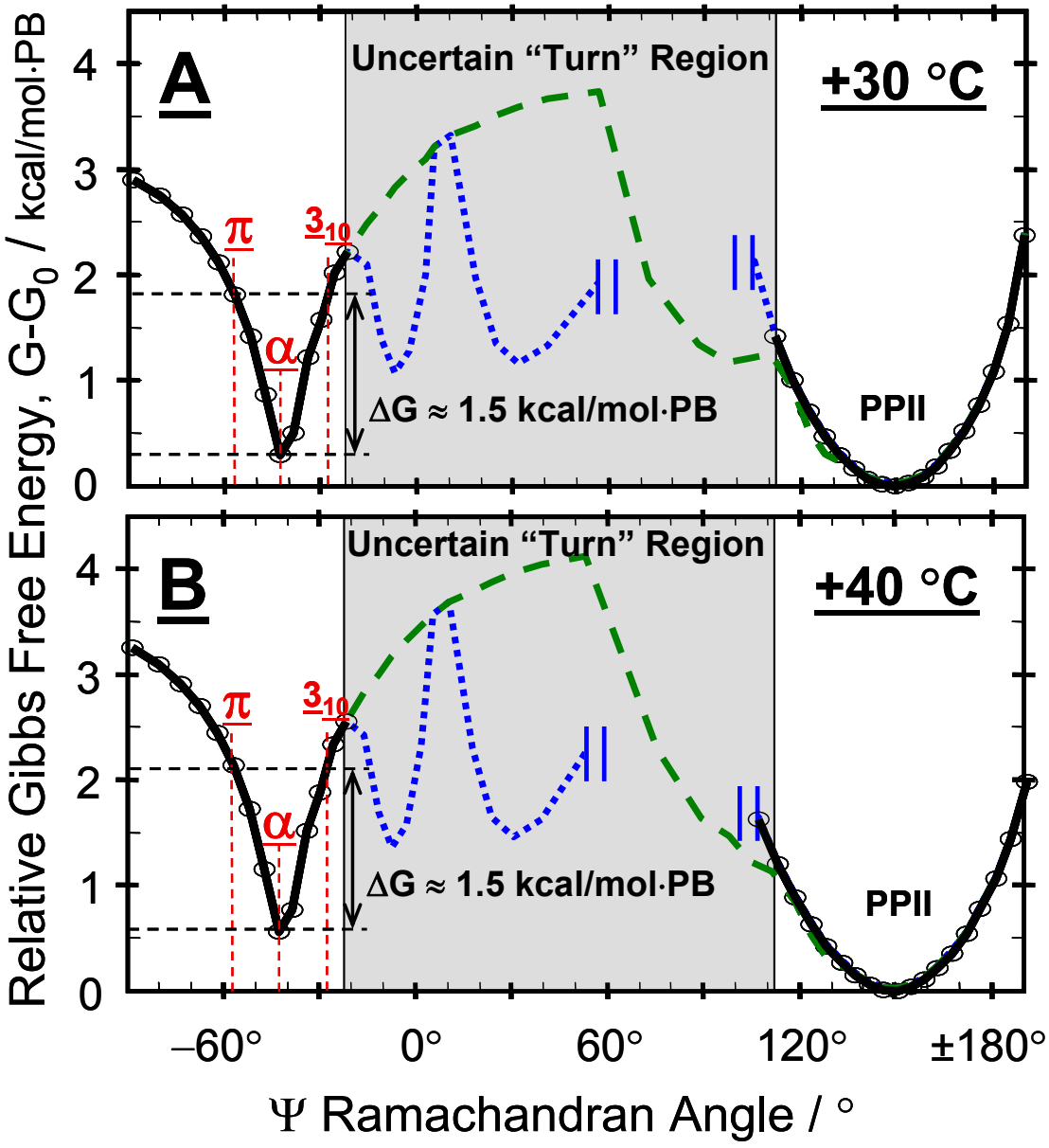

Figure 88. Relative equilibrium Gibbs free energy landscapes (GFEL) for AdP at different temperatures: (A) +30 °C, (B) +40 °C. Black lines with circles represent well-determined portions of the GFEL in the α-helix and PPII regions of the Ramachandran plot. The dotted blue line in the uncertain "turn" regions of the Ramachandran plot, assumes that the turns T1 and T2 exist at Ψ≈–10° and +30°, respectively.[145] The dashed green line assumes that turns T1 and T2 exist at Ψ≈+130° and +90°, respectively.[145]

The dotted blue line in Fig. 88 shows a very roughly estimated Ψ angle GFEL in the uncertain "turn" regions of the Ramachandran plot, by assuming that the detected minor turn conformations occur at Ψ≈–5° and +34°, respectively.[145] In this case, it is not possible to determine the portion of GFEL between Ψ values of ~60° and 100°, nor to reliably determine the energy barrier between the α-helix and the PPII conformations (60° to 100°, Fig. 6). However, we can estimate that the barriers at the other angles are <3.6 kcal/mol·peptide bond (kcal/mol·PB).

The dashed green line in Fig. 88 shows another option for the GFEL in the "turn" region of the Ramachandran plot, which assumes that the turns T1 and T2 (or β-strand) exist at Ψ≈+133° and +94°, respectively.[145] Under this assumption, we estimate that the energy barriers between the α-helix and PPII conformations are between ~3.5 and 4.2 kcal/mol·PB (Fig. 88).

We estimated from our Chapter 9 kinetic data that a 5.4–19.8 kcal/mol·PB *unfolding* and 0–11.3 kcal/mol·PB *folding* Gibbs free energy activation barriers exist between the α-helix and PPII conformations (Table 18). The higher kinetic activation barrier found for unfolding (Table 18) than that estimated from the equilibrium GFELs (Fig. 88) may indicate the existence of the additional intermediate states involved in the α-helix unfolding reaction of AdP. These additional states would slow down the α-helix unfolding rates at low temperatures, making the serial calculated unfolding free energy activation barrier higher than any of the individual barriers.